INVESTIGATIONS ON ALUMINA CERAMIC FORMING USING NATURAL RUBBER LATEX AS A BINDER

A thesis submitted

in partial fulfillment for the Degree of

Doctor of Philosophy

by

RAKESH KRISHNAN P P

DEPARTMENT OF CHEMISTRY

INDIAN INSTITUTE OF SPACE SCIENCE AND TECHNOLOGY

THIRUVANANTHAPURAM- 695 547

SEPTEMBER 2023

To my father, mother, wife, son, teachers, and friends

CERTIFICATE

This is to certify that the thesis entitled **Investigations on alumina ceramic forming using natural rubber latex as a binder**, submitted by Rakesh Krishnan P P, to the Indian Institute of Space Science and Technology, Thiruvananthapuram, in partial fulfillment for the award of the degree of Doctor of Philosophy, is a *bona fide* record of research work carried out by him under our supervision. The contents of this, in full or in parts, have not been submitted to any other Institution or University for the award of any degree or diploma.

Dr. P. Arun Kumar
Deputy Director
Earth Storable Engines and Stages
Liquid Propulsion Systems Centre
Thiruvananthapuram

Dr. K. Prabhakaran
Professor
Department of Chemistry
Indian Institute of Space Science and Technology
Thiruvananthapuram

Thiruvananthapuram - 695 547
September 2023

Countersignature of the HOD with seal

DECLARATION

I declare that this thesis entitled **Investigations on alumina ceramic forming using natural rubber latex as a binder**, submitted in partial fulfillment of the degree of **Doctor of Philosophy** is a record of original work carried out by me under the supervision of **Dr. K. Prabhakaran** and **Dr. P. Arun Kumar**, and has not formed the basis for the award of any degree or diploma, in this or any other Institution or University. In keeping with the ethical practice in reporting scientific information, due acknowledgements have been made wherever the findings of others have been cited.

Rakesh Krishnan P P

SC18D013

Thiruvananthapuram – 695 547

25.09.2023

Acknowledgments

I express my sincere gratitude to my guide, Dr. K. Prabhakaran for allowing me to work with his group. His guidance, patience, involvement with the work, supervision, ideas, and valuable time are gratefully acknowledged. His wealth of knowledge, passion for research, and work ethic have been sources of great inspiration to me, and which I sincerely wish to emulate in my professional career. I express gratitude to my guide, Dr. P. Arun Kumar for letting me work under his guidance and moreover, for his motivation, guidance, support, suggestions, and valuable time are greatfully acknowledged. My research supervisors had spent enough time discussing the experiments, data analysis, and paper writing and gave me a lot of suggestions and support to overcome the difficulties during my Ph.D. tenure.

I also take this opportunity to thank Dr. V. Narayanan, Director, LPSC for providing all the facilities and encouragement to carry out this research. I also take this opportunity to thank Dr. V. K. Dadhwal, former Director, IIST, and Dr. Unnikrishnan Nair, Director, IIST, for providing all facilities to accomplish my research. It is also a pleasure to extend my heartfelt gratitude to Prof. Kuruvilla Joseph, Dean (Student Activities), IIST for his support throughout my research tenure. I am also thankful to Shri. Jacob Panicker, P.C, former Deputy Director, ESES/LPSC, Shri. Shajimon A Cherian, former Group Director, ESEG/LPSC, Shri. Vinodha Kumar. M, former Group Head/TPTG, Shri. Mahesh. M, Group Director, ESEG, and Shri. Benny Peter, ESEG for permitting me to do a part-time Ph.D. and for their encouragement and support during my Ph.D. tenure. I would like to thank all my doctoral committee members, Dr. Nirmala Rachel James (IIST), Dr. Renjith Devasia (VSSC), Dr. Jobin Cyriac (IIST), Dr. V.S. Sooraj (IIST) and Dr. T.D.P. Rajan (NIIST) for

their valuable time, suggestions, guidance, future directions and criticism for improving the quality of the research work. I express thanks to all the faculty members of the Department of Chemistry for their motivation and support. I am extremely thankful to all my colleagues, Shri. Jipsu P Eldo, Shri. Aseem K.S, Shri. Anish Andrews, Shri. Tomy Francis of Earth Storable Engines Group, LPSC for their close co-ordination with this research work, their help, motivation, support, and guidance. I am grateful to the members of NIIST, VSSC, SCTIMST, SAW, Kerala University, and AML/LPSC for supporting the various characterization techniques which are the back bone of the research.

I also thank Shri. Nellori Dileep Kumar, Shri. Santhosh Kumar, and Shri. Bodasingi Thavitiraju of AML/LPSC for their support with the characterization of samples. I am grateful to, Dr. Sujith Vijayan, Dr. Praveen Wilson, Dr. Chithra A, and Ms. Raji S, former and current members of my research group for their help in my experimental work and for their fruitful discussions in analyzing the research data and writing the thesis. I am also thankful to Dr. Dheeraj B.D.S, Ms. Varsha. M. V, Govind Kumar Sharma, and all my fellow researchers for their support during my tenure in IIST. I am also thankful for the assistance received from the members of the staff viz. Mr. Loveson Albert, Mrs. Bindu J.M., Mrs. Jayasree R, Mrs. Jayasree L, and Mrs. Bindhu P C. Above all, I am forever thanks to my parents, wife, and son for their endless love and encouragement. Words cannot express my love and affection towards my son for his patience through the journey of my research work. I thank everyone who helped and inspired me in the last five years.

Rakesh Krishnan P P

Abstract

Ceramics are the major category of materials that have attractive mechanical, thermal, and electrical properties, resistance to high temperature, chemical inertness, and biocompatibility. Therefore, these materials have been employed in various advanced applications in the automotive, aerospace, defense, nuclear, and bio-medical sectors. The fabrication of high-quality complex-shaped ceramic components is particularly needed for achieving specific functions. The machining of sintered ceramics to make complex shapes is an energy-intensive, costly, and slow process. In this respect, the near-net shaping strategy is an essential part of ceramic fabrication. Ceramic fabrication techniques such as powder pressing, slip casting, tape casting, gel casting, injection molding, extrusion, and additive manufacturing are extensively used to produce ceramic components of various shapes and dimensions. Various processing additives such as solvents, dispersants, binders, plasticizers, lubricants, and antifoams are generally utilized in these processes to achieve specific processing requirements. Currently, most of the additives used are petroleum-based organic compounds that create environmental impacts and global warming. One of the approaches to avoid these problems is to replace toxic organic solvents with water and other synthetic additives with naturally renewable molecules. In the present work, natural rubber latex (**NRL**), a naturally renewable bio-polymer, has been utilized as a binder in the processing of alumina ceramic by powder pressing, slip casting, tape casting, and gel casting.

NRL is used as a binder in powder pressing of alumina. The ammonium poly(acrylate) dispersed alumina slurry and **NRL** form well-dispersed co-dispersions easily using magnetic stirring due to their high negative surface potentials in the pH range of 9.6 to 10. The granulated feedstock for powder pressing is prepared through co-coagulation of the co-dispersions using a formic acid solution followed by centrifugation, drying, and grinding. The average particle size of the coagulated co-dispersions increases from 0.34 to 12.30 μm when the concentration of **NR** increases from 0 to 10 wt.%. The feedstock granules prepared using 6 and 8 wt.% **NR** concentrations have superior flow properties as evidenced by the flow time and Hausner ratio measurements. The powder-pressed compacts achieve a maximum green density of 67.7 %T.D. at a relatively low compaction pressure of 20 MPa due to the highly flexible **NRL** binder. The green compacts exhibit uniform microstructure. The green compacts prepared at 2 wt.% **NR** shows severe end capping due to poor mechanical strength. The green strength increases from 0.55-1.91 MPa when the **NR** concentration increases from 4 to 10 wt.%. A remarkable increase in green strength in the range of 2.30-9.39 MPa (almost 2.3 to 6 times) is achieved on annealing

the pressed compacts at 200°C due to the cross-linking of **NR** chains through the carbon-carbon double bonds induced by the Lewis acid character of alumina. The annealed green compact is amenable to machining by milling, drilling, and lathing using conventional machines and tools. The cross-linked **NRL** binder shows a near-steady state of burn-out without creating any crack in the green body. The powder-pressed bodies sintered at 1550 °C show 18% linear shrinkage, 97% T.D., and 1.8 μm average grain size.

NRL is studied as a binder in the slip casting of alumina and the results are compared with that of slip casting using a conventional polyvinyl alcohol (PVA) binder. The polyacrylate dispersed aqueous alumina slurry and **NRL** form co-dispersions easily due to their high negative surface potentials. The slip casting slurries prepared using the **NRL** binder achieves a high alumina loading in the range of 40 to 55 vol.% compared to the 41.1 vol.% achieved with 2 wt.% PVA binder. The alumina-**NRL** co-dispersions show shear thinning flow behavior with viscosity and yield stress values suitable for slip-casting. The cast layer thickness formed in one hour decreases from 8.5 to 4.2 mm when the **NR** concentration increases from 0 to 8 wt.% due to the gelation of **NR** binder at the mold-cast layer interface. The cast layer thickness formed in one hour at 4 wt.% **NR** concentration increases from 4.13 to 6.5 mm when the alumina slurry concentration increases from 40 to 55 vol.%. The cast layer thickness formed from alumina slurry containing **NRL** binder is nearly 3 times higher than that formed from an aqueous slurry of the same alumina concentration containing 2 wt.% PVA binder. The slip-cast alumina bodies produced using **NRL** binder exhibit higher green density in the range of 53.4 to 62.5 % T.D. compared to 52.1% T.D. achieved from alumina slurry containing 2 wt.% PVA binder. The binder migration normally noticed in slip casting using water-soluble PVA binder is not observed in **NRL** binder-based alumina slip casting. The green strength increases from 0.45 - 1MPa by increasing the **NR** concentration from 0 to 8 wt.%. The strength increases to 0.45 - 9.68 MPa on annealing the green bodies at 200°C due to the cross-linking of **NR**. The annealed slip-cast green bodies are amenable to machining by milling and drilling using conventional machines and tools. The slip-cast alumina bodies sintered at 1550°C show 97%T.D. with a homogeneous microstructure and 1.82 μm average grain size. The slip casting using **NRL** binder is capable of producing crucibles of wall thickness as low as 1.2 mm.

The **NRL** is proposed as an eco-friendly binder in the aqueous tape casting of alumina. The tape casting slurries prepared by mixing 58.2 vol.% alumina slurry dispersed using the ammonium poly(acrylate) dispersant and **NRL** show shear thinning flow behavior and adequate viscosity and yield stress values. Tape casting slurries of high total solids loading in

the range of 60.57 to 60.88 vol.% is achieved at **NR** concentrations in the range of 14.2 to 18.1 wt.%. The high solid content of the tape casting slurry formulations enables the fast drying of the cast tape within a reasonable time of 15 minutes at 70°C. The strength, modulus, and % elongation at break of the green alumina tape are in the ranges of 1.62 to 1.85 MPa, 267.5 to 50.8 MPa, and 41 to 254 %, respectively, at **NR** concentrations in the range of 14.2 to 18.1 wt.%. Annealing in between two glass plates transforms the flexible green tape to a rigid and brittle one due to the self-cross-linking of **NR** which avoids its curling at the edges during the binder removal. Roll pressing of the green tapes produces a remarkable improvement in microstructure and density at a thickness reduction of 20%. The roll-pressed green tape achieves a density of 98.5% T.D by sintering at 1600°C. The sintered tapes show a uniform microstructure with an average grain size of 3.2 μm.

NRL is employed as gelling agent and binder in the freeze-gel casting of alumina. The alumina-**NRL** co-dispersions prepared by mixing ammonium poly(acrylate) dispersed 58.2 vol.% aqueous alumina slurry and concentrated **NRL** show low viscosity and yield stress values required for gel casting. The gelation of the co-dispersions is achieved by freezing in a mold and subsequent mold removal and thawing in an acetone medium. The growing ice crystals disrupt the protein layer on the latex particles leading to their coagulation. The exchange of water with acetone during thawing in an acetone medium strengthens the alumina-**NR** particle network by further coagulation. The minimum concentration of **NR** required to percolate and form a stable alumina-**NR** gel is 8 wt.% by weight of the alumina powder. The strength and modulus wet gel achieved are 60 kPa and 640 kPa, respectively, which are sufficient for handling during further processing. The frozen body passes through a semi-fluid state during thawing which enables the gel to flow and fill the space created by the melting of ice crystals leading to dense ceramics. The acetone exchange enables faster drying of the gel bodies at room temperature without creating any deformation or crack. The diametrical compressive strength and modulus of the dried green body are 0.34 MPa and 18 MPa, respectively. The diametrical compressive strength and modulus improve to 2.14 MPa and 150 MPa, respectively, on annealing at 200 °C due to cross-linking of **NR** chains. The green bodies on debinding and sintering at 1550°C produce alumina ceramics of uniform microstructure with ~96% T.D and 1.3 μm average grain size. The freeze-gel casting using **NRL** binder has the capability to fabricate near-net shape alumina ceramics.

NRL functions as a pores stabilizer and binder for the preparation of macroporous alumina ceramics by freeze-gel casting without freeze drying. The gels prepared by freezing and

thawing the alumina powder-**NRL** co-dispersions achieve shape stability at a minimum **NR** concentration of 20 wt.%. A 20 wt.% **NR** is required to stabilize the pores in gels prepared at alumina slurry concentrations in the range of 42.72 - 25.44 vol.% whereas 30 wt.% **NR** is required to prevent pore collapse in gels prepared from a slurry of alumina concentration up to 15 vol.%. Two-times acetone exchange removes ~ 96.5 % of the water present in the gels which results in fast drying, low drying shrinkage, and a smooth green body surface. The diametrical drying shrinkage varies from 2.1 to 10.32 % when the alumina slurry concentration varies from 42.74 to 15 vol.%. The cross-linking of **NR** chains by annealing at 200 ℃ prevents the melting of **NR** and thereby avoids pores collapse during binder removal. The achieved porosity (44.5 to 71.12 % at alumina slurry concentration in the range of 42.74 to 15 vol.%) by acetone exchange followed by air drying is lower by 10-15 % of the porosity obtained by freeze-drying of the corresponding frozen bodies. Macroporous ceramics produced from the frozen bodies by both the acetone exchange followed by air drying and freeze-drying methods exhibit a similar lamellar pore structure. The lamellar pore width in ceramic obtained by the acetone exchange followed by the air drying route is lower by nearly 42 % than that obtained by freeze-drying due to the pore shrinkage during air drying of the acetone exchanged bodies. The macroporous ceramics show a compressive strength and Young's modulus in the ranges of 3.8 to 35.3 MPa and 306.2 to 1486.5, respectively, at an alumina slurry concentration in the range of 15 to 42.74 vol.%.

Table of Contents

List of Tables

List of Figures

Abbreviations

PSD	Particle size distribution
NRL	Natural rubber latex
Al_2O_3	Alumina
ZrO_2	Zirconia
MgO	Magnesium oxide
$BaTiO_3$	Barium titanate
$PbZrxTi_{1-x}O_3$	Lead Zirconium Titanate
SiC	Silicon carbide
BN	Boron nitride
AlN	Aluminium nitride
TiB_2	Titanium diboride
ZrB_2	Zirconium diboride
$MoSi_2$	Molybdenum disilicide
T.D	Theoretical density
PVA	Polyvinyl alcohol
PEG	Polyethylene glycol
TBA	Tertiary butyl alcohol
PVP	Polyvinyl pyrrolidone
PAM	Polyacrylamide
HA	Hydroxyapatite
DHF	2,5- dimethoxy-2,5-dihydrofuran
PAA	Polyacrylic acid
SEM	Scanning Electron Microscopy

MA	Methacrylate
MMA	Methyl methacrylate
EHA	2-ethyl hexyl acrylate
MAA	Methacrylic acid
MC	Methylcellulose
CMC	Carboxymethyl cellulose
IEP	Isoelectric point
EDL	Electrical double layer
DLVO	Derjaguin-Landau-Verwey-Overbeek
PMMA	Polymethyl methacrylate
HPMC	Hydroxypropyl methyl cellulose
PIBM	Co-polymer of isobutylene and maleic anhydride
TiO_2	Titanium dioxide or Titania
AM	Additive manufacturing
SLS	Selective Laser Sintering
TGA	Thermogravimetric analysis
RPM	Rotation per minute
DMA	Dynamic mechanical analysis
PVC	Polyvinyl chloride
DTG	Derivative Thermogravimetric

Notations

σ_f	Fracture stress
E	Elastic modulus
γ	Shear rate
κ^{-1}	EDL thickness
N_i	Valence of the counter ions
k	Boltzmann constant
ψ_o	Surface potential
V_R	Repulsive potential energy
V_A	Attractive potential energy
V_T	Total potential energy
η	Viscosity of the liquid/slurry
Rc	Resistivity to liquid transport
ε_o	Permittivity of vaccum
ε_r	Dielectric constant of the medium
F	Faraday constant
h	Distance between the surface
τ	Shear stress
τ_o	Yield stress

n	Exponent
K	Consistency index
t	Casting time
T	Temperature
vol.%	Volume percentage
wt.%	Weight percentage
F_{max}	Load at fracture
MPa	Megapascal

Chapter 1

1. Introduction

Ceramics are one of the major categories of materials that are defined as "inorganic, non-metallic solids" (Kingery et al., 1976). The word 'ceramic' came from the Greek word '*keramikos'* meaning 'burnt stuff' in Greek or 'to burn' in Sanskrit. Ceramic materials are specially characterized by their physicochemical properties such as high strength, high-temperature stability, high hardness, low thermal and electrical conductivity, chemical inertness, and low fracture toughness (P.Greil et al.,2002; M.Vallet-Regí et al.,2001; S.F.Wang et al.,2013; L.Levinson.,2020). A strong covalent or ionic bonding or a combination that exists between the atoms in ceramics is the reason for their remarkable properties. Consequently, ceramics are increasingly used in structural and functional applications in aerospace, defense, nuclear, automotive, environmental, and pharmaceutical sectors (D.W. Richerson et al., 2018; T.E.Steyer et al., 2013). Generally, ceramics are classified as traditional and advanced ceramics. Traditional ceramics are made from clay-based natural raw materials and are mostly porous, non-uniform, multi-phase microstructure after heat treatment. These ceramics are employed in refractories and household applications. On the other hand, advanced ceramics are made from natural or synthetic raw materials of high purity, controlled particle size distribution (PSD), and chemical composition, using sophisticated technologies that resulted in tailored microstructure and properties (S.Somiya et al., 2013). Advanced ceramics are further classified based on chemical composition as oxides and non-oxides. Alumina (Al_2O_3), zirconia (ZrO_2), magnesia (MgO), barium titanate ($BaTiO_3$), lead zirconium titanate ($PbZr_xTi_{1-x}O_3$) are some of the oxide ceramics. Important candidates of the non-oxide ceramics include silicon carbide (SiC), silicon nitride (Si_3N_4), boron nitride (BN), aluminum nitride (AlN), titanium diboride (TiB_2), zirconium diboride (ZrB_2) and molybdenum disilicide ($MoSi_2$). According to W.M. Sigmund, advanced ceramic materials should have high reliability,

sufficient strength, and easy processability to produce near-net shape components (W.M. Sigmund., 2000).

The strength of the ceramic material is given by the Griffith equation (Griffith., 1921) as in equation (1),

$$\sigma_f = A\sqrt{E\gamma/c} \qquad (1)$$

Where σ_f is the fracture stress, E is the elastic modulus, γ is the fracture energy, c is the flaw size and A is a constant that depends on the specimen and flaw geometries. Here, the strength varies inversely with the square root of flaw size. So, the presence of defects or heterogeneities like cracks, agglomerates, pores, and inclusions in ceramics greatly affects its final strength. According to F.F. Lange, the strength limiting heterogeneities in ceramic such as soft and hard agglomerates, organic and inorganic inclusions, large grains, and surface cracks may co-exist and it varies with the ceramic material and processing method (F.F. Lange.,1989). These heterogeneities act as stress concentrators and strength-limiting factors. Therefore, a large number of processing techniques are developed to reduce the strength-limiting flaws and to produce more reliable ceramics with near-net-shapes.

1.1. Ceramic forming

The production of ceramic materials through melt casting is not a practical option since ceramic materials have a high melting point (1000 - 3000°C). G. Liu et al described the high gravity combustion synthesis such as melt-casting, and melt-infiltration for preparing bulk ceramics, glasses, and cermets in metal ingots through melt solidification (G.Liu et al., 2012; G Liu et al., 2013) and synthesized Al_2O_3 ceramic with 93 % theoretical density (T.D). The problem of porosity and uncontrolled grain growth occurs during solidification.Noreover, the ceramics such as Si_3N_4 and SiC undergo decomposition before the melting point restricted their melt casting (M. N. Rahaman., 2017; F. F. Lange., 1989). Therefore, the ceramic processing is

shifted from the melt-casting technique to the consolidation of fine powders to near-net-shapes followed by sintering. The basic steps in advanced ceramic processing include (1). Preparation of feedstock powder granules or powder suspensions, (2). consolidation to the green body (shape forming), (3). Drying and de-binding, and (4). Sintering (M.Trunec et al., 2014).

Generally, the starting materials for the fabrication of advanced ceramics are sub-micron or nanometer-sized ceramic powders. Further, the ceramic powders are consolidated into shapes by various forming techniques. The selection of a processing method is based on the size and shape of the component, cost, production rate, reproducibility, reliability, and environmental impact (H. K.Bowen., 1983). Based on the intermediate feedstock, the ceramic forming can be classified as powder metallurgical, slurry-based casting, plastic forming routes (R. Moreno., 2012), and the recently developed additive manufacturing (G.V. Franks et al., 2017; E. Peng, 2018). Alternatively, based on the mechanism of powder consolidation such as compaction, fluid removal through filtration and evaporation, particle flow, flocculation, coagulation, and gelation, ceramic forming is also classified. (J. A. Lewis, 2000; L.Bergstrom, 2001; R. Moreno, 2012). The corresponding forming processes are termed as powder pressing, slip casting, tape casting, electrophoretic deposition, gel casting, direct coagulation casting, injection molding, extrusion, and additive manufacturing.

Various additives are used in ceramic forming to achieve specific functions during powder consolidation (D.J. Shanefield., 2013; M.Trunec et al., 2014). Some of the important additives are solvents, binders, dispersing agents, plasticizers, lubricants, and anti-foaming agents. The consolidated shapes after the removal of the solvent by drying are known as the “green body” (unfired body). The desirable characteristics of a green body are (L.Bergstrom., 2001):

i. Uniform packing of particles.
ii. High density.

iii. Small pores and narrow pore size distribution.

iv. High strength for handling, storage, machining, and heat treatment

v. No defects such as agglomerates, cracks, warpage, etc.

1.2. Processing additives in ceramic forming

As mentioned above, various types of additives are used in ceramic processing for attaining specific functions during powder dispersion and particle consolidation. The additives provide a supporting role in ceramic processing. Criteria for the selection of additives are that they should meet the respective function with a minimum quantity and should get rid of the consolidated body through evaporation or burnt-out without making any kind of defects. The names of various additives and their functions are briefly described below:

1.2.1. Solvents:

Solvents act as a medium for the dispersion of ceramic powders and to dissolve other additives such as dispersants, binders, and plasticizers. The criteria for the selection of a solvent are low viscosity, easy wettability of the particle surface, low boiling point, non-reactivity with ceramic powder, non-toxic, low-cost, and compatibility with other additives (D. McKinney et al., 2013). Ceramic forming is carried out using both aqueous and non-aqueous solvents (X. Ba et al., 2013; M.Michálek et al., 2015). Organic solvents like methyl ethyl ketone, trichloroethylene, toluene, ethanol, and cyclohexanone are commonly used in ceramic forming that have the benefits of low viscosity, low surface tension, and low latent heat of vaporization as compared with water (D.J. Shanefield., 2013). As a result, organic solvents are preferred in the tape casting process where the drying and smooth surface of the tape are required to achieve in a shorter time (M. N. Rahaman., 2017). The demerits of using organic solvents are high cost, toxicity, flammability, personal hazards, and environmental pollution due to waste disposal. Water is commonly employed as a solvent in ceramic forming as it is a universal solvent, largely available and non-toxic. Water has a high dielectric constant of 80 as compared to

organic solvents. So, the ionization of surface functional groups such as carboxylic groups (–COOH or $–COO^-M^+$), sulphonic acid and their salts($-SO_3H$ or $SO_3^-M^+$), basic amino groups ($-NR_3$), quarternary ammonium groups ($-NR_4^+X^-$) that promote dispersion of particles occurs in an aqueous medium. The hydrogen bonding interaction between various additives that promote gelation also occurs in an aqueous medium (D.Hanaor et al., 2012). Moreover, the stable dispersion of ceramic particles through an electrostatic mechanism by pH adjustment and electrosteric stabilization using a polyelectrolyte dispersant is possible in an aqueous medium (B.P. Singh et al., 2005). The dispersion stability is controlled by ionic strength, pH, surface charge density, and concentration of dispersant. In addition, water acts as a plasticizer for the binders like polyvinyl alcohol (PVA) and polyethylene glycol (PEG) in powder pressing (C.W.Nies et al.,1984; S.D.Nunn et al.,1996). However, water is not a good solvent medium for ceramic powders such as $BaTiO_3$, and AlN as they react with water during the processing. However, the low evaporation rate and slightly high viscosity compared to organic solvents are other demerits of water as a solvent in ceramic processing.

1.2.2 Dispersing agents:

The dispersing agent provides stability to ceramic particles against flocculation. This facilitates homogeneous dispersion of particles in the solvent leading to low-viscosity slurries of high solids loading (R.R.Rao et al.,2001; J. Kim et al.,2022). Generally, the dispersing agents used in an aqueous medium are ionizable simples molecules and polymers and ions. The dispersing agent is adsorbed on the ceramic particle surface and provides stability to the ceramic powder suspensions through either electrostatic, steric, or electrosteric mechanisms. The dispersant can be a simple molecule of low molecular mass such as citric acid (P.Hidber et al.,1996), diammonium hydrogen citrate, sodium pyrophosphate (K.S.Chou et al., 1989), sodium carbonate (R.Jewad et al.,2008) and 4,5- dihydroxy-1,3-benzene disulfonic acid (Tiron) (L. Jiang et al.,2003), or a high molecular weight polyelectrolytes such as sodium carboxymethyl

cellulose, ammonium lignosulfonates, ammonium poly(acrylate) and ammonium poly(methacrylate) (D. Hotza et al.,1995; A.J. Ruys et al.,1996). Low molecular weight dispersing agents provide stabilization for dispersions of moderate concentrations through short-range electrostatic repulsion of the electrical double layer (EDL). On the other hand, poly(acrylates) provide electrosteric stabilization for highly concentrated powder dispersions. The structure of various dispersants used in ceramic forming is presented in **Fig.1.1**

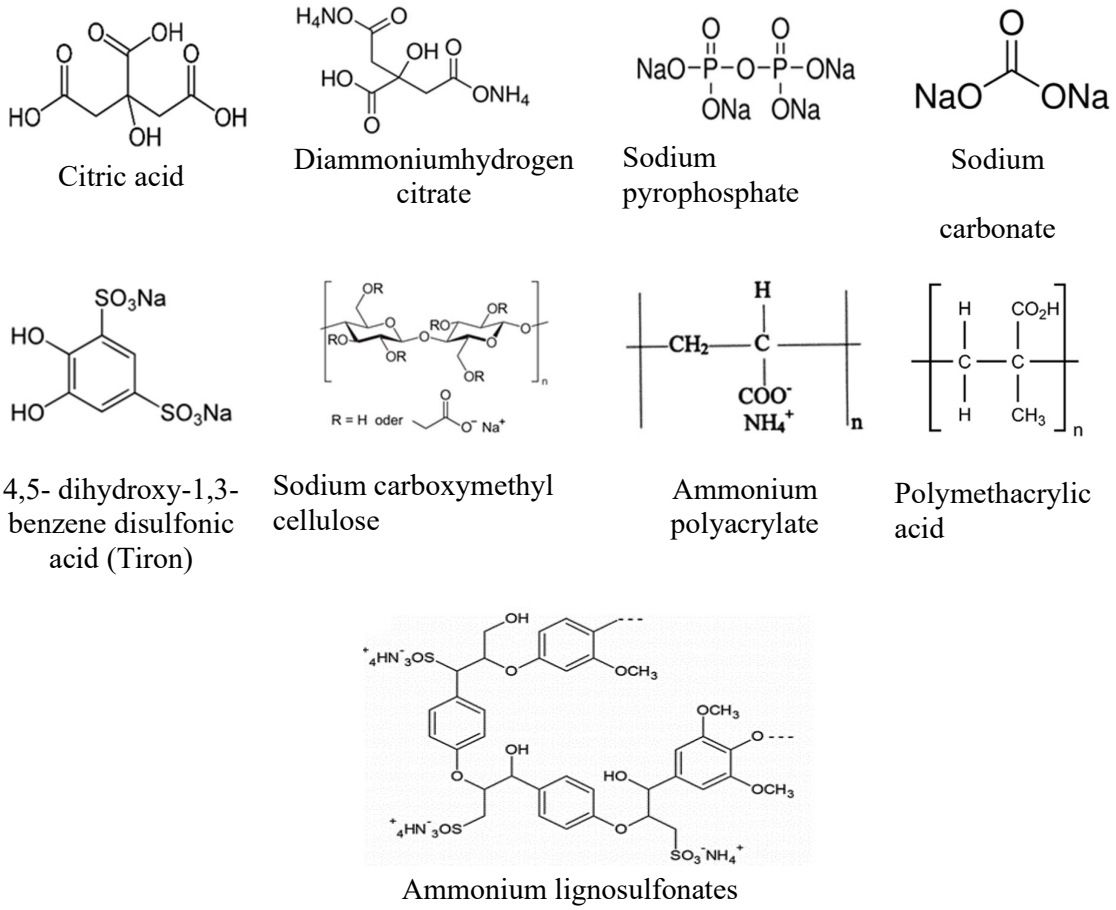

Fig.1.1 Molecular structures of aqueous dispersing agents

The dispersion of ceramic powder in a non-aqueous medium is by the steric mechanism. Block co-polymers with hydrophilic and hydrophobic segments and polyethyleneimine offer steric stabilization in a non-aqueous medium. J. Zhang et al used high molecular weight polyvinyl pyrrolidone as a dispersant for the non-aqueous processing of SiC (J. Zhang et

al.,2005). On the other hand, short-chain molecules such as fish oil, vegetable oils, phosphate esters, glycerol trioleate, and long-chain fatty acids, amines, and alcohols offer semi-steric stabilization in non-aqueous medium to prepare slurries for the process like tape casting (U.Paik et al.,1998; L.Guo et al., 2016). The structure of dispersing agents used in the nonaqueous medium is given in **Fig.1.2**.

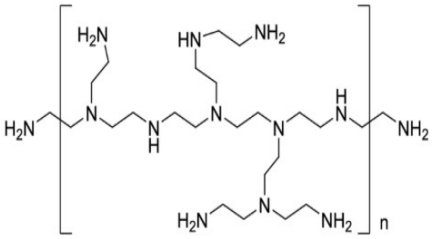

Polyethyleneimine (J. Xue et al.,2010)

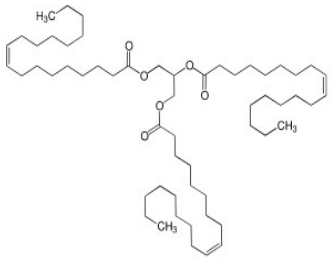

Glycerol trioleate (L.Jay Deiner et al.,2013)

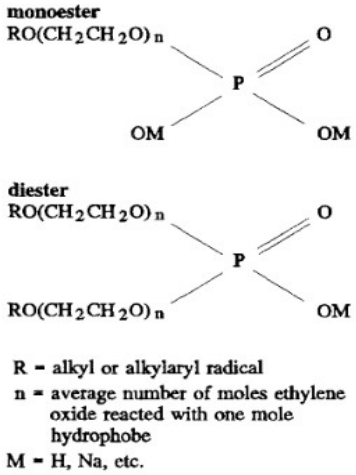

Phosphate ester (C.F.Hadson et al.,1993)

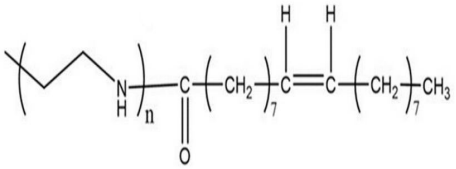

Polyethyleneimine-Oleic acid (M.Lijima et al.,2018)

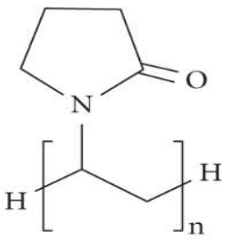

Polyvinyl pyrrolidone (J.Zhang et al.,2005)

Fig.1.2 Molecular structures of non-aqueous dispersing agents

1.2.3 Binder

The binders provide strength to the green bodies for handling, storing, machining, and heat treatment (S.D.Nunn et al.,1996; S.Dhara et al., 2005; C.Falamaki et al.,2006). Binders may also act as a dispersant, plasticizer, liquid retention agent, and rheology modifier depending on their type and the forming method used (J.S. Reed.,1995). The binders can be either inorganic or organic simple molecules or bulky polymers. They can be either synthetically prepared polymers or naturally renewable molecules (J.S. Reed.,1995; M. N. Rahaman., 2017). The selection of a binder for a ceramic shape forming is based on the following desirable characteristics (M. N. Rahaman., 2017; D.J. Shanefield., 2013).

i. Low cost and high availability.

ii. Low glass transition temperature.

iii. Slow and steady burnout

iv. Low ash content.

v. Good compaction behavior.

vi. High green strength.

vii. Compatibility with other additives.

Bentonite (G.P. Jiang., 2009), ball clay and kaolin (Y. Y. Li et al.,2001) are some of the inorganic clay-based binders that are used in ceramic forming as their colloidal dispersions in water. Here, the charged clay particles adsorbed on ceramic particles are bonded together due to the opposite charges on their edges and faces as shown in **Fig.1.3** to generate plasticity and yield strength to the green body (J.A.Lewis., 2000).

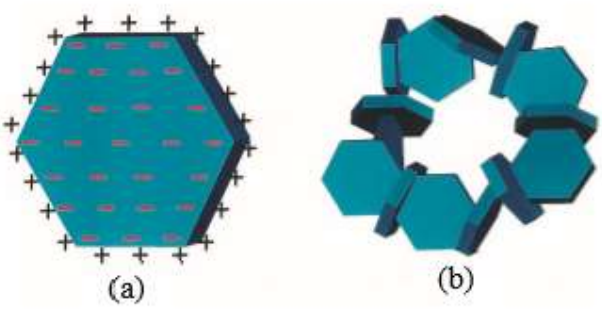

Fig.1.3 (a). Clay-particle dispersed in water, (b). hetero-coagulation of clay particles due to opposite charged edges and faces (J.A. Lewis.,2000).

Other inorganic binders are soluble silicates, organic silicates, colloidal alumina, colloidal silica, aluminates, and phosphates (D.W. Richerson et al., 2018). Inorganic binders do not burn off from the green body and they become part of the ceramic component. X.Xu et al studied the effect of three inorganic binders such as silica particles, SiO_2-B_2O_3 mixture, and silicon particles on the properties of mullite fibrous ceramics by tertiary butyl alcohol (TBA)-based gel-casting (X. Xu et al., 2017). They found that the binders played an important role in tailoring the microstructure and properties of the ceramics. Additionally, the ceramic prepared using silica as binder sintered at 1500 °C exhibited relatively low compressive strength compared to the SiO_2-B_2O_3 mixture as a binder. Further, according to them, the silicon binder is found most suitable for the high-temperature environment as silicon could transform into the silica phase with a high melting point.

In the processing of advanced ceramics, synthetically prepared organic polymeric binders are used for achieving high green strength (B.P.Singh et al.,2004; M.D.Vlajic et al., 2002). These binders can be of low or high molecular weight polymers which are either soluble in water or organic solvents. Water-based acrylic polymer emulsions are also used as binders (J.Moon et al.,2002; C.Pagnoux et al.,1998; M.Szafran et al.,2001). These acrylic emulsion binders have advantages such as low viscosity and high solid content compared to the water-

soluble binders. In ceramic shape forming processes like gelcasting polymers produced *in-situ* from organic monomers and the cross-linking agent are used to bind the ceramic particle (A.C.Young et al.,1991; M.A.Janney et al.,1998; K.Cai et al.,2005;).The major benefit of organic binders is the easy burn-out with little ash content and other contaminations compared to inorganic binders. The burn-out residue in acrylic emulsion binder, PVA, and PEG are 0.2-0.4, 0.4, and 0.4 %, respectively (X. K. Wu et al., 1997). The structure of some of the binders soluble in the aqueous and non-aqueous medium is presented in **Fig.1.4**.

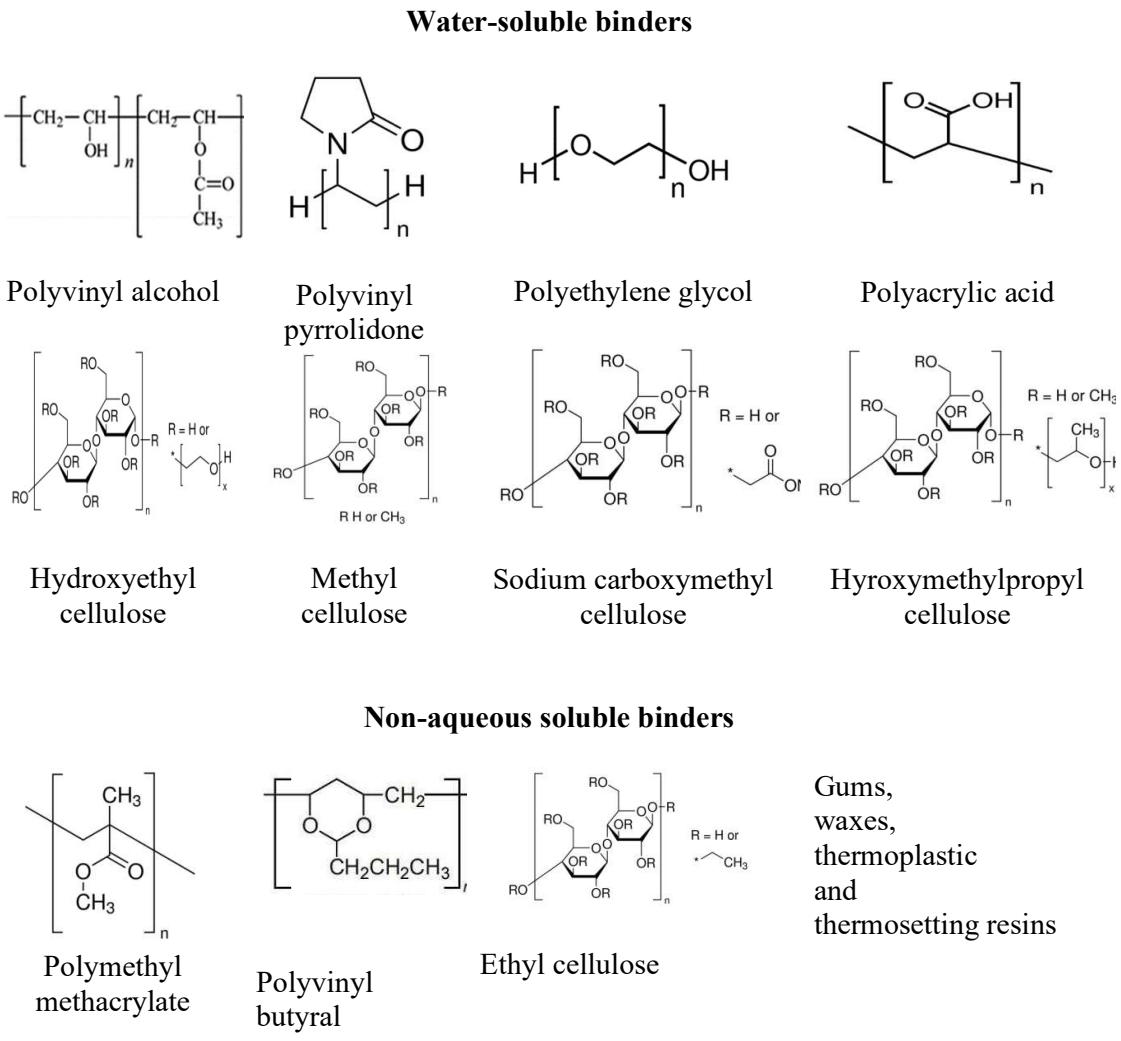

Fig.1.4. Molecular structure of polymeric binders soluble in aqueous and non-aqueous medium.

The polymeric binders are used as their low molecular weight liquid form called resin, as a solution in a suitable solvent and in molten condition (G.Y.Onoda Jr.,1976). The strength of the green body is decided by the bonding between the binder molecules or the binder and ceramic particles. The different types of bonding are Van der Waals attractive forces, hydrogen bonding, and covalent bonding through polymerization and cross-linking. The strength of the binder may be explained by the resistance to the de-bonding fracture that occurs by the action of mechanical force (S.A. Uhland et al., 2001). The de-bonding occurs in two ways: one is a binder-binder fracture and the other is through the binder-ceramic particles fracture. A schematic representation of the mode of fracture in ceramic green bodies is presented in **Fig.1.5**.

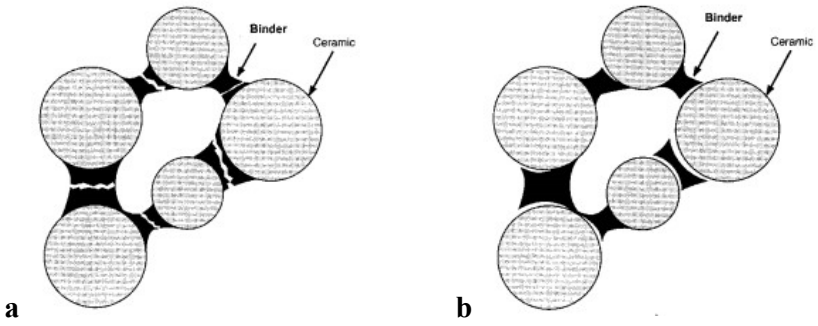

Fig.1.5 Schematic representation of modes fracture of ceramic green body a). binder-binder b).binder-ceramic (S.A.Uhland et al., 2001)

The force required to break a bond or the strength of a binder is given in equation (2) as,

$$F = S_o A \qquad \textbf{(2)}$$

where S_o is the cohesive or adhesive strength of a binder and A is the cross-sectional area of a binder at the particle neck (S.A.Uhland et al., 2001; G.Y.Onoda Jr.,1976). The distribution of binder significantly affects the strength of the green body. G.Y.Onoda Jr, classified binder distribution on ceramic particles in a green body into non-wetting type, the pendular, and

coated type depending on the wetting behavior, viscosity of the liquid, and capillary forces (G.Y.Onoda Jr.,1976). A schematic representation of different modes of binder distribution on particle surface in a green body is shown in **Fig.1.6**. Further, they concluded through strength measurements that the pendular type distribution is highly effective compared to the coated type. Additionally, the other parameters that decide the green strength are the density of the green body, the molecular weight of the binder, and the cohesive or adhesive strength of the binder.

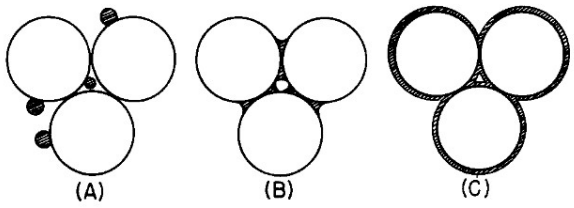

Fig.1.6 Organic binder distribution on ceramic particles (A). non-wetting, (B).wetting (pendular type), (C).coated-type (G.Y.Onoda Jr.,1976).

1.2.3.1 Chemical interaction of binders

Van der Waals forces including hydrogen bonding and covalent bonding through polymerization and cross-linking are the different types of interactions between the additives and additives with the ceramic powders (D. J.Shanefield et al., 2013). This interaction decides the physical properties such as density, mechanical strength, and machinability of the green bodies. Q.Wei et al studied the cohesive energy density, mechanical properties, bonding behavior, and surface morphology of three polymer binders such as polyvinyl pyrrolidone (PVP), polyacrylamide (PAM), and polyvinyl alcohol (PVA) through the molecular dynamics simulation using hydroxyapatite (HA) ceramics (Q.Wei et al., 2017). In that study, they calculated the cohesive energy density of the polymer binders for evaluating the interaction force between molecules or among functional groups with HA. Further, all properties related to material interactions, such as solubility, compatibility, and viscosity are intrinsically linked

to cohesive energy. Moreover, the trend of compressive strength is consistent with the simulated binding energies.

The cross-linking of polymers in solution through simple molecules and the interaction of polymers with the surface of ceramic particles are used to improve the strength of bonding in ceramic green bodies. S. B. Johnson et al reported that the cross-linking of chitosan using 2,5- dimethoxy-2,5-dihydrofuran (DHF) improves the strength of green ceramics (S.B. Johnson et al., 2002). M.Potoczek et al. introduced polyurethane emulsion binder in the powder pressing of alumina and the chemical interaction between the binder and the ceramic powder is mainly hydrogen bonding, which improved the polymer adhesion to the ceramic particles (M. Potoczek et al., 2003). The schematics of the cross-linking of chitosan through DHF and the interaction between polyurethane binder and alumina particles surface are shown in **Fig.1.7**.

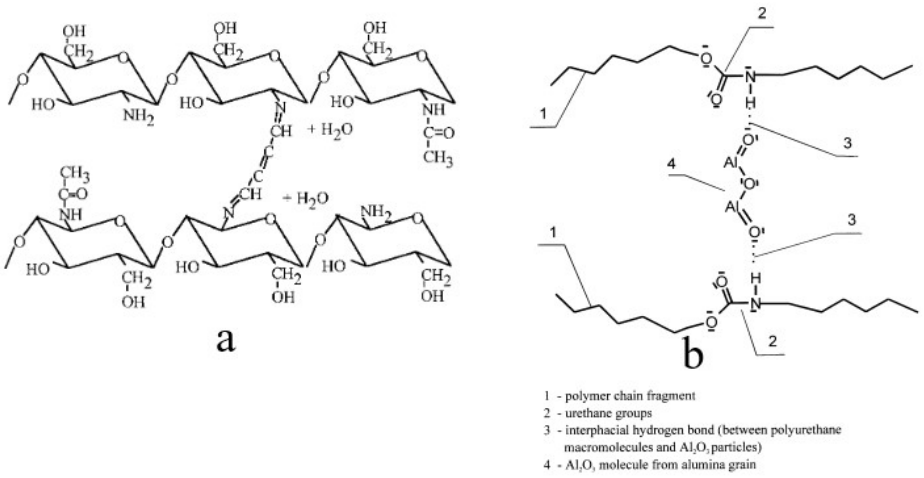

Fig.1.7 The schematics of (a) the cross-linking of chitosan using DHF (S.B. Johnson et al., 2002), (b) the H-bonding interaction between the polyurethane polymer and alumina ceramic powder (M.Potoczek et al., 2003).

1.2.4 Plasticizer

Plasticizers are required in the ceramic forming processes such as tape casting, injection molding, and extrusion to provide flexibility and plasticity to the green body (D.Hotza et al.,1995; Z.Xie et al., 2005). The function of a plasticizer is to reduce the glass transition

temperature of the binder and make it flexible at the processing temperature. The plasticizing effect depends on chemical composition, molecular weight, and functional group. The plasticizer decreases the green strength and modulus but it increases the percentage elongation (D. H. Kim et al., 2004). Polyethylene glycol, polypropylene glycol, glycerol, dibutyl phthalate, butyl benzyl phthalate, and dioctyl phthalate are some of the commonly used plasticizers. Among them, glycerol, polyethylene glycol, and polypropylene glycol are water-soluble plasticizers (D. Hotza at al.,1995). The chemical structure of some of the plasticizer molecules employed in ceramic forming is shown in **Fig.1.8**. J. Nie et al employed polyethylene glycol and dibutyl phthalate as plasticizers that affect the rheological characteristics of the ceramic paste and quality of the green body in the stereolithography-based additive manufacturing of alumina ceramics (J. Nie et al., 2021). Z. Xie et al studied the effects of different plasticizers including dibutyl phthalate, organic alcohol glyceryl, caster oil, and surfactants including stearic acid, oleic acid, and Tween 80 on the behavior of zirconia suspensions for the injection molding using polypropylene, paraffin wax, and ethylene-vinyl-acetate binders (Z. Xie et al., 2005). They concluded dibutyl phthalate as a plasticizer and stearic acid as a surfactant for the process through the measurements of rheological properties, density, flexural strength, and hardness.

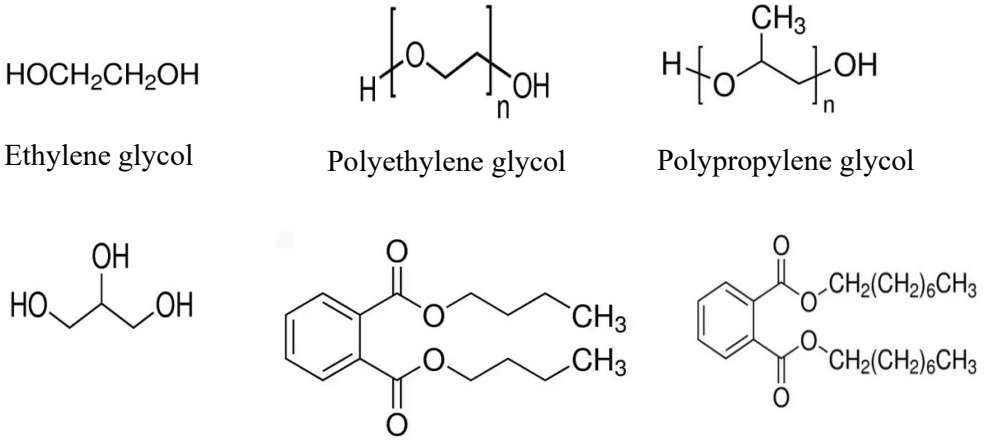

Fig.1.8 The molecular structure of commonly used plasticizers.

1.2.5 Antifoaming agent

The antifoaming agents are surface active agents that are added to prevent the foaming action of dispersing agents and binders in a ceramic powder suspension. The most common examples are long-chain alcohols such as octanol-1, octanol-2, oleic acid, and cetyl alcohol (B.P. Singh et al., 2004). The molecular structure of the commonly used antifoaming agents are shown in **Fig.1.9.**

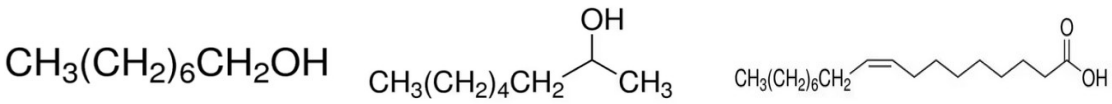

Octanol-1 Octanol-2 Oleic acid

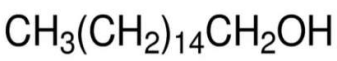

Cetyl alcohol

Fig.1.9 Molecular structure of some antifoaming agents.

1.2.6 Lubricant

The function of a lubricant is to reduce inter-particle and die-wall friction in the ceramic forming process such as powder pressing, injection molding, and extrusion (D.W. Richerson et al., 2018). In powder pressing, the lubricants are classified as external lubricants and internal lubricants (M.Uppalapati et al., 2005). Internal lubricants are added to the ceramic slurry before spray drying. This reduces particle friction, promotes better flow under high pressure, decreases the number of defects, and improves green density. On the other hand, external lubricants are dry mixed with spray-dried powder which lubricates the die and punches and improves the tool life (E. J. Motyl., 1963; H. J. Glass et al., 1995). Stearic acid is a commonly used lubricant in ceramic forming. W.J.Tseng et al studied the effect of stearic acid as a lubricant on particle packing and microstructure in the injection molding of zirconia using a wax binder (W.J.Tseng et al., 1999). **Fig.1.10** depicts the molecular structure of stearic acid.

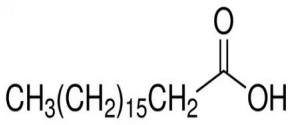

Stearic acid

Fig.1.10 Molecular structure of stearic acid

1.3 Ceramic forming processes

There are various ceramic shape-forming processes such as powder pressing, slip-casting, gel-casting, direct coagulation casting, tape casting, extrusion, injection molding, and additive manufacturing. The ceramic components are prepared from the respective powders by adopting a suitable shape-forming process. The processing method is selected based on the size and complexity of the shape, reliability requirement of the final ceramic component, the volume of ceramic components required, production rate, and cost (S.Leo et al.,2014, R.J.Brook .,1985; E.C.Hammal et al., 2014). The properties and performance of advanced ceramic materials depend on so many factors like purity, chemical composition, particle size, particle size distribution and specific surface area of ceramic powders, processing method, microstructure, chemical bonding, and grain size (L.F.Francis., 2015, C.Tallon et al.,2010; R.Moreno et al.,2020, W.E. Lee et al., 1994). Of which, if we keep raw material's quality and their properties as optimum (flaws or defects from the raw powders at the minimum level), then the processing route is the dominant parameter that determines the microstructure and the performance of a ceramic component. Nowadays, environmental pollution and global warming are the major issues. One of the ways to reduce these issues is to replace the synthetically prepared processing additives with naturally renewable, eco-friendly bio-based materials (A.Vinod et al., 2020; P.Wiecinska et al., 2020). A detailed review of the ceramic forming techniques with a focus on binders is presented in the following session.

1.3.1 Powder pressing

Powder pressing is the most widely used method for the production of a large number of ceramic components of relatively simple shapes in a short duration of time (S.J. Glass et al., 1997). More complex shapes could be achieved by a combination of powder pressing and green machining approaches. Powder pressing has been used for the production of magnetic, and dielectric ceramics, cutting tools, ceramic tiles, porcelain products, structural clay products, and grinding wheels (D.W.Richerson et al., 2018; T.A.Otitoju et al., 2020). In this method, the freely-flowing ceramic granules are compacted in hardened steel dies by applying a high compaction pressure using a mechanical or hydraulic machine. The granulation of ceramic powder is achieved through the spray drying of an aqueous ceramic powder suspension containing a suitable binder and a lubricant (S.N.Grigoriev et al.,2022; S.J.Lukasiewicz et al.,1989). Normally high-density green compacts are obtained through pressing (R.Oberacker et al.,2011). The moisture or water content in the green body is generally less than 2 wt. %. Consequently, drying-related defects such as cracks and binder-migration are limited in powder pressing. The machinability of the green compacts depends on the green strength (B.Su et al., 2008; S.D. Nunn et al.,1996). A schematic of powder pressing and morphology of typical granulated feedstock for powder pressing are shown in **Fig.1.11** and **Fig.1.12**, respectively.

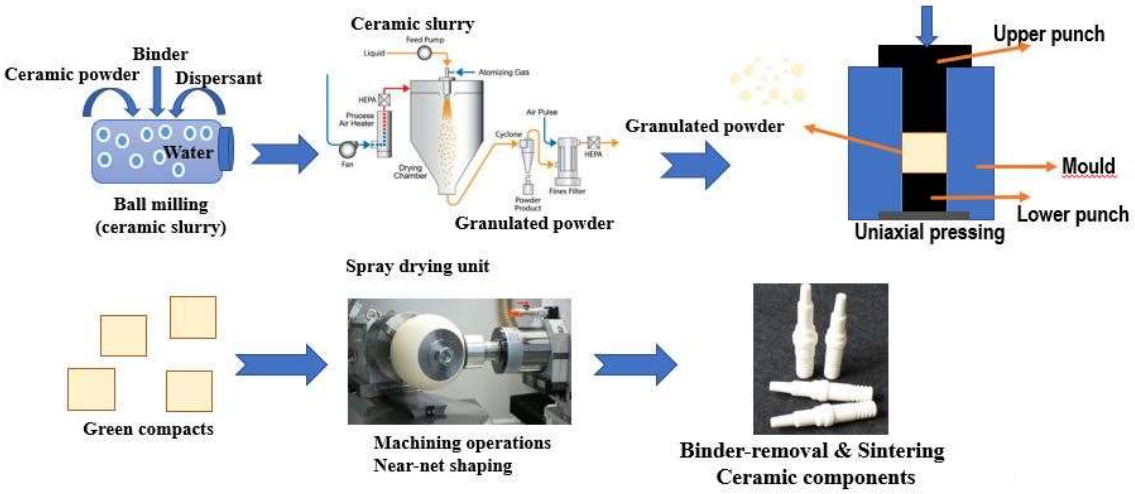

Fig.1.11 Outline of a typical dry pressing process

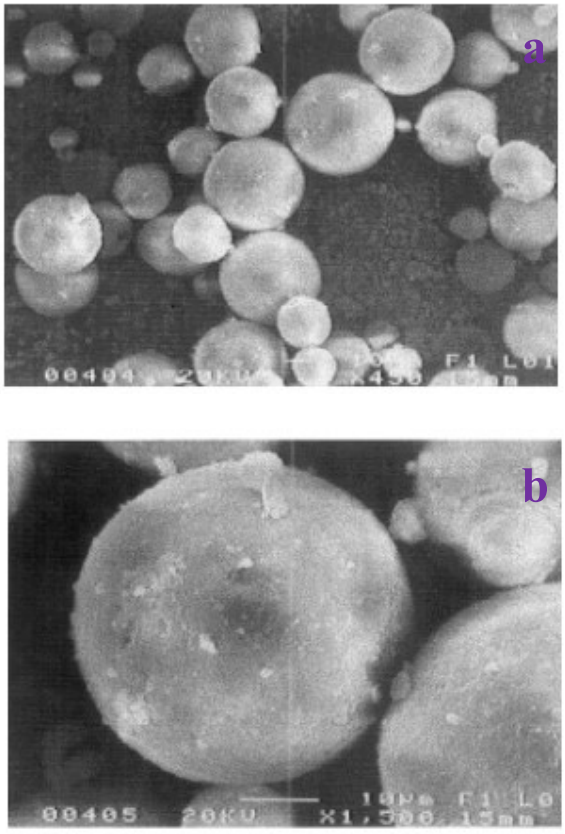

Fig.1.12 A low (a) and high (b) magnification image of spray-dried alumina granules (A.Tsetsekou et al.,2001).

The defects such as delamination, end-capping, ring-capping, crack, and residual porosity in sintered ceramics are commonly reported in powder pressing (P. Balakrishna et al.,1996; S.J. Glass et al., 1997). Low strength of the green body, non-homogeneous density, friction between the particles as well as particles and mold wall, and the presence of agglomerates are some of the reasons for these defects. During compaction, the distribution of the pressure is not homogeneous from the top surface to the bottom of the green body, and the density of the compacts is directly related to the compaction pressure. Due to this, the density gradient in the sample prepared by uniaxial pressing is normally observed. In addition, the uniaxial powder pressing is limited to relatively simple shapes. To some extent, these defects can be eliminated by cold isostatic pressing. In cold isostatic pressing, the granulated powder filled in a deformable mold (rubber mold) is pressurized in a fluid medium to achieve uniform compaction of the powder. The steps involved in industrial powder pressing are:

1. Mold filling with the granulated powder
2. Compaction of the powders to green body
3. Ejection of the green body
4. Machining, if required
5. Binder removal and Sintering

Powders in the form of granules are desirable in pressing for a good flow to fill into the mold and making the process continuous. Normally granulation of the fine powders (1-10μm) is carried out by spray-drying or spray granulation (S.J.Lukasiewicz et al.,1989; R.G.Frey et al., 1984). The spray drying converts the fine powders into spherical agglomerates of size in the range of 40-400 μm with an average size of 100 to 200μm which is the preferred size distribution of granules for powder pressing. These granules have less inter-particle friction with a good flow behavior. The slurry for spray-drying consists of various additives like a

solvent, binder, plasticizers, and lubricants. Each additive provides specific functions, as mentioned above, to the feedstock powders.

In powder pressing, the binders provide high green density, and high green strength for avoiding the defect during spring back, handling, storage, and machining (J. S. Reed., 1995; A. Kumar et al.,2014). Additionally, the binders determine the properties of the granules such as bulk density, flow rate, and compaction behavior (R.Taktak et al.,2011; S.Begum et al.,1998) and the microstructure and mechanical properties of the ceramics (R.Taktak et al.,2011). The glass transition temperature of the binder is an important parameter that decides the mode of fracture and strength of the granules, green density, and green strength (M.Potoczek et al., 2003; S.Baklouti et al.,1997; X.K. Wu et al., 1997).

Polyvinyl alcohol (S. Baklouti et al., 2001), polyethylene glycol (X.K.Wu et al., 1997; R.Taktak et al.,2011), and polyacrylic acid (M.Imran Zainuddin et al.,2008) are the most studied water-soluble binders in powder pressing. Binder migration along with the moisture flow during the spray drying and its segregation at the outer surface of the granule is a problem with some of the water-soluble binders such as PVA (S.J.Lukasiewicz et al.,1989; S. Baklouti et al., 1998). S.Tanaka et al. studied the migration of PVA in comparison with polyacrylic acid (PAA) through the analysis of binder distribution in the spray-dried alumina granules, their compaction behavior, and the flexural strength of green bodies (S.Tanaka et al., 2006). The migration is low in the case of the PAA binder compared to the PVA binder due to strong Coulombic attraction between the carboxylic acid group of the PAA and alumina particles which is evidenced by liquid immersion photomicrographs of spray-dried granules using PVA and PAA binders shown in **Fig.1.13**. In the case of PAA, the binder is homogeneously distributed in the granules, and for PVA, a brittle layer is formed on the granule surface due to binder migration that resists fracture and deformation. The powder granule with PVA binder deforms at a stress of 0.45 MPa whereas the deformation of the granule containing PAA is at

a low stress of 0.1 MPa. The binder migration adversely affects the flexural strength of the ceramics. A flexural strength of 580 and 485 MPa, is reported using PAA and PVA binder, respectively.

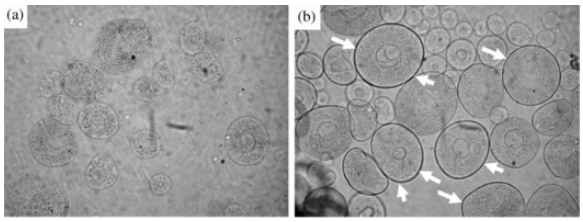

Fig.1.13 The liquid immersion photomicrograph of granules prepared using a). polyacrylic acid binder and b). polyvinyl alcohol binder (S. Tanaka et al., 2006).

The effect of the glass transition temperature of binders (PVA: 79°C and PEG: -60 °C) on the fracture behavior of spray-dried granules and mechanical strength of green and sintered ceramics have been studied (S. Baklouti et al., 1997; R.Taktak et al., 2011). The green strength of alumina compacts prepared with the same amount of PEG and PVA binder are 0.3 and 0.6 MPa, respectively. Further, the fracture mode of granules changes from intragranular to intergranular as evidenced by the micrographs shown in **Fig.1.14**. when the glass transition temperature of the binder increases.

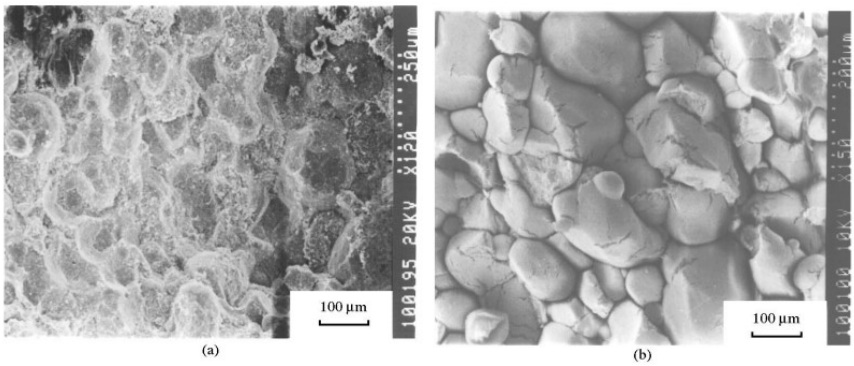

Fig.1.14 The mode of fracture of granules with (a) polyethylene glycol binder, and (b) polyvinyl alcohol binder (S. Baklouti et al., 1997).

R.Taktak et al studied the effect of PVA and PEG binders on the flowability and mechanical strength of ceramics using alumina powder (R.Taktak et al., 2011). The powder granulated by spray drying achieves good flow properties at 1 to 3 wt.% PVA and 3 wt.% PEG binder. Further, sintered alumina obtained using PVA binder shows comparatively lower strength due to the high Tg value of PVA, brittle outer granule surface, intergranular microcracks, and densification of the ceramic with the granules.

D.B. Rohini et al synthesized acrylic emulsions binders with various co-monomers such as styrene (S), methylmethacrylate (MMA), methacrylate (MA), 2-ethylhexyl acrylate (EHA), and methacrylic acid (MAA) in different ratio and used them as a binder in the powder pressing of lanthanum chromite and strontium chromite (D. B. Rohini Kumar et al., 2000). Here, these acrylic emulsion binders are ready to use colloidal emulsions of particle size in the range of 0.05-0.5 μm. The concentration of acrylic emulsion binder studied varies from 2 to 5 wt.%. The viscosity of these emulsions and Tg of the polymers are in the ranges of 75-100 mPa.s and -23 to 103 ℃, respectively. Further, their Tg could be tailored by the appropriate selection of monomer combinations which results in changes in the strength, density, and plasticity of the green bodies. Comparatively, the co-polymer from MA: MMA (30:70 wt.%) and EHA: MMA (60:40 wt.%) shows superior green density, and the co-polymer from MA: MMA (30:70 wt.%) and EHA: MMA: MAA (55:43:2 wt.%) shows superior green strength. Further, X. Kevin Wu et al studied the green density, green strength, viscosity, ash residues, and moisture sensitivity of four binders: PVA, PEG, Acrylic emulsions: Duramax B-1007 and Duramax B-1020 (X. Kevin Wu et al., 1997) using alumina as a ceramic powder. **Table 1.1** shows some of the important results of X.K.Wu et al.

Table 1.1 Comparison of the slurry viscosity, green density and strength, and ash contents of four binders used for powder pressing of alumina (X.K. Wu et al., 1997).

Binder (1-5 wt.%)	**Slurry viscosity, mPa.s**	**Green density, % T.D**	**Green strength, MPa**	**Ash residues in air, %**
PVA	> 2200	46 – 52	0.4 – 0.9	0.4
PEG	~ 200	50 – 53.5	0.3 – 0.4	0.4
Duramax B-1007	~ 200	49 – 53	0.37 – 0.9	0.2
Duramax B-1020	~ 200	51 – 55	0.42 – 1.15	0.4

M. Szafran et al prepared water-thinnable acrylic emulsion binders using different compositions of monomers such as butyl acrylate, styrene, acrylic acid, and a built-in amphiphilic macromonomer which act as a surface active agent and internal plasticizer for powder pressing of alumina (M. Szafran et al., 2001). The molecular weight of the binder is in the range of 400000 to 600000 g/mol and the glass transition temperature varies from 1.8 to -13.2℃. Here, the highest thickening is achieved for a binder containing a high amount of amphiphilic macromonomer. A high green density, high Weibull modulus, and less porosity are obtained for the ceramics prepared using these acrylic emulsion binders compared to that prepared using PVA and methylcellulose binders. In another work, M.Szafran et al. synthesized water-thinnable acrylic emulsion binders such as poly(acrylic-styrene), poly(vinyl-allyl), poly(acrylic-allyl), and poly(vinyl-acetate-co-allyl ether) with non-ionic hydrophilic long poly(oxyethylene) side chains. They compared the density and mechanical strength of the green bodies with that of green bodies obtained using a PVA binder. Here, the Tg of the prepared acrylic emulsions binders is in the range of 1.8 to –59.2℃ (M.Szafran et al., 2004). Further, they concluded that due to the low Tg and hydrophilic-hydrophobic balance of the co-

polymers, a high green density, and strength are achieved compared to the PVA binder. S. Begum et al studied the slurry viscosity, powder flow characteristics, and green properties of zinc oxide varistor powder using acrylic latex binders named Ltx A to Ltx E and compared the results with a PVA binder (S. Begum et al., 1998). The binder concentration studied is in the range of 1 to 1.60 wt.%. These acrylic emulsion binders provide superior granule flow properties compared to the PVA binder. The green strength obtained with latex binder is 1.5 MPa against <0.8 MPa for PVA binder due to the strong interaction between the latex binder with alumina powder. M.R. Ben Romdhane et al synthesized a co-polymer from acrylic acid and vinyl acetate with the molecular structure shown in **Fig.1.15**, which functions as a binder and dispersing agent for alumina (M.R. Ben Romdhane et al., 2007). In that co-polymer, the carboxylic acid groups present are responsible for strong adsorption on the alumina particle surface and provide electrostatic stabilization and the -OH groups provide higher mechanical strength. They achieved a green density and green strength of 59.04 % T.D and 4.2 MPa, respectively, at an optimum binder concentration of 1.5 wt.% and a compaction pressure of 120 MPa. With the same concentration, the PVA binder provides a green density of 57.03 % T.D and a green strength of 1.8 MPa.

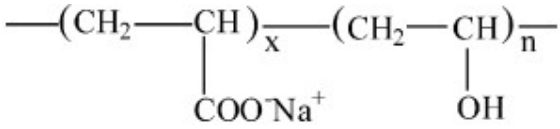

Fig.1.15 Molecular structure of co-polymer (M.R. Ben Romdhane et al., 2007).

Ajay Kumar et al studied sucrose as an eco-friendly binder in the powder pressing of alumina (A. Kumar et al.,2014). They studied the effect of green density, green strength, microstructure, and machinability as a function of sucrose concentration. The studied sucrose concentration is in the range of 0.6 - 10.8 wt.%. Further, they achieved the density and flexural strength of the green bodies in the range of 45-63 % T.D and 0.6-12.5 MPa, respectively, at

sucrose concentrations in the range of 0.6 to 10.8 wt.%. They studied the machinability of the green body by drilling using conventional machines and tools. The green bodies could withstand the stresses during drilling at sucrose concentrations greater than 3.6 wt.%. The reason for the high density and strength of green bodies is the inter-molecular hydrogen bonding of sucrose and water molecules with the alumina surface. Recently, V.P. Jyoti et al used a combination of aloe vera gel and sucrose as a binder in the dry pressing of alumina (V. P. Jyoti et al., 2022) and achieved a green density and flexural strength of 64 % T.D and 13.5 MPa, respectively. The high strength is due to better particle packing achieved by plasticizing properties of aloe vera gel and sucrose coated on the alumina particle surface.

1.3.2 Colloidal processing

The particle agglomerates present in the dry-pressed components produce residual porosity during sintering which limits the strength and reliability of ceramic materials. In colloidal processing, the powder particles are well separated in a liquid medium and the particles dispersed in the medium are subsequently consolidated to produce green ceramics of uniform microstructure (without much particle agglomerates). Therefore, the strength-limiting flaws will be minimum in ceramic components obtained by sintering the green bodies produced by colloidal processing. The steps involved in colloidal processing are (i) dispersion of ceramic powder in a solvent medium (ii) consolidation of the dispersed particle to produce desired shape (iii) drying (iv) binder removal and (v) sintering. The fundamentals of powder dispersion in a liquid medium are discussed in the following section.

1.3.2.1 Ceramic powder dispersion

Improved reliability of ceramic components is the benefit of the colloidal processing route compared to powder pressing (C.Tallon et al.,2011; G.V.Franks et al.,2017; R. J. Pugh et al.,2017). In colloidal processing, the heterogeneities in the powders are eliminated by sedimentation/filtration and inducing surface forces between the particles (F. F. Lange.,1989).

Colloids are particles of the size in the range of 1 nm – 1 μm dispersed in a liquid medium. Due to the large surface area, the surface interactions between the particles and the interaction of particles with the medium are important. Ceramic powder particles in a liquid medium attract each other due to the Van der Waals forces leading to agglomeration. The Van der Waals forces have components from Keesom (permanent dipole-permanent dipole), Debye (permanent dipole-induced dipole), and London (induced-induced dipole) dispersion forces. These agglomerated particles settle due to gravity resulting in an unstable dispersion. The way to achieve a stable colloidal dispersion is to overcome the Van der Waals attraction between the particles by providing repulsive interactions which are greater than the Van der Waals attractive forces. The repulsive interaction between particles is achieved through electrostatic, steric, and electrosteric mechanisms.

The electrostatic mechanism of powder dispersion mainly operates in a polar medium like water. In the electrostatic mechanism, identical charges are created on particle surfaces leading to strong electrostatic repulsion which overcomes the weak van der Walls attractive forces. The surface charge on particles suspended in a medium is created by various methods. In the case of a clay-based colloidal system, surface charge transfer phenomena such as adsorption of ions and surfactants, anion and cation-exchange reactions, and intercalation of organic molecules create the surface charge and controlling its stability (G. Lagaly et al., 2013). The surface chemical reactions or surface forces on a colloidal particle in a medium can be altered by varying the pH, and the addition of ions, surfactants, and other molecules. That is, by varying the chemical environment of the particles, stable colloidal suspensions and weakly flocculated or coagulated ceramic systems can be prepared. The pH adjustment of the dispersion medium is one of the commonly used methods for the preparation of powder dispersions. The pH adjustment away from the isoelectric point (I.E.P) of the powder creates either a positive or negative charge by protonation or deprotonation of surface functional

groups. For example, in the case of oxide ceramic powders protonation of surface hydroxyl groups at pH below the isoelectric point creates a positive surface charge and deprotonation at pH above the isoelectric point produces a negative surface charge as shown in **Fig.1.16.**

Fig.1.16 Oxide ceramic powder surface charging by changing the pH of the medium.

Another mechanism of powder dispersion in an aqueous medium is the electrosteric using polyelectrolytes as dispersing agents. The polyelectrolytes adsorb on the surface of the particles and create a monolayer coverage at its optimum concentration. The ionization of the functional groups present in the adsorbed polyelectrolyte provides an identical charge on the particle surface resulting in electrostatic repulsion. The adsorbed polymer layer on the particle surface provides additional stability by osmotic and entropy contribution called steric stabilization. A schematic of the electrosteric stabilization of ceramic particles in an aqueous medium is shown in **Fig.1.17.**

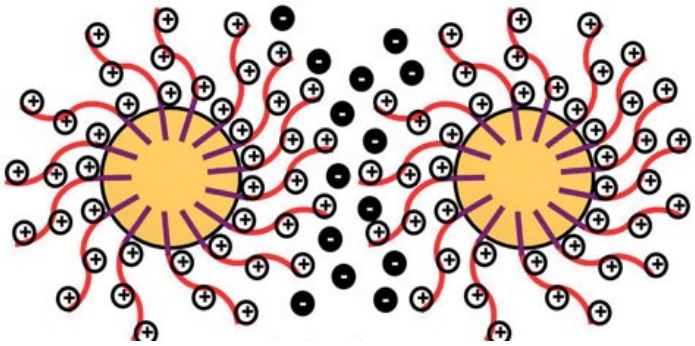

Fig.1.17 Schematic of electrosteric stabilization of ceramic particles in an aqueous medium.

The stability of a colloidal particle in an aqueous medium is explained by the electrical double layer (EDL) theory. The suspended charged particles attract the oppositely charged counter-ions in the medium towards its surface and create an immobile adsorbed layer called

the Stern layer. A cloud of co-ions and counter-ions forms a diffuse layer. That is, the EDL consists of a Stern layer and a diffuse layer. The potential of the particle decreases with distance from the surface. The distance from the surface at which the potential becomes $\psi_o/2.718$ (where ψ_o is the surface potential) is called the thickness of the EDL which depends on the ionic strength of the medium as shown in equation (3).

$$1/\kappa = \sqrt{\left(\varepsilon_r \varepsilon_o kT / F^2 \sum N_i z_i^2\right)} \qquad \textbf{(3)}$$

Where κ^{-1} is the electrical double-layer thickness, ε_r is the dielectric constant of the medium, ε_o is the permittivity of vacuum, N_i is the number of ions, z_i is the valence of the counter-ions, F is the Faraday constant, k is the Boltzmann constant and T is the absolute temperature.

The EDL repulsion is affected by zeta potential (the potential at the shear plane) and the Debye-Huckel screening length (the thickness of the EDL). Higher surface potential and lower ionic concentration enhance electrostatic stabilization.An increase in ionic concentration compresses the EDL such that the powder dispersion destabilizes upon the addition of excess electrolyte. When a potential difference is applied, the colloidal particle with the Stern layer moves toward one electrode and the colloidal medium with the ionic atmosphere moves in the opposite direction. Potential at the slippage plane is called zeta potential which is a measure of surface charge on the particle and stability of the powder dispersion. A zeta potential value of more than 25 mV provides stability to fine particles suspended in an aqueous medium. A schematic representation of an EDL around a colloidal particle suspended in a medium is shown in **Fig.1.18.**

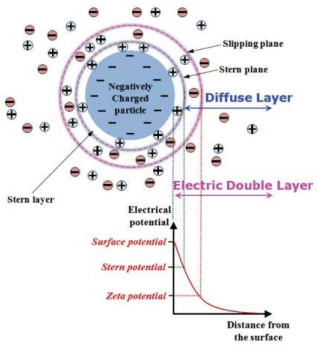

Fig.1.18 Schematic representation of an electrical double layer around a colloidal particle suspended in a medium (S.J.Park et al., 2011).

In the case of powder dispersion in non-aqueous solvents, the main mechanism is steric stabilization. Here, the Van der Waals attraction between the ceramic particles is hindered by the adsorbed polymer molecules.In this, polymeric molecules with hydrophilic and hydrophobic segments are used as dispersing agents. The polymeric dispersing agents adsorb on the particle surface and form a monolayer coverage at an optimum dispersant concentration. When particles with adsorbed polymer layers approach each other, the concentration of polymer in the inter-particle region increases which increases the osmotic pressure and decreases the configurational entropy. Now the solvent flows between the particles and separates them apart and thereby preventing agglomeration. A schematic of steric stabilization is shown in **Fig.1.19**. Simple molecules such as fish oil, vegetable oils, phosphate esters, long-chain alcohols, acids, and amines offer stability to particles dispersed in a non-aqueous medium (U.Paik et al.,1998; P.M. Raj et al.,2001). They do not have enough chain length to offer full steric stabilization and are therefore called semisteric stabilizers.

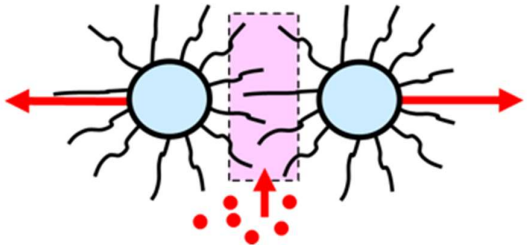

Fig.1.19 Schematic showing the steric stabilization.

The adsorbed polymer layer thickness, its density, polymer-ceramic bonding, conformation of the polymers, solvent quality, and molar volume of the solvent are the important parameters affecting steric stabilization. The different types of polymers provide different conformations on the particle surface (J.A.Lewis., 2000) as shown in **Fig.1.20.**

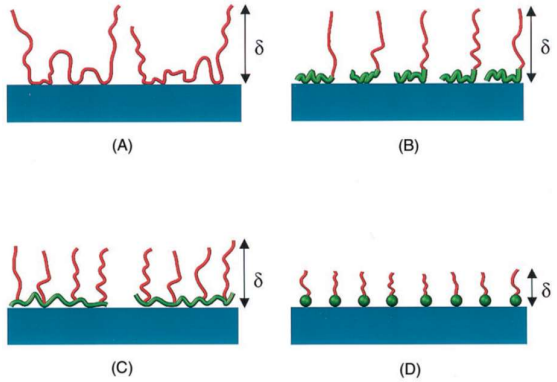

Fig.1.20 The different conformations of polymers adsorbed on the particle surface (a). homopolymer, (b). diblock co-polymers, (c). comb-like copolymers, (d). short chain dispersant. (J.A. Lewis., 2000).

The stability of a powder suspension in a medium is explained by the Derjaguin-Landau-Verwey-Overbeek theory (DLVO) (R. Hogg et al.,1966). According to DLVO theory, the total potential between the suspended particle in a medium is the sum of attractive potential originating from the Van der Waals forces and repulsive potential originating from the electrostatic, steric, or electrosteric mechanisms.

$$V_T = V_A + V_R$$

Where V_T is the total potential, V_A is the attractive potential and V_R is the repulsive potential. The attractive potential depends on the dielectrics of the particle and dispersion medium. On the other hand, the repulsive potential depends on the size and shape of particles, the distance between the particle, the electrical double-layer thickness, surface charge density,

and the dielectric constant of the medium. For two spherical particles of diameter 'a' the potential energy of repulsion U_R, is obtained by the equation **(**4**)**.

$$U_R = \frac{\epsilon_r a^2 \psi_0^2}{4(h + a)} \exp - \left(\frac{h}{\kappa^{-1}}\right) \qquad \textbf{(4)}$$

Where ψ_o is the surface potential, h is the distance between the surfaces and κ^{-1} is the electrical double layer thickness. The attractive, repulsive, and total potential of interaction between colloidal particles as a function of interparticle distance is shown in **Fig.1.21**. The repulsive potential increases and the attractive potential decreases with a decrease in interparticle distance. On the other hand, the total potential increases with a decrease in interparticle distance to reach a maximum and then decreases to a primary minimum. The primary minimum occurs when the particle separation is of the order of molecular dimension. The maximum potential is called the energy barrier which prevents the particle from falling into the primary minimum (agglomeration). In the case of large flat particles, a shallow secondary minimum is also observed at an interparticle distance approaching the particle dimension. An increase in electrolyte concentration and a decrease in zeta potential decreases the height of the potential barrier so that the particle falls into the deep primary minimum leading to permanent coagulation. On the other hand, the secondary minimum being very shallow, particles in the secondary minimum can easily go to the dispersed state by gentle mechanical agitation.

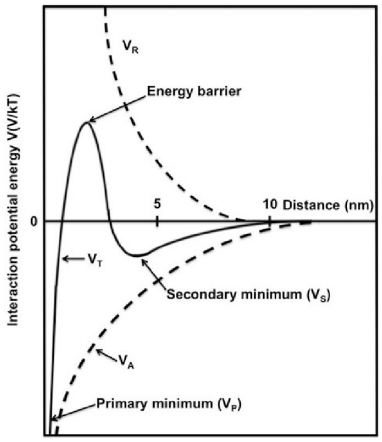

Fig.1.21 The changes in the interaction potential with interparticle distance (E.Piacenza et al., 2018).

Among the various dispersion mechanisms, the electrosteric is considered the most efficient one. L. Palmqvist et al studied the stabilizing mechanism of three dispersing agents viz., polyacrylates, lignosulfonates, and a comb copolymer through zeta potential, adsorption, and atomic force measurements (L.Palmqvist et al.,2006). For polyacrylates, high solid loading of up to 59 vol.% is achieved due to electrosteric stabilization. Instead, in the case of lignosulfonates, the stabilization is mainly through electrostatic and slurries up to 57 vol.% solid loadings can be prepared. In the case of a comb-like copolymer, the stabilization mechanism is steric and slurries of only medium solid loading can be prepared efficiently.

1.3.2.2 Rheological characteristics of colloidal dispersions

Rheology is the study of the deformation behavior of fluids under shear forces. The interaction between the polymers and particles dispersed in a fluid can be quantitatively analyzed using rheology. Rheological measurements yield the apparent viscosity, yield stress, and viscoelastic properties like storage modulus, loss modulus, and tan δ. The colloidal processing of ceramics generally requires well-dispersed slurries of low viscosity and high solids loading. The ceramic slurry rheology mainly depends on inter-particle forces and the concentration of the ceramic particles (F.F. Lange.,1989). Based on the deformation under shear stress, the fluids can be

classified as Newtonian and non-Newtonian. Well-dispersed ceramic powder suspensions at lower solids concentration (< 30 vol. %) exhibit Newtonian flow behavior (J.A. Lewis et al., 2000). For Newtonian fluids, the viscosity remains constant irrespective of the shear rate. If the viscosity decreases with an increase in shear rate, the flow behavior is known as shear-thinning. The shear-thinning flow behavior with some yield stress value is called pseudo-plastic. Well-dispersed suspensions of solids loading> 30 vol.% generally show the pseudoplastic flow behavior. The pseudoplastic behavior is due to the breakdown of temporary flocs formed in concentrated suspensions at higher shear forces. The powder suspensions used in the majority of the ceramic forming processes exhibit pseudoplastic flow behavior. If the viscosity of a suspension increases with an increase in shear rate, the flow behavior is shear-thickening or dilatant. The well-dispersed suspensions at the maximum limit of solids loading exhibit dilatant flow behavior. Bingham fluids have the Newtonian flow characterized by some yield stress value. The thixotropic and rheopectic flow behavior is time-dependent. Thixotropy means the decrease in viscosity with time with shear rate. The opposite behavior is known as rheopectic. **Fig.1.22** depicts the different flow behavior of colloidal dispersions. Plastic flow behavior is needed for plastic forming techniques such as Injection molding and extrusion. The presence of flocculated particles in a slurry can be detected by rheological measurements. Generally, the presence of particle agglomerates tends to increase the viscosity, shear thinning behavior, and yield stress of powder suspensions. The flow models presented in **Table 1.2** are used to explain the rheological behavior of powder dispersions.

The slip casting and tape casting processes require slurries of sufficient yield stress for the consolidated slurry layer on the mold surface to maintain its shape while draining the excess slurry and the cast tape to maintain the thickness uniformity, respectively (M. N. Rahaman., 2017). On the other hand, processes such as gel casting and direct coagulation casting demand slurries of low viscosity and yield stress to flow into the intricate parts of the mold. M.Jabbari

et al made a flow analysis and explained various rheological behavior of slurries for tape casting and found that the rheology strongly affects the final properties and quality of the product (M.Jabbari et al. 2016). B.Bitterlich et al characterized aqueous yttria-stabilized zirconia tape casting slurries using acrylic emulsion binders by static and dynamic measurements. The slurries exhibited pseudoplastic behavior and distinctive elastic properties below critical shear stress. Further, they demonstrated that the viscosity and its time-dependent behavior which in turn give the internal bonding between the particles and binder are excellent tools for the characterization of the tape casting slurry (B. Bitterlich et al., 2002). A.Mukherjee et al investigated a correlation between slurry rheology and density of green and sintered yttria-stabilized zirconia tapes using two different dispersants namely, menhaden fish oil and phosphate ester, and established a remarkable effect of slurry rheology on green and sintered densities (A.Mukherjee et al., 2001).

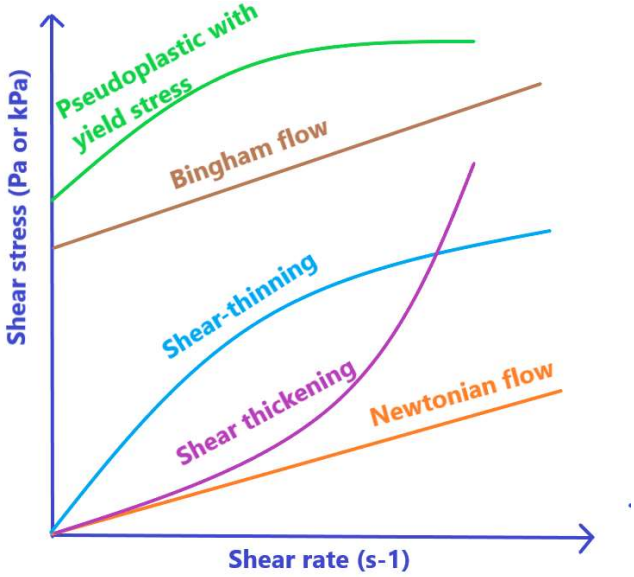

Fig.1.22 Different flow behaviors of ceramic powder dispersions

Table 1.2 Different flow models of the ceramic powder dispersions

Flow model	Formula	Parameters
Power-law	$\tau = K\gamma^n$	
Bingham model	$\tau = \tau_o + K\gamma$	τ: Shear stress
Herschel-Bulkley model	$\tau = \tau_o + K\gamma^n$	γ: Shear rate
		τ_o: Yield stress
Casson model	$\sqrt{\tau} = \sqrt{\tau_o} + \sqrt{K\gamma}$	K: consistency index
		n: exponent

1.3.2.3 Colloidal shape-forming processes

The well-dispersed ceramic powder suspensions in the aqueous or nonaqueous medium are consolidated into green bodies of near-net-shape with uniform microstructure by various forming processes. The details of different colloidal shape-forming processes are presented in the following sections.

1.3.2.3.1 Slip casting

Slip casting is originally developed for the consolidation of aqueous clay suspensions to produce green bodies of both simple and complex shapes. Later the process is adopted for the production of advanced ceramic components. The process uses a porous mold made of plaster of Paris. In slip casting, the ceramic powder suspension in a solvent medium (preferably water) cast into a mold is consolidated by draining the solvent through the pores in the mold. The draining of the solvent through the pores in the mold is due to the capillary action and gravity. The removal of solvent through the porous mold forms a gelled slurry layer (cast layer) on the surface of the mold. The thickness of the gelled layer increases with time. There, are two versions of slip casting called (i) drain casting and (ii) solid casting. In drain casting, the excess

slurry in the mold is poured out when the slurry layer gelled on the surface of the mold achieves sufficient thickness. This produces hollow components like tubes, crucibles, etc. On the other hand, in solid casting, the slurry is replenished until the gelled layer fills the mold cavity. Solid casting is used for the preparation of non-hollow components. A schematic of the slip-casting of ceramics is shown in **Fig.1.23**. The slurry with a shear-thinning flow behavior and adequate yield stress is desirable for the slip casting as it resists the preferential settling of larger particles during the consolidation (K.S. Chou et al.,1989; J.H.D. Hampton et al.,1988). Generally, the viscosity of the slurry should be less than 2000 mPas at a shear rate of 1-10 s^{-1} for effective pouring and mold filling (J. S Reed.,1995).

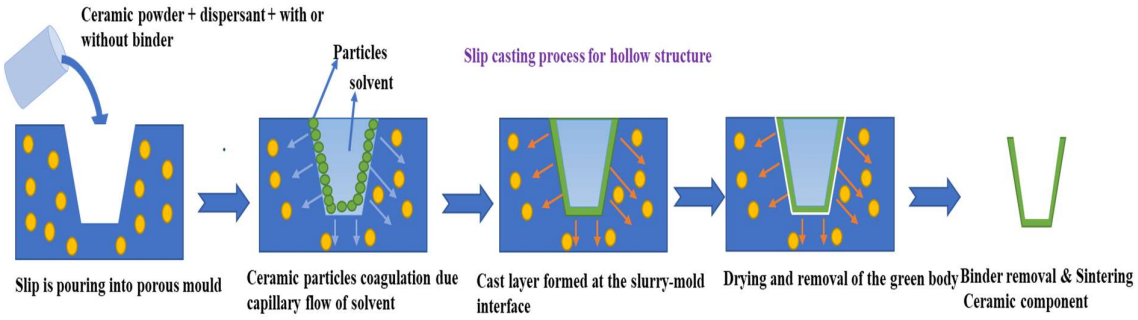

Fig.1.23 Schematic of slip casting for the preparation of hollow ceramic shapes

During the partial drying, shrinkage of the cast body detaches it from the mold surface and enables removal from the mold. This can be further dried, binder-removed, and sintered to get a ceramic body.

The cast-layer thickness is obtained from equation (5),

$$L = \sqrt{\left(\frac{2J\Delta Pt}{\eta Rc}\right)} \qquad \textbf{(5)}$$

Where J - the volume of cast/ volume of the liquid removed

ΔP - apparent mold suction

Rc - resistivity to liquid transport in the mold

t - casting time

η - viscosity of the liquid transported

The rate of cast thickness formation depends on casting time, slurry solids loading, the viscosity of the medium, temperature, and the residual or already absorbed liquid in the mold. At the beginning of the casting, more free pores are available on the mold surface and the solvent absorption is maximum. As time passes, the pores are filled by the solvent which further reduces the flow. Moreover, the already formed cast layer on the mold surface increases resistance to the flow of liquid which reduces the casting rate mentioned as the Rc factor in the equation (5). Generally, the rate of cast thickness development increases with an increase in slurry solids loading, an increase in temperature, and a decrease in the viscosity of the medium. The rate of cast thickness formation decreases when the same mold is used for many casting as the residual water in the pores of the mold decreases its water absorption capacity. One of the major problems with slip casting using plaster of Paris mold is the low production rate. The updated versions of the slip casting process are pressure casting, vacuum casting, and centrifugal casting where the rate of cast thickness formation can be enhanced by the application of pressure, vacuum, or centrifugal force, respectively. This is achieved by keeping the high-pressure difference (ΔP) between the slurry contact area and the outside of the mold. In the case of clay-based systems, the faster cast layer thickness formation is facilitated through inter-particle coagulation (J.S. Reed.,1995; W. Brodie.,2009).

A suitable binder that is soluble in the solvent medium is used in slip casting. The binder provides yield strength to the cast layers. Otherwise, during draining the excess slurry, the cast layer collapses and flows back which reduces the thickness of the slip cast body. The strength of the cast layer is based on the particle packing, the interparticle interactions, and the bonding induced by the binder **(**S.M.Olhero et al.,2002; Q.Xu et al.,2014; A.Gubernat et al.,2015). Normally the cast layer thickness produced at a fixed casting time decreases with the addition of a binder. For example, the casting rate of 2.4 mm/min for alumina using a pressure of 140 kPa is reduced to 0.3 mm/min with the addition of 0.5 wt. % of polyvinyl alcohol binder (J.S

Reed., 1995). This reduction in thickness is due to the gelation of the binder at the mold-slip interface. Further, the formed gelled layer resists the flow of the solvent. This reduces the permeability of the cast and the rate of cast thickness formation. In non-clay ceramics, the gelation of binder provides yield strength to the cast layer on the mold surface and increases the strength of the green body for handling, machining, and heat treatment (N. Dermirkol et al., 2007; A.Gubernat et al., 2015; K.M. Lindqvist et al., 2005; J.S.Reed,1995). Polyethylene glycol (K. A. Appiagyei et al.,2008; Q. Xu et al., 2013), polyvinyl alcohol (C.Promdej et al., 2008; M. Barmala et al., 2009; K.Somton et al., 2019), sodium carboxymethyl cellulose (A.J. Ruys et al.,1996), carboxymethyl cellulose (S.I.Conceicao et al.,2003) and acrylic latex emulsions (K.M. Lindqvist et al., 2005; A.Gubernat et al., 2015) are the binders reported in slip-casting. Here, the acrylic latex emulsion is a colloidal dispersion-type binder and all others are water-soluble binders. A styrene-acrylic acid co-polymer emulsion is reported for the preparation of complex-shaped alumina by slip casting using molds made by solid freeform fabrication (K.M. Lindqvist et al., 2005). The cast layer thickness formed varies inversely with the binder concentration due to the filtration resistance caused by the gelled binder at the slurry-mold interface. The green density decreases from 64 to 56.1 % of T.D and the green strength increases from 0.2 to 2 MPa when the binder concentration increases from 0 to 5 wt.%. A.Gubernat et al studied the acrylic emulsion binder, Duramax B-1000, for the production of dense SiC using Al_2O_3 and Y_2O_3 as sintering additives. With the addition of binder, only a minor increase in viscosity in the range of 120-320 mPa.s is noticed. A decrease in cast layer thickness with an increase in binder concentration is also observed due to the sealing of pores on the mold surface. The green ceramics produced using the acrylic emulsion binder exhibit sufficient strength to enable machining. Final sintering at 2050 ℃ resulted in 98 % T.D and single-phase SiC polycrystals. A photograph of green SiC crucibles made by slip-casting using acrylic latex emulsion binder before and after finishing by machining is shown in **Fig.1.24.**

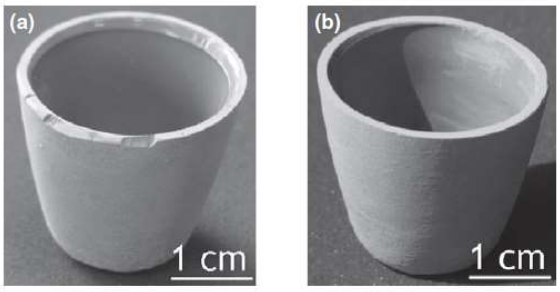

Fig.1.24 Green SiC crucibles prepared using acrylic emulsion binders (a). before, (b). after machining (A. Gubernat et al., 2015).

N. Dermirkol et al studied acrylic emulsion binder, Duramax B-1007, for the processing of low-clay translucent whiteware (N. Dermirkol et al., 2007). Here, the green strength increases from 1 to 4 MPa when the binder concentration increases from 0 to 6 wt.%. The high green strength obtained is due to the strong bonding between the ceramic particles and the binder through a carboxylic acid group of the binder and hydrogen bonding interaction between the binder molecules. S.I.Conceicao et al used carboxymethyl cellulose (CMC) binder in the slip casting of kaolin suspensions and studied its rheological characteristics and green density. With the addition of 0.2 wt.% of CMC binder, a high green density of 63 % T.D is achieved. In the case of water-soluble binders such as Na-CMC, even the addition of a small amount increases the slurry viscosity due to the long polymer chains (K.M. Lindqvist et al., 2005). As an example, a 2 wt.% aqueous solution of Na-CMC has a significantly high viscosity of 75 Pa.s at 25 ℃ (C.Falamaki et al., 2009). Another problem related to water-soluble binders in slip casting is the migration of binders and their segregation during the fluid flow (K.M. Lindqvist et al., 2005). H.Taguchi et al studied the effect of milling time on relative density and crystallographic phase change of partially stabilized ZrO_2 using sodium salt of polycondensation product of β-naphthalene sulfonic acid and formaldehyde as a binder (H.Taguchi et al.,1985). The relative density increases with binder addition and milling time. W. Xu et al used eco-friendly lactose and tannin as a binder and source of carbon in the

preparation of carbon-alumina ceramic filter foams for molten metal filtration through the slip casting process (X. Wu et al., 2022).

1.3.2.3.2 Tape casting

The tape casting was developed by G.N.Howatt et al for the production of thin sheets of titania (TiO_2) and alkaline titanates based ceramic dielectrics for capacitors (G.N. Howatt et al., 1947). Thereafter, tape casting has been utilized for the production of substrates materials, multilayered ceramic circuits/packages, electrolytes for solid oxide fuel cells, functionally graded ceramics, and textured ceramics (M.Jabbari et al. 2016; R.E. Mistler., 1995). In tape casting, the concentrated deflocculated ceramic powder slurry prepared in an aqueous or non-aqueous solvent using dispersant, binder, plasticizer, and an antifoaming agent is spread on a moving carrier film (Mylar sheet) using a double doctor blade (D.Hotza et al., 1995; P Wiecinska et al., 2015). Subsequent solvent removal by evaporation induced by hot air flow resulted in a green tape. The green tape removed from the substrate is rolled on a flywheel and stored. A schematic of tape casting is presented in **Fig.1.25**. On the other hand, batch tape casting uses a glass plate instead of the flexible mylar film as a substrate. The binder-removal and sintering of the green tape results in ceramic tape. The function of binder and plasticizer in tape casting is to provide sufficient strength and flexibility, respectively, to the green tape. The amount of binder and plasticizer is optimized to achieve adequate strength and flexibility of the green tape (S. L. Natividad et al., 2011; F. Doreau et al., 1999). The rheological behavior of the casting slurry plays a significant role in the tape casting process. The optimum viscosity of the slurry for tape casting is in the range of 1 to 1.5 Pa.s at a shear rate of 20 s^{-1} (C.Pagnoux et al.,1998).

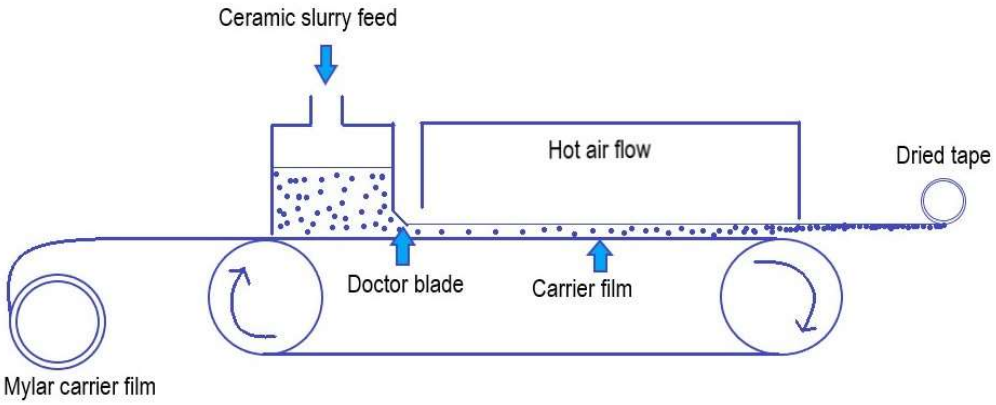

Fig.1.25 The schematic of the tape casting.

The continuous tape casting practiced in industries prefers organic solvents as aqueous tape casting systems require a long drying time and faces other drying-related issues such as formation of wrinkles and cracks on the surface. The advantages of organic solvents in continuous tape casting are their low boiling point, low heat of vaporization, and low viscosity. Trichloroethylene, ethyl alcohol, methyl ethyl ketone (MEK), and toluene are some of the organic solvents employed in non-aqueous tape casting. Azeotropic solvent mixtures such as MEK-ethanol and trichloroethylene-ethanol are also preferred. Polyvinyl butyral is the binder, phthalic esters, and polyethylene glycol are the plasticizers, and semi-steric stabilizers like fish oil and phosphate esters are the dispersing agents commonly used in industrial tape casting. R. Mistler et al used triethylene glycol di-2-ethyl hexanoate as an environmentally friendly plasticizer for polyvinyl butyral binder for tape casting and compared the results with a commercial plasticizer, butyl benzyl phthalate (R. Mistler et al., 2007). The proposed plasticizer performed well in terms of Tg and properties of green and sintered tapes. K. Prabhakaran et al used cardanol, a C_{15} alkyl chain substituted phenol obtained from cashew nut shell liquid as a dispersant and plasticizer for polymethylmethacrylate (PMMA) binder in the non-aqueous (toluene) tape casting of alumina (K. Prabhakaran et al., 2001).

High cost, flammability, and environmental pollution associated with the spent organic solvents instigated research activities on the development of eco-friendly water-based tape casting systems. Most commonly employed binders in aqueous tape casting are water-dispersible type acrylic emulsions (C.Pagnoux et al.,1998; A.Kristoffersson et al., 1997; C.A.Gutierrez et al.,2001; F.Doreau et al., 1999) and water-soluble binders such as PVA (C. Zhou et al., 2016; S.Li et al., 2009; A.Kristoffersson et al., 1998) and cellulose ethers (A.Kristoffersson et al., 1997; D.Hotza et al., 1995; T.Chartier et al.,1993). **Table 1.3** shows the comparative study made by A. Kristoffersson et al on three different aqueous binders in the tape casting of alumina (A.Kristoffersson et al., 1998). It has been reported that in the case of acrylic emulsion binders, tailorable Tg, high solid content, low viscosity, high green density, and lower drying shrinkage are achieved compared to PVA and hydroxypropyl methylcellulose (HPMC) binder-based tape casting formulations. F. Doreau et al studied the suitability of a combination of two acrylic emulsion binders, Duramax B-1035 and Duramax B-1050 in the aqueous tape casting of alumina (F. Doreau et al.,1998). The concentration of the binder combination used is up to 15 wt.%. By using the combination, they achieved, low viscosity slurries of shear thinning flow behavior, low foaming of the slurry, homogeneous tape, and higher critical cracking thickness. In addition, F. Doreau et al studied the mixture of acrylic emulsion binders of different Tg on the strength and flexibility of the green tapes (F. Doreau et al.,1999). Here, the green tape with a higher Tg value showed a brittle character while with a lower Tg, the green tape attained elastoplastic nature.

Table 1.3 Comparison of physicochemical properties of binders in aqueous tape casting (A.Kristoffersson et al., 1998).

Binder	**Tg (°C)**	**Solid content, wt.%**	**Viscosity (Pa.s)**	**Green density (%T. D)**	**Drying shrinkage (%)**	**Sintered density (% T.D)**
Acrylic-styrene latex, non-ionic	-16	50	8.5	52.6	20.3	97.6
Acrylic-styrene latex, Anionic	-6	55	0.100-0.400	54.1	20.5	93.0
Acrylic-styrene latex, Anionic	-40	55	< 0.200	54.8	21.5	93.2
4 % aq. Solution of PVA	-	38.9	0.032 – 0.038	50.7	36.3	95.1
2 % aq. Solution of HPMC	-	19.4	4	50.8	74.7	96.0

S.Li et al studied the PVA binder for the aqueous tape casting of microwave ceramic component, $Li_{1+x-y}\ Nb_{1-x-3y}Ti_{x+4y}O_3$, and characterized the effect of ceramic powder loading on green density, porosity, green strength, and sintered density of the tape (S.Li et al.,2012). T. Chartier et al studied the aqueous tape casting of alumina using hydroxypropyl methylcellulose binder (T.Chartier et al.,1993). The effect of the binder and plasticizer content on the green density, green strength, and strain at failure is established. Q. Shang et al proposed a new gel-tape casting process for the preparation of aluminum nitride ceramic sheets using an effective and environmentally friendly additive PIBM (a water-soluble copolymer of isobutylene and maleic anhydride). Herein, the PIBM acts as both a dispersant and gelling agent and PEG acts as a plasticizer (Q.Shang et al., 2017). The green tapes produced from slurry with a solids loading of 40 vol.% and binder content of 3 wt.% are smooth, uniform, and without cracks.

The average grain size and thermal conductivity of the sintered tape obtained are 7 μm and 161 W/(m·K), respectively. S. Nayak et al introduced biopolymer, gelatin as a binder in the aqueous tape casting of yttria-stabilized zirconia using glycerol as a plasticizer. They studied the flow behavior and gelling characteristics of the slurries and the strength and flexibility of the green tape. The flexible green tapes produced by the aqueous system sintered to 99 % of T.D (S. Nayak et al., 2011). J Marie et al studied the bio-based binders such as citrus pectin, microcrystalline cellulose, and psyllium along with ammonium lignosulfonate dispersant and glycerol as a plasticizer for the aqueous tape casting of alumina (J.Marie et al.,2017, 2021). The slurries using citrus pectin binder show shear thinning behavior. On the other hand, slurries prepared using psyllium and microcrystalline cellulose show anti-thixotropy and thixotropy, respectively. The green tapes of strength parallel and perpendicular to the casting directions were in the range of 0.34 to 0.44 MPa and 0.09 to 0.74 MPa, respectively, that were sintered to a density in the range of 90 to 94% TD. The molecular structure of PIBM is shown in **Fig.1.26.**

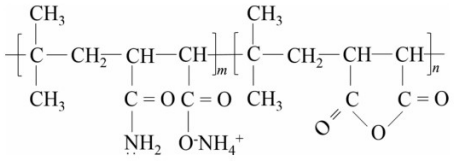

Fig.1.26 Molecular structure of PIBM

1.3.2.3.3 Gel casting

Gel casting is a ceramic shape-forming process developed in 1980 at Oak Ridge National Laboratory, USA (A. C. Young et al., 1991; O.O.Omatete et al.,1997). In this, a highly concentrated (>50 vol.%) ceramic powder suspension of low viscosity (<1 Pa.s) prepared in a solution of organic monomer and a crosslinking agent is cast in a mold. The *in situ* polymerization of the monomer and crosslinking agent initiated by an initiator and a catalyst

set the slurry into a strong gel. The gelled body removed from the mold is dried under the humidity-controlled condition to produce the green ceramics. Binder removal followed by sintering of the green body produces the ceramic component. The gelcasting is schematically represented in **Fig.1.27**. Gel casting has the benefits of strong and machinable green bodies at low binder content, homogenous binder distribution, complex-shape capability, high green density, moderate production rate, and improved reliability (A. C. Young et al., 1991; J. Yang et al.,2011). A photograph of near-net-shape ceramic components produced by gelcasting is shown in **Fig.1.28**. Gelcasting uses both aqueous and non-aqueous solvents. The non-aqueous version originally developed with acrylate monomers is replaced by the aqueous version due to the high cost and environmental hazards associated with the spent organic solvents (M.A.Janney et al.,1998). The initially developed aqueous version also faces industrial hesitation due to the neurotoxicity of the acrylamide monomer (O.O.Omatete et al.,1997; J.Yang et al., 2011). A large number of low toxic monomer-crosslinker systems has been reported for the aqueous gelcasting of ceramics (M.Potoczek et al.,2004; M.Kokabi et al.,2006; C.Tallon et al.,2007; C. Zhang et al.,2012). The low-toxic monomer systems studied for gelcasting of ceramics are given in **Table 1.4**.

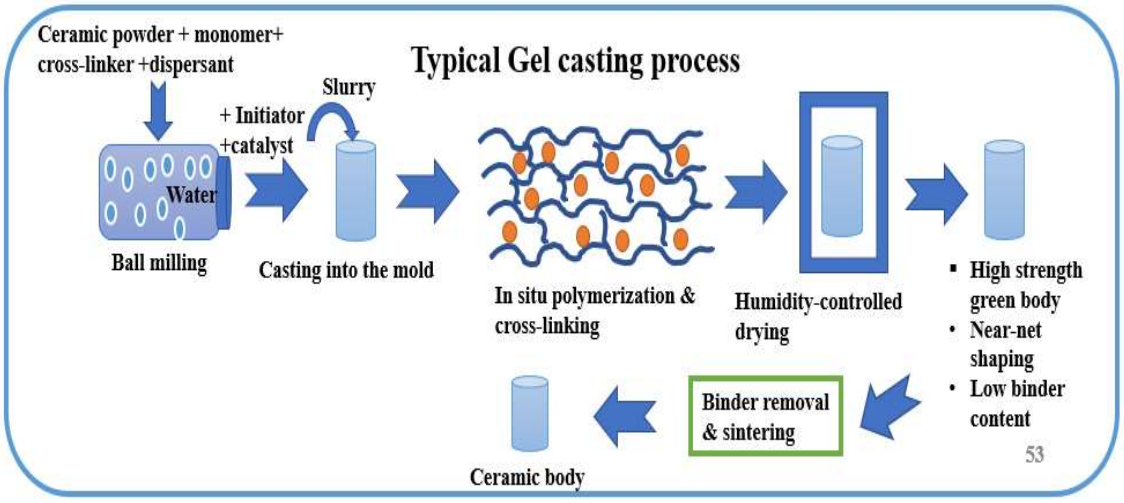

Fig.1.27 Schematic of gel casting

Fig.1.28 Complex near-net-shape ceramics fabricated by gelcasting (M.A.Janney et al.,1998).

Table 1.4 The low toxic monomers and cross-linkers used in gel casting.

Monomer	**Cross-linkers**	**References**
Methacrylamide Poly (ethylene glycol) methyl ether methacrylate 1-vinyl-2-pyrrolidone Acrylic acid Dimethyl aminoethyl methacrylate Hydroxyethyl acrylate Hydroxyethyl methacrylate Hydroxypropyl acrylate Hydroxypropyl methacrylate Methoxy poly(ethylene glycol) mono methacrylate Methacrylatoethyl trimethyl ammonium chloride Methacrylamidopropyle trimethyl ammonium chloride Methacrylic acid p-Styrene sulfonic acid (sodium salt) Glycerol monoacrylate Dimethyl acrylamide Copolymer of isobutylene and maleic anhydride 3-O-acrylic-D-glucose	N,N′-methylenebisacrylamide poly(ethylene glycol) dimethacrylate Diallyl tartardiamide Poly (ethylene glycol) diacrylate Poly (ethylene glycol) dimethacrylate Trialyl amine Tetraethylenepentamine	M. Potoczek et al., 2014; M. Kokabi et al., 2006 ; M. A. Janney et al., 1998; C. Tallon et al., 2007; C. Zhang et al., 2012; Q.Wu et al., 2023; P. Bednarek et al., 2010

In addition to the *in situ* polymerization of a monomer-crosslinking agent, thermally induced gelation of proteins and polysaccharides and crosslinking of polymers in solution by the suitable cross-linking agent are studied for aqueous gel casting of ceramics (S.Leo et al., 2014). Sodium alginate (Y. Jia et al., 2002), gelatin (Y.Chen et al., 1999), agarose (E. Adolfsson.,2006), carrageenan (A.J.Millan et al., 2002), gellan gum (Y. Zhang et al., 2014), egg-white protein (X. He et al., 2011), curdlan (J. Xu et al., 2015) are some of the polysaccharide and protein-based natural gelling agents studied for the gel casting of ceramics. In these, aqueous ceramic powder suspensions containing a gelling agent prepared at higher temperatures (80 to 90°C) undergo gelation by cooling in a mold. Here the gelation of the slurry is due to the secondary interactions between the molecules of the gelling agent. The major drawback of this process is the relatively low ceramic powder loading achieved in the suspension due to the higher viscosity of the polymeric gelling agent solutions compared to the monomer solutions. The molecular structure of naturally renewable gelling agents used for gelcasting is shown in **Fig.1.29**.

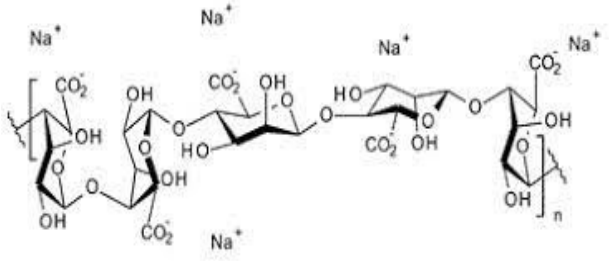

Sodium Alginate

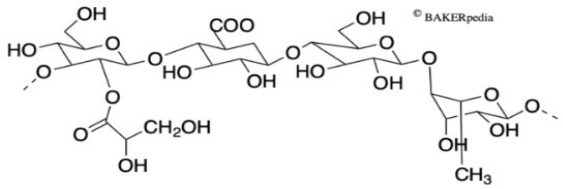

Gellan gum

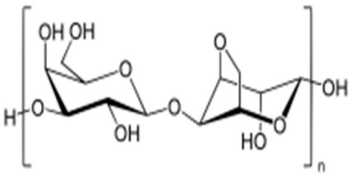

Agarose

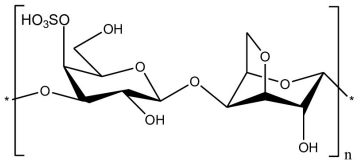

Carrageenan

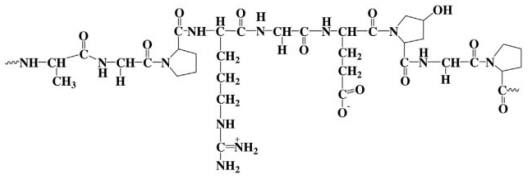

Gelatin

Fig.1.29 Molecular structures of the naturally renewable gelling agents.

The cross-linking of polyvinyl alcohol induced by 2,5- dimethoxy-2,5-dihydrofuran (DHF) (F. Chabert et al., 2008) and organotitanate coupling agent (S.L.Morissette et al., 1999) which results in the formation of gels are studied for the gel casting of ceramics. The cross-linking of chitosan, a biopolymer with glutaraldehyde (M. Bengisu et al., 2002) and DHF (S.B. Johnson et al., 2002) is also utilized for gel casting of alumina. The cross-linked structures of PVA induced by DHF and organotitanate and chitosan induced by glutaraldehyde and DHF are shown in **Fig.1.30.**

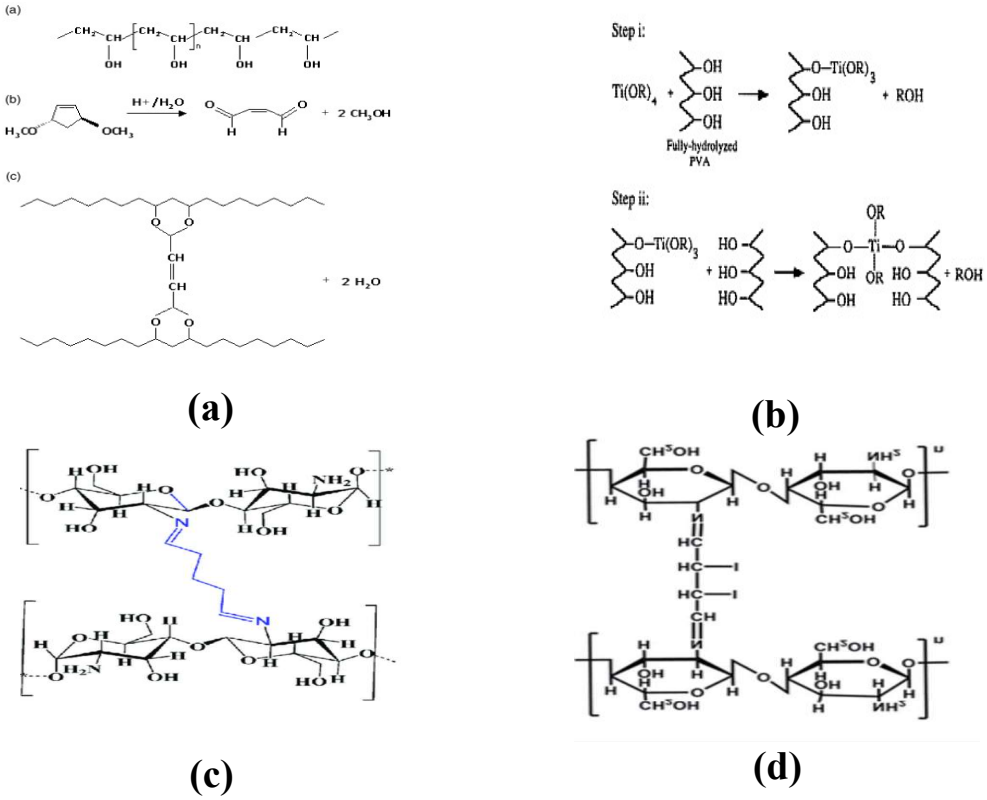

Fig.1.30 Cross-linking of PVA by (a) DHF, (b) organotitanate coupling agent, and the cross-linking of chitosan by (c) glutaraldehyde, (d) DHF.

1.3.2.3.4 Freeze casting

Freeze casting is a process mainly for the preparation of porous ceramics from a powder suspension in a suitable liquid medium. In this, a ceramic powder suspension cast in a mold is set by freezing the dispersion medium. During solidification by freezing, the growing solvent crystals reject the ceramic particle in the inter-crystal space. The removal of the solvent crystals from the frozen slurry by sublimation followed by sintering creates porous ceramics. Here, the solvent crystals act as a template for the pores. That is, the space created by the removal of solvent crystals by sublimation remains as pores in the ceramic. A flow chart of the freeze-casting process is shown in **Fig.1.31** and a schematic showing the ice growth and formation of porous ceramics is presented in **Fig.1.32**. The process is simple and capable of producing near-net-shape without any troublesome binder removal step (K. Araki et al., 2004; S. Deville., 2008). Various solvents such as water, camphene, t-butyl alcohol, and naphthalene-camphor mixture are investigated for freeze casting of ceramics. Among them, aqueous freeze casting using water as a medium is eco-friendly and sustainable. In freeze casting, the porosity of the ceramics could be very well modulated by the slurry solids loading. On the other hand, various pore architecture and pore alignment could be achieved by incorporating additives and manipulating the direction of freezing, respectively.

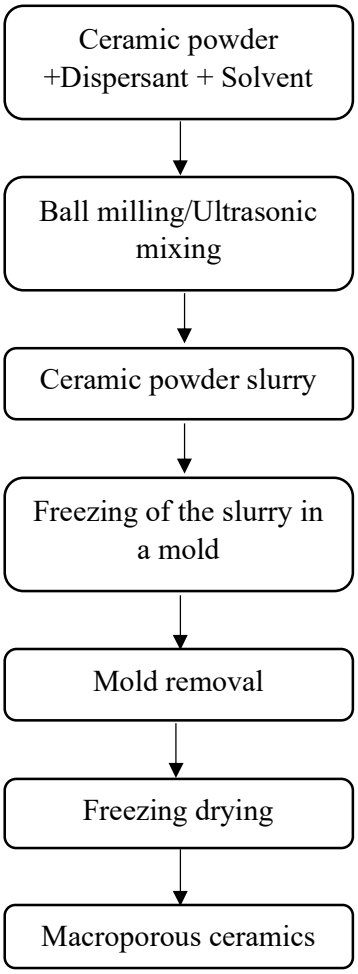

Fig.1.31 Flowchart of freeze-casting process

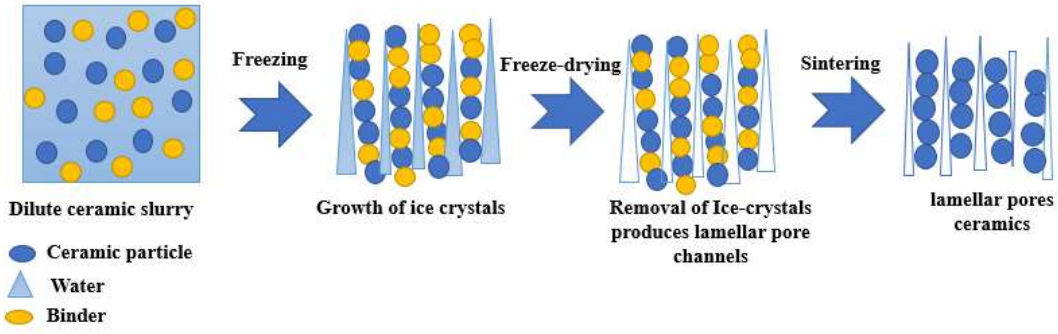

Fig.1.32 Schematic showing the formation of pores in freeze casting

Various additives such as glycerol (S.W. Sofie et al., 2001; Y. Zhang et al., 2010), polyvinyl alcohol (K.H.Zuo et al., 2010; L.Ren et al., 2009; D. Zhang et al., 2012), polyethylene glycol

(C. M. Pekor et al., 2008), gelatin (M. Fukushima et al., 2014; Y. Zhang et al., 2009), ethanol & 1-propanol (Z.Jing et al., 2014) are incorporated into the ceramic powder suspensions for freeze casting that interact with the growing ice crystals and modify the final macroporous structure and influence the properties. Y. Zhang et al studied the effect of glycerol (10 wt.%) on the microstructure and strength of sintered porous alumina ceramics prepared by freeze casting. It is found that the addition of glycerol results in an improved connection between the lamellar channels. Moreover, an increase of axial and radial compressive strengths by 31.4 % and 154.9 %, respectively, is observed by the addition of glycerol (Y. Zhang et al., 2010). The effect of glycerol addition and powder loading on the microstructure of alumina ceramics prepared by freeze casting is shown in **Fig.1.33.**

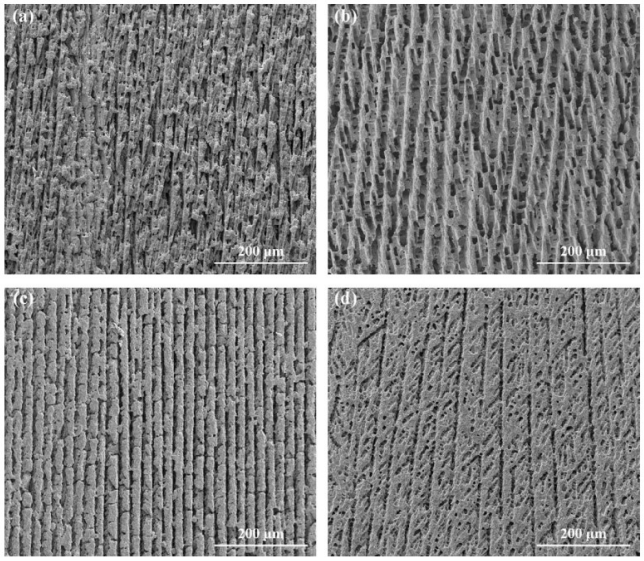

Fig.1.33 Microstructure of porous alumina ceramics prepared from (a) 20 vol.% slurry without glycerol, (b) 20 vol.% slurry with glycerol, (c) 30 vol.% slurry without glycerol, and (d) 30 vol.% slurry with glycerol. The direction of the cross-section is perpendicular to the ice front (Y. Zhang et al., 2010).

The effect of PVA concentration on the lamellar microstructure formed by freeze casting is studied by L.Ren et al using TiO_2 powder suspension (L.Ren et al., 2009). In his study, a change

of pore structure from dendritic to columnar type is observed when the concentration of PVA increases from 3 to 6 wt.%. The microstructure of freeze-cast TiO_2 ceramics prepared at 3 wt.% and 6 wt.% PVA showing the dendritic and columnar pore structure is given in **Fig.1.34**. K.H. Zuo et al studied the effect of PVA on the pore structure of hydroxyapatite ceramics prepared by freeze casting (K.H.Zuo et al., 2010). An increase in the interconnectivity of the pores in the hydroxyapatite ceramic is observed by the addition of PVA.

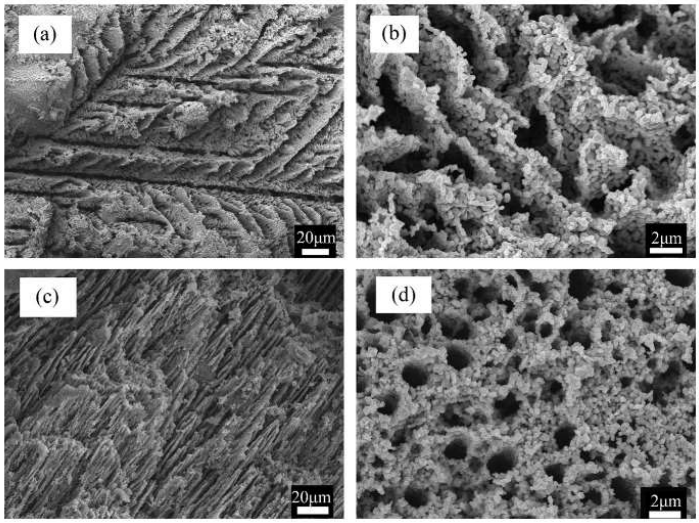

Fig.1.34 SEM images of porous TiO_2 with cross-section parallel and perpendicular to the ice growth direction. (a) 3 wt.% PVA, parallel; (b) 3 wt.% PVA, perpendicular; (c) 6 wt.% PVA, parallel; and (d) 6 wt. PVA, perpendicular.

C.M.Pekor et al studied the effect of PEG concentration at two different freezing conditions, ethanol/dry ice, and liquid nitrogen, on the three distinct microstructural scales, which include the colony size, the pore size, and the secondary dendrite spacing of porous alumina ceramics prepared by freeze casting (C.M.Pekor et al., 2008). The addition of PEG affected the pore size and secondary dendrite in ethanol/dry ice conditions. He concluded that the coarsening of the ice crystals during unidirectional freeze casting of ceramic slips is sensitive to both the volume fraction of ceramic particles and the addition of PEG. M.

Fukushima et al studied the effect of the concentration of gelatin on the porosity, compressive strength, and microstructure of porous alumina ceramics prepared by the gelation-freeze route (M. Fukushima et al., 2017). With an increase in gelatin concentration from 1 to 5 wt.%, the porosity increases from 86.2 to 87.1 % and the compressive strength increases from 10.8 to 19.2 MPa.

Apart from the preparation of porous ceramics, there are few reports on the preparation of dense ceramics by freeze casting (K. Araki et al., 2004; S.W. Sofie et al., 2001). K. Araki et al used molten camphene at 55℃ as a medium for the preparation of alumina slurry for freeze casting. The removal of camphene from frozen slurry by sublimation is achieved at room temperature in a fume hood. He obtained a sintered density of 98.4 % T.D at 1600 ºC for a freeze-cast body produced from a slurry with a solid content of 50.8 vol.% (K. Araki et al., 2004). S. W. Sofie et al studied the effect of glycerol, a cryoprotectant, in the freeze casting of aqueous alumina suspensions using an acrylic emulsion binder, Duramax B-1001(S.W. Sofie et al., 2001). Here, the viscosity of the slurry decreases, and green and sintered density increases with the addition of glycerol. Moreover, a dense sintered microstructure free of freezing defects with good grain interconnectivity is achieved. The microstructure of dense alumina ceramics prepared by freeze casting using glycerol as a cryoprotectant is shown in **Fig.1.35**.

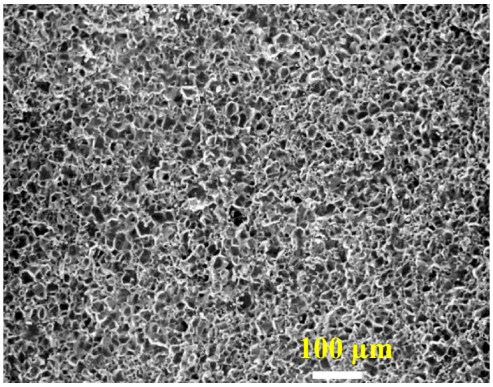

Fig.1.35 Microstructure of dense alumina ceramics prepared by freeze casting using glycerol as a cryoprotectant (S.W. Sofie et al., 2001).

1.3.3 Additive manufacturing

Additive manufacturing (AM) is a relatively new process for the preparation of near-net-shape ceramic components. In this, a 3D model of an object created in a computer is sliced into many layers with the help of software, and then the object is built on a platform layer-by-layer. The process has the benefits of complex shape manufacturing, low cost, shorter manufacturing time, and simplified procedure. The method is used for the preparation of metallic, polymeric, and ceramic components. Unlike metallic and polymeric materials, additive manufacturing for the commercial production of ceramic components is still in the infancy stage. The AM processes are capable of manufacturing dense and porous ceramics of complex shapes. A photograph of dense and porous alumina ceramic components fabricated by additive manufacturing is shown in **Fig.1.36**. The additive manufacturing techniques are mainly classified into seven types, material jetting, material extrusion, direct energy deposition, sheet lamination, binder jetting, powder bed fusion, and vat photo-polymerization (J.Deckers et al., 2014). Another classification by Z. Chen et al based on the feedstock form as powder-based (3D printing, selective laser sintering, selective laser melting), slurry-based (stereolithography, digital light processing, two-photon polymerization, inkjet printing, direct ink writing), and bulk solid-based (laminated object manufacturing, fused deposition modeling) (Z.Chen et al., 2019). Binders in polymeric or monomeric forms are inevitable for most ceramic additive manufacturing. X. Lv et al made a study on the binding mechanism of different AM processes and binders in binder jetting (X. Lv et al., 2019). They classified the liquid binders as tigger powder reactive (water and glycerol-based), self-adhesive (phosphoric acid, acrylic acid, polymer, isopropanol), and self- and powder-reactive (acidic calcium sulfate), and solid binder (polyvinyl alcohol, dextrin, instant alveoline, maltodextrin, starch).In powder-based selective laser sintering (SLS), various inorganic and organic binders are reported that glued the ceramic particles with melting (J. Deckers et al., 2014). HBO_2 (I.Lee., 2002) is an inorganic type and

stearic acid (M.C.Leu et al., 2008), carnauba wax (M.Rombouts et al., 2012), phenolic resin (B. Stevinson et al., 2006), epoxy resin (J.Liu et al.,2014), PMMA (K. Subramanian et al.,1995), polystyrene (J. Deckers et al.,2013) and polypropylene (K. Shahzad et al., 2014) are the organic type binders reported in SLS process. In AM by photocuring, photopolymerization of a slurry which contains monomers, oligomers, a photoinitiation system, and a ceramic filler with a concentration in the range of 40 – 60 vol.% (A. Zocca et al., 2015; B.Oezkan et al., 2021) occurs through the UV or laser beam. J. Nie et al studied the monomers 1,6-hexanediol diacrylate and ethoxylated (5) pentaerythritol tetraacrylate and a photoinitiator 1-hydroxycyclothexyl-phenyl-ketone for UV curing for the stereolithography based AM of alumina (J.Nie et al., 2021). H. H. Tang et al proposed slurry-based selective laser sintering (SLS) using insoluble semi-crystalline polyvinyl alcohol (PVA) coated alumina powder as a structural material and water-soluble PVA as an organic binder. They achieved an average flexural strength of 363.5 MPa and a relative density of 98% (H.H. Tang et al., 2011). Multi-functional photocurable acrylate systems such as an amine functional acrylate, pentaerythritol triacrylate, 6-hexanediol diacrylate, and trimethylolpropane triacrylate, modified acrylated polyether polyol are used to prepare the resins for SLS -3D printing as the acrylates undergo fast photo polymerization and produce ceramic green bodies of high fracture strength (M.Borlaf et al., 2019; C.Sciancalepore et al., 2017; H. J. Lee et al., 2021). T.F. McNulty et al reported a feedstock for the fused deposition of ceramics using a new family of thermoplastic binder system with an optimum concentration of 20 parts tackifier, 15 parts wax, 5 parts plasticizer, and 55 vol.% of lead zirconate titanate (PZT) powder (T.F. McNulty et al., 1998).

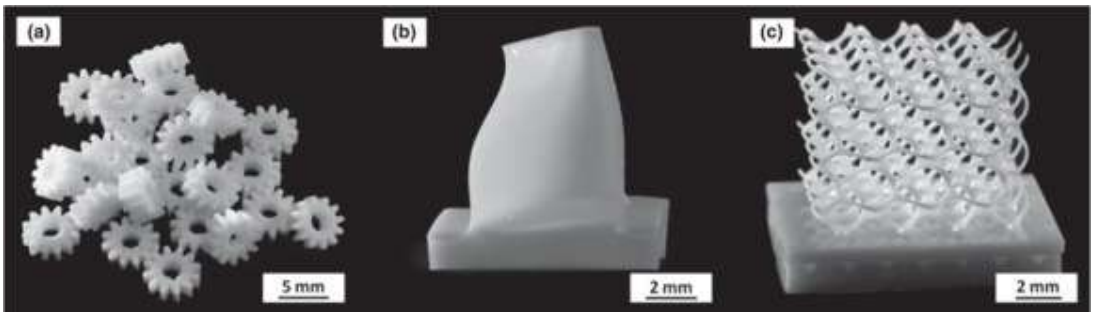

Fig.1.36 Sintered alumina parts fabricated using the LCM technique: (a) gear wheels; (b) a turbine blade; and (c) a cellular cube (M. Schwentenwein et al., 2015).

1.4 Scope and Objectives

Advanced structural ceramic materials are fabricated from fine ceramic powders using processing methods such as powder pressing, slip casting, tape casting, gel casting, freeze casting, injection molding, extrusion, and additive manufacturing. Various additives such as solvents, dispersing agents, binders, lubricants, and plasticizers are employed to enable shape forming from such fine powders. Out of these, the binders play a major role as it provides sufficient strength to the green body enabling handling and even machining in the green state. In addition, the binders used in the ceramic forming act as a rheology modifier, dispersing agent, and moisture retention agent. Several synthetic polymers have been exercised as binders in ceramic shape forming. Polyvinyl alcohol, polyethylene glycol, polyacrylic acid, and cellulose ethers are some of the water-soluble binders studied in ceramic shape forming. Polyvinyl butyral and polymethyl(methacrylate) are some of the non-aqueous binders studied in the shape forming of ceramics. Further, polymer-based emulsions prepared from acrylic monomers are also used as binders in ceramic processing. These emulsions possess high solid content (> 50 vol.%), and low viscosity and the polymers exhibit a wide range of glass transition temperatures. The acrylic emulsion binders provide superior properties in terms of green strength and flexibility and enable ceramic processing in an aqueous medium. In

addition, the emulsion-based binders easily disperse with the ceramic powder suspensions and produce co-dispersions of high solid content.

Sustainable development requires the use of eco-friendly and naturally renewable raw materials and processing additives. This instigates the search for naturally renewable binders for the aqueous processing of ceramic powders. The polysaccharides and proteins such as gelatin, pectin, sucrose, agarose, carrageenan, and egg white albumin are reported as binders in ceramic forming. Natural rubber latex (**NRL**) is a naturally renewable polymer emulsion obtained from the bark of the Hevea Brasiliensis tree.The ammonia-stabilized **NRL** is commercially available in the highly concentrated (~ 60 wt.%) form. Moreover, **NRL** has outstanding properties such as a high tensile strength, elasticity, and a low glass transition temperature (-70 °C). The high flexibility of **NR** at room temperature would eliminate the use of additional plasticizers. **NR** undergoes coagulation in the presence of acid, solvents, radiation, and by freezing. This can provide a handle for the gelation of co-dispersions of ceramic powder and **NRL**. In addition, the double bond in **NR** chains can form cross-links induced by metal oxides, sulfur, and radiation. Nevertheless, **NRL** is rarely studied as a binder in ceramic forming except for injection molding of alumina by C.F. Escobar (C.F. Escobar et al., 2015) and shape forming of hydroxyapatite for bio-medical applications by G.S. Sailaja (G.S.Sailaja et al., 2007). Therefore, the objectives of the present work are,

- To study the **NRL** as a binder in ceramic shape forming.
- To study alumina ceramic shape forming by powder pressing, slip casting, and tape casting using **NRL** binder.
- To study **NRL** as a gelling agent for the preparation of dense near-net-shape alumina ceramics by gel casting.
- To study **NRL** as a pore stabilizer for the preparation of porous alumina ceramics by freeze casting without freeze drying.

1.5 Organization of the thesis

The thesis explains alumina shape forming using **NRL** binder. The powder pressing, slip casting, tape casting, and freeze-gel casting of alumina is studied using **NRL** as a binder and the results are presented in seven chapters. A brief review of ceramic processing with a focus on binders is presented in **Chapter 1.**

Chapter 2 discusses the results of alumina powder pressing using the **NRL** binder. The preparation of powder pressing feedstock at various **NR** concentrations by co-coagulation of alumina-**NRL** co-dispersions using a formic acid solution and characterization of the resulting feedstock by the morphology of granules and flow time and Hausner ratio measurement is presented. The density and diametrical compressive strength of the pressed bodies prepared at various **NRL** concentrations and compaction pressures are measured and the results are discussed. The effect of annealing the green body on diametrical compressive strength is studied and presented. The cross-linking of rubber chains due to the Lewis acid character of alumina is proposed as a reason for a remarkable improvement in the strength of green bodies by annealing at 200°C. The green machining of annealed green bodies by lathing, milling, and drilling using conventional machines and tools is attempted and the results are presented. The ceramic prepared by binder removal followed by sintering at 1550°C of the pressed bodies is characterized by density measurement and microstructure analysis and the results are discussed.

The preparation of alumina ceramics by slip casting using the **NRL** binder is described in **Chapter 3**. The colloidal stability of the alumina-**NRL** co-dispersion is studied by zeta potential analysis and rheological measurements and the results are discussed. The thickness of the slip cast layer is investigated as a function of alumina slurry concentration, the concentration of **NRL** binder, and casting time. The **NR** cross-linking in the green body during annealing at 200°C is evidenced through diametrical compressive strength measurement before

and after annealing at 200°C. Homogeneity in the binder distribution is studied by thermogravimetric analysis of samples collected from various parts of a green body and the results are presented. The capability of the **NRL** binder-based slip-casting system for the quick preparation of thin-walled alumina crucibles is also demonstrated.

The **NRL** is successfully employed as a binder in the aqueous tape casting of alumina and the details are explained in **Chapter 4**. The colloidal stability and rheological characteristics of the tape casting slurries are studied using zeta potential and viscosity measurements. The tensile strength and flexibility (% elongation at break) of the green tape are measured as a function of **NRL** concentration and the results are discussed. A remarkable improvement in green density and microstructure achieved by roll-pressing of the green tapes is discussed. The shrinkage during sintering and density, microstructure, and average grain size, of the sintered alumina ceramic tapes are analyzed and presented.

Chapter 5 describes the use of **NRL** as a gel former and binder for the preparation of alumina ceramic shapes by freeze-gel casting. The mechanism of gelation by freezing concentrated alumina-**NRL** co-dispersions in a mold followed by thawing in acetone is explained. The shape stability of gels formed is studied as a function of **NR** concentration and presented. The compressive strength of the shape-stable gel is measured and the result is discussed. The effect of acetone exchange on the drying kinetics of the wet-gel body is investigated and explained. The effect of annealing at 200°C on the green strength and thermal decomposition of **NR** binder from the green body is discussed. The capability of freeze-gel casting using **NRL** as a gelling agent to fabricate complex neat-net-shape dense alumina ceramics is demonstrated.

NRL has been employed as a binder and pore stabilizer for the preparation of macroporous alumina ceramics by freeze-gel casting followed by air drying and the results are discussed in **Chapter 6**. The higher concentration of **NRL** stabilizes the macropores created

by the melting of ice crystals in the frozen body. The concentration of **NR** required to prevent the pore collapse at different alumina slurry concentrations is studied. The drying shrinkage, sintering shrinkage, porosity, and pore structure are evaluated and discussed in comparison with the samples prepared by freeze-drying the frozen bodies. The compressive strength and Young's modulus of the macroporous ceramics prepared by freeze-gel casting are evaluated and discussed. The summary of important findings in the study and future perspectives of the work are presented in **Chapter 7.**

Chapter 2

Alumina powder pressing using natural rubber latex as a binder

2.1 Introduction

Powder pressing is a simple and faster method for the production of ceramic shapes. The process achieves high green density at a relatively low amount of processing additives (M. H. Bocanegra-Bernal et al., 2004; G.H. Haertling et al.,1971). Powder pressing has been used for the fabrication of monolithic and composite ceramics, metal-ceramic composites, and functionally graded materials (J. Zhu et al., 2001; M. Dhanashekar et al.,2020). The process uses a granulated feedstock containing ceramic powder, a binder, a plasticizer, and a lubricant (J. L. Amoros et al., 2008). The incapability to produce complex shapes and development of density gradient in the green ceramic are the major drawback of the uniaxial powder pressing. Powder pressing followed by machining in the green state is utilized for the fabrication of more complex near-net-shape ceramic components (H. T. Larker et al.,1999; M. H. Bocanegra-Bernal et al., 2009; S. Leo et al.,2014). Green machining demands high green strength which is obtained only with a few binders reported in the literature (S. D. Nunn et al.,1996; M. Desfontaines et al., 2005). Strength of the green body is affected by chemical bonding interaction between the functional groups of the binder with ceramic powder or the interaction between the binders themselves and their glass transition temperature (C. W. Nies et al.,1984; M. Potoczek et al.,2003). Polyvinyl alcohol, polyethylene glycol, acrylic emulsions, methylcellulose, and wax emulsions are some of the reported binders in powder pressing (M. N. Rahaman., 2017). Among them, acrylic emulsion binders demonstrated superior strength for green machining. Recent researches focus on the use of natural renewable binders instead of synthetic one for sustainability and environmental friendliness (P. Wiecinska et al., 2020; N. P. Shapkin et al.,2021; M.F. Sanches et al.,2015)**.** Naturally renewable molecules such as

sucrose, and aloe vera gel are studied as binders in ceramic shape forming by powder pressing (A. Kumar et al., 2014; V. P. Jyoti et al., 2022). Although natural rubber latex (**NRL**) is available in highly concentrated form in stabilized condition attempts to use it as a binder in ceramic shape forming is rarely reported (C. F. Escobar et al., 2015; G. S. Sailaja et al.,2007). In this chapter, we discuss the use of **NRL** as an eco-friendly binder in the powder pressing of alumina. Unlike the spray drying process to obtain the granulated feedstock, the granules for the powder pressing in the present work are prepared through the coagulation of alumina-**NRL** co-dispersions using a formic acid solution. The flow properties of the granules, the green density, and the green strength are presented as a function of rubber concentration. We have also demonstrated green machining of uniaxial pressed alumina bodies using the **NRL** binder.

2.2 Experimental

2.2.1 Materials

A16SG α- alumina powder was procured from ACC Alcoa, Kolkata, India. The ammonia-stabilized concentrated **NRL** was procured from Hindustan Latex Ltd., Thiruvananthapuram, India. The solid content in the concentrated rubber latex was estimated gravimetrically by evaporating the water in a 50 ml beaker at 120 °C. The ammonium poly(acrylate) [Darvan 821A, 40 wt.% aqueous solutions] used as a dispersant was procured from Vanderbilt Company Inc., Norwalk, CA, USA. The ACS grade (98 to 100%) formic acid was supplied by Merck India, Mumbai. Distilled water was used for the preparation of powder dispersions and solutions. The surface area and average particle size of the alumina powder were measured using a surface area analyzer (Micromeritics Tristar II, USA) and a particle size analyzer **(**Nano ZS, Model ZEN 3600, Malvern, UK**)**, respectively. The specific surface area and average particle size of the alumina powder observed are 10.3 m^2/g and 0.34 μm, respectively. The particle size distribution of the alumina powder is shown in **Fig. 2.1a**. The

SEM analysis of the alumina powder shows irregular particle morphology as shown in **Fig.2.1b.**

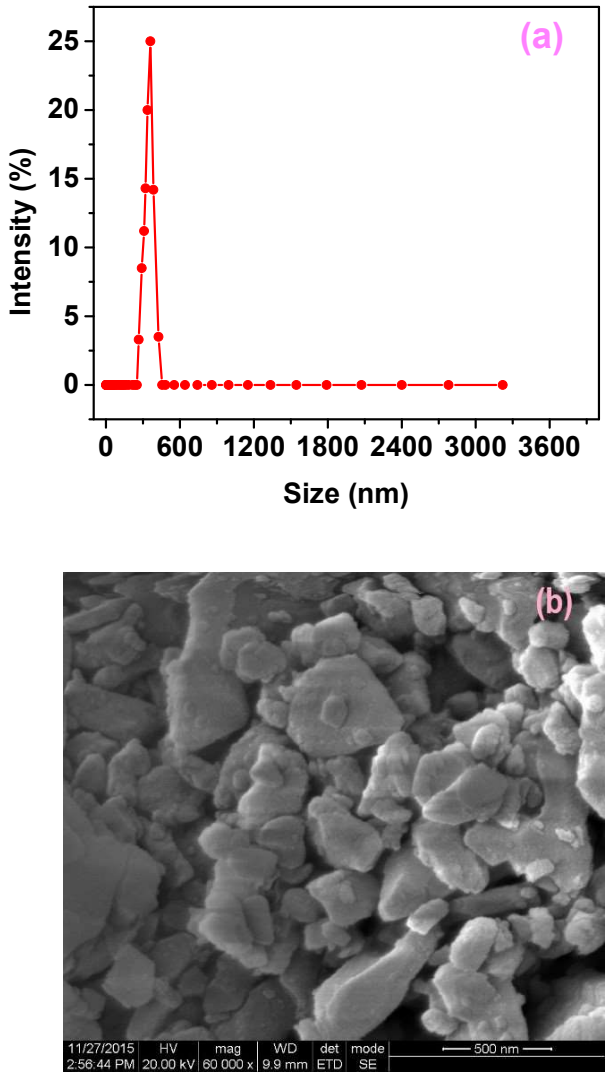

Fig.2.1 Particle size distribution (a) and SEM photomicrograph (b) of A16SG alumina powder

2.2.2 Preparation of feedstock for powder pressing

A 30 vol.% alumina slurry was prepared by dispersing 100 g alumina powder in distilled water using the ammonium poly(acrylate) dispersant in a 250 ml cylindrical

polypropylene bottle. The concentration of the dispersant was 0.4 wt.% of alumina powder. The slurry was ball milled for 12 hours using zirconia grinding media of 10 mm diameter in a roller ball mill. The alumina powder to zirconia ball weight ratio was 1:3. The alumina slurry was transferred into a 250 ml glass beaker and mixed thoroughly with the **NRL** using a magnetic stirrer for 30 minutes. The **NR** concentration in the slurry was varied in the range of 2 to 10 wt.% of the alumina powder. The alumina-**NRL** slurry was added dropwise from a burette into 2 liters of 10 mM formic acid solution under constant stirring using a mechanical stirrer. The stirring was continued for 10 minutes after the complete addition of the alumina-**NRL** slurry. The formed alumina-natural rubber aggregates were allowed to settle for another 30 minutes and the supernatant was decanted. The solid from the slurry was separated using a centrifuge (TC 4100F, Elektrocraft (India) Pvt. Ltd.) and dried at 50°C for 4 hrs. The dried alumina powder-rubber aggregates were ground using a mortar and pestle and sieved through a standard mesh to produce the powder-pressing feedstock. A flow chart for the preparation of alumina powder pressing feedstock is shown in **Fig. 2.2.**

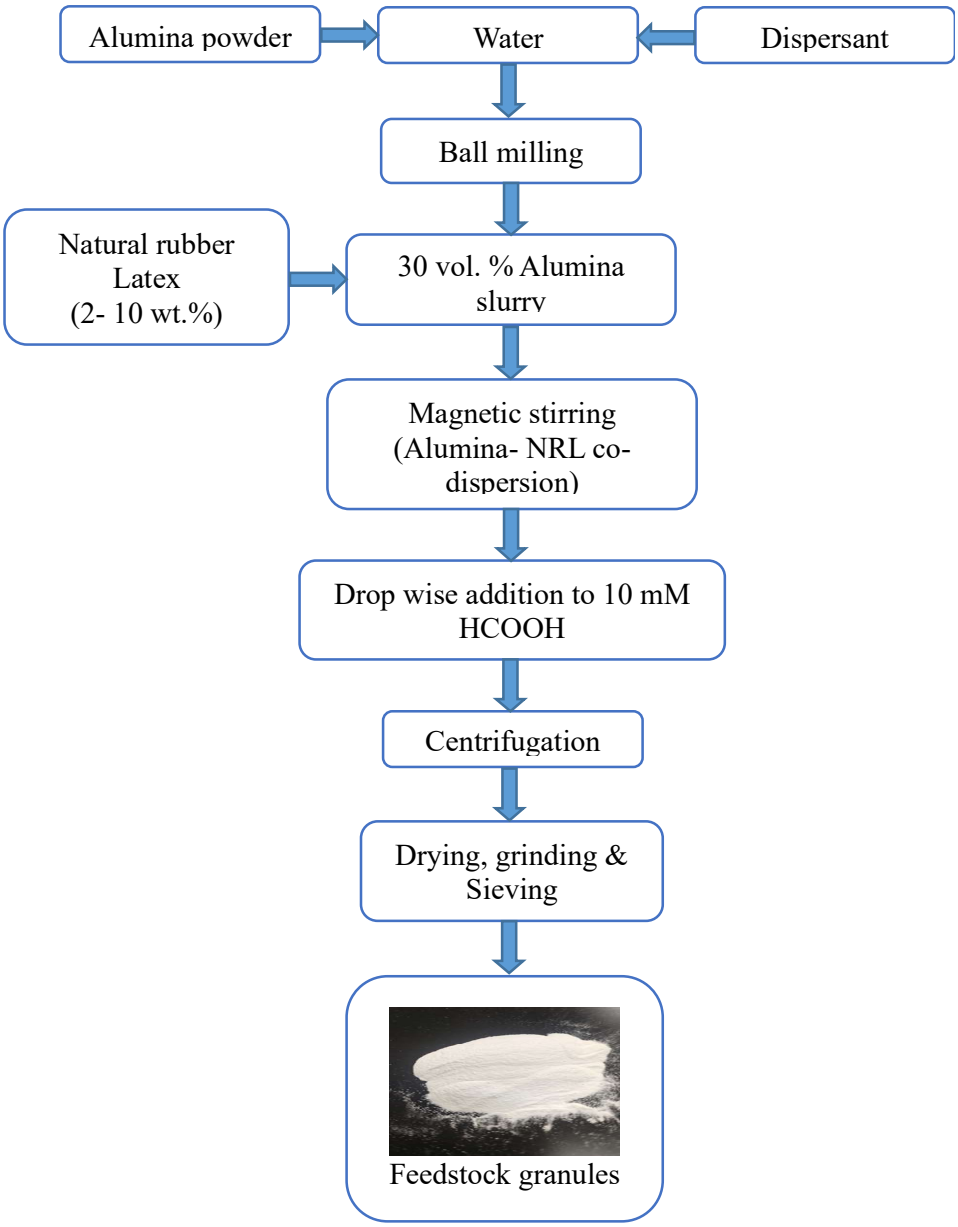

Fig.2.2 The flow chart for the preparation of feedstock granules.

2.2.3 Preparation of powder compacts and sintered ceramics

The powder pressing was carried out using a laboratory model hydraulic press. The feedstock powder filled in a hardened stainless steel mold was pressed uni-axially using a plunger to produce cylindrical green compacts. Green compacts of two different dimensions viz. 13 mm diameter and 5 mm height and 50 mm diameter and 100 mm height were prepared.

The compaction pressure was varied in the range of 5 to 25 MPa. The binder removal and sintering heat treatment of green samples were carried out in an electrically heated high-temperature furnace. The ramp rate was 1°C/min up to 600°C and 5°C/min from 600 to 1550°C. The samples were held for 1 hour at 600°C and 2 hours at 1550°C for completion of binder removal and sintering, respectively.

2.3 Characterization

2.3.1 Ash content & metal ion impurities in natural rubber latex

The ash content of the rubber in the concentrated latex was estimated through gravimetric analysis following ISO 247-1 2018. Ash content was obtained from the weight of the samples using a sartorius weighing balance of readability 0.1 mg before and after being heated to 550°C with a dwell time of 4 h in a muffle furnace. The obtained ash dissolved in dilute nitric acid was analyzed for the metal ion content using an inductively coupled plasma-optical emission spectrometer **(**ICP-OES, Optima 4300 V, Perkin Elmer, USA**).**

2.3.2 The solid content in natural rubber latex

The total solid content in natural rubber latex was analyzed as per ISO-124 2014. A known weight of **NRL** taken in a 50 ml beaker was heated in an air oven at 100 °C for 2h. The solid content was calculated from the weight of the initial latex and the final weight of rubber retained in the beaker.

2.3.3 Zeta potential analysis

The changes in zeta potential with pH were measured for the alumina powder dispersions, the **NRL**, and alumina-**NRL** co-dispersions using a Zetasizer (Nano ZS, Model ZEN 3600, Malvern, UK). A 0.1 wt.% suspension in distilled water was used for the zeta potential measurement. The pH adjustment of the suspensions was done using dilute HCl and NaOH solutions.

2.3.4 Particle size distributions

The particle size distribution of **NRL** was analyzed using a nano particle size analyzer (Nano ZS, Model ZEN 3600, Malvern, UK). The particle size distribution of alumina, **NRL**, and the alumina-**NRL** co-dispersions containing various amounts of natural rubber after the formic acid coagulation was analyzed using a Malvern Master Sizer 2000, UK.

2.3.5 Moisture content

The % moisture content in the powder pressing feedstock was estimated from the weight loss of the sample heated at 100 ℃ in an air oven for 4 hours using equation (6).

$$\text{Moisture content}=\frac{(M_{before}-M_{after})}{M_{before}}\times 100 \qquad \textbf{(6)}$$

where M_{before} is the mass of the sample before heating and M_{after} is the mass of the sample after heating at 100℃ for 4 hours.

2.3.6 Measurement of the flow time of powder pressing feedstock

The flow time of the powder pressing feedstock was measured using a standard funnel with a mouth diameter of 70 mm, tail diameter of 10 mm, and a tail length of 40 mm. 40 g of the powder pressing feedstock was transferred to the funnel, and time taken for the same to pass through the tail under gravity is noted. The reported values are the average of four measurements.

2.3.7 Measurement of Hausner ratio

The bulk density was estimated by measuring the volume of 10 g of the powder pressing feedstock in a 20 ml graduated measuring cylinder. The tapped density was estimated from the volume of the feedstock taken in the measuring cylinder after tapping on a rubber pad. 25

numbers of tapping were done before volume measurements in all the samples. The Hausner ratio was obtained as the ratio of tapped density to bulk density.

$$\text{Hausner ratio} = \frac{Tapped\ density}{Bulk\ density}$$

2.3.8 The density of the green and sintered bodies

The density of the green bodies was calculated from their masses and dimensions. The dimensions were measured using a Vernier caliper. The density value reported was an average of six measurements. The sintered density was measured by Archimedes' principle using the equation (7).

$$\text{The density of the sample} = \left({}^{M_{air}}/_{(M_{air} - M_{water})}\right) \qquad \textbf{(7)}$$

Where M_{air} is the mass of the sintered body in the air and M_{water} is the apparent mass of the body in water.

2.3.9 Green strength

The diametrical compressive strength of the as-prepared and annealed green bodies was measured using a universal testing machine (Instron 5500, USA). The diametrical compressive load-displacement measurement was carried on cylindrical alumina green bodies of 13 mm diameter and 5 mm height. The loading rate was 0.5 mm/min. The diametrical compressive strength was calculated using equation (8).The diametrical compressive strength values reported are averages of measurement made on six identical samples.

$$\boldsymbol{\sigma_f = \frac{2F_{max}}{\pi D h}} \qquad \textbf{(8)}$$

Where $\boldsymbol{F_{max}}$is the load at fracture, $\boldsymbol{D}$ is the diameter and $\boldsymbol{h}$ is the height of the sample.

2.3.10 Machinability of the green compacts

The machinability of the green compacts was checked by making rectangular slots by milling, holes by drilling, and recessed steps by lathing on a powder pressed body of 50 mm diameter and 100 mm height after annealing at 200°C. The machining was performed using the respective conventional machines and high-speed steel tools.

2.3.11 Thermogravimetric analysis

The TGA analysis of the green alumina samples was performed in an air atmosphere using a thermo-gravimetric analyzer (Q-50, TA Instruments, USA). The heating rate was 5°C/min.

2.3.12 Microstructure analysis

The microstructure of feedstock powders, green body, and sintered alumina ceramic samples was examined using a scanning electron microscope (FESEM, Carl Zeiss Gemini 500 field emission microscope, Germany). The samples were sputter-coated with Au-Pd alloy before the SEM analysis. The microstructure of green and sintered ceramics was observed on fractured surfaces. The size of feedstock granules was measured from the SEM micrographs using ImageJ software. The average grain size of the sintered alumina ceramic was measured from the respective micrograph using the linear intercept method.

2.4 Results and Discussion

2.4.1 Characterization of natural rubber latex

The solid content in the concentrated **NRL** is estimated as 61.6 wt. %. The ash content in natural rubber is 0.3 wt. % which is comparable to that of the other polymer binders (X. K. Wu et al.,1997). The metal ion impurities in natural rubber estimated by ICP-MS analysis of the ash dissolved in dil. HNO_3 solution are 0.083 wt. % of Ca, 0.019 wt. % of Mg, 0.011 wt. % Zn and 0.017 wt. % of aluminum. The particle size of **NRL** is in the range of 0.1 to 2 μm

with an average size of 0.5 µm. The particle size distribution graph of the **NRL** is given in **Fig.2.3**.

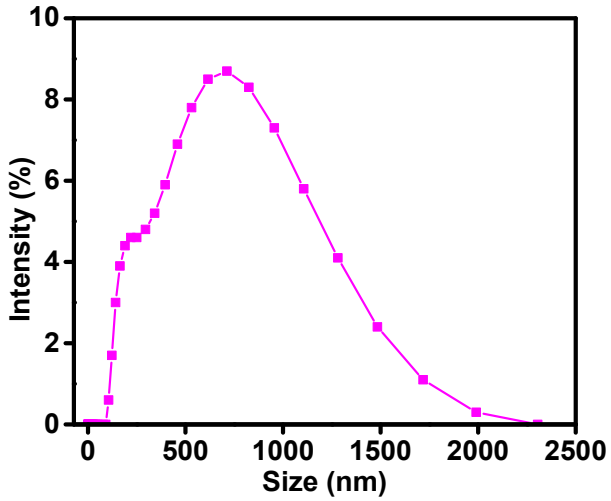

Fig.2.3 Particle size distribution of the **NRL**

2.4.2 Preparation of powder pressing feedstock

Powder pressing requires a uniform mix of ceramic powder and a polymeric binder having adequate flow properties as the feedstock. Conventionally, powder pressing feedstock is prepared by spray drying the ceramic powder dispersed in a binder solution. Contrary to this, in the present work, the co-coagulation of alumina powder-rubber latex co-dispersions has been used as a means of preparing a uniform powder-binder mix for pressing. Herein, the alumina powder forms a well-dispersed aqueous suspension in the presence of an ammonium poly(acrylate) dispersant. **Fig. 2.4** depicts the effect of pH on the zeta potential of alumina, **NRL**, and alumina-**NRL** co-dispersions. Generally, zeta potential is a measure of electrostatic repulsion between the charged particles, and a value ≥ 40 mV is considered highly stable colloidal dispersions (H. Bijarbooneh et al., 2013). In the present case, the pH and zeta potential values of the prepared aqueous alumina powder suspension are 9.6 and -57 mV, respectively.

The carboxylic acid group of ammonium poly(acrylate) adsorbed on alumina particles undergo ionization in the basic medium and stabilizes the particles electrostatically. In addition, the adsorbed ammonium poly(acrylate) provides steric stabilization to the particle as well (J. Davies et al.,2000; H Kamiya et al.,1999). The stabilized **NRL** also exhibits a pH and zeta potential value of 10.7 and -58 mV, respectively. The latex particles are electrostatically stabilized due to the ionization of surface carboxylic acid groups of proteins and lipids present on their surface (K. Nawamawat et al.,2011; J. Sansatsadeekul et al.,2011). As the alumina and rubber latex particles have negative surface charges, the aqueous alumina powder suspension and stabilized **NRL** easily mix to form a co-dispersion. The alumina powder suspension dispersed using the ammonium poly (acrylate) shows an I.E.P of 3.5. The I.E.Ps of both rubber latex and alumina-**NRL** co-dispersion are located at a pH of 4.1.

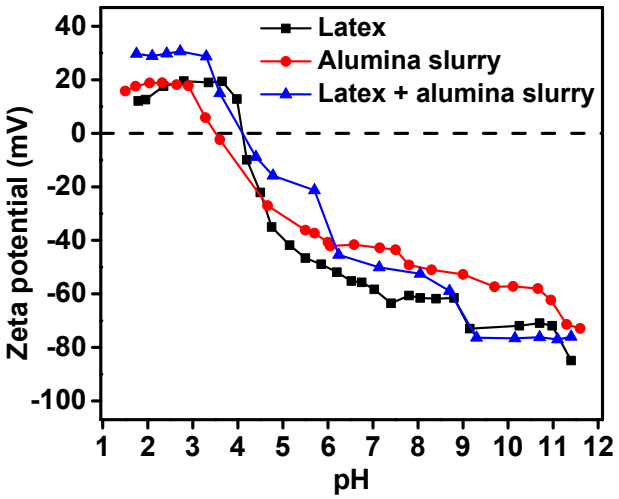

Fig. 2.4 The effect of pH on zeta potential of alumina, **NRL**, and alumina-**NRL** co-dispersions.

The coagulation of the co-dispersion can be accomplished by adjusting the pH to ~4 which is the I.E.P of the ammonium poly(acrylate) dispersed alumina powder-rubber latex co-dispersion. The 10 mM formic acid solution shows a pH of ~3. The pH of the formic acid

solution shifts to 4±0.2 up on the addition of alumina powder-rubber latex co-dispersion containing 100 g alumina to 2 liters of 10 mM formic acid solution affecting their co-coagulation. It has been observed that drop-wise addition of **NRL** to 10 mM formic acid solution under stirring results in the formation of bulky rubber precipitate which either sticks to the stirrer paddle or walls of the beaker. On the other hand, the rubber is not separated as a bulky precipitate when the alumina powder-rubber latex co-dispersion with rubber concentrations up to 10 wt.% of the alumina powder is added dropwise to the 10 mM formic acid solution under stirring. Instead, the co-dispersions slowly settle leaving a clear supernatant once the stirring stopped. To follow the sedimentation behavior, 100 ml of the acidified co-dispersion was taken in graduated measuring cylinders and the sediment volume is monitored with time. The sediment volume as a function of time is presented in **Fig.2.5**. The sedimentation rate of coagulated alumina dispersion is slow. On adding 2 wt.% natural rubber, a marginal increase in the sedimentation rate is observed. There is a significant increase in the sedimentation rate when the rubber concentration increases from 2 to 4 wt.%. Further increase in natural rubber concentration up to 10 wt.% produces a gradual increase in sedimentation rate. The sedimentation rate of a coagulated suspension depends on the size of the particle agglomerate produced during coagulation. The particle size distribution of the coagulated alumina powder-rubber latex co-dispersions containing various concentrations of rubber latex is shown in **Fig.2.6**. The coagulated alumina and alumina-rubber latex co-dispersions show uni-modal particle size distributions. The particle size distribution becomes wider as we increase the rubber latex concentration. The average particle size of alumina suspension increases from 0.34 to 1.64 μm during coagulation by formic acid. The incorporation of 2 wt.% of rubber latex produces a marginal increase in average particle size (2.27 μm) of the coagulated alumina-rubber latex co-dispersion. On the other hand, a further increase in rubber latex concentration rapidly increases the average particle size of coagulated alumina powder-

rubber latex co-dispersion. The average particle size increases from 2.27 to 12.30 μm when the rubber latex concentration increases from 2 to 10 wt.% of alumina.

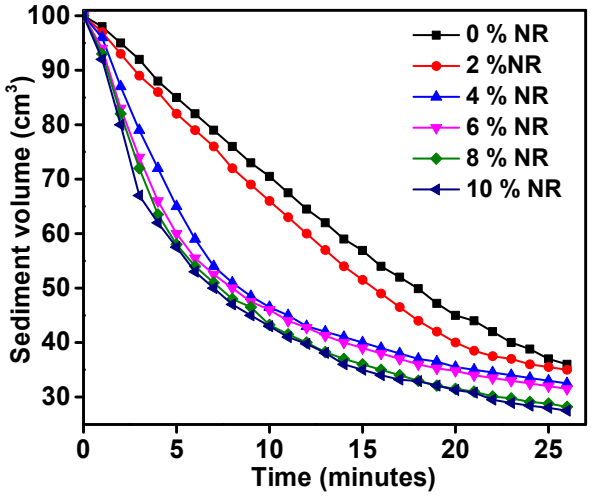

Fig.2.5 The effect of **NRL** concentration on the sedimentation behavior of coagulated alumina-**NRL** co-dispersion.

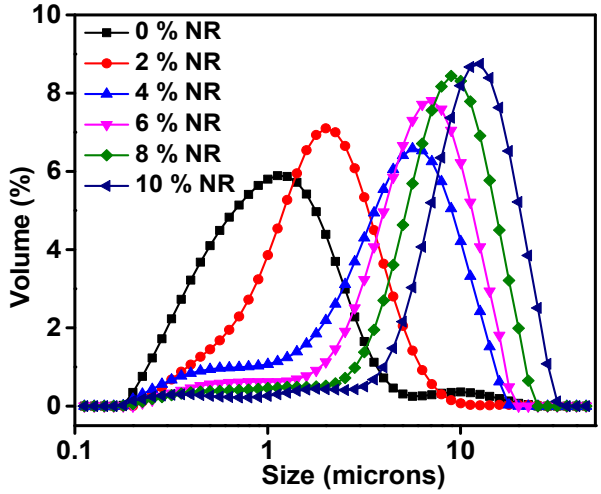

Fig.2.6 The effect of **NRL** concentration on the particle size distribution of coagulated alumina-rubber latex co-dispersions.

When the alumina-rubber latex co-dispersion is added to a 10 mM formic acid solution, the surface charge of both alumina and rubber latex particles changes from a high negative value to close to zero. This results in particle agglomeration due to Van der Waals attraction. There are possibilities for the self-agglomeration of alumina and rubber particles and their co-agglomeration. At lower rubber latex concentrations, there is a low probability of self-agglomeration of rubber latex particles. Instead, the smaller alumina particles (average particle size-0.34 μm) get attracted to the larger rubber latex particles (average particle size-0.5μm) leading to their agglomeration. As rubber latex concentration increases, the probability of self-agglomeration of rubber particles increases. However, the growth of the rubber particle to the stage of a bulky precipitate is prevented by the alumina particles on their surface. On the other hand, we have observed precipitation and separation of rubber latex during the coagulation of alumina powder-rubber latex co-dispersions containing rubber latex concentration higher than 14 wt.%. **Fig.2.7** shows a photograph of the precipitated natural rubber on the sides of the beaker and the stirrer paddle from an alumina powder-rubber latex co-dispersion containing 15 wt.% of rubber. This indicates that at higher rubber latex concentrations, growth by the self-agglomeration of rubber particles is fast enough to form a bulk precipitate.

Fig.2.7 Photograph showing the rubber precipitate formed on the walls of the beaker and stirrer paddle at a rubber concentration of 15 wt.%.

2.4.3 Flow properties of powder pressing feedstock

The powder pressing process demands good flow properties for the granulated powder feedstock for a continuous process and maintaining uniformity among the green bodies. Generally, the flow rate and Hausner ratio are some of the standard parameters measuring the flow property of a granulated powder (R. B. Shah et al., 2008; R.O. Grey et al., 1969). The relative flow property at various rubber concentrations is evaluated by measuring the time of flow of 40 g of alumina powder pressing feedstock through a glass funnel with a tail diameter of 10 mm. The alumina powder pressing feedstock without natural rubber and with 2 wt.% natural rubber take 41 and 20 seconds, respectively, to flow through the funnel even after several taping due to their poor flow property. On the other hand, the alumina powder pressing feedstock prepared using 4 to 10 wt.% rubber concentration flows through the funnel without tapping. The flow time decreases from 13 to 5 seconds when the rubber concentration increases from 4 to 8 wt.%. Further, an increase in rubber concentration to 10 wt.% results in an increase in flow time to 11 seconds. This observed trend in the flow time is further supported by calculating the Hausner ratio, the ratio of tapped density to the bulk density, of the powder pressing feedstock. Granulated powders with a Hausner ratio of less than 1.25 are considered to have good flow properties (A. Crouter et al., 2014). The feedstock containing 6 and 8 wt.% natural rubber exhibited a Hausner ratio of 1.23 and 1.07, respectively. The lowest flow time and Hausner ratio for the feedstock containing 8 wt.% natural rubber indicate its superior flow property. The observed trend in the flow time and Hausner ratio of the powder pressing feedstock may be due to the difference in the size distribution and morphology of the particle aggregates. The SEM micrographs of feedstock granules prepared at various natural rubber concentrations are given in **Fig.2.8.**

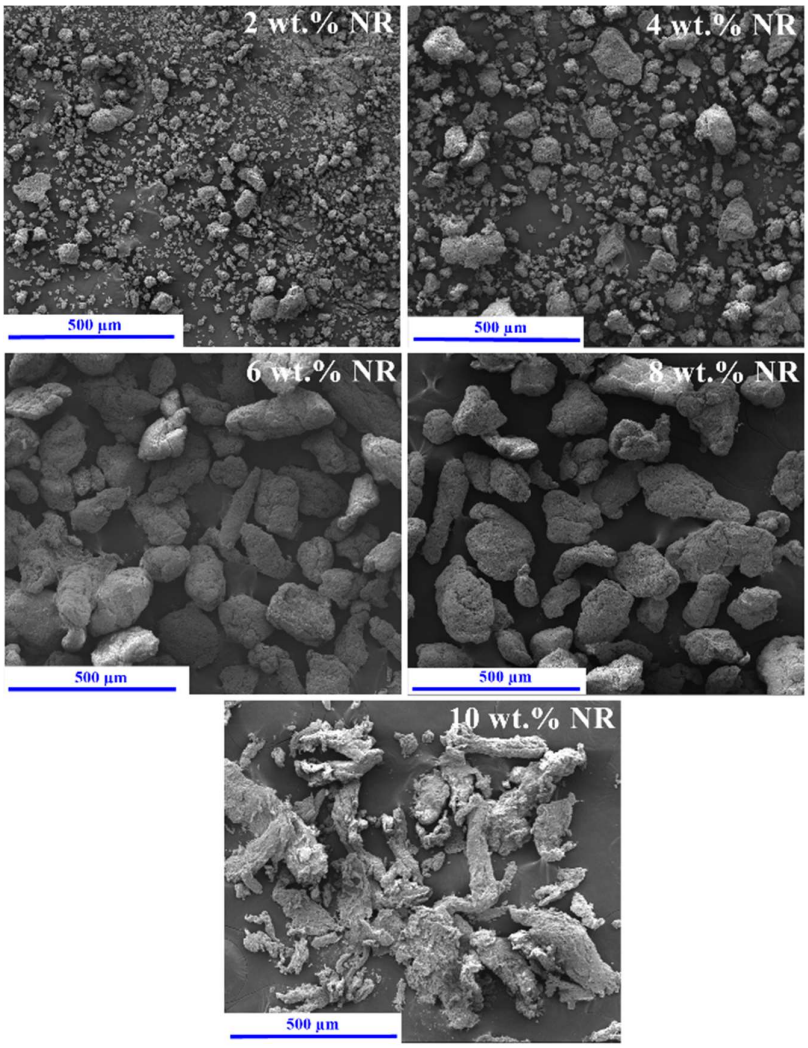

Fig.2.8 The SEM micrographs of powder pressing feedstock prepared at various natural rubber concentrations.

The powder-pressing feedstock contains granules of both irregular and near-spherical shapes. The size and shape of granules depend on the rubber concentration. The feedstock prepared at 2 and 4 wt.% rubber concentrations contain finer granules and the population of finer granules is more for the feedstock containing 2 wt.% rubber. The granule sizes observed at 2 and 4 wt.% rubber concentrations are in the ranges of 5 to 75 and 5 to 100 µm, respectively. The feedstocks prepared at 6 and 8 wt.% rubber concentrations contain granules of similar morphology and size distribution. The observed granule sizes are in the range of 50 to 250 µm. On the other

hand, the feedstock prepared at a rubber concentration of 10 wt.% depicts elongated granules with flaky morphology. Further, the large population of finer granules present at 2 and 4 wt.% rubber concentrations and elongated flaky morphology of granules at 10 wt.% natural rubber concentrations, respectively, are responsible for their poor flow property. The bulk density, tapped density, Hausner ratio, and flow time of alumina powder pressing feedstock prepared at various natural rubber concentrations are given in **Table 2.1**.

Table 2.1 The effect of rubber concentration on flow time, bulk density, tapped density, and Hausner ratio of powder pressing feedstock.

Rubber concentration (wt.%)	**Flow time (s)**	**Bulk density (gm/cc)**	**Tapped density (gm/cc)**	**Hausner ratio**
0	41	0.72	1.26	1.75
2	20	0.89	1.36	1.52
4	13	0.7	1.15	1.64
6	7	0.65	0.8	1.23
8	5	0.88	0.95	1.07
10	11	0.49	0.63	1.28

2.4.4 Compaction behavior of feedstock

During pressing in a mold, the particle aggregates present in the feedstock deform under relatively low pressure due to the low glass transition temperature of natural rubber. The effect of compaction pressure on the green density of powder compact obtained from alumina powder pressing feedstock at a rubber concentration of 10 wt.% is shown in **Fig.2.9**. The green density of the powder compacts increases from 64.1 to 67.7% of the theoretical density of alumina

when the compaction pressure increases from 5 to 20 MPa. Further, an increase in compaction pressure to 25 MPa does not have a significant effect on the green density. Therefore, a compaction pressure of 20 MPa is subsequently used for the preparation of green bodies. The optimum compation pressure in the present case is much lower than that used for powder pressing with the conventional binders which is reported in the range of **20 to 100 MPa** (J.S.Reed., 1995). A higher green density achieved at lower compaction pressure is due to the highly deformable nature of natural rubber binder at room temperature.

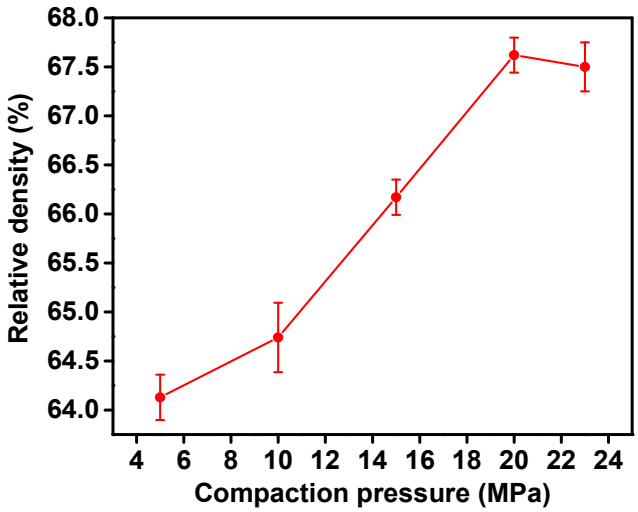

Fig.2.9 The effect of compaction pressure on the green density of alumina (rubber concentration 10 wt.% of alumina).

The alumina feedstock prepared at various rubber latex concentrations, except for 2 wt.%, exhibits good compaction behavior as evidenced by the defect-free green compacts produced with a high green density. Nevertheless, many of the green compacts prepared from the alumina feedstock at 2 wt.% rubber show defects such as end-capping which is shown in **Fig.2.10**. End-capping is a central cone-shaped separation occurred at the punching face during spring back due to poor strength of the green bodies (S. J. Glass et al.,1997; G. W. Egeland et al., 2010). It is inferred that the 2 wt.% rubber is not enough to provide sufficient strength to

the green compact to resist end-capping due to differential spring back. Therefore, the alumina feedstock prepared at a rubber concentration of 2 wt.% is discarded from further studies.

Fig.2.10 The photograph shows the end-capping defect noticed on the green compacts prepared using 2 wt.% rubber content.

The powder compact density increases with an increase in rubber concentration in the alumina powder pressing feedstock. The powder compact density increases from 63.6 to 67.7 % of the theoretical density of alumina when rubber concentration increases from 4 to 10 wt.%. It appears that the increase in rubber concentration increases the plasticity of the alumina feedstock which promotes powder compaction. The effect of rubber concentration on the density of alumina powder compacts prepared at a compaction pressure of 20 MPa is shown in **Fig.2.11**. The uniform powder compaction in the pressed samples is further evidenced by their uniform microstructure. The microstructure indicates the absence of particle aggregates in green ceramics. A typical SEM microstructure of the fractured surface of a green body and the EDS elemental mapping for aluminium, oxygen and carbon (indicating NR) are shown in **Fig.2.12.** It is clearly seen that the alumina ceramic particles and natural rubber binder are uniformly distributed throughout the green body. The photograph of cylindrical green compacts of various sizes prepared using **NRL** binder is shown in **Fig.2.13.**

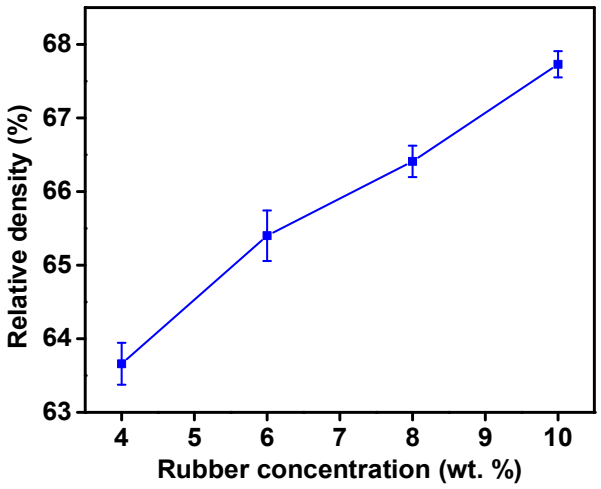

Fig.2.11 The effect of the rubber concentration on the green density of alumina.

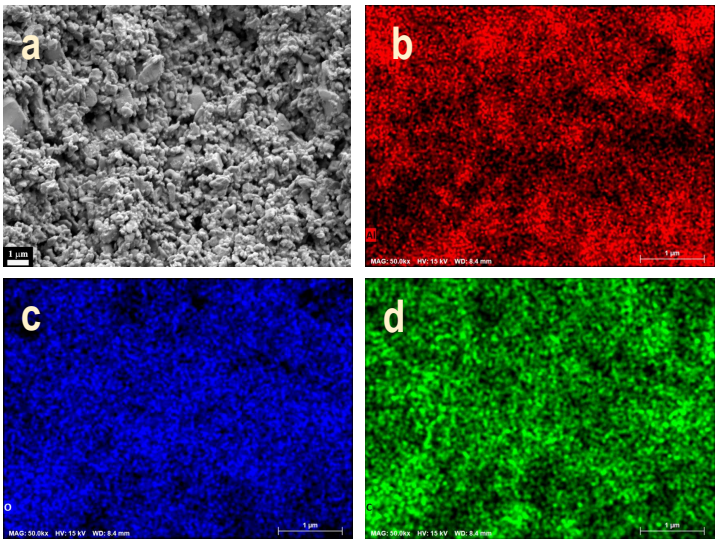

Fig. 2.12 a) Typical microstructure of fractured surface of green alumina sample prepared by powder pressing using **NRL** binder, b) EDS elemental mapping of aluminium, (c) oxygen and (d) carbon in the green body.

Fig.2.13 The photograph of alumina green bodies of various sizes prepared by powder pressing using **NRL** binder

2.4.5 Effect of annealing of pressed compacts on green strength

It is obvious to note that the strength of as-prepared green compacts increases with an increase in natural rubber concentration. The diametrical compressive strength of green bodies increases from 0.55 to 1.91 MPa when natural rubber concentration increases from 4 to 10 wt.%. The increase in strength is due to better compaction and binding of alumina particles achieved with an increase in rubber concentration. This moderate green strength of 0.55 to 1.91 MPa achieved is enough for the handling of the green bodies during further processing. However, this much green strength is not sufficient to carry out green machining. It has been reported that rubber undergoes a higher degree of thermal cross-linking through the double bonds present in the isoprene units in the presence of metal oxides (A. Smejda-Krzewicka et al., 2020). The cross-linking of the binder is expected to increase the strength of green bodies. To verify this and optimize the cross-linking temperature, the powder compacts prepared at 6 wt.% natural rubber concentration are heat-treated at various temperatures in the range of 60 to 240℃ for 2 hours and then evaluated for their diametrical compressive strength. The diametrical compressive strength of green compacts remains the same up to 100℃ and then increases slowly with heat-treatment temperature up to 140℃. Further, the diametrical compressive strength rapidly increases with an increase in heat-treatment temperature up to 220℃ and then decreases. This indicates that the optimum level of cross-linking of natural

rubber in alumina green compact is achieved at 220 ℃. The schematic structure of the cross-linked rubber is presented in **Fig.2.14**.

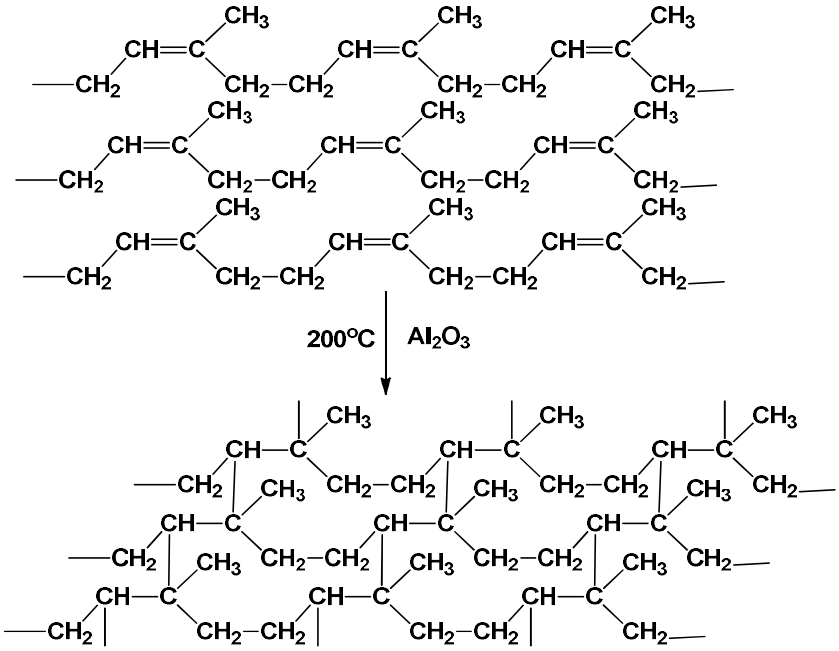

Fig.2.14 The schematic structure of cross-linked natural rubber.

The diametrical compressive strength observed at the optimum cross-linking is ~5.8 times that obtained before cross-linking. The effect of heat-treatment temperature on the diametrical compressive strength of alumina powder compacts prepared at 6 wt.% natural rubber binder is shown in **Fig.2.15**. The decrease in diametrical compressive strength at a heat-treatment temperature above 220℃ is due to the considerable decomposition of the natural rubber which is evidenced by the thermo-gravimetric analysis.

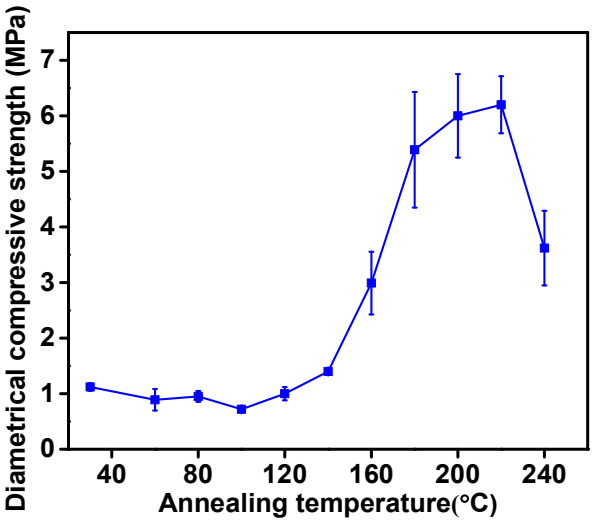

Fig.2.15 Effect of annealing temperature on the diametrical compressive strength of alumina green bodies prepared at a natural rubber concentration of 6 wt. %.

The cross-linking of rubber not only increases the strength but also changes the nature of failure during diametrical compression as evidenced by the load-displacement graph shown in **Fig.2.16**. The photograph of the green bodies after the diametrical compressive strength test that differentiated the nature of fracture before and after cross-linking is shown in **Fig.2.17**. The samples before cross-linking show a ductile region in the load-displacement graph after the formation of the crack due to sagging. This is due to the deformable nature of the uncross-linked rubber binder. On the other hand, the cross-linked samples show completely brittle failure and break into several pieces at the maximum load. Correspondingly, the load-displacement plots show only elastic regions with a high Young's modulus. Here, the deformation of the rubber binder is restricted due to the formation of the cross-links.

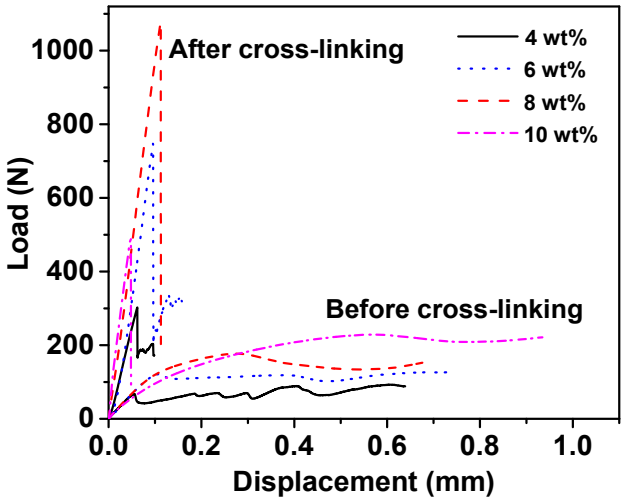

Fig.2.16 The diametrical compressive load-displacement graph of alumina green bodies prepared at various rubber concentrations before and after rubber cross-linking.

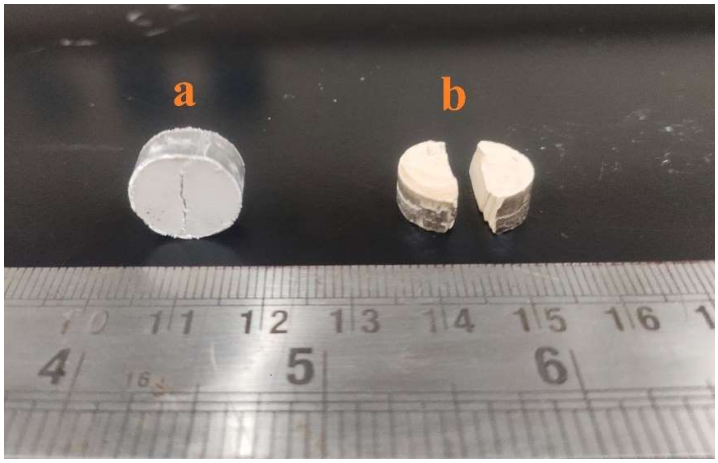

Fig.2.17 The photographs of the green bodies after the diametrical compressive test (a). before cross-linking and (b) after cross-linking

The alumina powder compacts prepared at 4 and 8 wt.% rubber after cross-linking shows 4.2 and 6.1, respectively, times the diametrical compressive strength before cross-linking. On the other hand, at 10 wt.% rubber concentration, the diametrical compressive strength of powder compacts after rubber cross-linking is only 2.3 times the original value. The

decrease in diametrical compressive strength observed at 10 wt.% rubber is explained as follows. As rubber concentration increases, the thickness of the binder between the alumina particles also increases. There is an optimum thickness below which the failure occurs by debonding at the alumina particle-binder interface. At binder thickness above the optimum level, cracks are generated in the thick brittle binder layer rather than the alumina-binder interface leading to failure at a low-stress level. It appears that the alumina-cross-linked rubber interfacial bond strength is higher than the cohesive strength between the cross-linked rubber molecules. The effect of rubber concentration on the diametrical compressive strength of powder compacts before and after the cross-linking heat treatment at 220℃ is shown in **Fig.2.18**. The maximum diametrical compressive strength (9.3 MPa) of green alumina bodies obtained is higher than that reported with most of the other binders. The diametrical compressive strength of alumina green bodies prepared using various binders reported in the literature is presented in **Table 2.2**

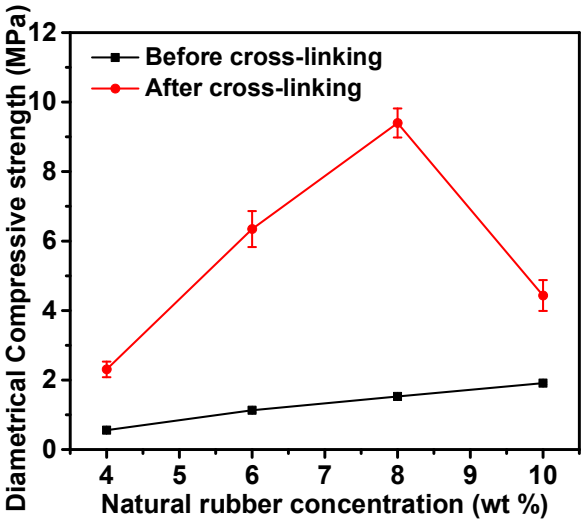

Fig.2.18 Diametrical compressive strength of alumina green bodies prepared at various rubber concentrations before and after the rubber cross-linking.

Table 2.2 The diametrical compressive strength of alumina green bodies reported using various binders.

Binder	Diametrical compressive Strength (MPa)	Binder Concentration (wt.%)	Method of preparation
Polyvinyl alcohol	0.6	3	Uniaxial pressing (S. Baklouti et al., 1998)
Polyethylene glycol	0.3	3	
Polyurethane	7	5	Uniaxial pressing (M. Potoczek et al., 2003)
Polyvinyl alcohol	~0.9	5	
Polyethylene glycol	~0.4	5	
Acrylic Duramax^{TM}B-1007	~0.9	5	Uniaxial pressing (X.K. Wu et al., 1997)
Acrylic Duramax^{TM}B-1020	~1.2	5	
Polyvinyl alcohol	0.16±0.03	3.07	Uniaxial pressing + Isostatic pressing (S.D. Nunn et al.,1996)
Polyvinyl alcohol +PEG	0.60±0.20	3.75 + 1.25	
Duramax^{TM} B-1031	6.5	5	Uniaxial pressing (X.L.K. Wu et al., 1995)
PVX-35 co-polymer containing –COOH and –OH groups	4.5	1.5	Uniaxial pressing (M.R. Ben Romdhane et al., 2007)
Sucrose	5.5	7.2	Uniaxial pressing (A. Kumar et al., 2014)
Gel casting using acrylamide	3	4-5	Uniaxial pressing (S.D.Nunn et al.,1994)
NRL	9.4	8	Uniaxial pressing (Present study)

2.4.6 Green Machining

Green machining of pressed powder compact is an efficient way to achieve near-net-shape ceramics as the machining of sintered ceramics consumes a large amount of energy and time (B. Su et al.,2008; S. Mohanty et al.,2013). To accomplish machining the green powder compacts should have sufficient strength to hold them in the conventional machines (S. D. Nunn et al., 1994). The alumina green bodies prepared at 6 and 8 wt.% natural rubber have sufficient strength to hold them in conventional machines without any damage due to rubber cross-linking during annealing at 220ºC. They could be machined by cutting recessed steps by lathing, rectangular slots by milling, and cylindrical holes by drilling. **Fig.2.19** is a photograph showing recessed steps, a rectangular slot, and a hole machined on cylindrical alumina green bodies prepared using the natural rubber binder.

Fig.2.19 Photograph of cylindrical alumina green bodies with rectangular slots, recessed steps, and a cylindrical hole made by milling, lathing, and drilling, respectively.

2.4.7 Binder removal and sintering

The thermal degradation of natural rubber takes place in two stages. The first stage of decomposition is at temperatures in the range of 235–385°C where almost 80 % of weight loss takes place. The major degradation products of natural rubber are small molecules such as isoprene, dipentene, and small amounts of p-menthene (N. Ahmad et al.,2016). The second stage at temperatures in the range of 440 – 530 °C is due to the decomposition of carbonaceous residues formed in the first stage. Approx.0.30 % of ash content is retained after 530°C. The observed ash content is comparable with that of other binders reported in the literature (X.K. Wu et al.,1997). The ash content reported for PEG, PVA, and acrylic binders is 0.4, 0.4, and 0.2 wt. %, respectively. The decomposition of natural rubber from the as-pressed green alumina sample shifted to a lower temperature. That is, the decomposition of rubber from the green alumina samples starts at a temperature of ~205℃ and ends at 490℃. This indicates that the alumina powder catalyzes the decomposition of natural rubber binder. On the other hand, the decomposition of binder from the alumina green body annealed at 220℃ is observed at a considerably higher temperature compared to that from the as-pressed samples. This is due to the higher thermal stability of the cross-linked binder (G.F. Levchik et al.,1999). It is interesting to note that the cross-linked rubber binder in the alumina green body exhibited a near steady-state decomposition. It has been reported that the binder with steady-state decomposition undergoes burn-out without creating any cracks. That is, the cross-linking of the rubber binder in the powder-pressed bodies not only improves diametrical compressive strength to aid green machining but also favors slow and near steady-state binder burnout. The TGA of neat natural rubber, green alumina samples containing uncross-linked and cross-linked (after annealing at 220 ºC) natural rubber binder is shown in **Fig.2.20**. The lower weight loss observed in the TGA of green alumina sample after annealing heat treatment is due to the removal of proteins, lipids and carbohydrates which are present in natural rubber during the annealing heat treatment.

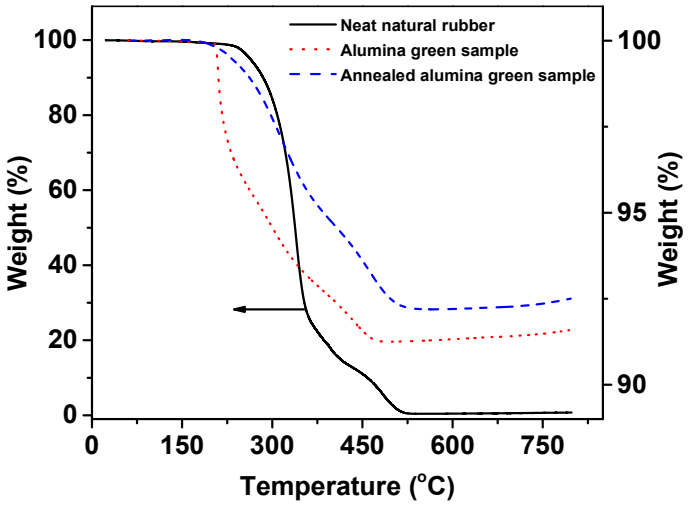

Fig.2.20 TGA of neat natural rubber, green alumina sample containing uncross-linked and cross-linked natural rubber binder (The NRL content in the green body is 8 wt.%)

The burn-out of cross-linked natural rubber binder by heating at a rate of 1°C/minute up to 600°C does not create any crack or deformation in cylindrical alumina bodies subjected to green machining. The binder removed bodies sintered to 97% of the theoretical density of alumina at 1550ºC. A linear sintering shrinkage of ~18% is observed. The photograph of sintered alumina bodies is presented in **Fig.2.21a**. The densification achieved is further evidenced by the microstructure. The SEM photomicrograph of the fractured surface of the sintered alumina ceramics is shown in **Fig.2.21b.** The microstructure shows a combination of inter-granular and transgranular fracture. The average grain size calculated from the SEM image using the linear intercept method is 1.8 μm.

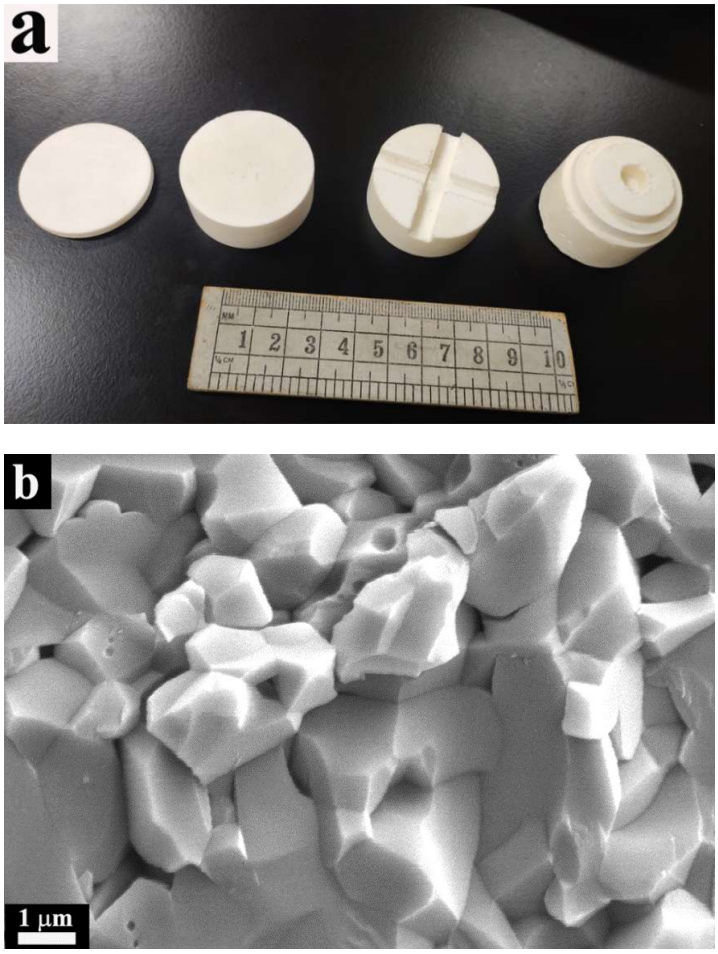

Fig.2.21 Photograph of sintered alumina bodies (a) and SEM photomicrograph of the fractured surface of the sintered alumina ceramics (b). The rectangular slots, recessed steps, and cylindrical holes are made by milling, lathing, and drilling, respectively, in the green state.

2.5 Conclusions

The study establishes **NRL** as a binder for the dry pressing of alumina powder. Instead of the spray drying method, the co-coagulation of alumina and rubber latex particles from their aqueous co-dispersions using formic acid followed by centrifugation, drying, and grinding is used for the preparation of the alumina powder-pressing feedstock. The alumina slurry mixes well with **NRL** easily and forms co-dispersions by the electrostatic stabilization due to the high

negative potential of alumina and rubber particle surfaces The formation of rubber aggregates at rubber concentrations in the range of 2 to 10 wt.% is prevented by the co-coagulation of alumina and rubber particles. Coagulation leading to the formation of the rubber precipitate is observed at a rubber concentration > 14 wt.%. The feedstock prepared at 6 and 8 wt.% natural rubber exhibits good flow properties as evidenced by their low flow time through a funnel and low Hausner ratio. A low compaction pressure of 20 MPa is sufficient to achieve a high green density of 67.7 % T.D due to the easily deformable rubber binder with a low glass transition temperature. The strength of pressed alumina powder compacts increases from 0.55 to 1.91 MPa when the rubber concentration increases from 4 to 10 wt.%. A remarkable increase in green strength (almost six times) is observed by annealing the pressed powder compacts at 220°C due to the cross-linking of the rubber binder in presence of alumina. A high diametrical compressive strength of 9.4 MPa obtained for the alumina green bodies with 8 wt.% rubber concentration is one of the highest values achieved for green bodies produced by powder pressing. Green bodies after annealing at 220°C are amenable to machining such as lathing, milling, and drilling using conventional machines and tools. The near steady-state burn-out of cross-linked rubber binders from the green body is advantageous for producing crack-free ceramics. The alumina ceramics sintered at 1550°C for 2 hours show a density of ~97% of the theoretical value. The microstructure analysis indicates intra-granular fracture and an average grain size of 1.8 μm.

Chapter 3

Slip casting of alumina using natural rubber latex as a binder

3.1 Introduction

Slip casting is a widely used shape-forming process in both traditional and advanced ceramic industries that produces ceramic components such as pottery, ceramic membranes, multi-layered composites, functionally graded ceramic structures, textured ceramics, and transparent ceramics (C. Hu et al.,2011; L. Jin et al., 2010; S. K. Amin et al.,2016). The major benefits of slip casting are simple, low production cost, high-density green bodies, and the capability to manufacture large and complex shape components. However, the longer time required for consolidation, non-uniform distribution of binder, and difficulty in green machining due to the poor green strength are the major limitations. Water is the preferred suspension medium for the preparation of slurries for slip casting due to its high availability, low cost, and environmental friendliness (D. W. Richerson et al.,2018; E. F. Adams.,1971). Water soluble binders such as polyvinyl alcohol (PVA), methylcellulose (MC), and carboxymethyl cellulose (CMC) are reported for the slip casting of ceramic powders (C.Falamaki et al., 2009; M.Barmala et al.,2009; K. Somton et al.,2019). Recently, acrylic emulsion binders are widely studied for the slip casting of aqueous ceramic powder suspensions (K. M. Lindqvist et al., 2005; A. Gubernat et al.,2015). In slip casting, the binders provide adequate yield stress for the consolidated slurry to resist deformation and flow while draining the excess slurry and subsequent partial drying and provide mechanical strength to the slip-cast bodies during drying, handling, and further heat treatment (J. S. Reed., 1995; J. S. Ha., 2000). The acrylic emulsion binders provide better performance in terms of green strength and rate of cast thickness formation compared to the PVA and cellulose-based binders.

Substitution of synthetic binders with naturally renewable polymers is very important for achieving sustainable development. However, slip casting using naturally renewable binders is seldom reported in the literature. In this chapter, slip casting of alumina using natural rubber latex (**NRL**), a low-cost eco-friendly biopolymer emulsion obtained from the bark of the Hevea Brasiliensis tree is discussed. The slurry rheology and cast layer thickness development as a function of **NRL** binder concentration, alumina loading, and casting time have been studied and presented. The slip-cast bodies achieved high green strength, which is comparable to that of gel-cast bodies reported in the literature. The efficacy of the binder to produce thin-walled alumina crucibles is also demonstrated.

3.2 Experimental

3.2.1 Materials

The α-alumina powder with an average particle size of 0.34 μm and a specific surface area of 10.3 m^2/g was procured from ACC Alcoa, Kolkata, India. Concentrated **NRL** of 61.5 wt.% solid content stabilized using ammonia was procured from Hindustan Latex Ltd, Thiruvananthapuram, India. Ammonium poly(acrylate) [Darvan 821A, 40 wt.% aqueous solutions] used as a dispersant was procured from Vanderbilt Company Inc., Norwalk, CA, USA. A silicon-free antifoaming agent was obtained from Sigma Aldrich, USA. The plaster of Paris was procured from J K Cement Ltd., New Delhi, India. Distilled water was used as a solvent medium for the preparation of slurries.

3.2.2. Preparation of mold for slip casting

700 g of the plaster Paris powder was thoroughly mixed with 1 L of water in a beaker to form a slurry. The slurry was poured into a square cardboard box of 160 mm x 160 mm x 6 mm size and allowed to set at room temperature for 2 hours. The rectangular plaster of Paris body removed from the cardboard box was first dried at 70°C for 10 hours and then at 100°C

for 2 hours in an air oven. The molds for the preparation of cylindrical slip-cast alumina green bodies were prepared by fixing PVC tubes of 30 mm diameter and 50 mm height on the rectangular plaster of Paris body using an adhesive. A photograph of the mold used for the preparation of cylindrical alumina green bodies by slip casting is shown in **Fig.3.1.**

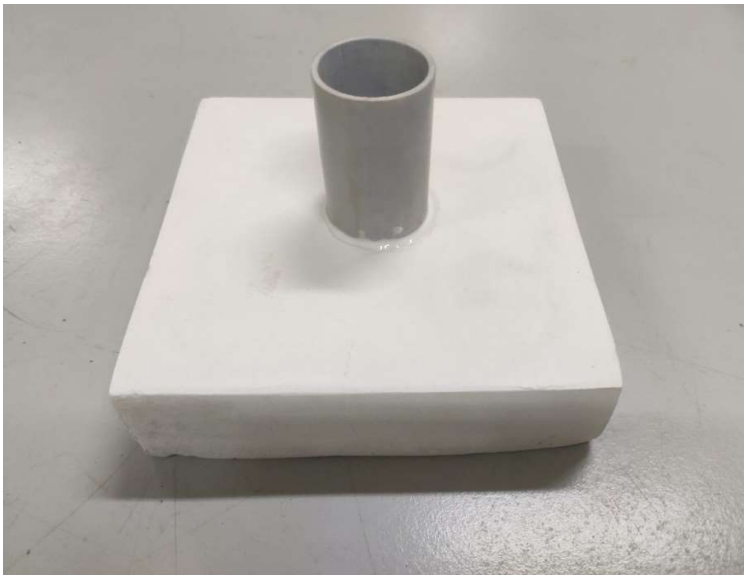

Fig.3.1 The photograph of the mold used for the preparation of cylindrical slip-cast bodies

3.2.3 Preparation of green and sintered alumina ceramics by slip casting

An aqueous slurry was prepared by dispersing the alumina powder in distilled water using the ammonium poly(acrylate) dispersant. The slurry taken in a 500 ml cylindrical polyethylene bottle was tumbled along with zirconia balls of 10 mm diameter on a roller ball mill for 12 hours. The alumina powder to zirconia ball weight ratio was 1:3. The concentration of ammonium poly(acrylate) was 0.5 wt.% of the alumina powder. The slurry was then poured into a beaker and mixed well with a calculated quantity of concentrated **NRL** and 0.20 wt.% of the antifoaming agent using a magnetic stirrer for 30 minutes. The concentration of rubber in the slurry was varied from 2 to 8 wt.% of the alumina powder and the alumina loading (with respect to total water in the slurry) was in the range of 40 to 55 vol.%. The slip casting slurries

thus obtained were poured into the PVC tube of the mold and aged for a different period for consolidation. The top of the PVC tube was covered with an aluminium foil to minimize the evaporation of water. The excess slurry was drained out after the pre-decided aging time. The slurry cast on the plaster of Paris surface was partially dried at room temperature for 12 hours and then removed from the mold. The slip-cast body removed from the mold was subsequently dried in an air oven at 70℃ for 12 hours. The dried green bodies were annealed at 200℃ for 2 hours at a ramp rate of 1℃/minute. The binder removal from the annealed bodies was performed by heating in an electrically heated muffle furnace at a rate of 1℃/minute up to 600℃ and holding at the final temperature for 2 hours. The sintering of the binder-removed bodies was carried out in a high-temperature sintering furnace at 1550℃ for 2 hours in an air atmosphere. The heating rate was 5℃/minute. A flow chart of the slip casting using the **NRL** binder is shown in **Fig. 3.2.**

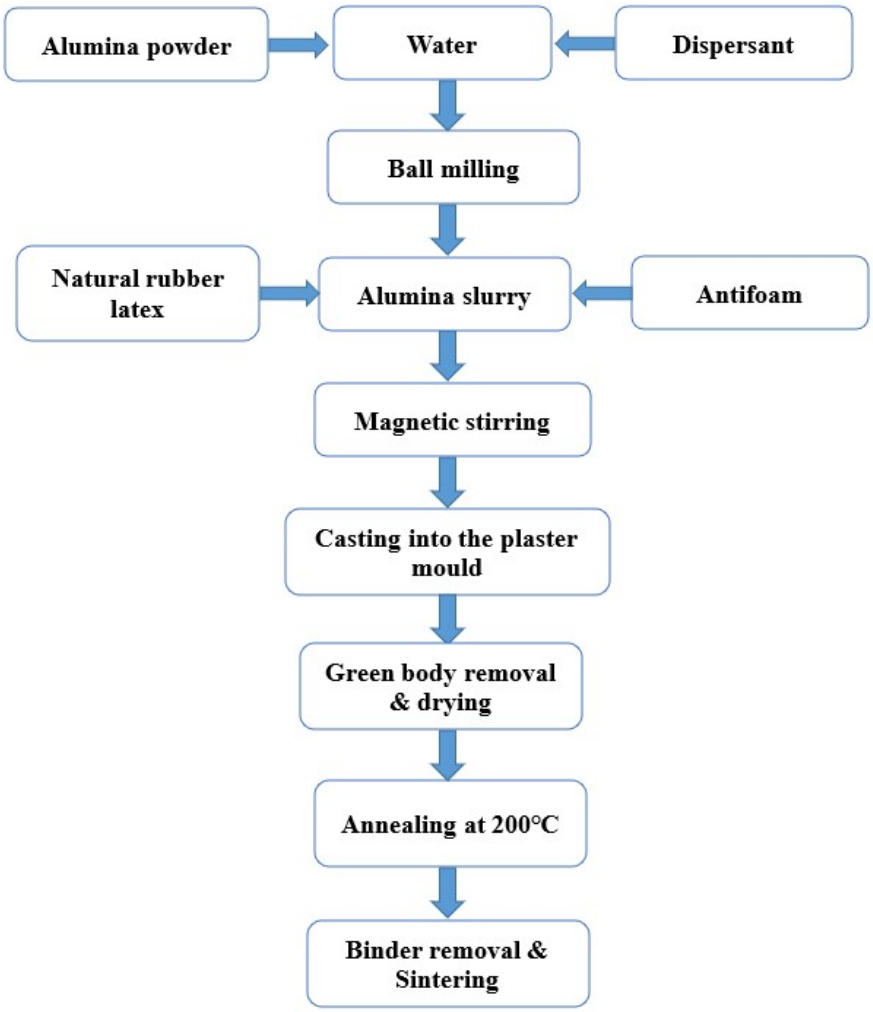

Fig.3.2 Flow chart of the slip casting process for the alumina ceramics using **NRL** binder.

3.3 Characterization

3.3.1 Zeta potential mesurement

The Zeta potential of alumina powder suspension, **NRL,** and alumina-NRL co-dispersions was measured as a function of pH using a Zeta sizer (Nano ZS, model ZEN 3600, Malvern, UK). The dispersion concentration used for the zeta potential measurement was 0.1 wt.%. Dilute NaOH and HCl solutions were used for pH adjustment.

3.3.2 Rheological properties of slip casting slurries

The viscosity of the slip-casting slurries at various shear rates was measured using a Brookfield viscometer (Brookfield Engineering Inc., Middleboro, MA) with a small sample adapter and a cylindrical spindle (SC21). The yield stress was calculated from the shear stress and shear rate data using the Casson Model (N. Q. Dzuy et al.,1983).

3.3.3 Cast layer thickness

The thickness of the green bodies was measured using a Vernier caliper. The thickness of the body was measured at a minimum of six locations and an average of the six measurements was reported.

3.3.4. Green and sintered densities

The density of the green bodies was measured from their weight and dimensions. The dimensions were measured using a Vernier caliper. The sintered density was measured using Archimedes' principle.

3.3.5 Green strength

The diametrical compressive strength of slip-cast green bodies was measured using a Universal Testing Machine (Instron 5500, Instron USA). The cylindrical samples of 13.5 mm diameter and 6.5 mm height were used. The strain rate was 0.5 mm/minute. The diametrical compressive strength was calculated from the load at break and sample dimensions using equation (8) given in **Chapter 2.**

3.3.6 Thermogravimetric analysis

The TGA of the green sample was performed in an air atmosphere using a Thermogravimetric analyzer (Q-50, TA Instruments, USA). The heating rate was 10 °C/min.

3.3.7 Microstructure analysis

The microstructure of fractured surfaces of green and sintered samples was observed using a scanning electron microscope (FESEM, Carl Zeiss Gemini 500 field emission microscope, Germany). The samples were sputter-coated with gold before the SEM analysis. The average grain size of the sintered alumina ceramic was measured from the SEM microstructure using the linear intercept method.

3.4 Results and Discussion

3.4.1 Colloidal stability

A well-dispersed slurry is required to get a uniform packing of particles and a defect-free final microstructure (L. Bergstrom., 2001). The slip casting slurries prepared by mixing alumina powder suspension and concentrated **NRL** show a pH in the range of 9.2 to 9.5. At this pH range, the zeta potential measured for the ammonium poly(acrylate) dispersed alumina particles is -53 mV. The zeta potential value observed for **NRL** particles at this pH range is -57 mV. That is, ammonium poly(acrylate) dispersed alumina particles, and the **NRL** particles in the suspension possess high negative surface charges at pH in the range of 9.2 to 9.5. In the case of **NRL** particles, the negative surface potential is attained by the ionization of the carboxyl groups of the proteins and lipids located at their surface. On the other hand, the ionization of carboxyl groups of adsorbed ammonium poly (acrylates) gives a negative surface potential to the alumina particles. These like charges on the particles provide electrostatic stabilization to the alumina and NRL particles in the co-dispersion. Therefore, a simple

magnetic stirring of alumina slurry and **NRL** leads to their easy mixing to form concentrated stable alumina-**NRL** co-dispersions for slip casting.

3.4.2 Rheological characteristics of slip casting slurries

The concentrated **NRL** and alumina slurries show shear-thinning flow behavior. The concentrated **NRL** shows viscosity in the range of 0.0625 to 0.0275 Pa.s at shear rates in the range of 3.7 to 93 s^{-1}. On the other hand, 50 vol. % alumina slurry displays a viscosity in the range of 0.875 to 0.14 Pa.s at shear rates in the range of 3.7 to 93 s^{-1}. The viscosity and shear-thinning behavior of the slip-casting slurries prepared at 50 vol.% alumina (with respect to water present in the slurry) increase with an increase in rubber concentration. Although the alumina concentration with respect to water in the slurry is kept constant (50 vol.%), the total solids concentration (including rubber) in the slurry increases from 50 to 57.8 vol.% when the rubber concentration increases from 0 to 8 wt.%. The observed increase in viscosity and shear thinning behavior are due to the increase in the total solid concentration. The viscosity at various shear rates of 50 vol.% alumina slurry containing different concentrations of **NRL** is shown in **Fig. 3.3.** Nevertheless, the viscosity and shear-thinning behavior of the slurries prepared at a constant natural rubber concentration of 4 wt.% increase with an increase in alumina loading. The viscosity versus shear rate plot of slurries of alumina loading in the range of 40 to 55 vol.% at **NRL** concentration of 4 wt.% is shown in **Fig.3.4.**

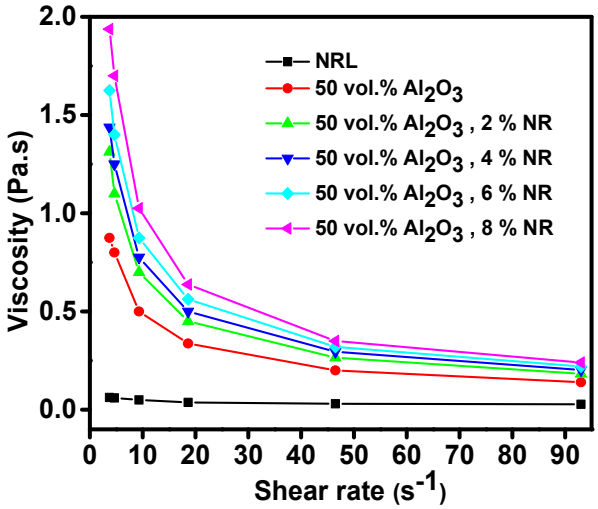

Fig.3.3 The viscosity vs. shear rate of 50 vol.% alumina slurry containing different concentrations of **NRL**

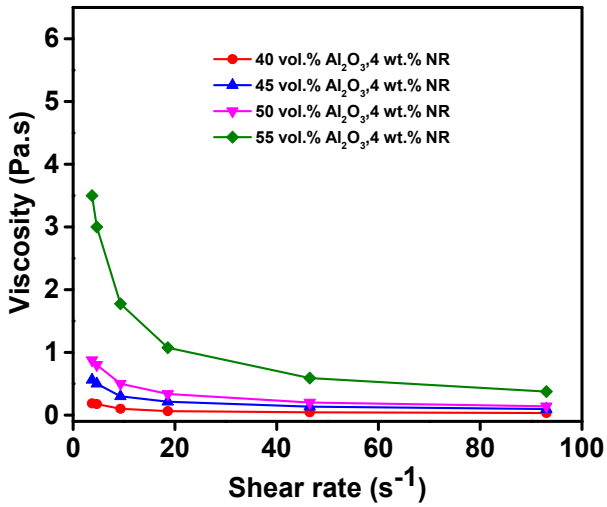

Fig.3.4 The viscosity vs. shear rate plot of slurries of alumina loading in the range of 40 to 55 vol.% at a fixed **NRL** concentration of 4 wt.%

It has been reported that a slurry viscosity of less than 2 Pa.s at a shear rate of 100 s^{-1} is adequate for slip casting to achieve good green densities (S. Leo et al., 2014). The viscosity of slurries

prepared at an alumina concentration in the range of 40 to 55 vol. % containing rubber concentrations from 2 to 8 wt. % of alumina shows a viscosity less than 2 Pa.s at 93 s^{-1}. That is, the viscosity of the slurries prepared is within the limit recommended for slip casting. On the other hand, a 41.1 vol.% alumina slurry containing 2 wt.% poly(vinyl alcohol) binder prepared by adding 10 wt.% aqueous PVA solution into 58.2 vol.% aqueous alumina slurry displays a viscosity in the range of 6.31 to 0.43 Pa.s at a shear rate in the range of 3.7 to 93 s^{-1}. This viscosity is much higher than that of 55 vol.% alumina slurry containing 4 wt.% **NRL** binder. It is worth noting that an increase of PVA concentration beyond 2 wt.% further decreases the alumina concentration in the slurry. This clearly shows that the use of concentrated **NRL** instead of conventional PVA binder facilitates the preparation of slip casting slurries of higher alumina powder loading with a wide concentration range of the binder. The viscosity at various shear rates of a 41.1 vol.% aqueous alumina slurry prepared at 2 wt.% PVA binder is shown in **Fig. 3.5.**

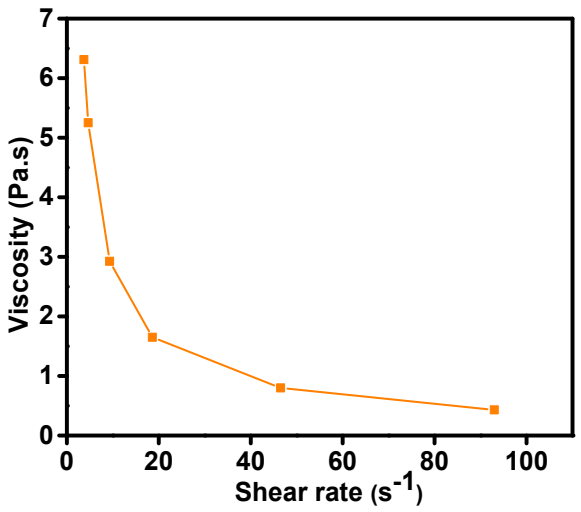

Fig.3.5 The viscosity vs. shear rate of a 41.1 vol.% aqueous alumina slurry prepared at 2 wt.% PVA binder

Generally, the rheological characteristics of concentrated ceramic powder suspensions showing shear thinning flow behavior are well explained by the Casson model (X. Zhu et al., 2002; W. J. Jr Walker et al., 1999; C. F. Escobar et al., 2015). In the present case, the flow behavior of the slip casting slurries fits well with the Casson model given as equation (9).

$$\boldsymbol{\tau^{\frac{1}{2}} = \tau_y^{1/2} + c\,\gamma^{1/2}} \quad \textbf{(9)}$$

Where τ and γ are the shear stress and shear rate, respectively, c is a constant and τ_y is the yield stress of the slurry. That is, a plot of the square root of shear stress versus the square root of shear rate gives a straight line. The yield stress of the slurry is calculated by extrapolating the straight-line graph to Y-axis. The Casson plot of the slip casting slurries is shown in **Fig.3.6**. The yield stress of 50 vol.% alumina slurries shows an increase from 2.84 to 4.79 Pa when the **NRL** binder concentration increases from 0 to 8 wt.%. On the other hand, the yield stress of slurries increases from 0.37 to 9.73 Pa when the alumina concentration increases from 40 to 55 vol.% at a fixed **NRL** binder concentration of 4 wt.%. In contrast, the 41.1 vol.% alumina slurry containing 2 wt.% PVA binder shows yield stress of 20.88 Pa. The moderate yield stress of the slip casting slurries using the **NRL** binder enables easy mold filling and provides adequate strength for the cast layer formed on the mold surface to resist deformation and flow while draining the excess slurry and subsequent partial drying before mold removal.

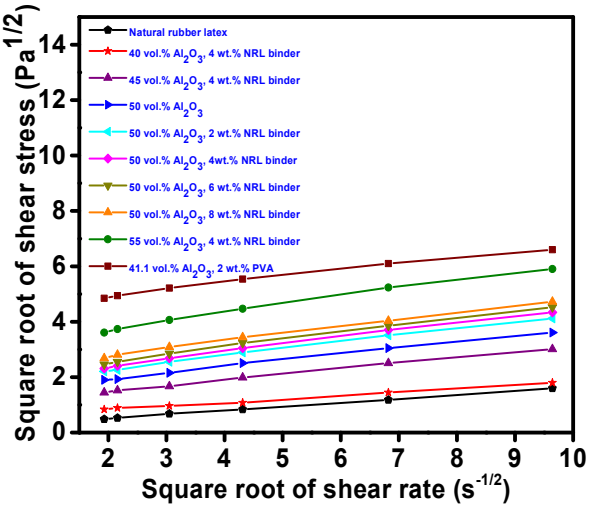

Fig.3.6 The Casson plot of slip casting slurries.

3.4.3 Effect of rubber concentration on casting rate

The efficiency of the slip casting can be explained in terms of the casting rate (the rate of formation of cast layer thickness) (L. F. Francis., 2015). Here, the thickness of the cast layer formed on the surface of the mold depends on the **NRL** binder concentration, alumina loading in the slurry, and casting time. The effect of **NRL** binder concentrations (2 to 8 wt.%) on the thickness of the cast layer is studied at a constant alumina slurry loading of 50 vol. % and a casting time of 1 hour. The reported cast layer thickness throughout this chapter is the thickness of the green body measured after drying at 70°C. The 50 vol.% alumina slurry without **NRL** binder forms a cast layer thickness of 8.5 mm in 1 hour. The thickness of the cast layer decreases with an increase in **NRL** binder concentration and the value reaches 4.2 mm when the binder concentration reaches 8 wt.%. In slip casting, a layer of slurry rapidly casts on the surface of the mold due to the absorption of water from the slurry by the capillaries present in the mold (J. S. Reed., 1995). Further growth of this layer depends on the permeability of the cast layer already formed. It appears that the rubber latex particles present in the inter-alumina particles region hinder the flow of water which results in a decrease in cast layer thickness with

an increase in rubber latex concentration. The thickness of the cast layer formed as a function of NRL binder concentration at a constant alumina loading of 50 vol.% and casting time of 1 hour is shown in **Fig.3.7**.

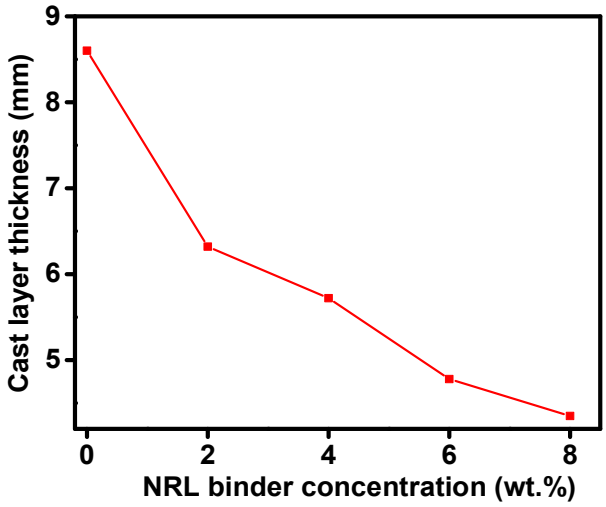

Fig.3.7 Effect of **NRL** binder concentration on the thickness of the cast layer formed at 1 hour from a slurry of 50 vol.% alumina loading.

3.4.4 Effect of casting time on casting rate

The effect of casting time on the thickness of the cast layer at **NRL** binder concentration of 4 wt. % of alumina and at an alumina slurry loading of 50 vol. % is shown in **Fig.3.8**. The thickness of the cast layer rapidly increases from 4.4 to 17 mm when the casting time increases from 30 to 240 minutes. Further, a slow down of the thickness development is observed and the cast layer thickness reaches only 18 mm in 480 minutes. The initial sharp increase in cast layer thickness is due to the availability of more free pores on the plaster mold for the capillary absorption of water. As the casting time increases, the pores in the mold are filled with water which results in lower water absorption by the mold. Another reason for the decrease in the

rate of cast layer thickness formation with an increase in time is the resistance to the permeation of water through the thick cast layer already formed on the mold surface.

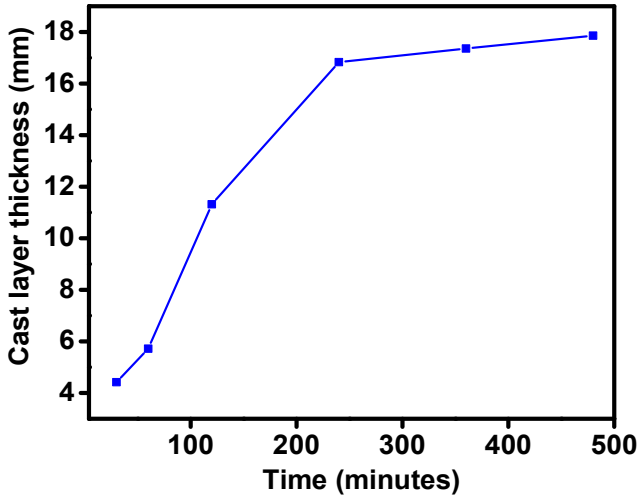

Fig.3.8 The effect of casting time on cast layer thickness at 4 wt.% **NRL** binder concentration from a slurry of 50 vol.% alumina loading.

3.4.5 Effect of alumina concentration in the slurry on casting rate

The third parameter deciding the rate of cast layer thickness formation is the alumina powder loading in the slurry. **Fig.3.9** shows the effect of alumina powder loading on the thickness of the cast layer developed at **NRL** binder concentration of 4 wt. % and at a casting time of 1 hour. The cast layer thickness increases from 4.13 to 4.55 mm when the alumina powder loading in the slurry increases from 40 to 45 vol. %. Further, an increase in slurry concentration to 55 vol.% rapidly increases the cast layer thickness to 6.5 mm. In the case of highly concentrated slurries, gelation can be achieved by draining a small amount of water leading to faster growth of the cast layer on the plaster mold surface. On the other hand, the 41.1 vol.% alumina slurry containing 2 wt.% PVA binder prepared for comparison shows a cast layer thickness of 2 mm in one hour. The thickness developed is nearly 2 times lower than

that produced from **NRL** binder-based slurry of similar alumina concentration. Further, the thickness developed is three times lower than that produced from the slip casting slurry of the highest alumina loading achieved with the **NRL** binder. This indicates the capability of the **NRL** binder system to produce slurries of higher alumina powder loading with viscosity ranges suitable for slip casting enabling faster cast layer thickness formation.

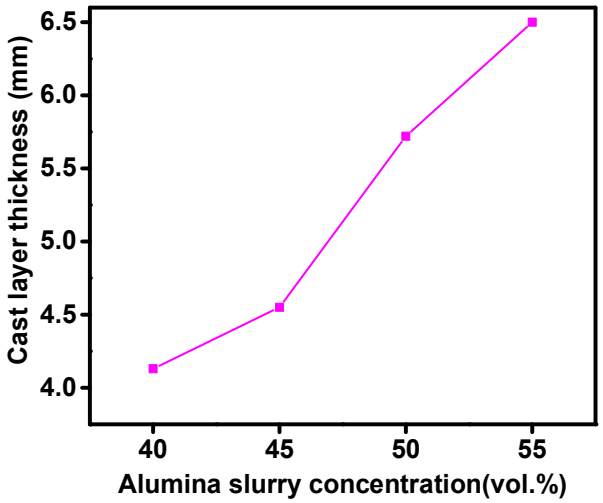

Fig.3.9 The cast layer thickness formed vs. alumina slurry concentration at 4 wt. % **NRL** binder concentration.

3.4.6 Green density and microstructure

The green bodies prepared at **NRL** binder concentrations in the range of 0 to 8 wt. % of alumina are evaluated for their density. The density of slip-cast green bodies as a function of **NRL** binder concentration is shown in **Fig.3.10**. The slip-cast body without the **NRL** binder shows a green density of 2.48 g cm^{-3}. This is 62.31% of the theoretical density of alumina. The green density decreases from 2.48 to 2.12 g cm^{-3} when the **NRL** binder concentration increases from 0 to 8 wt. % of alumina. These values are corresponding to 62.31 to 53.26% of the theoretical density of alumina. The theoretical density of alumina-natural rubber composites

containing 0 to 8 wt.% natural rubber calculated using the rule of mixtures is in the range of 3.94 to 2.64 g cm^{-1}. The density of natural rubber is taken as 0.93 g cm^{-1} for the calculation of the theoretical density of alumina-natural rubber composites. When the density of the composites is used as a base value for the calculation, the percentage of the theoretical density of the slip-cast green bodies containing 0 to 8 wt.% of NRL becomes in the range of 62.43 to 66.93. This indicates that the **NRL** binder does not hinder the packing of alumina particles during slip casting and the observed decrease in bulk density of the green body is due to the lower density of natural rubber compared to that of alumina. On the other hand, the 41.1 vol. % alumina slurry containing 2 wt.% PVA binder prepared for comparison produces slip-cast green bodies of density 2.05 g cm^{-1}. This is only 52.1% of the theoretical density of alumina. That is, the particle packing during consolidation is high in **NRL** binder-based slip casting slurries compared to the PVA binder-based slurries. It appears that the PVA binder bridges the alumina particles during consolidation leading to agglomeration which results in a lower particle packing. The high packing of alumina particles in the NRL binder-based green body is further evidenced by the SEM image of the fractured surface of the slip-cast green body. The SEM photomicrograph of the fractured surface of a slip-cast alumina green body prepared at 6 wt.% **NRL** concentration is shown in **Fig.3.11**. Few larger pores observed in the SEM image are formed by the removal of alumina particle-NR aggregates during fracture for sample preparation.

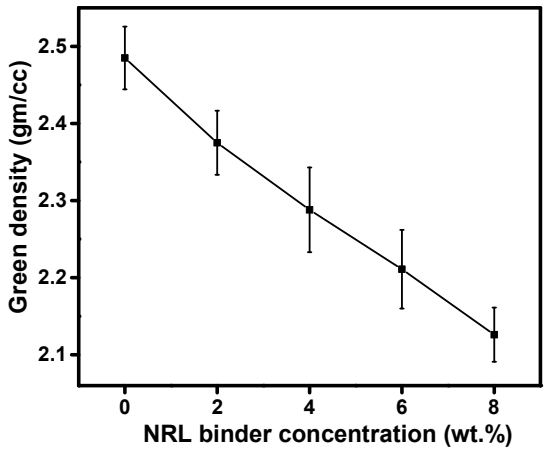

Fig.3.10 The plot of the green density of slip-cast bodies as a function of NRL binder concentration.

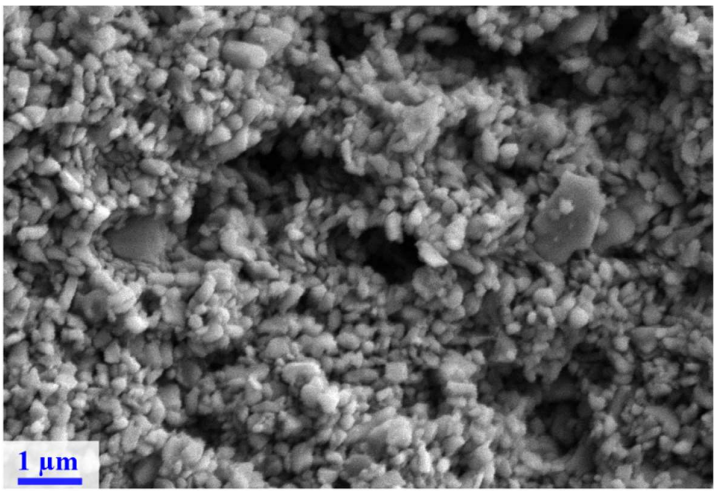

Fig.3.11 The SEM fractograph of a slip-cast alumina green body prepared from 50 vol.% alumina slurry and at 6 wt.% NR concentration.

3.4.7 Green strength

The strength of slip-cast green bodies is measured by diametrical compression after drying at 70°C and after annealing at 200°C for 2 hours. The load-displacement graph obtained during the diametrical compression of slip-cast alumina green samples containing different

concentrations of **NRL** binder is shown in **Fig.3.12**. In all the samples, a crack is formed along the diameter during the diametrical compression. In the case of green bodies dried at 70°C, the samples deform plastically after the formation of cracks as they are partially ductile due to the presence of the rubber binder. On the other hand, in the case of the samples annealed at 200°C, as soon as the crack develops, they break into pieces in a brittle manner. The load at which the crack developed on the sample is taken as the load at the break for the calculation of diametrical compressive strength. The diametrical compressive strength as a function of natural rubber concentration before annealing and after annealing at 200°C is shown in **Fig.3.13**. The diametrical compressive strength of green bodies dried at 70°C increases from 0.45 to 1 MPa when the rubber concentration increases from 0 to 8 wt. %. The strength of dried green bodies is comparable with that of slip-cast green bodies reported in the literature using other conventional binders (S. D. Nunn et al.,1994; K. Somton et al.,2019). However, in the case of green bodies containing natural rubber binder a drastic increase in the strength is observed after annealing at 200°C. On the other hand, the green body without a natural rubber binder does not show any improvement in strength by the annealing. The strength of annealed green bodies increases from 3 to 9.68 MPa when the rubber concentration increases from 2 to 8 wt.%. This corresponds to a 6 to 9.68 times increase compared to the green strength of the slip-cast bodies before annealing at 200°C. The partially ductile to brittle transition and the remarkable increase in the strength during annealing at 200°C are due to the cross-linking of rubber chains through the double bonds present in the isoprene units induced by the Lewis acid nature of alumina.

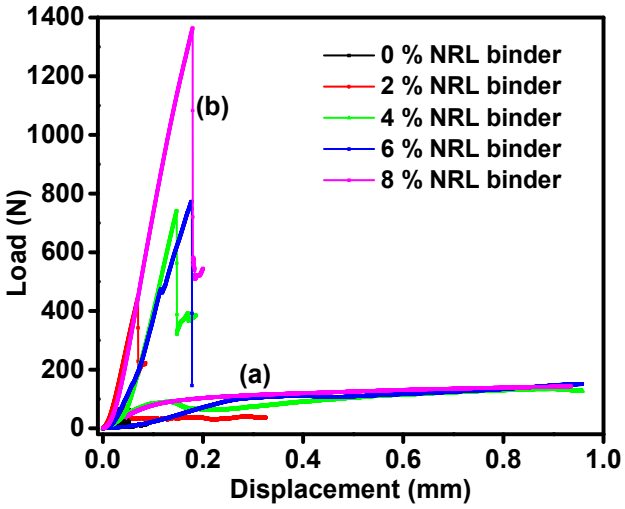

Fig.3.12 The load vs. displacement plot of slip-cast green alumina bodies prepared at different **NRL** binder concentrations after (a) drying at 70°C (before cross-linking) and (b) annealing at 200°C (after cross-linking).

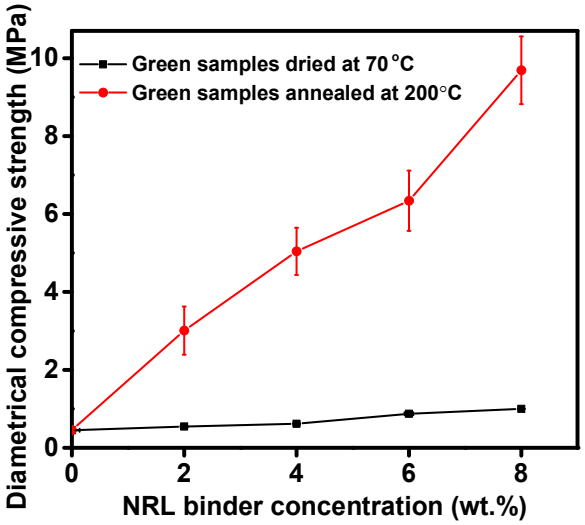

Fig.3.13 The variation of diametrical compressive strength as a function of **NRL** binder concentration of slip-cast green bodies after drying at 70°C and annealing at 200°C.

It has been reported in **Chapter 2** that at 2 wt.% natural rubber concentration, preparation of green samples by powder pressing is not feasible due to end-capping because of the poor green strength. Contrary to this, the slip-cast green body containing 2 wt.% NRL after annealing at 200°C shows a diametrical compressive strength of 3 MPa. At 4 wt.% NRL concentration, the slip-cast green body shows a diametrical compressive strength of 5 MPa in comparison to 2.3 MPa obtained for the powder-pressed sample. Beyond 4 wt.%, the diametrical compressive strength of green bodies prepared by powder pressing and slip-casting are more or less similar. In the powder pressing reported earlier, the feedstock is prepared by the coagulation of alumina powder-rubber latex co-dispersions using a formic acid solution. It appears that the coagulated rubber latex percolates at a concentration beyond 4 wt.% leading to stronger green bodies. On the other hand, co-consolidation from the well-dispersed suspension during slip-casting results in uniform distribution of the latex particles in the slip-cast green body even at a very low NRL concentration of 2 wt.%. The higher strength of slip-cast green bodies observed at a lower **NRL** binder concentration is due to the uniform distribution of the latex particles.

3.4.8 Green machining

Generally, the green bodies produced by slip casting show low strength (S. D. Nunn et al., 1994). The synthetic acrylic latex binders produce slip-cast bodies of considerably higher green strength compared to the solution-based polymer binders (K. M. Lindqvist et al., 2005; N. Demirkol et al., 2007). The strength of ceramic green bodies prepared using various binders reported in the literature is summarized in **Table 3.1**. It is important to note that the strength of slip-cast green bodies prepared using **NRL** binder after annealing at 200°C is much higher than that reported for the green bodies prepared using synthetic latex-based binders. It is worth noting that, due to the rubber cross-linking during annealing at 200°C, the strength of green bodies is enhanced to the level of green strength achieved by some of the best gel casting systems (S. D. Nunn et al., 1994). It has been reported that strength greater than 3MPa is

required for successful green machining (S. D. Nunn et al.,1994). The green bodies produced at **NRL** binder concentration of 2 wt.% exhibit strength of 3 MPa. That is, the green bodies produced at **NRL** binder concentration of 2 wt.% and above show sufficient strength for machining. The green bodies after annealing at 200°C are amenable to milling and drilling using conventional machines and high-speed steel tools. **Fig.3.14** is a photograph of a cylindrical slip-cast green body showing a slot made by milling and holes made by drilling.

Table 3.1 The strength of the slip-cast green bodies reported using different binders.

Ceramic powder	**Binder**	**Concentration of binder, wt. %**	**Strength, MPa**	**Reference**
Alumina	Acrylic latex emulsion	5	2 (Diametrical compression)	K. M. Lindqvist et al., 2005
Low clay white ware	Acrylic latex emulsion	7	4 (flexural)	N. Demirkol et al.,2007
Alumina	Polyvinyl alcohol	2	0.52 (flexural)	K. Somton et al., 2019
Alumina	Polyvinyl alcohol + Carbowax	3.75 + 1.25	1.88±0.04 (Diametrical compression)	S. D. Nunn et al., 1994
Alumina	Carboxymethyl cellulose	0.5	1.4 (flexural)	J. S. Ha et al., 2000
Alumina	**NRL**	4	5 (Diametrical compression)	Present study

Fig.3.14 Photograph of a cylindrical alumina green body showing a slot made by milling and holes made by drilling.

3.4.9 Thermogravimetric analysis

Non-uniform distribution due to the migration of binder during consolidation is reported in slip-cast bodies prepared using water-soluble polymeric binders (P.C.Hidber et al.,1995). **Fig.3.15** shows the TGA of the samples collected from the top and bottom portion of a cylindrical green body prepared by slip-casting using **NRL** binder. It is worth noting that the sample collected from the bottom (surface in contact with the plaster mold) of the cylindrical slip-cast green body shows a binder content of 4.83 wt. % whereas that collected from the top portion shows a binder content of 4.88 wt.% of alumina. This concludes that there is no appreciable binder migration during slurry consolidation by the slip casting. The particle size of the **NRL** is in the range of 0.1 to 2 μm with an average size of 0.5 μm. That is, NRL and alumina powder have more or less the same range of particle sizes. This leads to their co-consolidation rather than the migration of rubber latex particles along with the dispersion medium. This leads to uniform distribution of the NRL particles throughout the alumina green bodies. The TGA graphs further show the disintegration of natural rubber in the green alumina

sample at a temperature in the range of 200 to 550ºC. A near steady-state decomposition of the binder from the green sample is observed. The slip-cast alumina green bodies do not show cracks or deformation during the debinding by heating at a rate of 1ºC/minute.

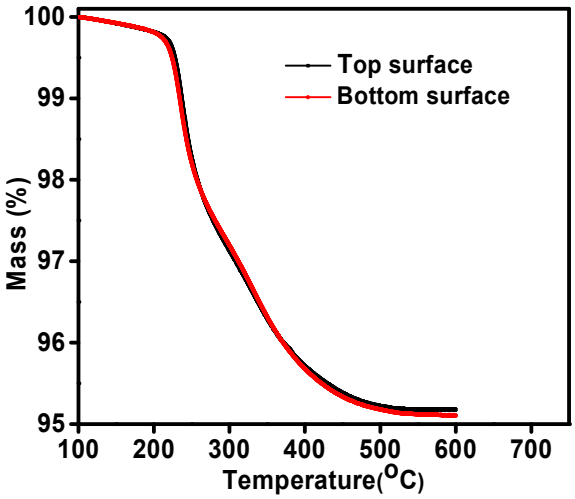

Fig.3.15 TGA of samples collected from the top and bottom surface of the slip-cast green body.

3.4.10 Sintering

The debinded green bodies sintered to ~ 97% of theoretical density at 1550 ºC. Nearly 13.57 % of diametrical and 14.88 % linear shrinkages are observed during the sintering of the cylindrical green bodies. **Fig.3.16** shows the SEM microstructure of the fractured surface of a slip-cast alumina body sintered at 1550ºC. The microstructure is homogeneous and dense. The average size of alumina grains in the sintered ceramics calculated from the SEM image using the linear intercept method is 1.82 µm.

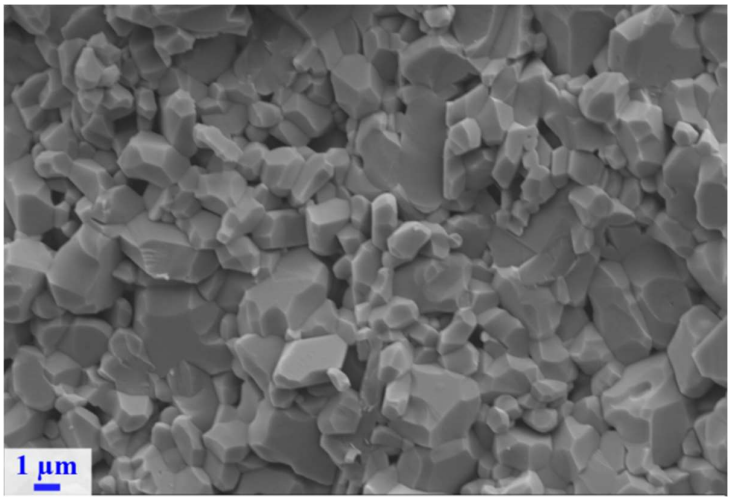

Fig. 3.16 The SEM image of the fractured surface of sintered slip-cast alumina ceramic.

3.4.11 Preparation of thin-walled crucibles

Fabrication of hollow ceramic components of low wall thickness (close to 1mm) by slip casting is challenging as the parts are likely to crack while mold removal and subsequent drying due to low strength. However, the slip casting using **NRL** binder can quickly produce thin-walled alumina crucibles. Sintered alumina crucibles of 1.7 and 1.2 mm thickness could be successfully produced at casting times of 5 and 2 minutes, respectively.**Fig.3.17** shows the photograph of thin-walled sintered alumina crucibles fabricated by slip casting using **NRL** binder.

Fig.3.17 Photograph of thin-walled sintered alumina crucibles prepared by slip-casting using **NRL** binder.

3.5 Conclusions

Slip casting of aqueous alumina powder suspensions is studied using a **NRL** binder. The slurry rheology, rate of cast layer thickness formation, green density, and green strength are evaluated in comparison with the commonly used PVA binder. Slip casting slurries of high (40-55 vol.%) alumina concentration at **NRL** binder concentrations in the range of 2 to 8 wt.% having suitable viscosity (<2 Pa.s at a shear rate of 100 s^{-1}) could be prepared due to the high and negative zeta potentials of latex and alumina particles at the suspension pH (9.2 to 9.5) and high solid content of the concentrated **NRL**. The green density and green strength observed are in the ranges of 62.43 to 53.42% TD and 0.45 to 1 MPa, respectively, at **NRL** binder concentrations in the range of 0 to 8 wt.%. The slip-cast alumina bodies show a 6 to 9.68 times increase in diametrical compressive strength by annealing at 200°C due to the cross-linking of rubber chains induced by the Lewis acid character of the alumina. The slip-cast green bodies after annealing are amenable to machining using conventional machines and tools. The **NRL** binder-based slip casting exhibits superior performance in terms of lower slurry viscosity, and a higher rate of cast layer thickness formation, green density, and green strength. A uniform distribution of natural rubber binder throughout the green body is evidenced from the TGA analysis of samples collected from different parts of a slip-cast green body indicating negligible binder migration during consolidation. The natural rubber binder shows a near steady-state burnout from the slip-cast green body. Alumina ceramics with a density of ~ 97% TD could be obtained by sintering the slip-cast bodies at 1550°C for 2 hours. Alumina crucibles with wall thickness as low as 1.2 mm could be quickly fabricated by slip casting using **NRL** binder. The sintered ceramics exhibit a dense microstructure with an average grain size of 1.8 μm.

Chapter 4

Aqueous alumina tape casting using natural rubber latex as a binder

4.1 Introduction

Tape casting is a process for the preparation of thin sheets of ceramics from powder suspensions containing a suitable binder and a plasticizer. The process is used for the preparation of ceramic substrates for integrated circuits, electrodes & electrolytes for solid oxide fuel cells, layered capacitors and sensors, and fabrication of complex shape monolithic and composite structural ceramic components through a multilayer fabrication route (R.E. Mistler.,1990; A.Roosen.,2001; K. P. Plucknett et al.,1994). Generally, the non-aqueous solvent systems such as toluene, MEK-ethanol, and trichloroethane-ethanol mixtures are employed for the preparation of tape casting slurries using polyvinyl butyral and poly(methyl methacrylate) as binders and phthalic esters and polyethylene glycol as plasticizers(R. Moreno.,1992; R.E. Mistler.,2000; A. Kristoffersson et al.,1998). Aqueous tape casting using water-soluble polymers [poly(vinyl alcohol) and cellulose ethers] and acrylic latex emulsions as binders along with plasticizers such as polyethylene glycol and glycerol have been widely investigated (A. Kristoffersson et al.,1998). Long drying time, drying-related cracks, and reactivity with some ceramic powders are the demerits of water-based tape casting systems (P. Nahass et al.,1990). The non-aqueous systems are preferred to aqueous tape casting systems by the industry for continuous production, despite the hazardous nature of non-aqueous solvents, due to the fast drying of organic solvents and smooth and crack-free green tapes. However, for achieving complete environmental friendliness and sustainability, there is a renewed interest in aqueous tape casting research using naturally renewable materials instead of synthetically prepared polymers as binders (W. W. Wolny et al.,2004). Natural renewable molecules such as gelatin and pectin as binders, glycerol, and linseed oil as plasticizers, and lignosulfonate as a dispersant have been studied for aqueous tape casting of ceramic powders

(F. Snijkers et al.,2004; J. Marie et al., 2017). However, detailed mechanical characterization of the green tape is not reported to understand the effectiveness of the used binders. In this chapter, we discuss the aqueous tape casting of alumina using concentrated **NRL** as a binder. The advantage of the system is that it does not require an additional plasticizer as the natural rubber is elastomeric. Moreover, the concentrated **NRL** binder system enables the preparation of tape casting slurries of high solid concentration which lead to faster drying of the cast tape.

4.2 Experimental

4.2.1 Materials

The A16SG α-alumina powder of average particle size 0.34 μm and specific surface area 10.3 m^2/g was procured from ACC Alcoa, Kolkata, India. The concentrated **NRL** stabilized with ammonia was obtained from Hindustan Latex Ltd, Thiruvananthapuram, India. Analytical grades nitric acid, hydrochloric acid, and sodium hydroxide were procured from Merck, India. A 40 wt.% aqueous ammonium poly(acrylate) solution (Darvan 121 A, Vanderbilt Company Inc., Norwalk, CA) was used as the dispersant. A silicon-free defoaming agent (Antifoam O-30) was procured from Sigma Aldrich, USA. Distilled water was used for the preparation of alumina powder suspensions.

4.2.2 Preparation of green and sintered alumina tapes

The flow chart of the tape casting process is shown in **Fig.4.1**. A 58.2 vol.% slurry was prepared by ball milling the alumina powder, water, and the dispersant taken in a cylindrical polyethylene container for 12 hours using zirconia balls of 10 mm size. The concentration of ammonium poly(acrylate) was 0.5 wt.% of the alumina powder. The alumina powder to zirconia ball weight ratio was 1: 3. The alumina slurry thus obtained was transferred to a borosilicate glass beaker. The calculated quantity of the concentrated **NRL** and the defoaming agent were added. The slurry was then mixed thoroughly using a magnetic stirrer for 30

minutes. Green alumina tapes of nearly 500 µm thickness were prepared by casting the slurry on silicon-coated Mylar films using a tape casting machine (Keko equipment, Zuzemberk, Slovenia) and a double doctor blade. The casting speed was 20 cm/min. The drying of the cast tape was performed by blowing hot air. The temperature of the drying chamber was 70°C. Rectangular samples of 50 mm length and 40 mm breadth prepared by cutting the green tape using a sharp blade were placed in between two glass plates and annealed at 200 °C for 2 h. The annealed green tapes were heated in an electrically heated sintering furnace for binder-removal and sintering. The heating rate was 1°C/min up to 600°C and 2°C/min from 600 to 1600°C. A holding time of 2 h was given at 1600°C.

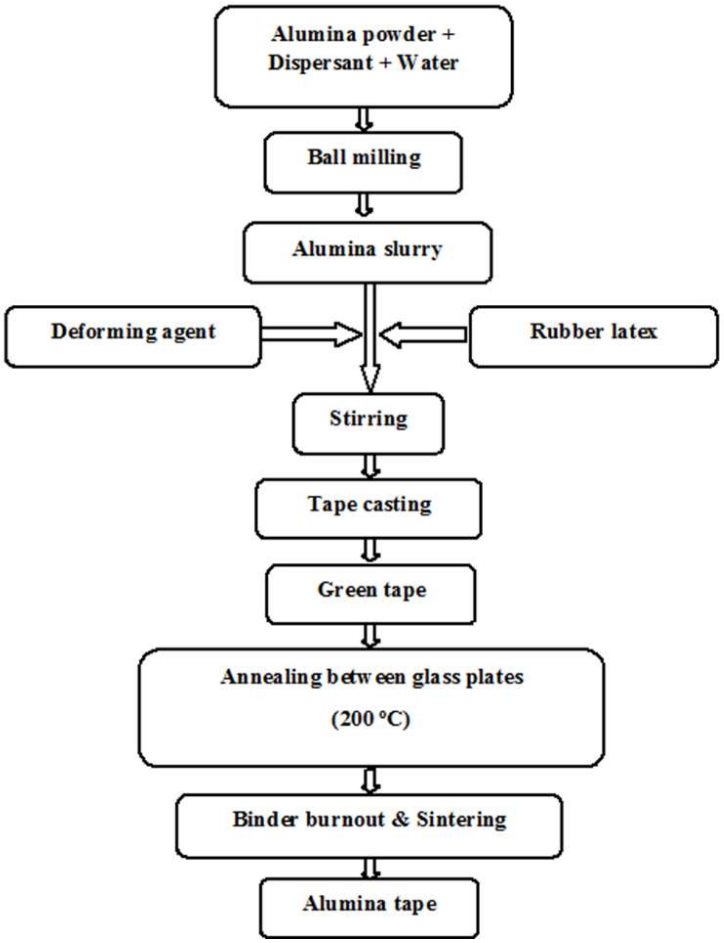

Fig.4.1 The flow chart of the tape casting process using **NRL** binder

4.3 Characterization

4.3.1 Rheological properties of tape casting slurries

The viscosity at various shear rates of the tape casting slurries was measured with a Brookfield viscometer (Brookfield Engineering Inc., Middleboro, MA) using a small sample adapter and a cylindrical spindle (SC21). The yield stress of the slurries was calculated from the shear rate and shear stress data using the Casson model.

4.3.2 Drying kinetics of green tapes

The drying kinetics of the slurry tape cast on a Mylar sheet is studied at room temperature and 70℃ by monitoring the weight loss at regular intervals of time. An electronic weighing balance of readability 0.1 mg was used for measuring the weight losses.

4.3.3 Thermogravimetric analysis

TGA of the dried and annealed green tape was carried out using a thermogravimetric analyzer (Q-50, TA Instruments, USA) in an air atmosphere at a heating rate of 5 °C/min.

4.3.4 Tensile strength measurement

The tensile stress-strain measurement of the green tapes was performed using a universal testing machine (Instron 5500, Instron USA). Dumbbell specimens (ASTM D412) prepared from the green tapes were used for the stress-strain measurement. The loading rate was 10 mm/min. The stress corresponding to yield point in the stress-strain graph was taken as the tensile strength and the slope of the initial linear region was taken as Young's modulus. The tensile strength and modulus reported were an average of a minimum of six measurements.

4.3.5 Dynamic mechanical analysis

The dynamic mechanical analysis of the green alumina tape was performed using a dynamic mechanical analyzer (DMA 800, Perkin Elmer, USA). The analysis was conducted in dual cantilever mode from -100 to +200°C at a heating rate of 2°C/min using rectangular samples of 50 mm in length and 10 mm in size.

4.3.6 Roll pressing of the green tape

The green tapes were passed through the rollers of a Hot roll pressing machine (Gelon group, Shandong, China) to reduce the thickness and enhance the particle packing. The roll pressing was performed at room temperature.

4.3.7 Measurement of sintering shrinkage

The sintering shrinkage was calculated from the dimension of the tape before and after sintering. Green tapes of 5 cm x 5 cm size were used for the sintering shrinkage studies. The dimensions were measured using a Vernier caliper.

4.3.8 Green and sintered density measurement

The green density was calculated from the weight and volume of green tapes of size 5 cm x 5 cm. The length, width, and thickness for the calculation of volume were measured using a Vernier caliper. The density of the sintered tape was measured using Archimedes' principle.

4.3.9 Microstructure analysis

The microstructure of fractured surfaces of binder removed green tapes and sintered alumina tapes was observed using a scanning electron microscope (FESEM, Carl Zeiss Gemini 500 field emission microscope, Germany). The samples were sputter coated with gold before the SEM analysis. The grain size of the sintered alumina tape was measured from the SEM microstructure by the linear intercept method.

4.4 Results and Discussion

4.4.1 Preparation of tape casting slurries

The tape casting formulations prepared by mixing the concentrated alumina slurry and concentrated **NRL** show a pH in the range of 10.3 to 10.5. At this, pH ranges the ammonium poly(acrylate) dispersed alumina and rubber latex particles possess high negative zeta potentials of -66 to -76 mV, respectively. This enables the easy mixing of the concentrated alumina dispersion with the concentrated **NRL** to form stable slurries for tape casting. The compositions of tape casting slurry formulations prepared by mixing the concentrated alumina slurry and rubber latex are given in **Table 4.1**. The rubber content used is in the range of 14.2 to 18.1 wt. % of the alumina powder. The alumina powder to rubber weight ratio is within the range of alumina powder to organic content (binder+ plasticizer) used in most of the reported tape casting formulations (P. Boch et al., 1986; T. Chartier et al., 1993). Tape casting slurry with a high solid-to-solvent ratio is desirable for faster drying to form a crack-free green tape.

Table 4.1. Composition of tape casting slurry formulations

Formulations	Alumina (g)	Water (ml)	Dispersant (g)	Rubber latex * (g)	Antifoaming agent (g)	Solid loading (vol.%)
A	100	18	0.35	27 (16.63)	0.20	60.57
B	100	18	0.35	30 (18.48)	0.20	60.69
C	100	18	0.35	33 (20.32)	0.20	60.78
D	100	18	0.35	36 (22.17)	0.20	60.88

*Values given in parenthesis are the weight of the rubber

The aqueous tape casting slurry formulations prepared using synthetic and natural binders show relatively low total solid content (J. Marie et al.,2017; S. Nayak et al., 2011). This may be due

to the low solubility and high viscosity of the polymeric binders in water. On the other hand, emulsion-based binders produce tape casting slurry with a high solid content since aqueous emulsion binders have relatively high solid content and low viscosity. Doreau et al achieved a maximum solid (ceramic powder + binder) loading of nearly 55 vol.% in aqueous alumina tape casting slurry prepared using an acrylic emulsion binder (F. Doreau et al., 1998). It is worth noting that the total solid content, the sum of alumina powder and rubber, in all the studied slurry formulations is higher than 60 vol.%. This is higher than that of most of the reported aqueous tape casting slurry formulations. The density of natural rubber is taken as 0.93 g/cm^3 for the calculation of solid content.

In the conventional preparation of tape casting slurry, ball milling is continued after the addition of binder and plasticizer to ceramic powder suspension to dissolve the polymeric binder and to achieve a homogeneous mixing of the ingredients. However, in the present case, an attempt to ball mill the slurry after the addition of concentrated rubber latex results in the formation of lumps of rubber. This is due to the mechanically induced aggregation of rubber particles in the alumina slurry medium. That is, the latex particles coming in between the colliding grinding balls stick to each other due to the mechanical force of the collision to form larger particles. These particles grow to the size of large lumps with continued ball milling. A photograph of a lump of rubber produced in the alumina tape casting slurry during ball milling is shown in **Fig.4.2**. On the other hand, mixing by stirring using a magnetic stirrer does not produce any such lump. Further, the slurry easily achieves homogeneity by stirring with a magnetic stirrer as the rubber latex and alumina slurry are in colloidal form with high negative particle surface charges. Therefore, the mixing of alumina slurry with rubber latex is carried out by stirring using a magnetic stirrer for 30 minutes.

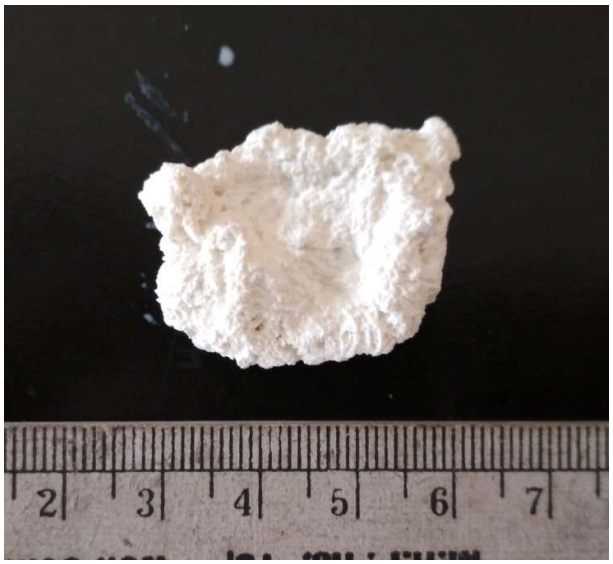

Fig.4.2 Photograph of a lump of rubber formed during ball milling of concentrated aqueous alumina powder dispersion and **NRL**

4.4.2 Rheological properties of tape casting slurries

The tape casting requires a slurry with shear thinning flow behavior with relatively high yield stress. The plot of viscosity versus the shear rate of the concentrated alumina slurry, rubber latex, and tape casting slurries prepared by mixing them are shown in **Fig.4.3**. The concentrated (58.2 vol.%) aqueous alumina slurry shows shear thinning flow behavior with a viscosity in the range of 3.05 to 0.48 Pa.s at shear rates in the range of 4.65 to 93 s^{-1}. On the other hand, the concentrated rubber latex shows near Newtonian flow behavior with low viscosity in the range of 0.05 to 0.045 Pa.s at shear rates in the range of 4.65 to 93 s^{-1}. The tape casting slurries prepared by mixing the concentrated alumina slurry and rubber latex show shear thinning flow behavior with viscosities in between that of the alumina slurry and rubber latex. The tape casting slurries containing 14.2 to 18.1 wt.% (with respect to alumina) natural rubber show a viscosity in the range of 1.1 to 1.15 Pa.s at a shear rate of 4.65s^{-1}. The slurry viscosity decreases to the range of 0.18 to 0.21 Pa.s when the shear rate increases to 93s^{-1}. The tape casting slurries obey the Casson flow model. That is, a plot of the square root of shear

stress versus the square root of shear rate gives a linear graph as shown in **Fig.4.4.** The yield stress of the slurries calculated from the Casson plots are in the range of 3.29 to 2.97 Pa. The observed shear thinning flow behavior and viscosity and yield stress ranges of the slurries are suitable for tape casting.

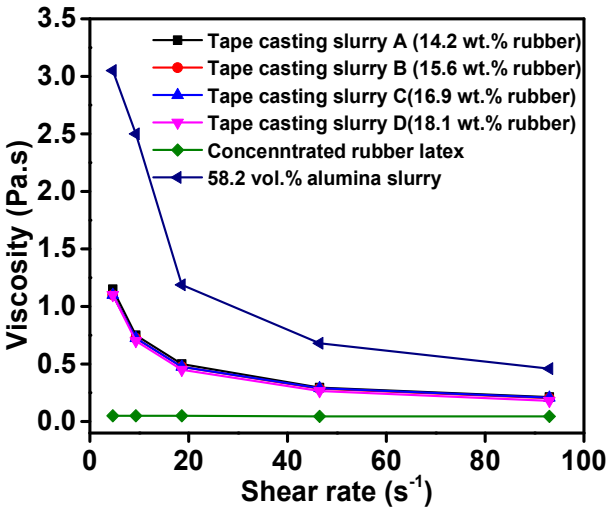

Fig.4.3 Viscosity at various shear rates of tape casting slurries prepared at various rubber concentrations

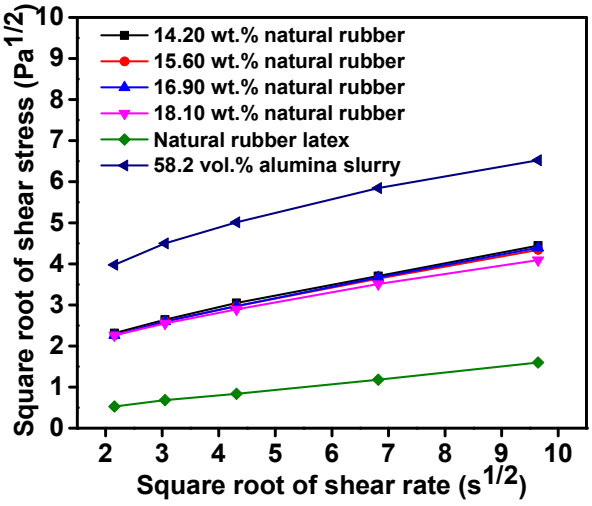

Fig.4.4 The Casson plot of tape casting slurries.

4.4.3 Stability of tape casting slurries during aging

The long-term stability of the tape casting slurry formulations is studied by measuring their viscosity with time at a shear rate of 9.3 s^{-1}. The viscosity of the tape casting slurries slowly increases with time. The variation of viscosity with the time of a tape casting slurry formulation (formulation B) is shown in **Fig.4.5**. The viscosity of the slurry increases from 0.675 to 1.5 Pa.s when the aging time increases from 0 to 9 h. The alumina slurry and concentrated rubber latex do not show any change in viscosity during aging.

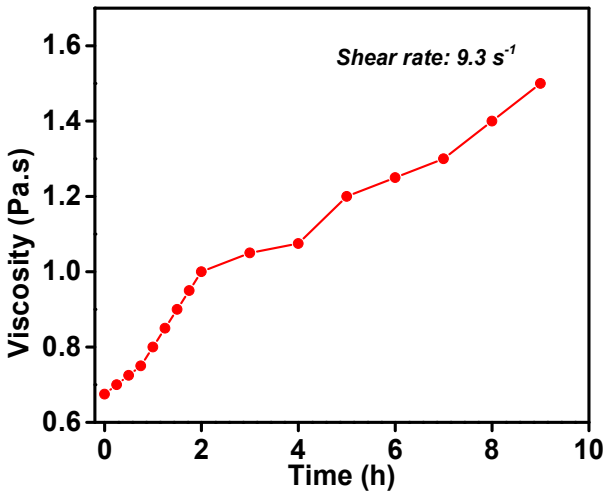

Fig.4.5 Viscosity variation with time of tape casting slurry formulation B (rubber concentration-15.6 wt.% of alumina)

A similar increase in viscosity with time was reported by Pagnoux et al in tape casting slurries prepared using acrylic emulsion binders and 4,5-dihydroxy-1,3-benzene sulfonic acid disodium salt as a dispersant (C. Pagnoux et al.,1998). The explanation offered was the aggregation of acrylic emulsion particles induced by some of the cations such as Na^+ slowly released from impurities present in the A16SG alumina powder. A similar explanation is valid in the present case also as the tape casting slurry is prepared from a similar alumina powder

and rubber latex particles have a similar surface charge. Alternatively, the increase in viscosity of the tape casting slurry may be due to the slow aggregation between latex particles and alumina particles caused by polymer bridging through the ammonium poly(acrylate) chains adsorbed on the alumina particle surface. To counter this aggregation phenomenon, the tape casting slurries prepared by mixing the alumina slurry and concentrated rubber latex are cast within 30 minutes. The viscosity increase observed within 30 minutes is from 0.675 to 0.725 Pa.s.

4.4.4 Drying kinetics

The major hurdle to continuous tape casting with aqueous slurries is their long drying time (P. Nahass et al.,1990). The drying behavior at room temperature (~ 30°C) and at 70°C of the slurry formulation B tape cast on the Mylar substrate is shown in **Fig.4.6**. At room temperature, a slow and near-steady water loss is observed up to 300 minutes at which nearly 90% of the water present in the slurry is removed. The tape can be easily peeled off from the substrate at this stage. On the other hand, a much faster drying rate is achieved at 70°C. Nearly 97% of the water is removed in 15 minutes. The relatively low drying time is due to the high solid content (> 60 vol.%) of the tape casting slurries. No crack is observed on the tape during drying. The green tape peeled off from the substrate shows a smooth surface and adequate flexibility. A photograph of green tape exhibiting its flexibility and smooth surface is shown in **Fig.4.7**.

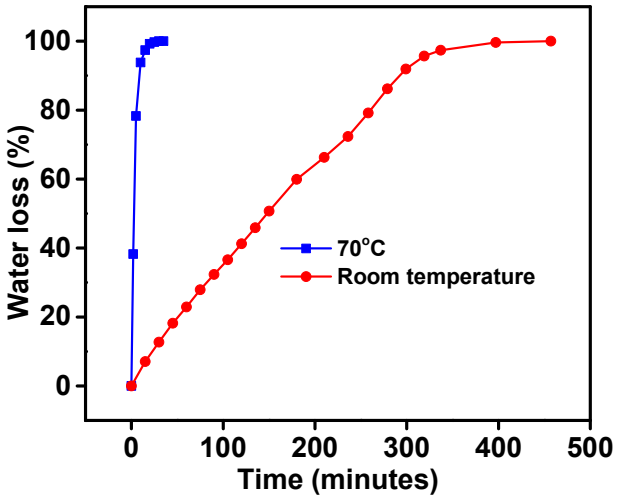

Fig.4.6 Drying behavior of slurry formulation B tape cast on Mylar substrate

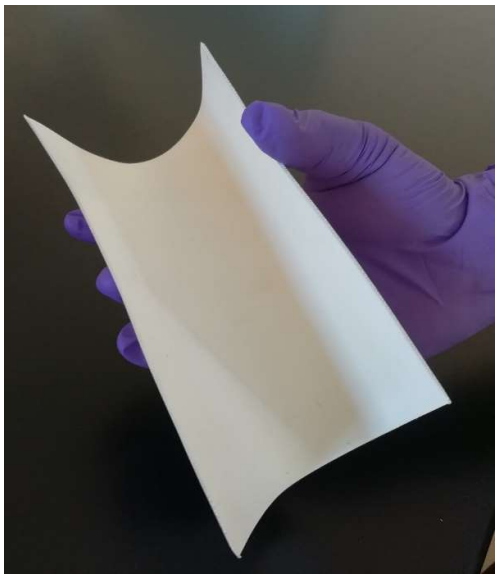

Fig.4.7 Photograph showing the flexibility of alumina green tape prepared at a rubber concentration of 15.6 wt.%.

4.4.5 Green strength

The strength of green tapes is measured in the tensile mode using dumbbell-shaped specimens shown in **Fig.4.8**. The tensile stress-strain graph of green tapes prepared at various

rubber concentrations is shown in **Fig.4.9**. The tensile stress of the green tapes shows an initial rapid and linear increase with strain up to a yield point. The yield point is observed at a strain value of 1.5 % for green tape prepared at a rubber concentration of 14.2 wt.%. For all other compositions, the yield point is observed at a strain value of 2.5 to 3%. After the yield point, the tensile stress very slowly increases with an increase in strain and reaches a maximum. All the samples break immediately after reaching the stress maximum. The slow increase of stress with an increase of strain after the yield point is due to strain hardening caused by the uncoiling and alignment of rubber chains at higher tensile stress (stress-induced crystallization of rubber). The stress corresponding to the yield point is taken as the tensile strength of the samples. The tensile strength of the green tape marginally increases from 1.81 to 1.85 MPa when the rubber concentration increases from 14.2 to 15.6 wt.%. Further, increase in rubber concentration to 18.1 wt.% decreases the tensile strength to 1.62 MPa. The highest tensile strength observed at a rubber concentration of 15.6 wt.% indicates the better reinforcement of the rubber matrix by the alumina particles. On the other hand, Young's modulus rapidly decreases from 267.5 to 79.3 MPa when the rubber concentration increases from 14.2 to 15.6 wt.%. Further increase in rubber concentration to 18.1 wt.% slowly decreases the Young's' modulus to 50.8 MPa. The effect of rubber concentration on tensile strength and Young's modulus of green tapes is shown in **Fig.4.10**.

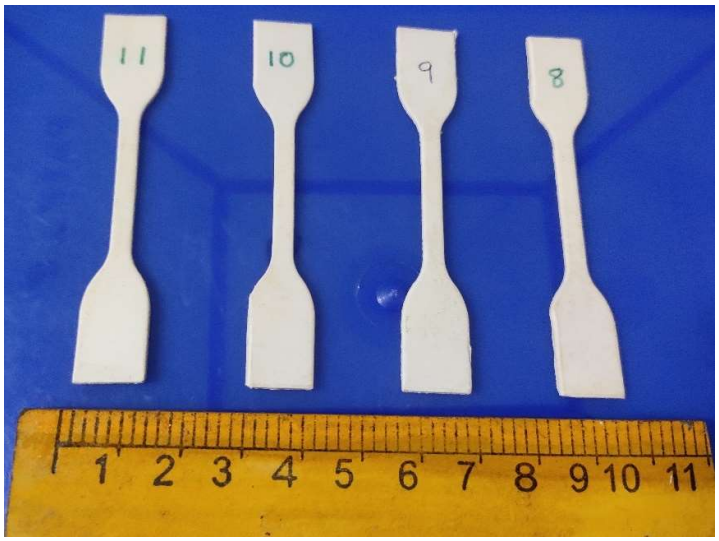

Fig.4.8 The dumbbell-shaped tensile specimens

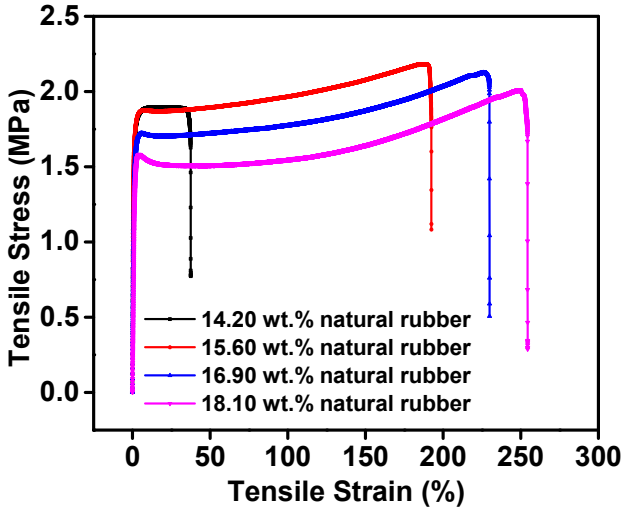

Fig.4.9 The tensile stress-strain graph of alumina green tapes prepared at various rubber concentrations

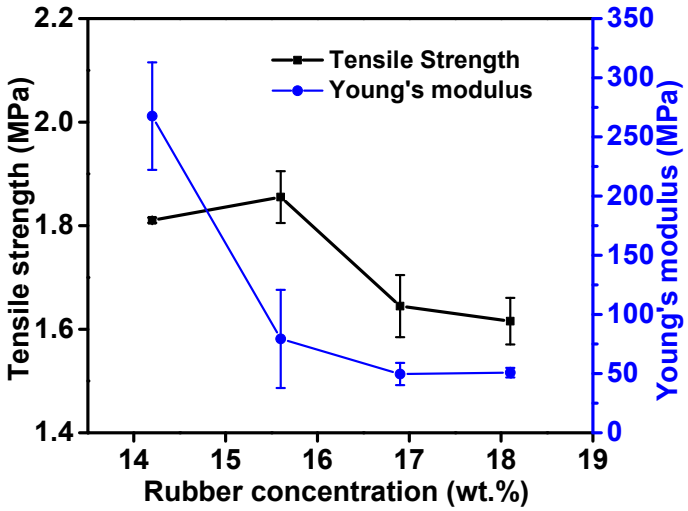

Fig.4.10 Effect of rubber concentration on the tensile strength and Young's modulus of alumina green tapes

The alumina green tapes should have sufficient flexibility to be peeled off from the substrate after drying. The percentage strain at the failure point is a measure of the flexibility of the green tape. The strain at the failure point increases from 41 to 193% when the rubber concentration increases from 14.2 to 15.6 wt.%. Further increase in rubber concentration to 18.1 wt.% slowly increases the strain at the failure to 254%. That is, the flexibility of the green tape increases with an increase in rubber concentration. The strain at the failure point is plotted as a function of rubber concentration in **Fig.4.11**. Conventionally, plasticizers such as phthalic esters, polyethylene glycol, glycerol, etc. are added to the tape casting slurries to make the used binders such as poly(vinyl butyral), poly (methyl methacrylate) and polyvinyl alcohol flexible. In the present case, natural rubber is an intrinsically flexible polymer at room temperature (Tg ~ -70°C). Therefore, the green alumina tapes achieve enough flexibility without the use of any additional plasticizing agent. The strain at the failure point observed for the green tape prepared at a rubber concentration of 14.2 wt.% is sufficient for peeling off the cast tape from the substrate without any failure. However, the green tape prepared at a rubber concentration of

15.6 wt.% exhibits slightly higher tensile strength and very high flexibility. Therefore, the green tape prepared at a rubber concentration of 15.6 wt.% is used for further sintering studies.

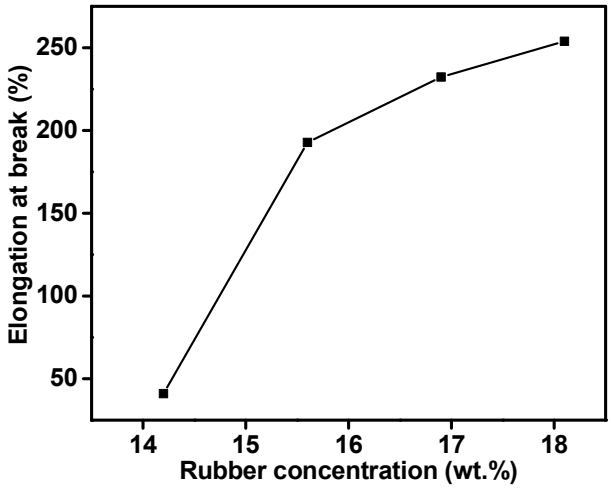

Fig.4.11 Effect of rubber concentration on the strain at failure of alumina green tape

4.4.6 TGA and DMA

The TGA graph of the green tape is shown in **Fig.4.12**. The burn-out of rubber from the green tape starts at a temperature of ~ 200℃. The weight loss slowly increases with an increase in temperature and the complete removal of rubber from the green tape takes place at a temperature of ~ 490℃. A slow and steady burnout of rubber from the green tape is observed. This type of burnout characteristic is considered beneficial for binder removal without creating cracks in the green tape. It has been observed that the flexible green tape turned into a rigid one when annealed at 200℃ for 1 hour even though the TGA shows negligible weight loss before 200℃. This may be due to the self-cross-linking of rubber chains in the green tape through the double bonds. The neat natural rubber obtained by drying the concentrated rubber latex did not form a rigid mass when annealed at 200℃. This indicates that the alumina powder catalyzes the self-cross-linking of natural rubber in the green tape.

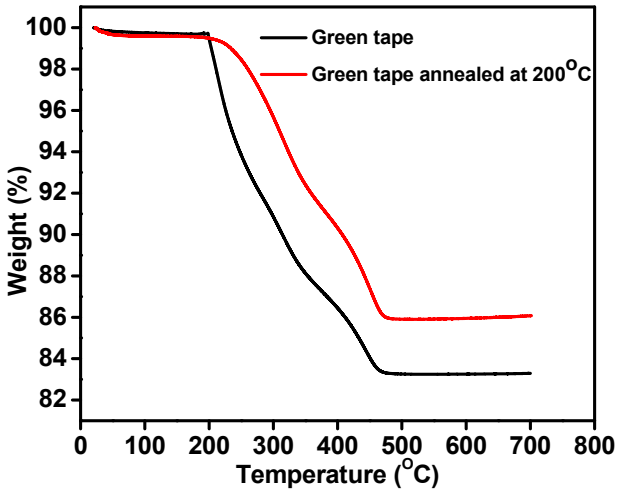

Fig.4.12 TGA of green alumina tape prepared from slurry formulation C (16.9 wt.% rubber)

The Lewis acid sites on the alumina particle surface may induce the self-cross-linking of natural rubber by a cationic mechanism. The cross-linking of polymers is evidenced by the DMA study. Generally, in the rubbery region, the storage modulus increases in the event of a cross-linking reaction (K. P. Menard et al., 2002). The modulus of both the green alumina tape and neat natural rubber sample decreases with an increase in temperature and a rapid decrease is observed at a temperature corresponding to the glassy to rubbery transition (glass transition temperature, Tg). The tanδ shows a peak corresponding to the Tg. The rubber in the alumina green tape shows a Tg of -51°C. On the other hand, the neat natural rubber sample shows a Tg of -46.7°C. After the Tg, the modulus of neat natural rubber remains constant up to 175°C indicating the absence of any cross-linking reaction. However, the modulus of green alumina tape shows a slow increase in the temperature range of 50 to 150°C and the test abruptly stops at a temperature of nearly 175°C due to the breaking of the specimen. The debris obtained after the DMA test are highly brittle. The increase in modulus observed in the temperature range of

50 to 150ºC is due to the self-cross-linking of rubber in the green alumina sample. The DMA graph of alumina green tape and neat natural rubber sample is shown in **Fig.4.13.**

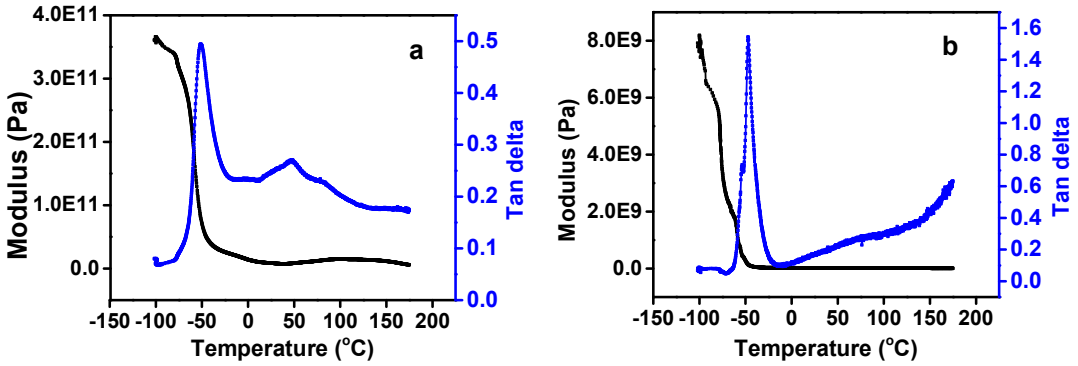

Fig.4.13 The DMA graph of (a) alumina green tape and (b) natural rubber sample

The self-cross-linking of rubber in the green tape is further evidenced by the TGA of the green tape annealed at 200°C (**Fig.4.12)**. The rubber in the annealed green tape sample decomposes at temperatures ~ 75°C higher than that present in the unannealed sample. It is well known that cross-linking increases the thermal stability of polymers (G. F. Levchik et al.,1999; N. Reddy et al.,2010). A lower weight loss observed in the annealed green tape sample may be due to the removal of proteins, carbohydrates, and lipid components associated with the natural rubber during the annealing at 200°C (A. Subramaniam.,1995).

The conversion of flexible tape into a rigid one by cross-linking of rubber has some advantages. The slight curling of green tape may be occurring at the edges during heating for binder removal. This can be avoided by annealing the green tapes at 200°C by keeping them between two glass plates. A photograph of green tapes annealed at 200°C is shown in **Fig.4.14**. It is clear from the figure that the green tape annealed by keeping it between the glass plates shows perfect flatness. On the other hand, slight curling at one corner is observed in green tape annealed by keeping it on a glass plate. This may be due to the residual stress retained during the cutting of the green tape.

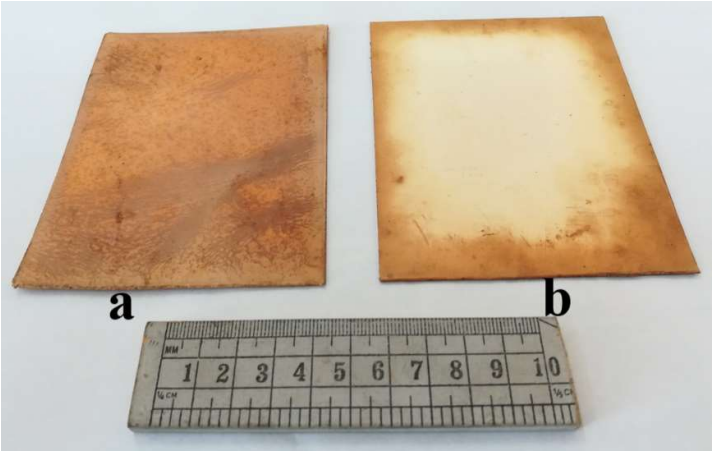

Fig.4.14 Alumina green tapes annealed at 200 ℃, (a) placed on a glass plate (b) placed between two glass plates.

4.4.7 Effect of roll pressing

The binder removal from the annealed tape results in green tape with good integrity and adequate strength for handling. However, the microstructure of the binder removed tape shows a considerable number of pores with a size in the range of 0.5 to 2 μm. The SEM photograph of the binder removed green tape is shown in **Fig.4.15** The particle size analysis of the **NRL** reveals the presence of a significant fraction of rubber particles with a size in the range of 0.5 to 2 μm. The particle size distribution of rubber latex is given in **Chapter 2** as **Fig.2.3**. The pores observed in the green microstructure are due to the removal of these larger rubber particles.

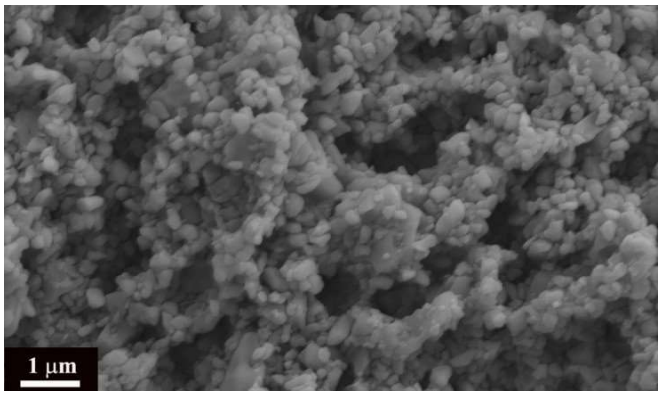

Fig.4.15 The SEM photograph of a binder removed the green tape.

To improve the green density and microstructure by avoiding the larger pores, the green tape is rolled into a roll pressing machine at room temperature before annealing. **Fig.4.16** shows the photograph of a green tape being rolled using a roll pressing machine. A remarkable improvement in the density and microstructure of the green tape (after binder removal) was observed with a decrease in thickness up to 20% by rolling. Further decrease in thickness does not make any change in the green microstructure. **Fig.4.17 a and b** show the microstructure of the green tape after thickness reduction by rolling to 10 and 20 %, respectively, of its original thickness. It appears that during the rolling, the shear forces cause the larger latex particles and aggregates to deform and infuse between the alumina particles to create a green tape with a more uniform microstructure.

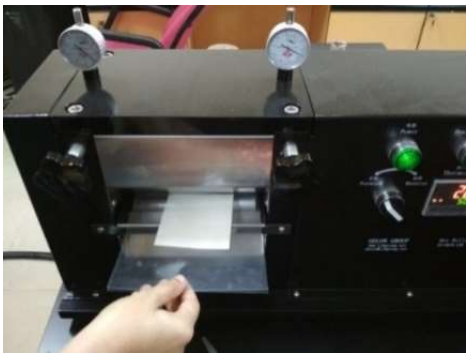

Fig.4.16 The photograph showing the thickness reduction of a green tape using a roll press machine.

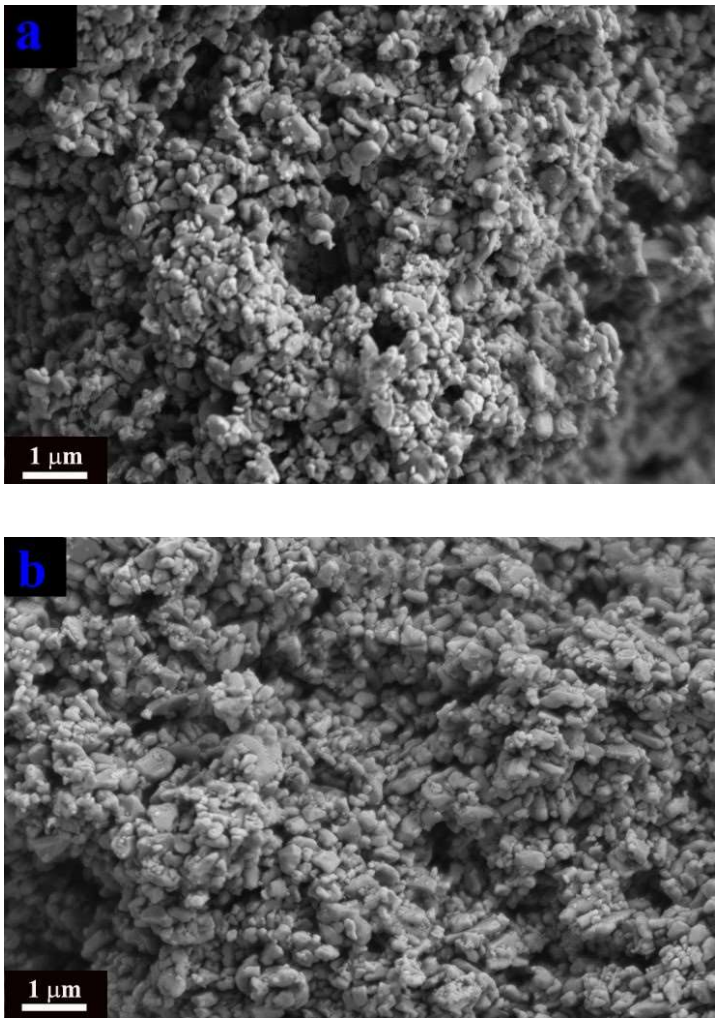

Fig.4.17 The SEM photograph of (a). binder removed alumina green tape after thickness reduction to 10 % and (b). 20%.

The density of green tape before roll pressing is in the range of 53.14 to 50.25 % T.D at rubber concentrations in the range of 14.2 to 18.1wt.%. An exceptional increase in density to the range of 65.71 to 58.04 % T. D is observed in green tapes after a 20% thickness reduction by the roll pressing. The observed improvement in green density is nearly 15 to 23.65% of the original value. The improvement in green density observed at lower rubber concentrations is higher than that observed at higher rubber concentrations. **Fig.4.18** shows the effect of a roll pressing on green density at various rubber concentrations. It appears that the soft natural

rubber particles deform and mix with alumina powder up on roll pressing to produce a more uniform and compact microstructure.

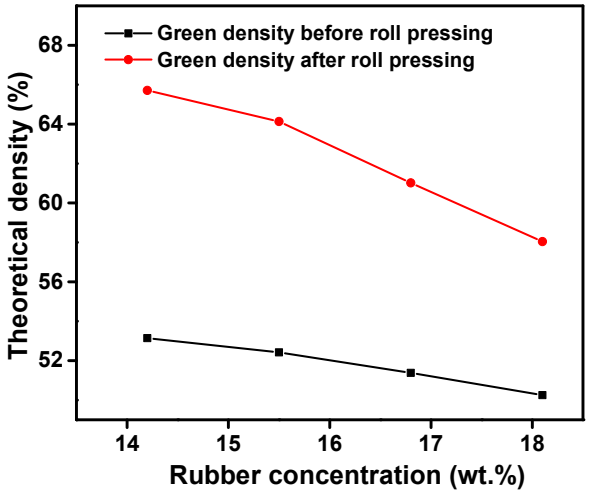

Fig.4.18 Effect of a roll pressing on green density at various rubber concentrations.

The green tape without roll pressing and with roll pressing did not show any crack or warpage during binder removal and sintering. However, the green tape without roll pressing achieves a density of only 93 % of the theoretical value on binder removal and sintering at 1600ºC. However, sintered density increases with a thickness reduction of the green tape by rolling. The green tape rolled to 10 and 20 % of its original thickness achieve a sintered density of 97.5 and 98.5%, respectively, of the theoretical value. Further decrease in thickness does not make any change in the sintered density. A photograph of the sintered alumina tape is shown in **Fig. 4.19**. **Fig.4.20** shows the SEM micrograph of the sintered alumina produced from green tape without roll pressing and roll pressing to 20 % of its original thickness. Residual pores are visible in the SEM photograph of the sintered alumina produced from green tape without roll pressing. On the other hand, the sintered alumina tape produced from a green tape roll pressed to 20% of its original thickness exhibits a dense microstructure. The microstructure of the sintered alumina shows fine and uniform grains.

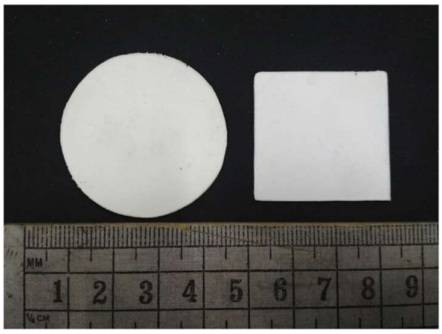

Fig.4.19 Photograph of sintered alumina tape.

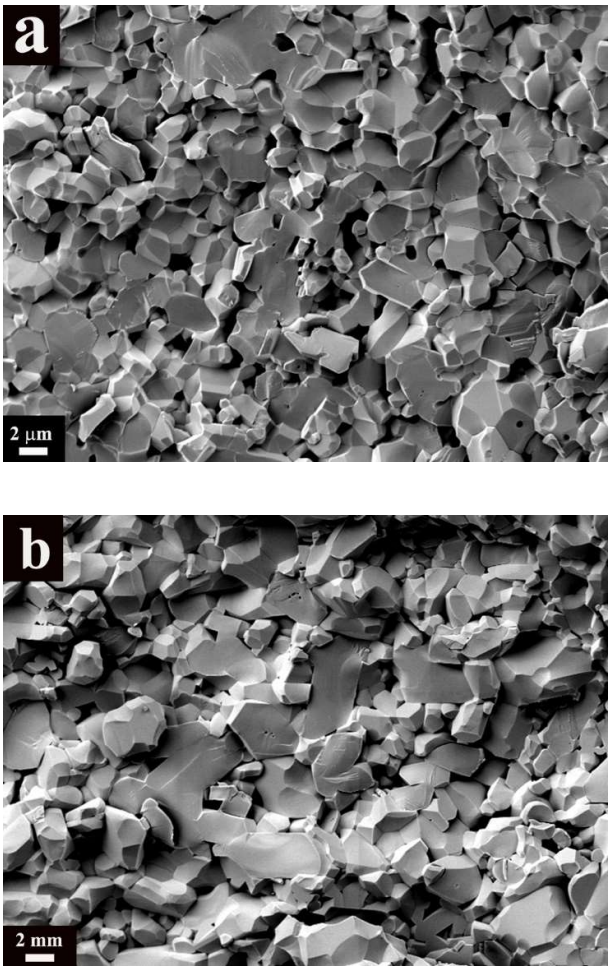

Fig.4.20 The SEM micrograph of the sintered alumina produced from green tape (a). without roll pressing and (b). roll pressing to 20 % of its original thickness.

The average grain size calculated from the SEM photograph by the linear intercept method is 3.2 μm. If we consider the tape casting formulation B, 18.48g of rubber produces 0.055 g of ash in 100g alumina during binder burn-out. That is, the amount of impurity incorporated because of natural rubber is only 0.055 wt.% of alumina. The uniform and small grain size observed in the microstructure indicate that the impurities produced from the **NRL** binder do not produce any exaggerated grain growth in the alumina ceramics.

4.5 Conclusions

NRL is used as a binder for the tape casting of ceramics for the first time. The high negative value of zeta potential of -66 and -76 mV exhibited by the ammonium poly(acrylate) dispersed alumina powder suspension and **NRL**, respectively, enables their co-dispersion at pH in the range of 10.3 to 10.5 to form the tape casting slurries. The slurries prepared at rubber concentrations in the range of 14.2 to 18.1 wt.% of alumina powder show shear thinning flow behavior with suitable viscosity (1.1 to 1.15 Pa.s at 4.65 s^{-1}) and yield stress values (2.97 to 3.27 Pa) for tape casting. The high solid (alumina + rubber) content in the range of 60.55 to 60.88 vol.% of the tape casting formulations achieved due to the concentrated rubber latex enables the drying of the cast tape within a reasonable time of 15 minutes at 70°C. The green alumina tape with rubber content in the range of 14.2 to 18.1 wt.% exhibited adequate tensile strength and elastic modulus in the ranges of 1.62 to 1.85 MPa and 267.5 to 50.8 MPa, respectively. The high flexibility in terms of % elongation at break in the range of 41 to 254 % achieved without the use of a plasticizing agent enables easy peeling off from the substrate. The flexible alumina green tape transforms into a rigid and brittle one during annealing at 200°C due to the self-cross-linking of natural rubber induced by Lewis acid sites of alumina powder. The cross-linking of the rubber enables a near-steady state of binder removal and facilitates the preparation of flat tapes by avoiding the curling of the edges during the binder removal. A remarkable improvement in microstructure and density of the green tape is

achieved by a 20 % reduction in thickness by roll pressing of the flexible green tapes. The roll-pressed green tape achieves a sintered density of 98.5% T.D as compared to 93% T.D achieved without roll pressing. The sintered alumina tape shows a uniform microstructure with an average grain size of 3.2 μm indicating that the trace amount of impurities introduced in the ceramic from the natural rubber binder does not produce any exaggerated grain growth. The process is completely eco-friendly and sustainable as it is not using any synthetic solvent, binder, and plasticizer.

Chapter 5

Freeze-gel casting of alumina using natural rubber latex as a gelling agent and a binder for dense near-net-shape ceramics

5.1 Introduction

Near-net-shape fabrication of ceramic components is increasingly important as it avoids energy-intensive machining of sintered ceramics (P. Greil.,1999). Gel casting has emerged as one of the relatively faster production methods for near-net-shape ceramic components from powder suspensions (J. Yang et al., 2011; R. Gilissen et al.,2000). The gel casting process has aqueous and non-aqueous versions (S. Leo et al., 2014). The non-aqueous versions using acrylic ester monomers are less attractive due to the costly and environmentally hazardous organic solvents (H. Li et al., 2020). The aqueous gel casting system initially developed suffered hesitation from the industry due to the neurotoxicity of the acrylamide monomer (A. C. Young et al.,1991). Later, aqueous gel casting using several low-toxic organic monomer systems has been developed (P. Bednarek et al., 2010; M. Kokabi et al., 2006; M. A. Janney et al.,1998; L. Montanaro et al., 2019). Freezing of aqueous powder suspensions in a mold is also used for setting them into various shapes. The process is called freeze casting. The shapes produced by freeze casting are subsequently freeze-dried and sintered to produce the ceramic components. Herein, the space created by the removal of ice crystals from the freeze-cast bodies remains as pores in the sintered ceramics (T. Fukasawa et al., 2001; T. Moritz et al.,2007). Freeze casting is widely used for the preparation of porous ceramics with a wide range of porosity and a variety of pore architecture. The polymers such as gelatin and polyethylene glycol are effectively used to engineer the pore architecture in various ceramic systems by the gelation-freezing route (M. Fukushima et al.,2016; C.M. Pekor et al.,2008). On the other hand, the preparation of dense ceramics by freeze casting is rarely reported. Sofie et al achieved dense alumina ceramics by freeze casting aqueous powder suspensions of high

solids loading and using antifreeze compounds such as glycerol (S. W. Sofie et al.,2001). The advantage of freeze casting is the quick turnaround of the mold during production as setting by freezing can be achieved very fast. However, the subsequent freeze-drying is time-consuming and requires costly machinery. The setting of powder suspensions by freezing as in freeze casting and subsequent drying in ambient conditions would be an attractive alternative. It has been reported that rubber latex undergoes coagulation on freezing (A. S. Siti Nuraya et al., 2019; W. M. Cole et al.,2017). The present chapter explores the gelation of concentrated alumina-NRL co-dispersions by freezing in a mold to produce dense near-net-shape ceramic components. Herein, the gelation of the aqueous alumina powder suspension is accomplished by freezing the suspension cast in a mold followed by thawing in an acetone medium.

5.2 Experimental

5.2.1 Materials

The α-alumina powder (A16SG) was procured from ACC Alcoa, Kolkata, India. The particle size and surface area of the powder were 0.34 μm and 10.3 m^2/g, respectively. The concentrated (61.6wt.%) ammonia-stabilized NRL was received from Hindustan Latex Ltd., Thiruvananthapuram, India. A 40 wt.% ammonium poly(acrylate) [Darvan 821 A] dispersant was procured from Vanderbilt Company Inc., Norwalk, CA, USA. Analytical reagent grade acetone was obtained from Merck India Ltd. Mumbai. Distilled water was used for the preparation of slurries. A silicon-free defoaming agent (Antifoam O-30) was procured from Sigma Aldrich, USA. Distilled water was used for the preparation of alumina powder suspensions.

5.2.2 Preparation of alumina ceramics by freeze-gel casting

An aqueous slurry of 58.2 vol. % solid loading was prepared by dispersing the alumina powder in distilled water using the ammonium poly(acrylate) dispersant. The ammonium poly

(acrylate) used was 0.5 wt.% of the alumina powder. The slurry in a polypropylene bottle along with zirconia grinding media was tumbled on a roller ball mill for 12 hours. The slurry after the ball milling was poured into a borosilicate glass beaker. The concentrated NRL and the defoaming agent were then added to the alumina slurry and then thoroughly mixed by stirring using a magnetic stirrer for 30 minutes. The concentration of rubber was in the range of 2 to 10 wt.% of the alumina powder. The concentration of defoaming agent was 0.2 wt.% of the alumina powder. The slurry after thorough mixing was cast in cylindrical PVC mold and then cooled in a deep freezer at -55^{o}C for setting for 12 h. The frozen bodies removed from the mold were aged in acetone for 12 hours. Nearly 300 ml of acetone in a 500 ml glass beaker was used for aging a frozen body of 30 mm diameter and 50 mm length. The aged bodies were removed from acetone and dried at room temperature for 6 hours and then at 70^{o}C in an air oven. The dried bodies were annealed at 200^{o}C for cross-linking of rubber to achieve high green strength. Burn-out of rubber from the green bodies was accomplished by heating at a rate of 1^{o}C/minute up to 600^{o}C. The binder-removed bodies were sintered at 1550^{o}C in an electrically heated furnace for 2 hours. The heating rate was 5^{o}C/minute. The flowchart of the freeze-gel casting using NRL binder is shown in **Fig.5.1**.

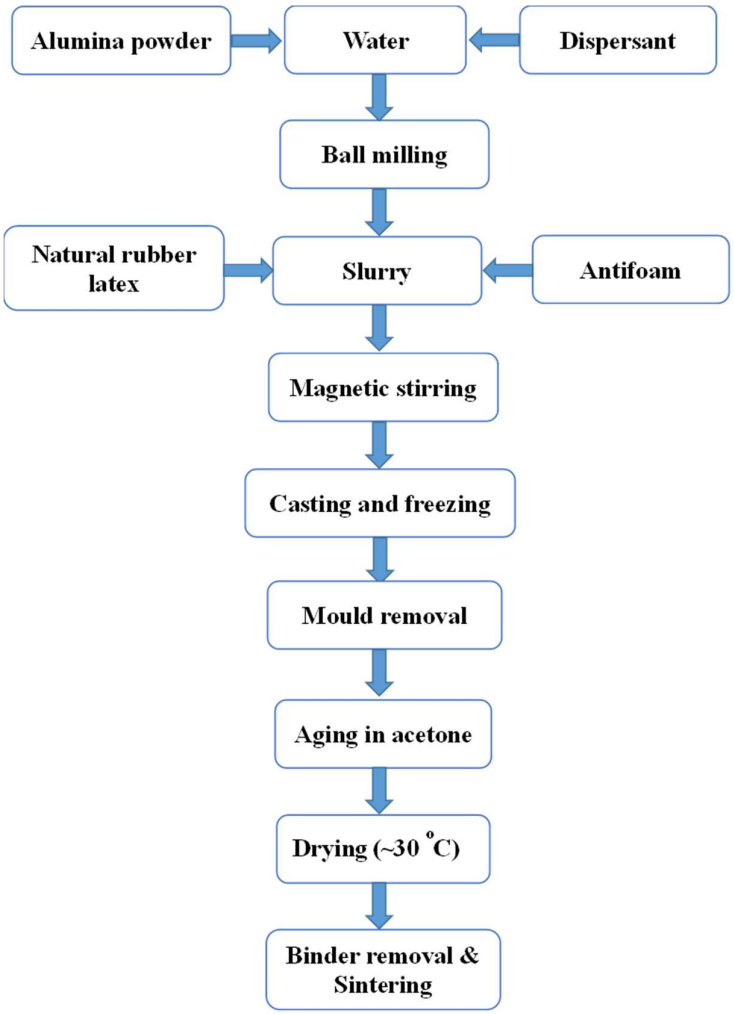

Fig.5.1 Flowchart of freeze-gel casting using NR latex binder.

5.3 Characterization

5.3.1 Rheological characterization

Viscosity and yield stress measurement of the slurries was carried out using a Brookfield viscometer (Brookfield Engineering Inc., Middleboro, MA) coupled with a small sample adapter and a cylindrical spindle (SC 21). The yield stress of the slurries was obtained from the shear rate-shear stress data using the Casson model.

5.3.2 Measurement of gel strength and green strength

The mechanical strength of gelled wet bodies and green bodies was measured using a Universal Testing Machine (Instron5500, Instron USA). The strength of wet gelled bodies was measured by applying compressive stress on cylindrical samples of 50 mm height and 30 mm diameter and noticing the strain at a loading rate of 0.5 mm/minute. The compressive strength and Young's modulus were obtained from the stress-strain graph. The strength of green bodies was measured by diametrical compression using cylindrical samples of 15mm length and 30 mm diameter. The cross-head speed was 0.5mm/minute. The diametrical compressive strength was calculated from the breaking load using equation (8) given in Chapter 2.

5.3.3 Shrinkage measurement

The drying and sintering shrinkages were calculated from the diameter and height of samples measured using a Vernier caliper of readability 0.01mm.

5.3.4 Green and sintered density measurements

The green density was measured from the weight and the dimensions of cylindrical bodies. The dimensions were measured using a Vernier caliper. The sintered density was measured using Archimedes' principle.

5.3.5 Thermogravimetric analysis

The thermogravimetric analysis (TGA) of the gel-cast green ceramic sample was conducted in an air atmosphere using a thermo-gravimetric analyzer (Q-50, TA Instruments, USA). The heating rate was 5°C/minute.

5.3.6 Microstructure analysis

The microstructure of the green and sintered ceramics was observed on fractured surfaces using a scanning electron microscope (FE-SEM, Carl Zeiss Sigma HD, Germany). The samples

were sputter-coated with gold before the SEM analysis. The average grain size was calculated from the SEM images using the linear intercept method.

5.4 Results and discussion

5.4.1 Preparation of freeze-gel casting slurry

The alumina-**NRL** co-dispersions prepared by mixing 58.2 vol.% alumina slurry and concentrated **NRL** shows pH in the range of 9.6 to 9.9. At this pH range alumina and NRL, particles have very high negative surface potentials leading to well-dispersed stable co-dispersions. The composition of slurries prepared at various **NRL** concentrations is given in **Table 5.1**. The concentration of alumina with respect to total water present in the slurry decreases from 56.58 to 50.7 vol.% when the rubber concentration increases from 2 to 10 wt.% alumina. On the other hand, the total solid (alumina+rubber) content in the slurry increases from 58.62 to 59.76 vol.%.

Table 5.1 The composition of the freeze gel casting slurries

Concentration of natural rubber, wt.%	Alumina (gm)	Water (ml)	Dispersant (wt.%)	**NRL** (gm)	Total solid loading (vol.%)	Conc. of alumina with respect to water (vol.%)
0	100	18	0.40	0	58.20	58.20
2	100	18	0.40	3.32 (2.04)*	58.62	56.58
4	100	18	0.40	6.77 (4.16)	58.97	54.95
6	100	18	0.40	10.37 (6.38)	59.25	53.31
8	100	18	0.40	14.14 (8.69)	59.51	51.72
10	100	18	0.40	18.06 (11.11)	59.76	50.17

*Values given in the parenthesis are the mass of the natural rubber

5.4.2 Rheological properties of freeze-gel casting slurries

The viscosity of the co-dispersions containing various concentrations of NRL is shown in **Fig.5.2**. The viscosities of 58.2 vol.% alumina slurry and the concentrated NRL measured at a shear rate of 9.3 s^{-1} are 2.18 and 0.05 Pa. s, respectively. The co-dispersions show shear-thinning flow behavior. The viscosity of 58.2 vol.% alumina powder suspension decreases with the incorporation of concentrated **NRL**. The co-dispersions prepared at rubber concentrations in the range of 2 to 10 wt.% of alumina powder show viscosity in the range of 1.2 to 0.6 Pa.s at a shear rate of 9.3 s^{-1}. The flow behavior of the slurries follows the Casson model. That is, the plot of the square root of shear rate versus the square root of shear stress gives a straight line. **Fig.5.3** depicts the Casson plot of all the freeze-gel casting slurries prepared at various rubber concentrations. The yield stress of the slurries obtained by extrapolating the straight line to zero shear rates is presented in **Table 5.2**. The 58.2 vol.% alumina slurry shows a high yield stress value of 11.83 Pa. The yield stress value decreases to 3.10 Pa when the rubber concentration increases to 10 wt.% of alumina. The observed viscosity and yield stress ranges of the slurries are sufficiently low to flow and fill any intricate shape mold and therefore suitable for gel casting.

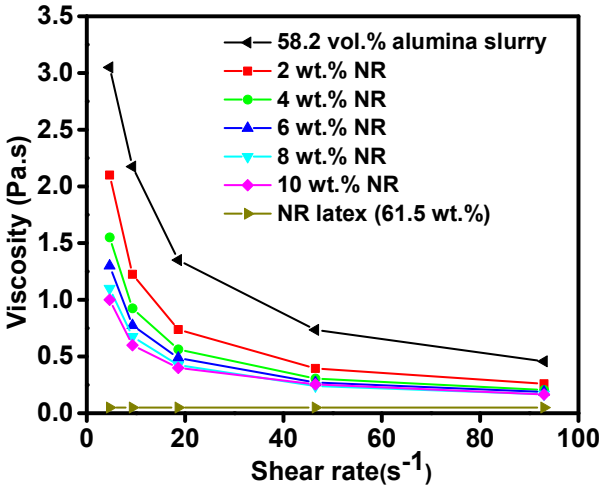

Fig.5.2 Viscosity versus shear rate plot of alumina, NR latex, and alumina-NR latex co-dispersions.

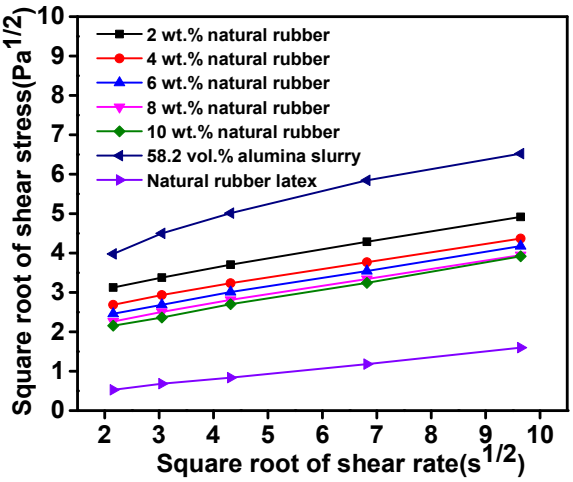

Fig.5.3 The Casson plot of freeze gel casting slurries.

Table 5.2 The Yield stress values from the Casson flow model

Rubber concentration (wt.% of alumina)	0	2	4	6	8	10
Yield stress, Pa	11.83	6.97	5.02	4.04	3.46	3.10

5.4.3 Shape stability of the gels

The concentrated aqueous alumina powder suspensions containing NRL cast in cylindrical PVC molds undergo setting while cooling in a deep freezer. The frozen bodies removed from the mold when exposed to room temperature (~30^{o}C) show different shape stability depending on the rubber concentration. The body prepared without rubber latex starts to deform in 30 minutes due to the melting of ice. On the other hand, the stability of the frozen bodies against deformation during thawing increases with the rubber concentration. The frozen body prepared at 8 wt.% rubber concentration shows only minor deformation after 1 hour when placed horizontally without any disturbance. However, the body is highly soft and flexible and collapses while handling. The photograph of cylindrical freeze-gel cast wet alumina bodies prepared at various concentrations of **NRL** immediately after mold removal, after 30 minutes, and after 1 hour is shown in **Fig.5.4**.

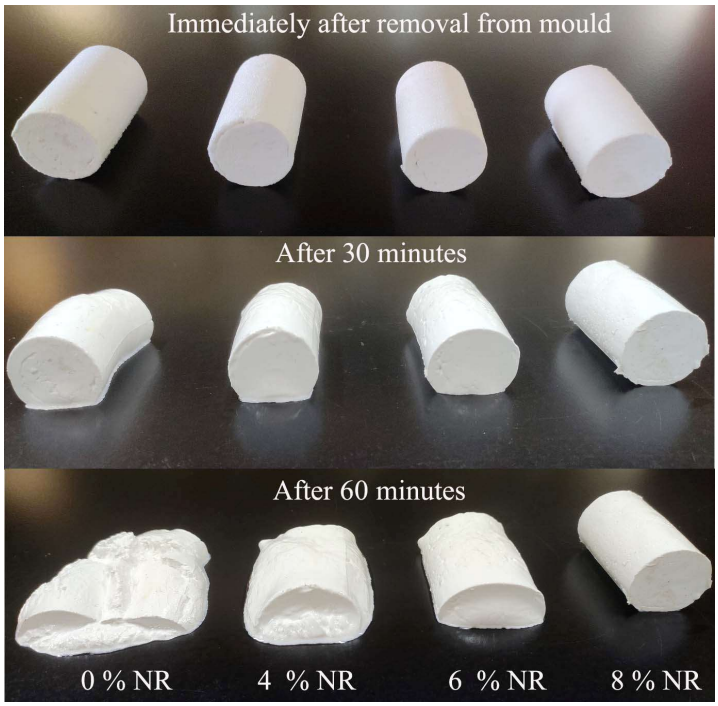

Fig.5.4 The photograph of cylindrical freeze-gel cast wet alumina bodies containing various concentrations of rubber latex immediately after mold removal, after 30 minutes and 1 hour.

Even though the cylindrical frozen body of 30 mm diameter and 50 mm length prepared at 8 wt.% rubber concentration exhibits reasonable shape stability when placed in the horizontal position, collapses by sagging after 30 minutes when placed in the vertical position. This indicates that the gel strength after the melting of ice is not sufficient to resist deformation due to its weight. On the other hand, the frozen body removed from the mold when immersed in water-miscible solvents like acetone and ethanol exhibits shape stability in the vertical position also. When immersed in the solvent (acetone or ethanol), the water produced by the melting of ice in the body is exchanged with the solvent. The alumina and rubber in contact with the solvent further coagulate and strengthen the alumina-rubber gel network leading to improved gel strength. **Fig.5.5** shows photographs of freeze-cast cylindrical wet alumina bodies aged in a vertical position in the air and acetone. The body kept in the air atmosphere starts deformation in 30 minutes due to its weight whereas the body aged in an acetone medium remains stable. Therefore, the frozen bodies removed from the mold are aged for 12 hours in acetone for solvent exchange and thereby achieve higher gel strength. It appears that when the frozen body is immersed in acetone the alumina-rubber gel network on the surface of the body gets strengthened first due to coagulation in contact with the acetone. The melting of ice in the frozen body also starts from the surface. That is, the melting of ice and strengthening of the alumina-rubber gel network progresses from surface to interior with the progress of aging time. This enables the body to resist the deformation due to its weight during the melting of ice. It is worth noting that frozen bodies produced at rubber concentrations up to 6 wt.% of alumina undergo crack and then disintegrate when immersed in acetone for solvent exchange. This further confirms that the percolation of rubber latex particles to produce a stable alumina-rubber gel network is possible at a minimum concentration of 8 wt.%.

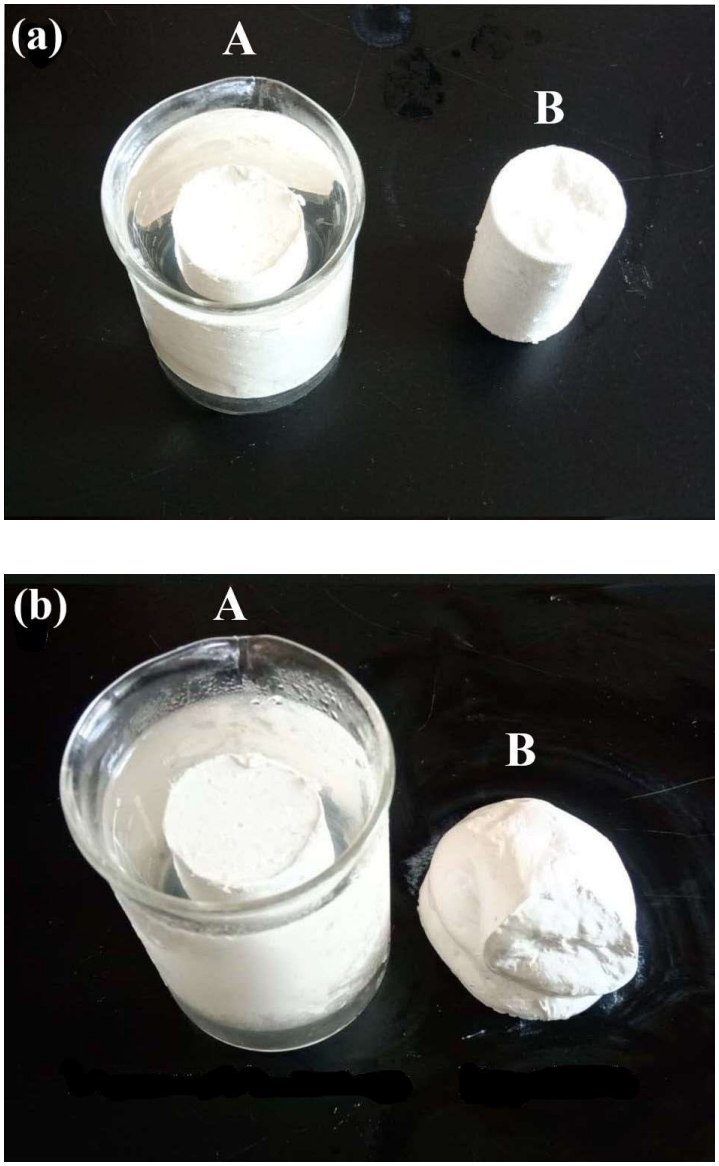

Fig.5.5 Photograph showing freeze-cast cylindrical wet alumina bodies aged in the vertical position in acetone (A) and in air (B). (a) at the start of aging and b) after 30 minutes.

5.4.4 Mechanism of gel formation

It is well known that the rubber particles in latex are stabilized in an aqueous medium due to the protein layer on their surface (Y. Wei et al.,2017; J. Sansatsadeekul et al.,2011; C.C.Ho et al.,1996). It has been reported that the freezing of rubber latex results in the aggregation of particles leading to coagulation (A. S. Siti nuraya et al.,2019; E. G.

Cockbain.,1969). Herein, the particle rejection due to the ice crystallization compels the rubber particles to come closer. This disrupts the protein cloud around the rubber particle. The rubber particles with broken protein clouds coalesce leading to the formation of lumps. Therefore, freezing and thawing are widely used instead of coagulation using acid for the separation of solid rubber from latex (W. M. Cole et al.,2017). During the freezing of alumina powder suspension containing **NRL**, particle rejection due to the ice crystal growth compresses the alumina and rubber particles together. This disrupts the protein layer on the latex particles leading to their adhesion on alumina particles and neighboring rubber particles. This alumina-to-rubber and rubber-to-rubber adhesion provides stability against deformation even after the melting of ice. It can be inferred that the percolation of rubber particles to achieve shape stability by holding the water produced by melting ice is attained at a minimum rubber concentration of 8 wt.%. The mechanism of stable gel formation by freezing and thawing of the alumina-**NRL** co-dispersion is schematically represented in **Fig.5.6**. The rubber concentration higher than 8 wt.% is not attempted for gel casting as water present in the rubber latex dilutes the slurry. At 8 wt.% **NR**, the alumina concentration in the slurry with respect to the water reaches 51.72 vol.%. It is well known that slurries of high ceramic powder loading are desirable for gel casting to minimize drying and sintering shrinkages (A.C.Young et al.,1991). In addition, a higher binder concentration is also detrimental as it tends to create pores in the sintered ceramics.

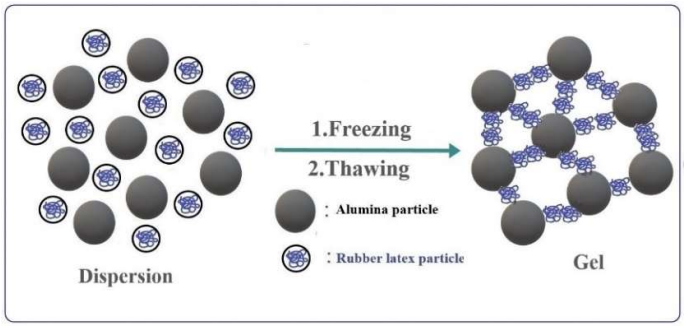

Fig.5.6 Schematic showing the mechanism of formation of alumina-rubber gel.

5.4.5 Gel strength

The solvent-exchanged wet bodies achieve sufficient strength for handling during drying. The stress-strain graph of a solvent-exchanged wet gel cast body is shown in **Fig.5**.The stress-strain graph shows an initial linear increase of stress with strain followed by a strain hardening. Bulging of the gel with a vertical crack on the surface is observed at strain beyond 10%. The photograph of the wet gel before and after the compression test is given as an insert in **Fig.5.7**. The stress at 10% strain is taken as the compressive strength, and the slope of the initial linear region is taken as Young's modulus. The solvent exchanged wet gel shows a compressive strength of ~60 kPa and Young's modulus of 640 kPa. The strength of wet alumina gel cast bodies prepared using agarose binder (~ 98 kPa at 3 wt.% agarose) is higher than that of alumina wet gels produced at 8 wt.% **NR** (T. Zhang et al., 1994; A. J. Fanelli et al., 1989). On the other hand, the strength of the wet gel cast alumina bodies reported with 8 wt.% gelatine binder (~60 kPa) is matching well with the strength of wet alumina gels produced in the present study with the **NRL** binder (Y. Chen et al.,1999). The observed compressive strength is sufficient for easy handling of the gel before drying.

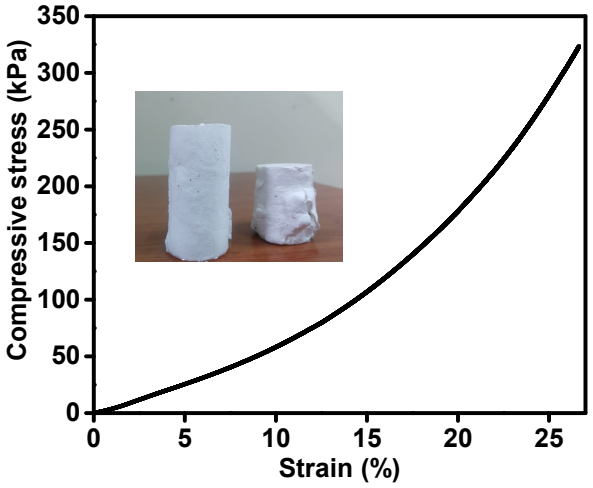

Fig.5.7 Stress-strain plot of solvent exchanged wet alumina gel.

5.4.6 Drying kinetics

The drying of conventional gel cast bodies is accomplished under controlled humidity and temperature conditions to avoid the formation of cracks and warpage (A.C.Young et al.,1991). On the other hand, solvent removal from freeze-cast bodies is done by sublimation in a lyophilizer (T.Fukasawa et al.,2001; Y. Zhang et al.,2010). In both cases, drying requires costly machinery and takes a relatively long time. In the present case, the solvent exchanged wet gels dries quickly in an air atmosphere at room temperature. The weight loss from a solvent-exchanged wet gel body with time is presented in **Fig.5.8**. Nearly 75% of the solvent present in the body is removed within 6 hours at room temperature. The removal of the remaining solvent is accomplished by heating in an air oven at 70℃. This indicates that water present in the gelled body is not completely exchanged with acetone. Nearly 25% of water is likely to retain even after aging in acetone for 12 hours. However, replacing the spent acetone with a fresh one at the end of 12 hours and continuing the aging for another 12 hours results in the exchange of ~97% water. Nevertheless, the removal of 97% of acetone is not warranted as the sample aged in acetone for 12 hours does not develop any crack or deformation during the subsequent drying. Herein, the high volatility of the acetone made the drying faster and its low surface tension allows drying without creating much capillary pressure (S. J. Yoon et al.,2001). It is worth noting that the solvent exchange not only improve the gel strength but also made the gel drying easier and faster. The body undergoes a diametrical shrinkage of ~1.5% during the drying. The green body shows a density of 2.02g/cc. This is equivalent to 50.82%T.D of alumina.

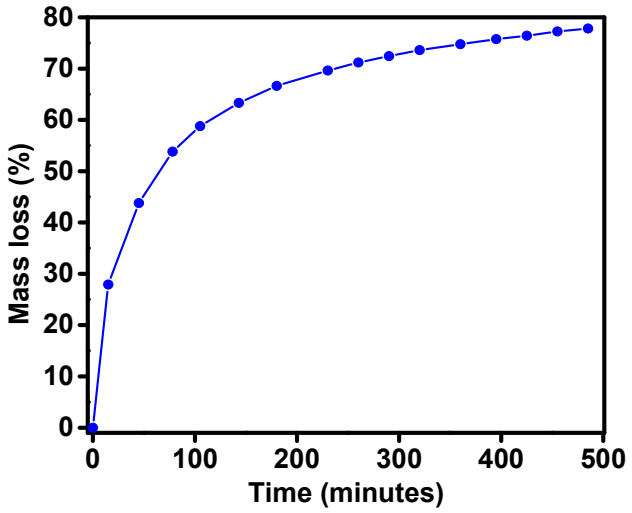

Fig.5.8 The drying kinetics of a solvent exchanged wet alumina gel body.

5.4.7 Green strength

The green body produced by drying the solvent-exchanged gel has sufficient strength for minor finishing using an emery paper. The strength of the dried green body is measured by a diametrical compression test. The diametrical compressive load-displacement plot of the green body is shown in **Fig.5.9**. The load increases slowly with displacement until a vertical crack is developed at the center of the body. The corresponding load is taken as the breaking load. Further, there is a small decline in load followed by strain hardening. That is, the body exhibited almost plastic-like behavior. The diametrical compressive strength calculated from the breaking load is 0.34 MPa. It has been reported in the previous chapters that the rubber latex in the presence of alumina powder undergoes self-cross-linking when heated at a temperature of ~200°C. The Lewis acid sites on the alumina particle surface catalyze the self-cross-linking through the carbon-carbon double bonds present in natural rubber by a cationic mechanism. The green gel cast bodies on annealing at 200°C in an air oven for 2 hours show higher strength and brittle behavior due to the self-cross-linking of the rubber binder. The

diametrical compressive load-displacement graph of the green body annealed at 200°C shows a rapid and linear increase in load with displacement and reaches a maximum at a displacement of ~0.25 mm. Thereafter, the body undergoes brittle failure by breaking along the diameter. The diametrical compressive strength of the annealed body is calculated as 2.14 MPa. The Young's modulus of the green body increases from 18 to 150 MPa due to annealing at 200°C. The photograph of dried and annealed green bodies after the compression test showing their mode of failure is given in **Fig.5.10**.

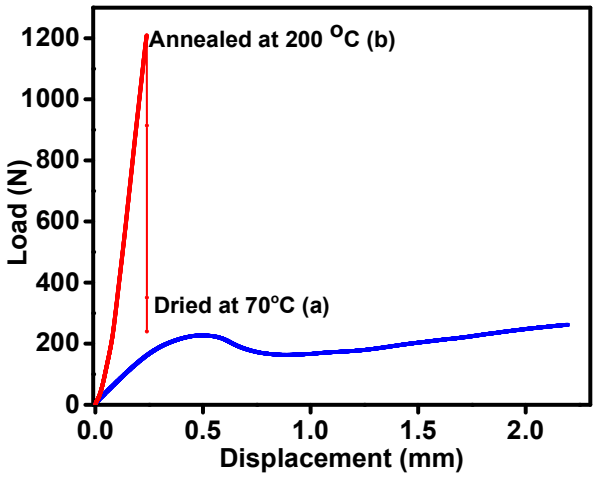

Fig.5.9 Diametrical compressive load-displacement graph of the green body dried at 70°C and annealed at 200°C.

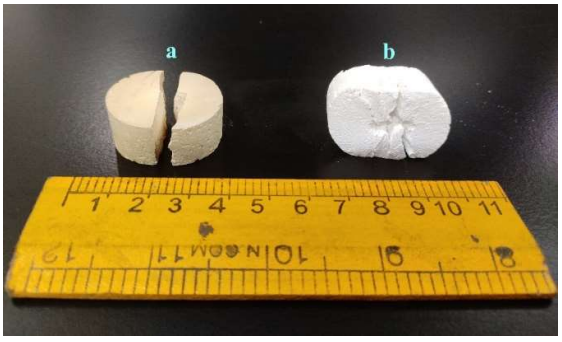

Fig.5.10 The photograph of annealed (a) and dried (b) bodies after the compressive strength test showing their mode of fracture.

5.4.8 Green microstructure

The low magnification SEM image of the gel-cast green body does not show any pores evidencing ice crystal growth during freezing. On the other hand, it is interesting to note that the green body produced by direct freeze-drying of the frozen bodies in a lyophilizer shows lamellar-type pores due to the ice crystals produced during freezing. The low-magnification SEM images of green bodies obtained by solvent exchange followed by conventional drying and direct freeze-drying are shown in **Fig.5.11a** and **Fig.5.11b**, respectively. This indicates that ice crystals are growing during the freezing of the slurry even though the total solid (alumina + rubber) concentration is nearly 60 vol.%. It appears that the water produced during the melting of ice crystals is reabsorbed in the alumina-rubber gel network. This makes the gelled body almost like a semi-fluid as evidenced by its deformation when vertically placed at room temperature. That is, during aging in acetone, the frozen body passes through a semi-fluid state. That is, the transformation of the strong frozen body to a gel of reasonable strength takes place through an intermediate semi-fluid state. This transformation takes place layer-by-layer from the surface to the interior of the body. This layer-by-layer transformation saves the frozen body from collapse during aging in acetone even though there is an intermediate weak semi-fluid state. It appears that this semi-fluid nature allows the soft gel to flow and reorganize to fill the space created by the melting of the ice crystals. That is, during thawing in acetone the soft semi-fluid like alumina-**NR** gel produced flows and fills the pores created by the melting of ice crystals before achieving strength by further coagulation. This transformation produces a uniform gel without the lamellar-type pores and facilitates the preparation of dense ceramics from the frozen bodies. This is further evidenced by the microstructure of the green body obtained by solvent exchange followed by conventional drying of the frozen body. The green body shows a homogenous compact microstructure with uniform distribution of alumina and

rubber particles, unlike the one with lamellar pores observed for samples prepared by freeze-drying the frozen bodies.

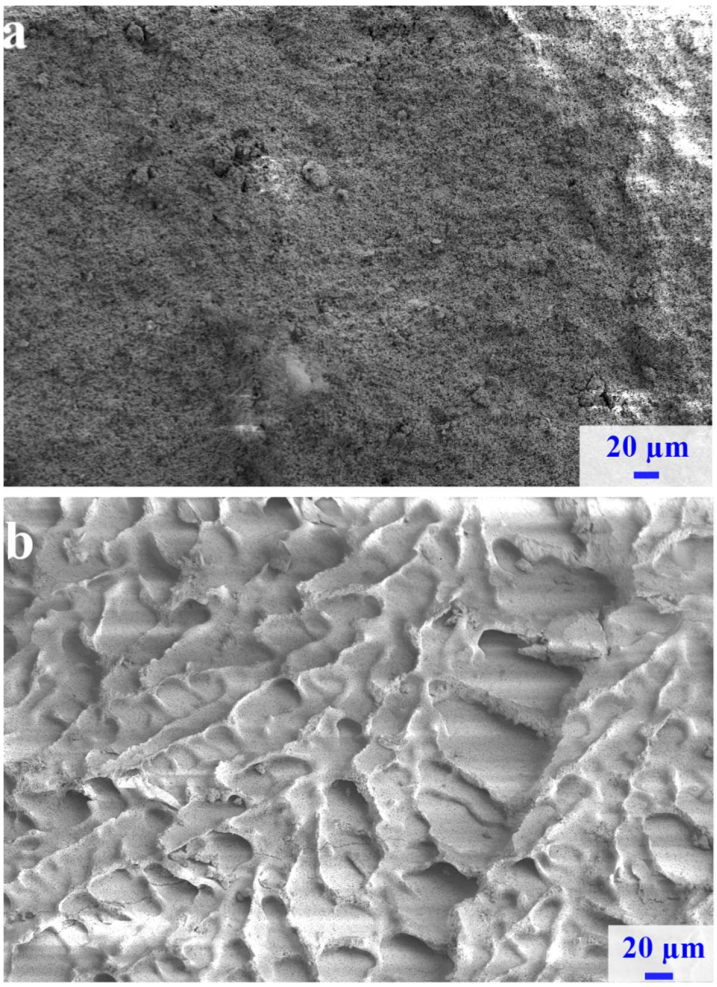

Fig.5.11 Low magnification SEM image of the fractured surface of the green body produced by solvent exchange followed by ambient drying (a) and direct freeze-drying (b) of freeze-gel cast bodies.

5.4.9 Binder removal

The TGA graph of annealed alumina gel cast green body is shown in **Fig.5.12**. The thermal degradation of cross-linked rubber from the green alumina sample starts at 210°C. The cross-linked rubber binder in the gel-cast body undergoes decomposition in two steps as

evidenced by the DTG graph. The decomposition proceeds with near steady-state kinetics and completes at ~525℃. The slow and steady decomposition of the polymeric binder is advantageous in binder removal without creating any cracks in the green body (R. V. Shende et al., 2002). The gel cast alumina bodies did not show any crack or deformation during binder removal by heating at a rate of 1℃/minute up to 700℃ in a muffle furnace. The binder-removed body shows enough strength for further handling before sintering.

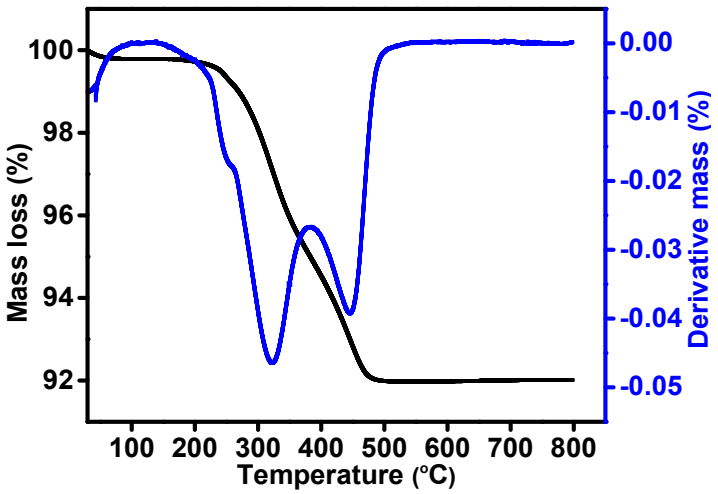

Fig.5.12 TGA-DTG graph of the annealed green body containing 8 wt. % rubber.

5.4.10 Sintering

The binder removed bodies on sintering at 1550℃ achieve ~96% of theoretical density. The linear and diametrical shrinkages observed during sintering are 15 and 16 %, respectively. The low and high-magnification SEM images of fractured surfaces of sintered alumina ceramics prepared by freeze-gel casting are shown in **Fig.5.13a & b**, respectively. It is further confirmed from the low magnification image that the lamellar-type pores noticed in the case of the freeze-dried samples due to ice crystal growth are completely absent in the samples produced by acetone exchange and air drying of the frozen bodies. The high magnification

image shows a dense microstructure with fine grain size. The mean grain size calculated from the SEM image by the linear intercept method is 1.3μm.

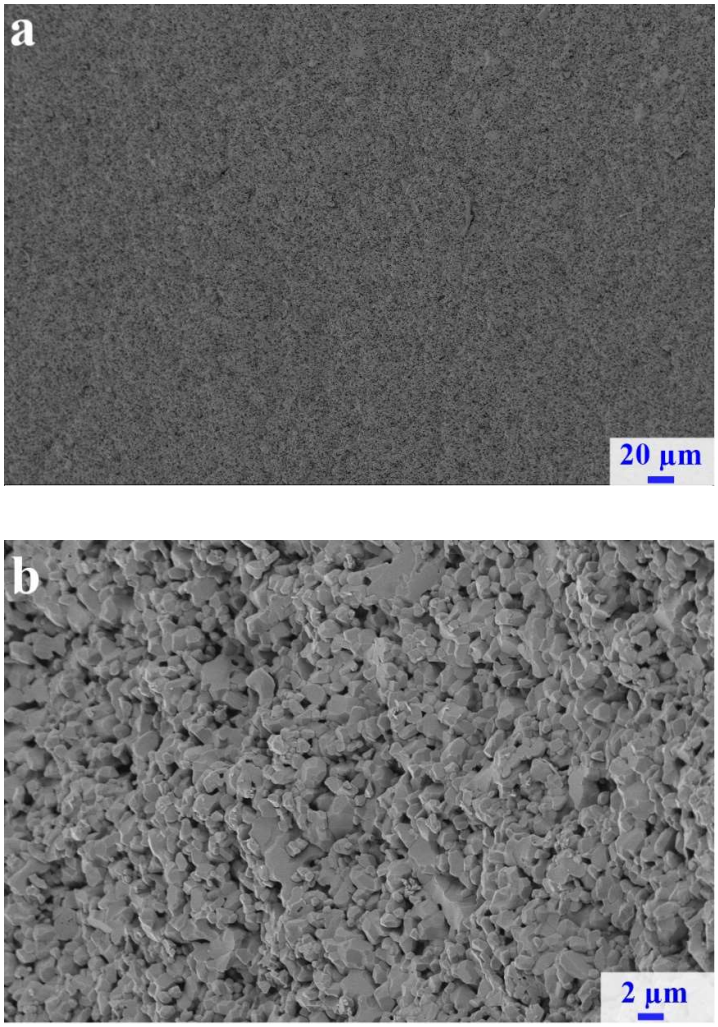

Fig.5.13 Low (a) and high (b) magnification SEM images of the fractured surfaces of sintered alumina ceramic prepared by freeze-gel casting.

5.4.11 Near-net shaping capability

The preparation of complex near-net-shape ceramic components of defect-free microstructures is very important (M. H. Bocanegra-Bernal et al.,2009). Here, like the conventional aqueous gel casting using organic monomers, freeze-gel casting using **NRL** can produce complex shapes by freezing the slurry in molds made of metals, plastic, and wax. The

complex shapes produced are very strong in the frozen condition to resist any deformation during mold removal. A photograph of green and sintered alumina spur gear fabricated by the freeze-gel casting in a wax mold is shown in **Fig.5.14**. The thin section (teeth of the gear wheel) did not show any deformation during the acetone exchange and subsequent air drying. Moreover, the green and sintered bodies show a good surface finish. Unlike organic monomer-based gel casting systems, freeze-gel casting using **NRL** is sustainable, environmentally benign, and non-toxic.

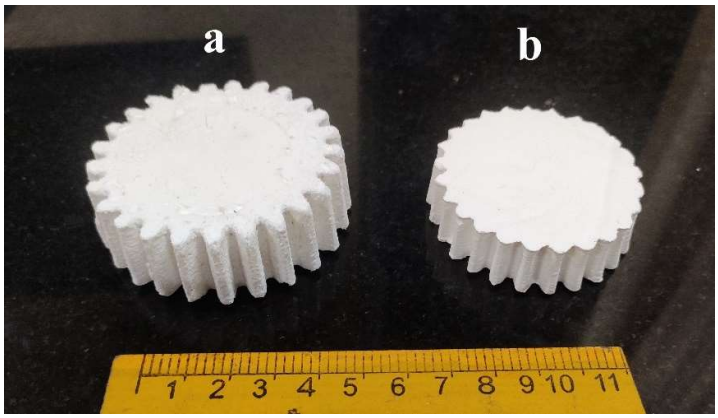

Fig.5.14 Photograph of an alumina spur gear fabricated by freeze-gel casting in a wax mold. a) green and b) sintered bodies.

5.5 Conclusions

Gel casting of aqueous alumina powder suspensions using **NRL** as a gelling agent and binder has been studied. Gelation of alumina-**NRL** co-dispersions is achieved by the coagulation of the latex particles by freezing the slurry in a mold and subsequently thawing in an acetone medium. During freezing, particle rejection due to the growing ice crystals compresses the alumina and rubber latex particle together leading to the breaking down of the surface protective protein and lipid layer of the rubber latex particles resulting in coagulation. The water produced by the melting of ice crystals reabsorbs in the alumina-rubber gel network resulting in a soft, and pliable gel. The minimum concentration of rubber required to percolate

and form a stable alumina-rubber gel is 8 % by weight of the alumina powder. The aging of the frozen body in acetone strengthens the alumina-rubber gel network by further coagulation due to solvent exchange results in strong wet gels. The compressive strength (60kPa) and modulus (640 kPa) of the wet gel are sufficient for further handling during drying. The frozen body passes through a semi-fluid state during thawing which enables the gel to flow and fill the space created by the melting of ice crystals leading to dense ceramics. The acetone exchange enables faster drying of the gel cast bodies at room temperature without creating any deformation or crack. The diametrical compressive strength of the dried green body is 0.34 MPa. A remarkable increase in the diametrical compressive strength of the green body from 0.34 to 2.14 MPa (6.3 times higher) and modulus from 18 to 150 MPa, is achieved on annealing at 200℃ due to cross-linking of rubber chains. The cross-linking benefits the binder removal enabling a slow and steady burnout as evidenced by the TGA. The green bodies on debinding and sintering at 1550℃ produce alumina ceramics of uniform microstructure with ~96% T.D and 1.3 μm average grain size. The non-toxic and sustainable gel casting system produces complex near-net-shape alumina ceramics.

Chapter 6

Freeze gel casting of aqueous alumina powder suspensions using natural rubber latex as a binder and pore stabilizer for macroporous ceramics

6.1 Introduction

Macroporous ceramic materials find application in the area of high-temperature thermal insulation, catalyst support, molten metal filtration, and bio-implants (I. Nettleship.,1996; E. C. Hammel et al.,2014). Fugitive particle templating, polymer foam replication, foaming and setting of powder suspensions, and freeze casting are used for the preparation of macroporous ceramics from ceramic powders (T. Ohji et al., 2012; S. Deville.,2008). Among them, freeze casting is a simple and cost-effective method that produces tailored porosity and pore structure by appropriately selecting a solvent medium, the volume fraction of ceramic in the slurry, the direction of freezing, and using some additives such as alcohol, glycerol, gelatin, and polyethylene glycol (D.Zhang et al.,2012; S.Deville.,2008). Water, naphthalene, naphthalene-camphor mixture, camphene, tertiary butyl alcohol, tertiary butyl alcohol-water mixture, cyclohexane, and tertiary butyl alcohol-cyclohexane mixture are studied as a dispersion medium for freeze casting of ceramics. Among them, ice templating using water as a medium is the most attractive one due to the wide availability, low cost, and environmentally friendly nature of water. However, the removal of ice crystals from the frozen ceramic powder suspensions by freeze drying requires a lyophilizer. It works at a low temperature and high vacuum, typically below the triple point of water. This would hurdle the scale-up of the ice-templating process to produce macroporous ceramics. Therefore, the removal of ice crystals from the frozen body using methods other than freeze drying without pore collapse is of utmost importance. The present chapter explores the freeze-casting of aqueous alumina powder-**NRL** co-dispersions at higher rubber concentrations to produce macroporous ceramics without a freeze-drying step. The large concentration of rubber prevents the formation of a semi-fluid

state during the thawing of frozen powder suspensions and thereby stabilizes the pores created by the melting of ice crystals.

6.2 Experimental

6.2.1 Materials

The α-alumina (A16SG) powder of average particle size 0.34 mm and specific surface area 10.3 m^2/g was procured from ACC Alcoa, Kolkata, India. Concentrated **NRL** of 61.5 wt.% solid content was obtained from Hindustan latex, Thiruvananthapuram India. Ammonium poly(acrylate) aqueous solution (40 wt.%) procured from Vanderbilt, USA was used as the dispersing agent. Analytical reagent grade acetone was procured from Merck India Ltd. Mumbai. Distilled water was used for the preparation of powder dispersions.

6.2.2 Preparation of macroporous alumina ceramics

A 58.2 vol.% alumina slurry was prepared by dispersing the alumina powder in water using the ammonium poly(acrylate) dispersant and tumbling in a cylindrical polyethylene bottle along with zirconia balls of 10 mm size on a roller ball mill for 12 hours. The concentration of dispersant was 0.5 wt.% of the alumina. The alumina powder to zirconia ball weight ratio was 1:3.The slurry poured into a beaker was mixed with an adequate quantity of concentrated **NRL** and additional water to adjust the alumina concentration in the slurry. The slurry was stirred for 30 minutes using a magnetic stirrer for homogeneous mixing. The alumina volume percentage expressed throughout this chapter is with respect to the water present in the slurry and the rubber concentration is in weight percentage with respect to the alumina powder. The composition of slurries used for freeze-casting for the preparation of macroporous alumina ceramics is given in **Table 6.1**. The prepared slurry was cast in open cylindrical molds of 30 mm inner diameter and 30 mm height fabricated by fixing PVC tubes on a glass plate using an adhesive. The slurries cast in the mold were kept in a deep freezer at

-58°C for freezing of water. The frozen bodies were removed from the mold and thawed in an acetone medium. The bodies were aged in acetone for 48 hours for the exchange of water with acetone. The acetone-exchanged bodies were dried in air at room temperature for 10 hours and then in an air oven at 70°C. The dried bodies were heated in an air atmosphere sintering furnace at 1550°C for binder removal and sintering. The heating rate was 1°C/minute from room temperature to 500°C and then 3°C/minutes up to 1550°C. The samples were held for 2 hours each at 200, 500, and 1550°C.

Table 6.1 The composition of slurries used for freeze-casting for the preparation of macroporous alumina ceramics.

Alumina (gm)	**Dispersant (wt.%)**	**Water (ml)**	**NRL (gm)**	**Concentration of alumina to water (vol.%)**
100	0.40	18	40.65 (25.00)*	42.75
100	0.40	28	40.65 (25.00)	36.53
100	0.40	38	40.65 (25.00)	31.89
100	0.40	48	40.65 (25.00)	28.30
100	0.40	58	40.65 (25.00)	25.44
100	0.40	68	40.65 (25.00)	23.10
100	0.40	58.63	18.07 (11.11)	30
100	0.40	58.63	28.69 (17.65)	30
100	0.40	58.63	40.65 (25.00)	30
100	0.40	73.67	69.69 (42.86)	20
100	0.40	140.66	69.69 (42.86)	15
100	0.40	199.29	69.69 (42.86)	10

*The mass of natural rubber given in brackets.

6.3 Characterization

6.3.1 Diametrical shrinkage

The diametrical shrinkages during drying and sintering were determined from the respective change in diameter measured using a Vernier caliper. The reported diametrical shrinkages are the average of measurements taken on six samples.

6.3.2 Porosity

The porosity of the sintered bodies was calculated from their densities using the following formula. The density of sintered ceramics was calculated from their weight and volume. The volume of the cylindrical bodies was determined from their height and diameter measured using a Vernier caliper. The reported porosity is the average of measurements taken on six samples.

$$\text{Porosity } = (1 - \frac{\rho_b}{\rho_{td}})100$$

Where ρ_b is the bulk density and ρ_{td} is the theoretical density (3.98 g/cc).

6.3.3 Compressive strength measurement

The compressive strength of the sintered porous alumina samples was measured using a Universal testing machine (Instron 5500, Instron, USA) at a cross-head speed of 0.5 mm/minute. The cylindrical samples of approximately 22 mm diameter and 25 mm height were used.

6.3.4 Microstructure analysis

The microstructure of the sintered ceramics was observed using a scanning electron microscope, FE-SEM, Carl Zeiss Sigma HD, Germany. The sample for SEM analysis was

prepared by cutting the cylindrical bodies using a hacksaw blade. The samples were sputter-coated with gold before the SEM analysis.

6.4 Results and Discussion

6.4.1 Shape stability

When the frozen bodies prepared from dilute alumina slurries containing **NRL** of concentrations higher than 8 wt.% is immersed in acetone at room temperature, the ice crystals melt and the liquid water produced retains within the pores. The soft gel thus produced initially has poor strength, especially at lower alumina and rubber concentrations. Therefore, the bodies sag due to their weight during thawing. To determine the minimum concentration of rubber required to resist the deformation, the frozen bodies produced from 30 vol.% aqueous alumina slurries containing 10, 15, and 20 wt.% of natural rubber are subjected to thawing in an acetone medium. It has been observed that the shape stability of the frozen bodies during thawing in acetone medium improves with rubber concentration and the body prepared at 20 wt.% rubber survives without any deformation. On the other hand, the frozen bodies prepared at 10 wt.% rubber undergo severe collapse, and the one prepared at 15 wt.% rubber exhibits partial collapse. Therefore, a rubber concentration of 20 wt.% is used for the freeze casting of slurries of various alumina concentrations. A photograph showing the frozen bodies prepared from 30 vol.% alumina slurry at 10,15 and 20 wt.% rubber after aging in acetone for 48 hours and drying in the air are shown in **Fig.6.1.**The observed deformation of the body is produced during the thawing in acetone medium.

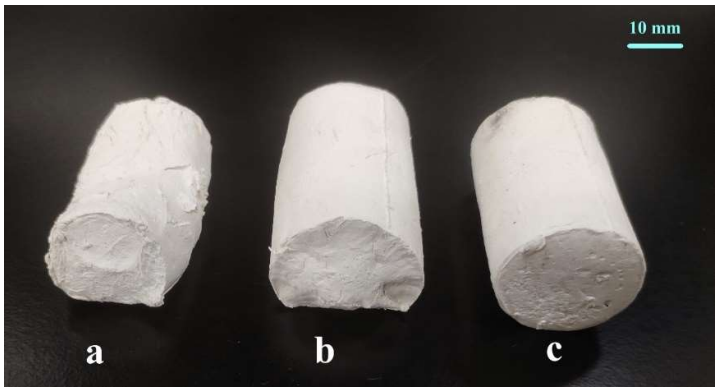

Fig.6.1 The photographs of the frozen bodies prepared from 30 vol. % alumina slurry at rubber concentrations of a). 10 wt.%,b). 15wt. % and c). 20 wt.%.

6.4.2 Acetone-exchange and drying kinetics

During aging in acetone, the water produced by the melting of ice is exchanged with acetone. The acetone exchange improves the strength of the gels by strengthening the alumina particle-rubber network through further coagulation. The extent of exchange of water in the frozen body with acetone also decides the stability of the pores against collapse during drying. The frozen body aged in acetone for 24 hours on drying in air at room temperature shows a loss of ~ 82.0 wt.% of the total solvent in 8 hours. The remaining 18 wt.% of the solvent removed on heating at 70℃ is mostly water. On the other hand, if the spent acetone is replenished and aging is continued for another 24 hours, 96.5 wt.% of the total solvent could be removed by drying in air at room temperature for 8 hours. That is, the residual water present in the body after the second time acetone exchange is only 3.5 wt.%. The residual water in the acetone exchanged body has a remarkable influence on the drying kinetics and pore stability as evidenced by their drying shrinkage and appearance of the surface after drying. A rapid removal of solvent from the two-time acetone-exchanged body is observed against a relatively slow removal of solvent from the one-time acetone-exchanged body. The drying kinetics of bodies after one-time and two-time acetone exchange is shown in **Fig.6.2**.The slow removal of

solvent from the one-time acetone exchanged body is due to the presence of a large quantity of residual water. That is, the acetone-water mixture with a higher concentration of water exhibits lower vapor pressure. The one-time acetone-exchanged body undergoes a higher diametrical drying shrinkage of 10.5% compared to 5.6% exhibited by the two-times acetone-exchanged body. Moreover, a wrinkled surface appearance, an indication of pore collapse is observed on a one-time acetone-exchanged body in comparison with the smooth surface of a two-time acetone-exchanged body. The higher shrinkage of the one-time acetone exchanged body is attributed to the shrinkage of pores due to the higher surface tension of the 18 wt.% residual water present. A photograph of one-time and two-times acetone exchanged bodies after drying is given in **Fig.6.3**. It is worth noting that the time for the exchange of water in the thawed frozen body with acetone could be considerably reduced by using a Soxhlet extraction unit. Nearly 97% of water could be removed from the thawed frozen body in 24 hours by continuous extraction with acetone using the Soxhlet extraction unit.

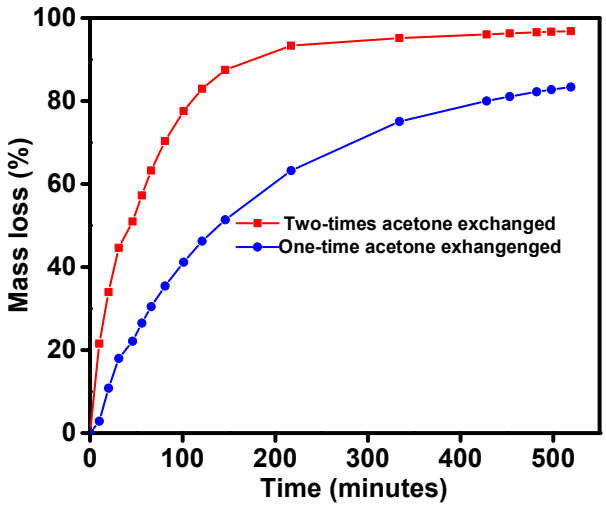

Fig.6.2 The drying kinetics of one-time and two-times acetone exchanged bodies.

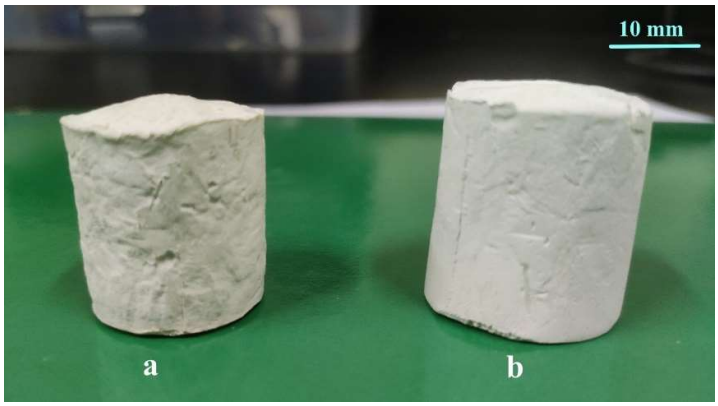

Fig.6.3 The photograph of a). one-time and, b) two-times acetone exchanged body after air drying.

6.4.3 Drying shrinkage

It is well known that the frozen powder suspensions do not show any appreciable shrinkage during freeze-drying. Unlike in freeze drying, the acetone exchanged frozen bodies undergo considerable shrinkage during further drying. The drying shrinkage depends on the alumina slurry concentration. The effect of alumina slurry concentration on the drying shrinkage of the acetone exchanged bodies is shown in **Fig.6.4**.

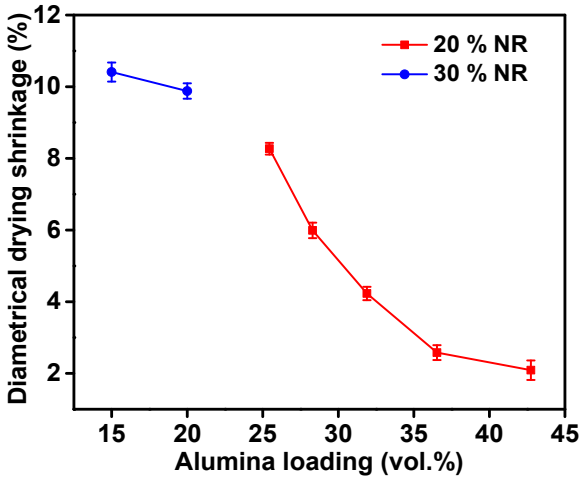

Fig.6.4 The diametrical drying shrinkage of acetone exchanged bodies as a function of alumina slurry loading.

The acetone exchanged bodies prepared at 42.74 vol.% alumina slurry shows a diametrical shrinkage of 2.1% during drying. The diametrical drying shrinkage slowly increases to 8.3% when the alumina slurry concentration decreases to 25.44 vol.%. The observed drying shrinkage is a result of the shrinkage of pores due to the surface tension effect of the acetone and the small amount of residual water present. Uniform shrinkage with the smooth surface of the dried body observed in this alumina slurry concentration range indicates the absence of pore collapse during drying. However, the further decrease of alumina slurry concentration to 23.10 vol.% results in large and non-uniform shrinkage with a highly wrinkled surface due to the pore collapse. It appears that at lower alumina slurry concentrations, the pore walls have insufficient strength to resist collapse due to their lower thickness. This is evidenced by the fact that further strengthening of pore walls by increasing the rubber concentration to 30 wt.% again results in uniform drying shrinkage and smooth surface of the dried bodies at lower alumina slurry concentrations of 20 and 15 vol.%. The diametrical drying shrinkage observed at 20 and 15 vol.% alumina slurry concentrations is 9.8 and 10.32 %, respectively. However, a further decrease of alumina slurry concentration to 10 vol.% again results in a large and non-uniform shrinkage and a highly wrinkled surface of the dried body. A photograph of the dried bodies prepared at 25.44 and 23.10 vol.% alumina slurries at 20 wt.% rubber concentration and at15 and 10 vol.% alumina slurries at 30 wt.% rubber concentration are shown in **Fig.6.5**.The non-uniform shrinkage with the wrinkled surface due to pore collapse is visible in dried bodies prepared at 23.10 vol.% alumina slurry with 20 wt.% rubber and 10 vol.% alumina slurry with 30 wt.% rubber.

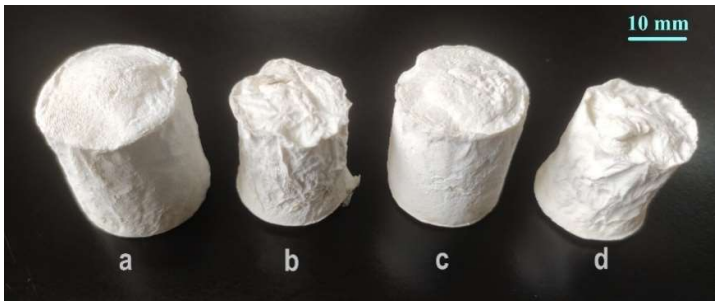

Fig.6.5 The photographs of bodies prepared by acetone exchange and air drying of frozen slurries of various alumina and rubber concentrations (a) 25.44 vol.% alumina & 20 wt.% rubber; (b) 23.10 vol.% alumina & 20 wt.% rubber; (c) 15 vol.% alumina & 30 wt.% rubber and (d) 10 vol.% alumina & 30 wt.% rubber.

6.4.4 Binder removal

The TGA graph of the dried alumina green sample is shown in **Fig.6.6**. The TGA shows a near-steady state weight loss from 200 to 480℃. That is, the rubber binder undergoes complete burn-out before 500℃. Natural rubber burnout takes place in two stages. The first stage in the temperature range of 200 to 370 ℃ involves nearly 78 % of the total mass loss due to the decomposition of natural rubber to isoprene, dipentene, and small amounts of p-menthene (S.Straus et al.,1956; N.Ahmad et al., 2018). The second stage at temperatures in the range of 390 - 480 °C is due to the burn-out of the carbon-rich residues produced in the first stage. The rubber binder presents in large quantities (20 & 30 wt.% of alumina) expected to collapse the pores if melts during the heat treatment for binder removal. However, our previous chapters indicate cross-linking of rubber in alumina green bodies through the double bonds present in the isoprene unit at 200℃ due to the Lewis acid character of alumina. That is, the rubber in the porous green bodies undergoes cross-linking when held for two hours at 200℃ during the heat treatment. This cross-linking prevents the melting of rubber and the collapse of pores during subsequent heat treatment. The burn-out of rubber leaves finer pores in the alumina-green body. That is, the binder-removed body contains pores created by the removal

of ice crystals and finer pores generated by the burnout of the rubber binder. These pores shrink and even some of the finer pores produced due to the rubber binder vanish during the subsequent sintering.

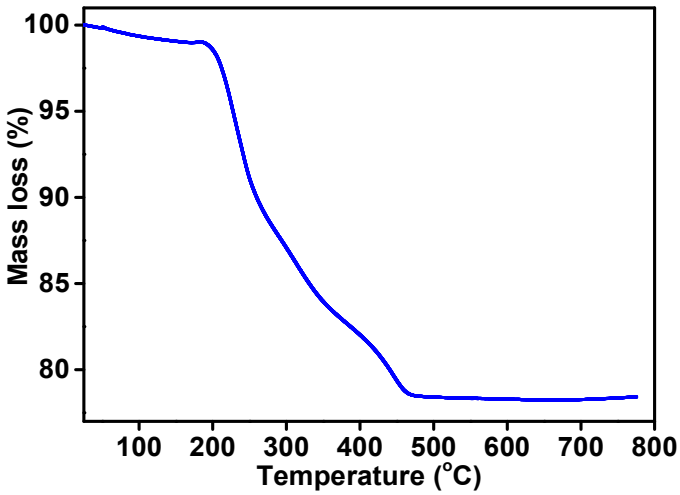

Fig.6.6 The TGA of the porous alumina green sample prepared at a rubber concentration of 20 wt. %.

6.4.5 Sintering shrinkage

The porous ceramics obtained by sintering the binder-removed bodies do not show any crack or deformation, however, show uniform shrinkage. The effect of alumina slurry concentration on the diametrical sintering shrinkage of porous alumina green bodies prepared by acetone exchange followed by air drying is shown in **Fig.6.7**. Unlike the drying shrinkage, sintering shrinkage decreases with a decrease in alumina slurry concentration. The diametrical sintering shrinkage decreases from 18.54 to 15.8% when the alumina slurry concentration decreases from 42.74 to 25.44 vol.%. The porous bodies prepared at 20 and 15 vol.% alumina slurry concentrations with 30 wt.% rubber exhibit a higher sintering shrinkage of 21 and 20.9 %, respectively. Although the sintering shrinkage follows a decreasing trend with a decrease

in alumina slurry concentration, the total shrinkage (shrinkage from the frozen body to sintered ceramics) exhibits an opposite trend. The porous green alumina bodies prepared by freeze-drying the frozen slurries for comparison show more or less similar diametrical shrinkage during sintering. The sintering shrinkage of freeze-dried samples decreases from 17.4 to 16.6 when the alumina slurry concentration decreases from 42.74 to 25.44 vol.%. The freeze-dried bodies prepared from slurries of 20 and 15 vol.% alumina concentration exhibit a sintering shrinkage of 19.98 and 22.8%, respectively.

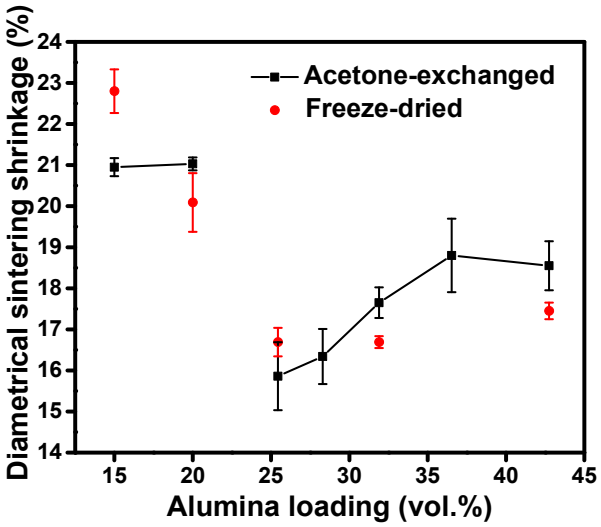

Fig.6.7 The sintering shrinkage of solvent exchanged and freeze-dried bodies vs. alumina slurry concentration.

6.4.6 Porosity

The properties and application of macroporous ceramics mainly depend on porosity, size, and shape of the pores, and the pore size distribution which are depending on the processing technique used for their preparation (D.M.Liu et al.,1997; R.W.Rice.,1993). Here, the effect of alumina slurry concentration on the porosity of the ceramics prepared by acetone exchange followed by air drying is presented in **Fig.6.8**. The porosity increases from 44.4 to

59.4% when the alumina slurry concentration decreases from 42.74 to 25.44 vol.% at a rubber concentration of 20 wt.%. The slurries at alumina concentrations of 20 and 15 vol.% prepared at a rubber concentration of 30 wt.% produce ceramics with 62.64 and 71.12 % porosity, respectively. The ceramics prepared by freeze-drying of the frozen bodies followed by sintering exhibit porosity in the range of 51.74 to 79.91% at the same alumina slurry concentrations in the range of 42.74 to 15 vol.%. That is, the porosity obtained by acetone exchange followed by air drying and sintering is lower by nearly 10- 15% compared to that prepared by freeze-drying and sintering. The observed lower porosity is due to the shrinkage that occurred in acetone-exchanged bodies during air drying.

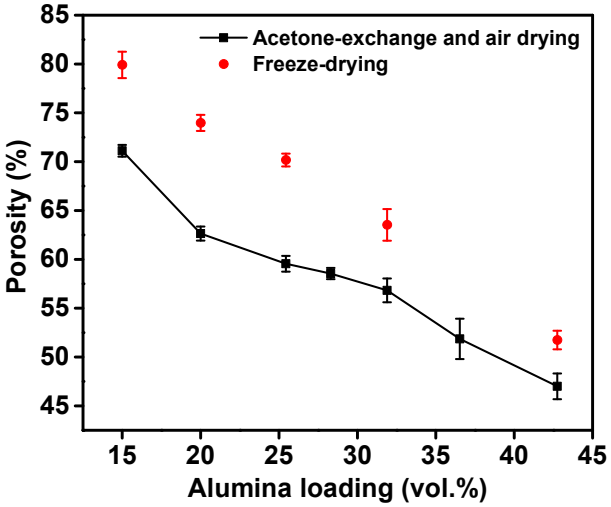

Fig.6.8 The porosity of sintered ceramics as a function of alumina slurry concentration prepared by freeze-casting followed by acetone exchange and air drying and freeze-drying.

6.4.7 Microstructure

The microstructure of the sintered ceramics shows mainly lamellar-type pores due to the removal of ice crystals. The lamellar-type pores are randomly oriented. This is due to the random growth of ice crystals during the isotropic freezing of the slurry. Pores due to the

removal of dendritic ice crystals formed during freezing are also rarely evidenced in the microstructure. **Fig.6.9** shows a typical low-magnification SEM image of porous ceramic showing the random orientation of lamellar pores and dendritic pores. The width of the lamellar pores increases whereas the lamellar wall thickness decreases with a decrease in alumina slurry concentration. The average lamellar pore width and lamellar wall thickness observed in ceramics prepared from 42.74 vol.% slurries are 26.95 and 65 μm, respectively. The corresponding values in ceramics prepared from a 15 vol.% slurry are 47 and 31μm, respectively. The porous alumina ceramics prepared by freeze casting followed by freeze-drying and sintering exhibited a similar pore structure. However, the width of the lamellar pores observed in ceramics obtained by acetone exchange followed by drying and sintering is smaller than that present in the corresponding freeze-dried samples. The average width of lamellar pores in freeze-dried samples is in the range of 28 to 109 μm at an alumina slurry concentration in the range of 42.74 to 15 vol.%. This is due to the shrinkage of pores during drying in the case of acetone exchange followed by air drying. The SEM images of porous ceramics prepared by acetone exchange followed by air drying in comparison to the corresponding freeze-dried samples showing their similar pore structure are given in **Fig.6.10**. In addition to the lamellar pores, the lamellar walls show finer pores in the size range of 0.70 to 1.0 μm. These finer pores are due to the burnout of natural rubber which is used in relatively large quantities to stabilize the lamellar pores during thawing, acetone exchange, and drying. The lamellar pores created by ice templates are connected through the finer pores on the lamellar walls produced by the rubber binder. A high-magnification image showing the finer pores created by the rubber binder is shown in **Fig.6.11**. The average grain size calculated from the high-magnification SEM image of the lamellar wall is 0.8 μm.

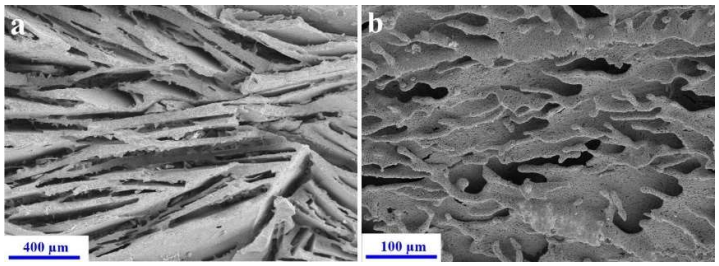

Fig.6.9 The low magnification SEM images showing a). randomly oriented lamellar pores and b). dendritic pores.

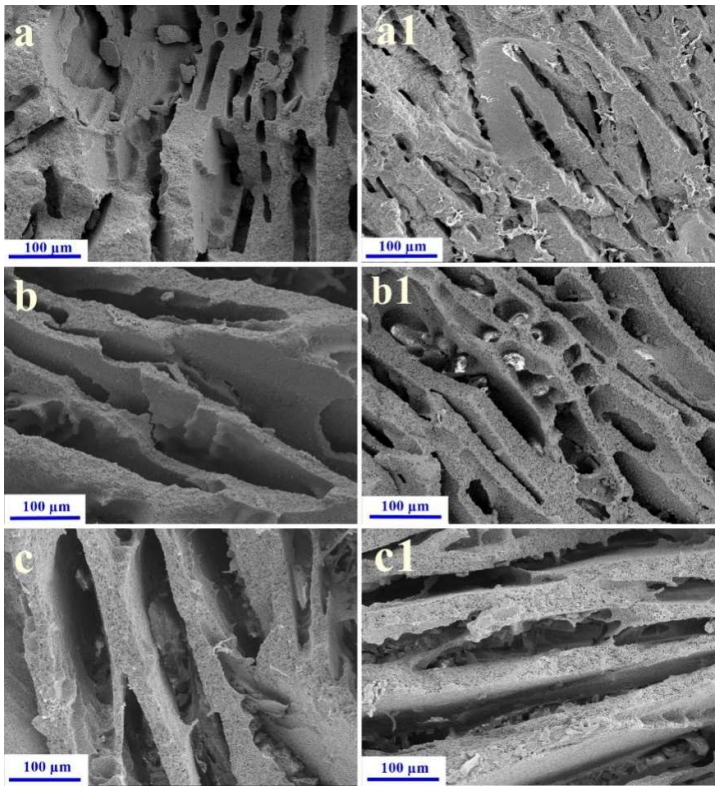

Fig.6.10 SEM photomicrographs showing similar pore structure of porous alumina ceramics prepared by freeze-drying and acetone exchange followed by air drying at various alumina slurry concentrations, a).42.74 vol.% freeze-dried, a1).42.74 vol.% acetone-exchanged, b) 25.44 vol.% freeze-dried, b1) 25.44 vol.% acetone-exchanged, c).15 vol.% freeze-dried,c1) 15 vol.% acetone-exchanged.

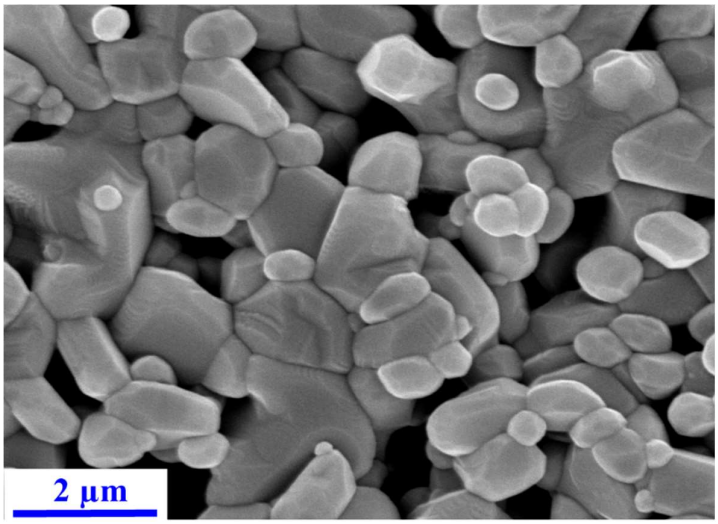

Fig.6.11 The SEM image showing the finer pores in the lamellar wall due to the removal of the rubber binder.

6.4.8 Compressive strength

The compressive stress-strain graph of the porous alumina ceramics is shown in **Fig.6.12**. The stress-strain graphs are similar to the typical plots observed for the brittle porous solids (I.Sabree et al.,2015; B.S.M.Seeber et al.,2013). The graphs show a linear increase of stress with strain until a maximum followed by a gradual decline of stress. In most cases, stress-maximum is exhibited at 2% strain. The slope of the initial linear region is taken as Young's modulus and the stress maximum in the stress-strain graph is considered as the compressive strength. The compressive strength of the porous ceramics increases slowly from 3.84 to 6.71MPa when the alumina slurry concentration increases from 15 to 31.89 vol.%. Further increase in alumina slurry concentration to 42.74 vol.% rapidly increases the compressive strength to 35.26 MPa. Young's modulus also follows the same trend. That is, Young's modulus increases slowly from 306.2 to 760.29 MPa when slurry concentration increases from 15 to 31.89 vol.% and then rapidly to 1486.5 MPa when slurry concentration further increases to 42.74 vol.%. At the lower alumina solid loading of 15 to 31.89 vol.%, after the yield point,

a constant long plateau region is noticed in the stress-strain graph. At higher solid loadings of 36.53 and 42.74 vol.%, the plateau region in the stress-strain graph is reduced. Instead, the samples show a more brittle fracture and a sudden drop in the stress value thereafter. The compressive strength and Young's modulus of the porous alumina ceramics as a function of alumina slurry concentration are presented in **Fig.6.13**. The increase in compressive strength and Young's modulus with an increase in alumina slurry concentration is due to the decrease in the porosity of the ceramics. The compressive strength of porous ceramics prepared by freeze-casting depends on pore morphology and alignment of pores. The ceramics with uni-directionally aligned pores obtained by directional freezing of slurries show much higher compressive strength compared to the ones with random orientation of pores produced by the isotropic freezing (B.H.Yoon et al., 2008; N. Zhang et al.,2022). Moreover, ceramics with prismatic pores are reported to have higher compressive strength compared to those with lamellar pores at the same porosity (M. Q. Sun et al.,2019). Muto et al reported a compressive strength of ~ 3.5 MPa at a porosity of ~75% in alumina ceramics prepared by isotropic freezing (D. Muto et al., 2020). Y.F. Tang et al achieved a high compressive strength in the range of 20 to 80 MPa at porosity in the range of 25 to 57 vol.% in alumina ceramics prepared by unidirectional freezing of powder suspensions (Y. Tang et al., 2014). Zhang et al achieved a high compressive strength in the range of ~95 to 225 MPa in alumina ceramics of porosity in the range of ~ 63 to 46 vol.% by directional freezing of aqueous alumina powder suspensions containing glycerol (Y. Zhang et al., 2010). The relatively lower compressive strength observed in the present study is due to the combination of two factors. One is the random orientation of lamellar pores due to the isotropic freezing and another is the presence of micro-pores in the lamellar walls due to the removal of natural rubber binder.

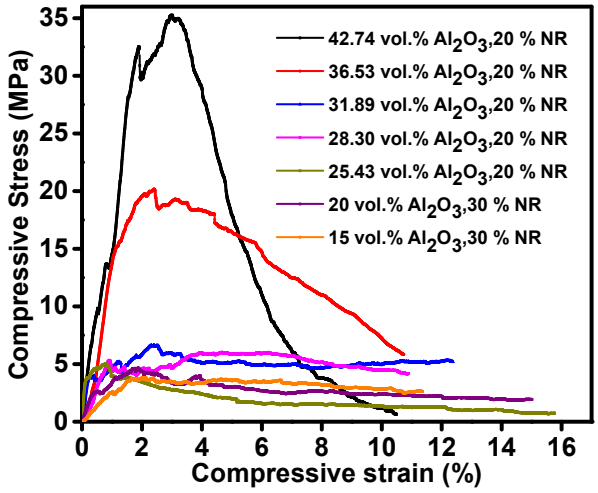

Fig.6.12 The compressive stress-strain plot of porous alumina ceramics prepared from slurries of various alumina loading.

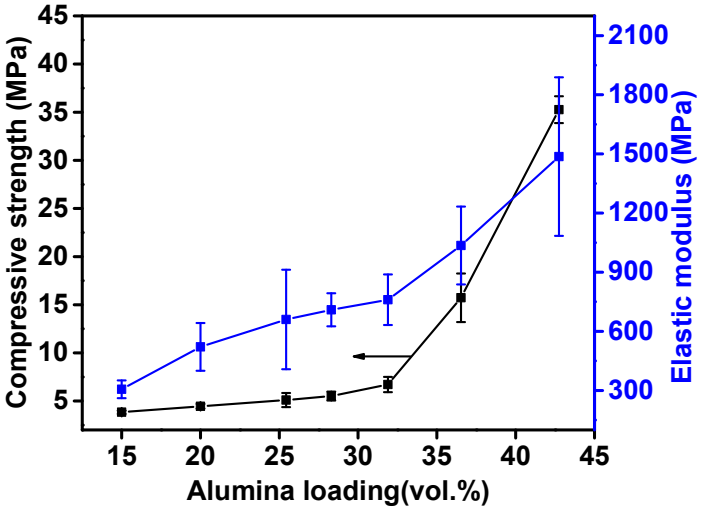

Fig.6.13 The compressive stress and elastic modulus of porous alumina ceramics as a function of alumina slurry concentration.

6.5 Conclusions

Freeze-casting followed by thawing in acetone medium, air drying, and sintering has been demonstrated for the preparation of macroporous alumina ceramics from alumina-**NRL** co-dispersions containing large concentrations of **NRL**. The **NRL**-alumina particle network in frozen slurries achieved sufficient strength in acetone medium that resist pore collapse during thawing, acetone exchange, and subsequent air drying at rubber concentrations in the range of 20 to 30 wt.% of alumina. A rubber concentration of 20 wt.% stabilizes the pores in gels prepared at alumina slurry concentrations up to 25.44 vol.% whereas 30 wt.% rubber is required to prevent pore collapse in gels prepared up to an alumina slurry concentration of 15 vol.%. Repeating the acetone exchange for a second time removes ~ 96.5 % of the total water present in the gel which results in fast drying, low drying shrinkage, and a smooth green body surface. The diametrical shrinkage varies from 2.1 to 10.32 % when the alumina concentration varies from 42.74 to 15 vol.%. The cross-linking of rubber chains by annealing at 200 ℃ prevents the melting of rubber and thereby avoids pores collapse during binder removal. The frozen slurries of alumina concentration in the range of 42.74 to 15 vol.% produced ceramics of porosity in the range of 44.5 to 71.12% by acetone exchange followed by air drying and sintering which is lower by nearly 10-15 % of that obtained by freeze-drying. The ceramics produced from the frozen alumina slurries by acetone exchange followed by air drying exhibited the same lamellar pore structure as the one produced by freeze-drying. The lamellar pore width in ceramic obtained by acetone exchange followed by drying and sintering is lower by nearly 42.65 % than that obtained by freeze-drying due to the pore shrinkage in acetone-exchanged bodies during air drying. The lamellar pores produced by ice templating are connected through the submicron pores created on the lamellar pore walls by the removal of the rubber latex binder. The porous ceramics showed compressive strength and Young's modulus in the ranges of 3.8

to 35.3 MPa and 306.2 to 1486.5, respectively, at alumina slurry concentrations in the range of 15 to 42.74 vol.%.

Chapter 7

7.1 Summary and Conclusions

Complex-shaped ceramic components have been increasingly used for various applications in aerospace, defense, nuclear, and medical fields. The manufacture of these ceramic components is carried out from the respective ceramic powders using advanced processing techniques such as powder pressing, slip casting, tape casting, gel casting, injection molding, extrusion, and the recently developed additive manufacturing. Various additives such as solvents, dispersants, binders, plasticizers, and antifoaming agents are used in ceramic forming for imparting specific functions. Most of these additives are petroleum-based synthetically produced chemicals that create global emissions and environmental pollution. Additionally, the organic solvents employed as a medium in ceramic forming techniques such as tape casting are costly, toxic, flammable, have personal hazards and cause environmental pollution. The development of eco-friendly processing routes that are safe for the personal as well as the environment is highly demanded. This is attained by using water as a solvent medium and naturally renewable molecules as processing additives. **NRL** (**NRL**) is an aqueous emulsion of poly(isoprene) obtained from the bark of Hevea Braziliansis. The **NRL** stabilized using ammonia is commercially available in a highly concentrated form. This thesis investigates **NRL** as a binder in the processing of alumina ceramic by powder pressing, slip casting, tape casting, and gel casting.

Chapter 1 describes the various ceramic forming techniques, additives used in ceramic forming, and their functions. A detailed literature review with a focus on binders used in various ceramic forming methods is also presented.

In **Chapter 2** the **NRL** is introduced as a binder in powder pressing of alumina. The metal ion impurities in **NRL** are analyzed as 0.083 wt. % of Ca, 0.019 wt. % of Mg, 0.011 wt. % Zn

and 0.017 wt. % of Al with a total ash content of 0.3wt.%. The **NRL** and the alumina powder dispersions using ammonium polyacrylate dispersant show very high zeta potential values of -58 mV and -57 mV, respectively, at pH in the range of 9.6 to 10 enabling the preparation of their co-dispersions at this pH range by simple mixing by magnetic stirring. The co-dispersions undergo co-coagulation by shifting the pH towards 4 using a formic acid solution. The average particle size of aggregates formed by the coagulation increases from 0.34 to 12.30 μm when the **NR** concentration increases from 0 to 10 wt.%. The precipitation of **NR** as lumps is observed only at an **NR** concentration ≥ 15 wt.%. The granulated feedstock for powder pressing is prepared through co-coagulation of the alumina-**NRL** co-dispersions using the formic acid solution followed by drying and grinding. The flow time and the Hausner ratio measurements indicate that the feedstock granules prepared at 6 and 8 wt.% **NR** concentrations have good flow properties. The powder compacts prepared by pressing the granulated feedstock show a maximum green density of 67.7 % T.D at a relatively low compaction pressure of 20 MPa due to the highly deformable nature of **NRL** binder with a low glass transition temperature. The binding effect of **NR** is evidenced by the powder compact density that increases from 63.6 to 67.7 % T.D of alumina at a compaction pressure of 20 MPa when the **NR** concentration increases from 4 to 10 wt.%. The green bodies prepared at 2 wt.% **NR** concentration exhibit severe end-capping due to poor strength. The strength of the pressed bodies increases from 0.55-1.91 MPa when the **NR** concentration increases from 4 to 10 wt.% of the alumina powder. Green strength shows almost a 2.3 to 6 times increase to the range of 2.30 - 9.39 MPa on annealing at 200 ^{o}C due to the cross-linking of rubber chains through the carbon-carbon double bonds induced by the Lewis acid character of alumina. The annealed green bodies are amenable to machining by lathing, milling, and drilling using conventional machines and tools. A near-steady state burn-out of the **NR** from the annealed green body is evidenced by the TGA

analysis. A linear shrinkage of 18 % is observed during the sintering of binder-removed bodies at 1550℃. The sintered ceramics show 97% T.D. with an average grain size of 1.8 μm.

Chapter 3 establishes **NRL** as a binder for the slip casting of alumina. The alumina-**NRL** co-dispersions show shear thinning flow behavior. The alumina slip casting slurries of concentration in the range of 40 to 55 vol.% prepared using the **NRL** binder show lower viscosity and yield stress compared to 41.1 vol.% aqueous alumina slurry prepared using the conventional PVA binder. The yield stress of 50 vol.% alumina slurries shows an increase from 2.84 to 4.79 Pa when the **NRL** binder concentration increases from 0 to 8 wt.%. At a fixed **NRL** concentration of 4 wt.%, the yield stress of slurries increases from 0.37 to 9.73 Pa when the alumina concentration increases from 40 to 55 vol.%. The 41.1 vol.% aqueous alumina slurry containing 2 wt.% PVA binder exhibits a high yield stress of 20.88 Pa. The cast layer thickness decreases from 8.5 to 4.2 mm when the **NR** concentration increases from 0 to 8 wt.% due to the gelation of **NR** at the mold-cast layer interface. The cast layer thickness increases from 4.13 to 6.5 mm when the alumina concentration increases from 40 to 55 vol.%. As a comparison, in the case of the PVA binder the cast layer thickness achieved is only 2 mm which is two times lower than that achieved from a slurry of the same alumina concentration containing **NRL** binder. The cast layer thickness increases with casting time and a high cast layer thickness of 18 mm is achieved within 480 minutes. The density of the green body (53.4 - 62.4 % T.D.) obtained for **NRL**-based alumina slip casting slurry is higher than that obtained for the green body (52.1 % T.D.) produced from alumina slurry containing the PVA binder. The green strength increases from 0.45 - 1MPa when the **NR** concentration increases from 0 to 8 wt.%. Almost 6 to 9.68 times increase in green strength to 0.45 - 9.68 MPa is achieved on annealing at 200℃ due to the cross-linking of rubber. The annealed slip-cast green bodies could be machined by milling and drilling using conventional machines and tools. The TGA analysis of samples collected from various parts of the slip-cast body indicated negligible

binder migration during consolidation. The slip-casting using the **NRL** binder could produce thin-walled crucibles (wall thickness as low as 1.2 mm). The slip-cast ceramics sintered at 1550℃ exhibits a homogeneous microstructure with 97 % T.D. and 1.82 μm average grain size.

In **Chapter 4**, the **NRL** is studied as a binder in the aqueous tape casting of alumina. The tape casting slurries of high total solids loading in the range of 60.57 to 60.88 vol.% could be prepared due to the high solid content (61.5 wt.%) of the concentrated **NRL**. The tape casting slurries prepared by mixing concentrated aqueous alumina slurry and the **NRL** show shear thinning flow behavior. The alumina slurries at **NR** concentrations in the range of 14.2 to 18.1 wt.% exhibit viscosity in the range of 1.1 to 1.15 Pa.s at a shear rate of 4.65 s^{-1} and yield stress in the range of 3.29 - 2.97 Pa, suitable for tape casting. The high solid (alumina + rubber) concentration in the slurry enables the drying of the cast tape within a reasonable time of 15 minutes at 70 ℃. The tensile strength of green alumina tape prepared at **NR** content in the range of 14.2 to 18.1 wt.% is in the range of 1.62 to 1.85 MPa which is comparable with the strength of green tapes obtained with other binders. The corresponding elastic modulus observed is in the range of 267.5 to 50.8 MPa.The green tapes show sufficient flexibility without using an additional plasticizer as evidenced by the 41 to 254 % elongation at break. The flexible green tape turned into a rigid one on annealing at 200 ℃ due to the cross-linking of **NR** chains induced by Lewis acid sites of the alumina powder. The annealing of the green tape between two glass plates for cross-linking of the **NR** enables a near-steady state binder removal and facilitates the preparation of flat tapes by avoiding the curling of the edges during the binder removal. A remarkable improvement in green density and microstructure is achieved by a 20 % reduction in the thickness of the green tape by roll pressing. The roll-pressed green tape achieves a sintered density of 98.5% T.D. as compared to 93% T.D. achieved without roll pressing. The sintered alumina tape shows a uniform microstructure with an average grain size

of 3.2 μm indicating that the trace amount of impurities introduced in the ceramic from the **NRL** binder does not produce any exaggerated grain growth. The aqueous tape casting using the **NRL** binder is completely eco-friendly and sustainable as it is not using any synthetic solvent, binder, and plasticizer.

Gel casting of aqueous alumina powder suspensions using **NRL** as a gelling agent and binder is investigated in **Chapter 5**. The viscosity of 58.2 vol.% aqueous alumina slurry prepared using the ammonium poly(acrylate) dispersant measured at a shear rate of 9.3 s^{-1}decreases from 2.18 Pa.s to 0.6 Pa.s up on the addition of 8 wt.% of **NRL**. The corresponding decrease in yield stress is from 11.83 to 3.10 Pa. Gelation is achieved by freezing the alumina-**NRL** co-dispersion in a mold followed by mold removal and thawing in an acetone medium. The disruption of the protein layer, responsible for the stability of **NRL**, by the growing ice crystals leads to its coagulation during freezing. The thawing in the acetone medium further promotes coagulation and thereby strengthens the alumina particle-rubber network. The shape stability of the wet gels increases with an increase in **NR** concentrations and a stable gel without deformation is achieved at a minimum rubber concentration of 8 wt.%. The minimum concentration of **NR** required to percolate and form a stable alumina particle-rubber gel is 8 % by weight of the alumina powder. The frozen body passes through a semi-fluid state during thawing which enables the gel to flow and fill the space created by the melting of ice crystals. The compressive strength and modulus of the wet gel are 60kPa and 640 kPa, respectively, which are sufficient for further handling during drying. The acetone exchange enables faster drying of the gel cast bodies at room temperature without creating any deformation or crack. The diametrical compressive strength and modulus of the dried green body are 0.34 MPa and 18 MPa, respectively. A remarkable increase in the diametrical compressive strength of the green body from 0.34 to 2.14MPa (6.3 times higher) and modulus from 18 to 150 MPa, is achieved on annealing at 200°C due to the cross-linking of rubber chains. The cross-linking

benefits the binder removal enabling a slow and steady burn-out as evidenced by the TGA. The green bodies on debinding and sintering at 1550°C produce alumina ceramics of uniform microstructure with ~96% T.D and 1.3 µm average grain size. The non-toxic and sustainable gel casting system produces complex near-net-shapes.

In **Chapter 6** large concentrations of **NR** are used as a pore stabilizer to prepare macroporous alumina ceramics by freeze casting followed by air drying. The **NRL**-alumina particles network in frozen slurries achieves sufficient strength in acetone medium that resist pore collapse during thawing, acetone exchange, and subsequent air drying at **NR** concentrations in the range of 20 to 30 wt. % of alumina. An **NR** concentration of 20 wt.% stabilizes the pores in gels prepared at alumina slurry concentrations in the range of 42.72 - 25.44 vol.% whereas 30 wt.% **NR** is required to prevent pore collapse in gels prepared up to an alumina slurry concentrations 15 vol.%. Acetone exchange for two times removes ~ 96.5 % of the water present in the gels which results in fast drying, low drying shrinkage, and a smooth surface of green body. The diametrical shrinkage of gels during drying varies from 2.1 to 10.32 % when the alumina slurry concentration varies from 42.74 to 15 vol.%. The cross-linking of **NR** chains by annealing at 200 °C prevents the melting of **NR** and thereby avoids pores collapse during binder removal. The frozen slurries of alumina concentration in the range of 42.74 to 15 vol.% produces ceramics of porosity in the range of 44.5 to 71.12% by acetone exchange followed by air drying and sintering. The porosity achieved by freeze gel casting followed by acetone exchange and air drying is 10 to 15 % lower than that achieved by freeze casting followed by freeze-drying at the same alumina slurry concentration due to the shrinkage observed during air drying of the acetone exchanged bodies. The porous ceramics obtained both by acetone exchange followed by air drying and freeze-drying of the frozen slurries exhibits a similar lamellar pore structure. The lamellar pore width in ceramic obtained by acetone exchange followed by air drying is lower by ~ 42 % compared to that obtained by

freeze-drying due to the pore shrinkage in acetone-exchanged bodies during drying. The lamellar pores produced by ice templating are connected through the submicron pores created on the lamellar pore walls by the removal of the **NRL** binder. The porous ceramics show a compressive strength and Young's modulus in the ranges of 3.8 to 35.3 MPa and 306.2 to 1486.5, respectively, at alumina slurry concentrations in the range of 15 to 42.74 vol.%. The process enables the preparation of macroporous ceramics by freeze casting without the use of a freeze-drying system.

7.2 Future scope of the work

In the present thesis, the **NRL** stabilized in an alkaline medium is used as a binder, gelling agent, and pore stabilizer for the preparation of dense and macroporous alumina ceramics. The alumina and rubber particles possess high negative surface potentials and form co-dispersions easily. By applying a pulsed electric field, the co-deposition of charged alumina and rubber particles can be achieved on a conducting substrate material through electrophoretic deposition. Here, the deposited layer thickness can be controlled by the parameters such as current density, deposition time, the distance between the electrodes, etc. The deposited alumina-rubber composite is expected to be easily peeled off from the substrate after drying due to the flexible nature of rubber. We propose to study this as an alternative to aqueous tape casting.

We have carried out the isotropic freezing of alumina suspensions containing **NRL** for the preparation of macroporous alumina ceramics containing randomly oriented lamellar pores. It has been reported that macroporous ceramics with aligned lamellar pore morphology results in high compressive strength. It is proposed to study the directional freezing of alumina-**NRL** co-dispersions followed by thawing in acetone and air drying to produce macroporous alumina ceramics of unidirectionally aligned pores.

Chemically, **NRL** is a cis-1, 4-polyisoprene polymer that contains a high level of unsaturation. Many reports are available on the radiation-induced cross-linking of polyisoprene polymers. The reported radiation sources are electron beams, microwaves, X-rays, and γ-rays. It is suggested to study the effect of the radiation cross-linking of **NR** in alumina-**NRL** co-dispersions to enable their gelation for the preparation of near-net-shape ceramic components by additive manufacturing.

It is also proposed to extend the study to other oxide and non-oxide ceramic systems. The preparation of co-dispersions of **NRL** with the aqueous slurries of other advanced ceramic powders, their colloidal stability, gelation characteristics, and the effect of different ceramic powders on cross-linking of rubber chains are to be investigated.

References

1. Adams, E. F. (1971). Slip-cast ceramics. High Temperature Oxides, 45.
2. Adolfsson, E. (2006). Gelcasting of zirconia using agarose. *Journal of the American Ceramic Society*, 89(6), 1897-1902.
3. Ahmad, N., Abnisa, F., & Daud, W. M. A. W. (2016). Potential use of natural rubber to produce liquid fuels using hydrous pyrolysis–a review. *RSC advances*, 6(73), 68906-68921.
4. Amin, S. K., Abdallah, H. A. M., Roushdy, M. H., & El-Sherbiny, S. A. (2016). An overview of production and development of ceramic membranes. *International Journal of Applied Engineering and Research*, 11(12), 7708-7721.
5. Amorós, J. L., Cantavella, V., Jarque, J. C., & Felíu, C. (2008). Fracture properties of spray-dried powder compacts: effect of granule size. *Journal of the European Ceramic Society*, 28(15), 2823-2834.
6. Appiagyei, K. A., Messing, G. L., & Dumm, J. Q. (2008). Aqueous slip casting of transparent yttrium aluminum garnet (YAG) ceramics. *Ceramics International*, 34(5), 1309-1313.
7. Araki, K., & Halloran, J. W. (2004). New freeze-casting technique for ceramics with sublimable vehicles. *Journal of the American Ceramic Society*, 87(10), 1859-1863.
8. Ba, X., Li, J., Pan, Y., Zeng, Y., Kou, H., Liu, W., ... & Guo, J. (2013). Comparison of aqueous-and non-aqueous-based tape casting for preparing YAG transparent ceramics. *Journal of alloys and compounds*, *577*, 228-231.
9. Baklouti, S., Bouaziz, J., Chartier, T., & Baumard, J. F. (2001). Binder burnout and evolution of the mechanical strength of dry-pressed ceramics containing poly (vinyl alcohol). *Journal of the European Ceramic Society*, 21(8), 1087-1092.

10. Baklouti, S., Chartier, T., & Baumard, J. F. (1997). Mechanical properties of dry-pressed ceramic green products: the effect of the binder. *Journal of the American Ceramic Society*, 80(8), 1992-1996.

11. Baklouti, S., Chartier, T., & Baumard, J. F. (1998). Binder distribution in spray-dried alumina agglomerates. *Journal of the European Ceramic Society*, 18(14), 2117-2121.

12. Balakrishna, P., Chakraborthy, K. P., & Singh, A. (1996). End-capping and other defects in pressed ceramic compacts. NISCAIR-CSIR, India, 196-200.

13. Barmala, M., Moheb, A., & Emadi, R. (2009). Applying Taguchi method for optimization of the synthesis condition of nano-porous alumina membrane by slip casting method. *Journal of Alloys and Compounds*, 485(1-2), 778-782.

14. Bednarek, P., Szafran, M., Sakka, Y., & Mizerski, T. (2010). Gelcasting of alumina with a new monomer synthesized from glucose. *Journal of the European Ceramic Society*, 30(8), 1795-1801.

15. Begum, S., Duff, A., Puyane, R., & Hashmi, M. S. J. (1998). Evaluation of latex binder in the processing of electronic ceramic powder. *Journal of Materials Processing Technology*, 77(1-3), 108-114.

16. Bengisu, M., & Yilmaz, E. (2002). Gelcasting of alumina and zirconia using chitosan gels. *Ceramics International*, 28(4), 431-438.

17. Bergstrom, L. (2001). Colloidal processing of ceramics. *Handbook of applied surface and Colloid chemistry*, 1, 201-217.

18. Bitterlich, B., Lutz, C., & Roosen, A. (2002). Rheological characterization of water-based slurries for the tape casting process. *Ceramics international*, 28(6), 675-683.

19. Bocanegra-Bernal, M. H. (2004). Hot isostatic pressing (HIP) technology and its applications to metals and ceramics. *Journal of Materials Science*, 39(21), 6399-6420.

20. Bocanegra-Bernal, M. H., & Matovic, B. (2009). Dense and near-net-shape fabrication of Si3N4 ceramics. *Materials Science and Engineering: A*, 500(1-2), 130-149.

21. Boch, P., Chartier, T., & Huttepain, M. (1986). Tape casting of Al_2O_3/ZrO_2 laminated composites. *Journal of the American Ceramic Society*, 69(8), C-191.

22. Borlaf, M., Serra-Capdevila, A., Colominas, C., & Graule, T. (2019). Development of UV-curable ZrO2 slurries for additive manufacturing (LCM-DLP) technology. *Journal of the European Ceramic Society*, *39* (13), 3797-3803.

23. Bowen, H. K. (1983). Ceramics as engineering materials: Structure-property-processing. MRS Online Proceedings Library (OPL), 24.

24. Brodie, W. (2009). Gelation Rate Index and Cast Quality. In *Whitewares-Materials and Equipment: A Collection of Papers Presented at the 1980 Fall Meeting and 83rd Annual Meeting, Volume 2, Issue 9/10* (No. 9-10, p. 917). John Wiley & Sons.

25. Brook, R. J. (1985). Processing technology for high performance ceramics. *Materials Science and Engineering*, 71, 305-312.

26. Cai, K., Huang, Y., & Yang, J. (2005). Alumina gelcasting by using HEMA system. *Journal of the European Ceramic Society*, 25(7), 1089-1093.

27. Chabert, F., Dunstan, D. E., & Franks, G. V. (2008). Cross-linked polyvinyl alcohol as a binder for gelcasting and green machining. *Journal of the American Ceramic Society*, 91(10), 3138-3146.

28. Chartier, T., & Bruneau, A. (1993). Aqueous tape casting of alumina substrates. *Journal of the European Ceramic Society*, 12(4), 243-247.

29. Chen, Y., Xie, Z., Yang, J., & Huang, Y. (1999). Alumina casting based on gelation of gelatine. *Journal of the European Ceramic Society*, 19(2), 271-275.

30. Chen, Z., Li, Z., Li, J., Liu, C., Lao, C., Fu, Y., ... & He, Y. (2019). 3D printing of ceramics: A review. *Journal of the European Ceramic Society*, 39(4), 661-687.

31. Chou, K. S., & Lee, L. J. (1989). Effect of dispersants on the rheological properties and slip casting of concentrated alumina slurry. *Journal of the American Ceramic Society*, 72(9), 1622-1627.

32. Cockbain, E. G., Gregory, J., Pillai, N. M., & Gorton, A. D. T. (1969). Freeze-resistant natural rubber latex concentrate. *Journal of Rubber Research Institute of Malaysia*.

33. Cole, W. M., Bohm, G. G., Tomaszewski, W., & Huang, Y. (2017). U.S. Patent No. 9,546,224. Washington, DC: U.S. Patent and Trademark Office.

34. Conceição, S. I., Velho, J. L., & Ferreira, J. M. F. (2003). Influence of deagglomeration and carboxymethyl cellulose binders on rheological behaviour of kaolin suspensions. *Applied Clay Science*, 23(5-6), 257-264.

35. Crouter, A., & Briens, L. (2014). The effect of moisture on the flowability of pharmaceutical excipients. *Aaps PharmSciTech*, 15, 65-74.

36. Davies, J., & Binner, J. G. P. (2000). Coagulation of electrosterically dispersed concentrated alumina suspensions for paste production. *Journal of the European Ceramic Society*, 20(10), 1555-1567.

37. Deckers, J., Kruth, J. P., Cardon, L., Shahzad, K., & Vleugels, J. (2013). Densification and geometrical assessments of alumina parts produced through indirect selective laser sintering of alumina-polystyrene composite powder. Strojniški vestnik-*Journal of Mechanical Engineering*, 59(11), 646-661.

38. Deckers, J., Vleugels, J., & Kruth, J. P. (2014). Additive manufacturing of ceramics: A review. *Journal of Ceramic Science and Technology*, 5(4), 245-260.

39. Demirkol, N., & Capoglu, A. (2007). Rheological and Green Strength Behaviour of Low-clay Translucent Whiteware Slurries with an Acrylic Type Emulsion Binder Addition. *In Proceedings of the European Ceramic Society for 10th International Conference and Exhibition of the European Ceramic Society* (pp. 434-38).

40. Desfontaines, M., Jorand, Y., Gonon, M., & Fantozzi, G. (2005). Characterisation of the green machinability of AlN powder compacts. *Journal of the European Ceramic Society*, 25(6), 781-791.

41. Deville, S. (2008). Freeze-casting of porous ceramics: a review of current achievements and issues. *Advanced Engineering Materials*, 10(3), 155-169.

42. Dhanashekar, M., Loganathan, P., Ayyanar, S., Mohan, S. R., & Sathish, T. (2020). Mechanical and wear behaviour of aa6061/sic composites fabricated by powder metallurgy method. *Materials Today: Proceedings*, 21, 1008-1012.

43. Dhara, S., & Su, B. (2005). Green machining to net shape alumina ceramics prepared using different processing routes. *International Journal of Applied Ceramic Technology*, 2(3), 262-270.

44. Doreau, F., Tarı, G., Guedes, M., Chartier, T., Pagnoux, C., & Ferreira, J. M. F. (1999). Mechanical and lamination properties of alumina green tapes obtained by aqueous tape-casting. *Journal of the European Ceramic Society*, 19(16), 2867-2873.

45. Doreau, F., Tarì, G., Pagnoux, C., Chartier, T., & Ferreira, J. M. F. (1998). Processing of aqueous tape-casting of alumina with acrylic emulsion binders. *Journal of the European Ceramic Society*, 18(4), 311-321.

46. Dzuy, N. Q., & Boger, D. V. (1983). Yield stress measurement for concentrated suspensions. *Journal of Rheology*, 27(4), 321-349.

47. Egeland, G. W., Zuck, L. D., Cannon, W. R., Lessing, P. A., & Medvedev, P. G. (2010). Dry bag isostatic pressing for improved green strength of surrogate nuclear fuel pellets. *Journal of Nuclear Materials*, 406 (2), 205-211.

48. Escobar, C. F., & dos Santos, L. A. (2015). New eco-friendly binder based on natural rubber for ceramic injection molding process. *Journal of the European Ceramic Society*, 35(13), 3567-3575.

49. Falamaki, C., & Beyhaghi, M. (2009). Slip casting process for the manufacture of tubular alumina microfiltration membranes. *Materials Science-Poland*, 27(2), 427-441.

50. Falamaki, C., Naimi, M., & Aghaie, A. (2006). Dip-coating technique for the manufacture of alumina microfilters using PVA and Na-CMC as binders: a comparative study. *Journal of the European Ceramic Society*, 26(6), 949-956.

51. Fanelli, A. J., Silvers, R. D., Frei, W. S., Burlew, J. V., & Marsh, G. B. (1989). New aqueous injection molding process for ceramic powders. *Journal of the American Ceramic Society*, 72(10), 1833-1836.

52. Francis, L. F. (2015). Materials processing: a unified approach to processing of metals, ceramics and polymers. Academic Press.

53. Franks, G. V., Tallon, C., Studart, A. R., Sesso, M. L., & Leo, S. (2017). Colloidal processing: enabling complex shaped ceramics with unique multiscale structures. *Journal of the American Ceramic Society*, 100(2), 458-490.

54. Frey, R. G., & Halloran, J. W. (1984). Compaction behavior of spray-dried alumina. *Journal of the American Ceramic Society*, 67(3), 199-203.

55. Fukasawa, T., Ando, M., Ohji, T., & Kanzaki, S. (2001). Synthesis of porous ceramics with complex pore structure by freeze-dry processing. *Journal of the American Ceramic Society*, 84(1), 230-232.

56. Fukushima, M., & Yoshizawa, Y. I. (2016). Fabrication and morphology control of highly porous mullite thermal insulators prepared by gelation freezing route. *Journal of the European Ceramic Society*, 36(12), 2947-2953.

57. Fukushima, M., Ohji, T., Hyuga, H., Matsunaga, C., & Yoshizawa, Y. I. (2017). Effect of gelatin gel strength on microstructures and mechanical properties of cellular ceramics created by gelation freezing route. *Journal of Materials Research*, 32(17), 3286-3293.

58. Fukushima, M., Yoshizawa, Y. I., & Ohji, T. (2014). Macroporous ceramics by gelation–freezing route using gelatin. *Advanced Engineering Materials*, 16(6), 607-620.

59. Gilissen, R., Erauw, J. P., Smolders, A., Vanswijgenhoven, E., & Luyten, J. (2000). Gelcasting, a near net shape technique. *Materials & Design*, 21(4), 251-257.

60. Glass, H. J., De With, G., De Graaf, M. J. M., & Van Der Drift, R. J. A. (1995). Compaction of homogeneous (Mn, Zn)-ferrite potcores. *Journal of Materials Science*, 30, 3162-3170.

61. Glass, S. J., & Ewsuk, K. G. (1997). Ceramic powder compaction. *Mrs. Bulletin*, 22(12), 24-28.

62. Greil, P. (1999). Near net shape manufacturing of ceramics. *Materials Chemistry and Physics*, 61(1), 64-68.

63. Greil, P. (2002). Advanced engineering ceramics. *Advanced Engineering Materials*, 4(5), 247-254.

64. Grey, R. O., & Beddow, J. K. (1969). On the Hausner ratio and its relationship to some properties of metal powders. *Powder Technology*, 2(6), 323-326.

65. Griffith, A. A. (1921). VI. The phenomena of rupture and flow in solids. Philosophical transactions of the royal society of london. Series A, containing papers of a mathematical or physical character, 221(582-593), 163-198.

66. Grigoriev, S. N., Soe, T. N., Malakhinsky, A., Makhadilov, I., Romanov, V., Kuznetsova, E., ... & Kurmysheva, A. Y. (2022). Granulation of Silicon Nitride Powders by Spray Drying: A Review. *Materials*, *15*(14), 4999.

67. Gubernat, A., Zych, Ł., & Wierzba, W. (2015). SiC products formed by slip casting method. International *Journal of Applied Ceramic Technology*, 12(5), 957-966.

68. Guo, L., Yang, J., Feng, Y., Qiu, T., Chen, B., & Wan, W. (2016). Preparation and properties of AlN ceramic suspension for non-aqueous gel casting. *Ceramics International*, 42(7), 8066-8071.

69. Gutierrez, C. A., & Moreno, R. (2001). Influence of slip preparation and casting conditions on aqueous tape casting of Al2O3. *Materials Research Bulletin*, 36(11), 2059-2072.

70. Ha, J. S. (2000). Effect of atmosphere type on gelcasting behavior of Al2O3 and evaluation of green strength. *Ceramics international*, 26(3), 251-254.

71. Hadson, C. F., Andrews, M. M., & Raghavan, S. (1993). Interaction of phosphate ester dispersants with calcined alumina. *Colloid and Polymer Science*, *271*, 56-62.

72. Haertling, G. H., & Land, C. E. (1971). Hot-pressed (Pb, La)(Zr, Ti) O3 ferroelectric ceramics for electrooptic applications. *Journal of the American Ceramic Society*, 54(1), 1-11.

73. Hammel, E. C., Ighodaro, O. R., & Okoli, O. I. (2014). Processing and properties of advanced porous ceramics: An application based review. *Ceramics International*, 40(10), 15351-15370.

74. Hampton, J. H. D., Savage, S. B., & Drew, R. A. (1988). Experimental analysis and modeling of slip casting. *Journal of the American Ceramic Society*, *71*(12), 1040-1045.

75. Hanaor, D., Michelazzi, M., Leonelli, C., & Sorrell, C. C. (2012). The effects of carboxylic acids on the aqueous dispersion and electrophoretic deposition of ZrO2. *Journal of the European Ceramic Society*, *32*(1), 235-244.

76. Hasani Bijarbooneh, F., Zhao, Y., Kim, J. H., Sun, Z., Malgras, V., Aboutalebi, S. H., ... & Dou, S. X. (2013). Aqueous colloidal stability evaluated by zeta potential measurement and resultant TiO2 for superior photovoltaic performance. *Journal of the American Ceramic Society*, 96(8), 2636-2643.

77. He, X., Su, B., Zhou, X., Yang, J., Zhao, B., Wang, X., ... & Qiu, H. (2011). Gelcasting of alumina ceramic using an egg white protein binder system. *Ceram. Silik*, 55(1), 1-7.

78. Hidber, P. C., Graule, T. J., & Gauckler, L. J. (1995). Competitive adsorption of citric acid and poly (vinyl alcohol) onto alumina and its influence on the binder migration during drying. *Journal of the American Ceramic Society*, 78(7), 1775-1780.

79. Hidber, P. C., Graule, T. J., &Gauckler, L. J. (1996). Citric acid—a dispersant for aqueous alumina suspensions. *Journal of the American Ceramic Society*, 79 (7), 1857-1867.

80. Ho, C. C., Kondo, T., Muramatsu, N., & Ohshima, H. (1996). Surface structure of natural rubber latex particles from electrophoretic mobility data. *Journal of Colloid and Interface Science*, 178(2), 442-445.

81. Hogg, R. T. W. D. W., Healy, T. W., & Fuerstenau, D. W. (1966). Mutual coagulation of colloidal dispersions. *Transactions of the Faraday Society*, 62, 1638-1651.

82. Hotza, D., &Greil, P. (1995). Aqueous tape casting of ceramic powders. *Materials Science and Engineering: A*, 202(1-2), 206-217.

83. Howatt, G. N., Breckenridge, R. G., & Brownlow, J. M. (1947). Fabrication of thin ceramic sheets for capacitors. *Journal of the American Ceramic Society*, 30(8), 237-242.

84. Hu, C., Sakka, Y., Tanaka, H., Nishimura, T., & Grasso, S. (2011). Fabrication of textured Nb_4AlC_3 ceramic by slip casting in a strong magnetic field and spark plasma sintering. *Journal of the American Ceramic Society*, 94(2), 410-415.

85. Iijima, M., Okamura, N., & Tatami, J. (2018). Effect of polyethyleneimine-fatty acid complex type dispersant structure on the overall processing chain of Si3N4 ceramics using multicomponent non-aqueous slurries. *Advanced Powder Technology*, *29*(12), 3440-3447.

86. Imran Zainuddin, M., Tanaka, S., & Uematsu, K. (2008). Effect of segregation of a polyacrylic acid (PAA) binder on the green strength of dry-pressed alumina compacts. *Journal of the American Ceramic Society*, 91(12), 3896-3902.

87. Jabbari, M., Bulatova, R., Tok, A. I. Y., Bahl, C. R. H., Mitsoulis, E., & Hattel, J. H. (2016). Ceramic tape casting: A review of current methods and trends with emphasis on rheological behaviour and flow analysis. *Materials Science and Engineering: B*, 212, 39-61.

88. Janney, M. A., Nunn, S. D., Walls, C. A., Omatete, O. O., Ogle, R. B., Kirby, G. H., & McMillan, A. D. (1998). Gelcasting, the handbook of ceramic engineering. Marcel Decker, New York.

89. Janney, M. A., Omatete, O. O., Walls, C. A., Nunn, S. D., Ogle, R. J., & Westmoreland, G. (1998). Development of low-toxicity gelcasting systems. *Journal of the American Ceramic Society*, *81*(3), 581-591.

90. Janney, M. A., Ren, W., Kirby, G. H., Nunn, S. D., & Viswanathan, S. (1998). Gelcast tooling: net shape casting and green machining. *Material and Manufacturing Process*, 13(3), 389-403.

91. Jay Deiner, L., Piotrowski, K. A., & Reitz, T. L. (2013). Mechanisms of Fatty Acid and Triglyceride Dispersant Bonding in Non-Aqueous Dispersions of NiO. *Journal of the American Ceramic Society*, *96*(3), 750-758.

92. Jewad, R., Bentham, C., Hancock, B., Bonfield, W., & Best, S. M. (2008). Dispersant selection for aqueous medium pressure injection moulding of anhydrous dicalcium phosphate. *Journal of the European Ceramic Society*, 28(3), 547-553.

93. Jia, Y., Kanno, Y., & Xie, Z. P. (2002). New gel-casting process for alumina ceramics based on gelation of alginate. *Journal of the European Ceramic Society*, 22(12), 1911-1916.

94. Jiang, G. P., Yang, J. F., Gao, J. Q., &Niihara, K. (2009). Characterization of porous silicon nitride ceramics using bentonite as binder and sintering additive. *Materials characterization*, 60(5), 456-460.

95. Jiang, L., & Gao, L. (2003). Effect of Tiron adsorption on the colloidal stability of nano-sized alumina suspension. *Materials chemistry and physics*, 80(1), 157-161.

96. Jin, L., Zhou, G., Shimai, S., Zhang, J., & Wang, S. (2010). ZrO2-doped Y2O3 transparent ceramics via slip casting and vacuum sintering. *Journal of the European Ceramic Society*, 30(10), 2139-2143.

97. Jing, Z. E. N. G., Zhang, Y., Zhou, K. C., & Zhang, D. (2014). Effects of alcohol additives on pore structure and morphology of freeze-cast ceramics. *Transactions of Nonferrous Metals Society of China*, 24(3), 718-722.

98. Johnson, S. B., Dunstan, D. E., & Franks, G. V. (2002). Rheology of cross-linked chitosan–Alumina suspensions used for a new gelcasting process. *Journal of the American Ceramic Society*, 85(7), 1699-1705.

99. Jr Walker, W. J., Reed, J. S., & Verma, S. K. (1999). Influence of slurry parameters on the characteristics of spray-dried granules. *Journal of the American Ceramic Society*, 82(7), 1711-1719.

100. Jyoti, V. P., Yadav, M. K., Mohanta, K., & Singh, V. K. (2022). Green Properties of Dry Pressed Alumina Compact Prepared Using Aloe Vera Gel and Sucrose as a Binder. *Transactions of the Indian Ceramic Society*, 81(1), 7-14.

101. Kamiya, H., Fukuda, Y., Suzuki, Y., Tsukada, M., Kakui, T., & Naito, M. (1999). Effect of polymer dispersant structure on electrosteric interaction and dense alumina suspension behavior. *Journal of the American Ceramic Society*, 82(12), 3407-3412.

102. Kim, D. H., Lim, K. Y., Paik, U., & Jung, Y. G. (2004). Effects of chemical structure and molecular weight of plasticizer on physical properties of green tape in BaTiO3/PVB system. *Journal of the European Ceramic Society*, 24(5), 733-738.

103. Kim, J., Choi, Y. J., Gal, C. W., Park, H., Yoon, S. Y., & Yun, H. S. (2022). Effect of dispersants on structural integrity of 3D printed ceramics. *International Journal of Applied Ceramic Technology*, 19(2), 968-978.

104. Kingery, W. D., Bowen, H. K., & Uhlmann, D. R. (1976). Introduction to ceramics (Vol. 17). John Wiley & sons.

105. Kokabi, M., Babaluo, A. A., & Barati, A. (2006). Gelation process in low-toxic gelcasting systems. *Journal of the European Ceramic Society*, 26(15), 3083-3090.

106. Kristoffersson, A., & Carlström, E. (1997). Tape casting of alumina in water with an acrylic latex binder. *Journal of the European Ceramic Society*, 17(2-3), 289-297.

107. Kristoffersson, A., Roncari, E., & Galassi, C. (1998). Comparison of different binders for water-based tape casting of alumina. *Journal of the European Ceramic Society*, 18(14), 2123-2131.

108. Kumar, A., Mohanta, K., Kumar, D., & Parkash, O. (2014). Green properties of dry-pressed alumina compacts fabricated using sucrose as binder. *Ceramics International*, 40(4), 6271-6277.

109. Kumar, D. R., Reddy, M. R., Mulay, V. N., & Krishnamurti, N. (2000). Acrylic co-polymer emulsion binders for green machining of ceramics. *European Polymer Journal*, 36(7), 1503-1510.

110. Lagaly, G., & Dékány, I. (2013). Colloid clay science. In Developments in clay science (Vol. 5, pp. 243-345). Elsevier.

111. Lange, F. F. (1989). Powder processing science and technology for increased reliability. *Journal of the American Ceramic Society*, 72(1), 3-15.

112. Larker, H. T., & Lundberg, R. (1999). Near net shape production of monolithic and composite high temperature ceramics by hot isostatic pressing (HIP). *Journal of the European Ceramic Society*, 19(13-14), 2367-2373.

113. Lee, H. J., Park, H. Y., Kim, E. H., Choi, H. H., Jin, J., Choi, J., ... & Jung, Y. G. (2021). Relationship between mechanical properties of ceramic green body and structures of photo-cured acrylate polymer for ceramic 3D printing based on photo polymerization. *Ceramics International*, 47(3), 3867-3875.

114. Lee, I. (2002). Influence of heat treatment upon SLS processed composites fabricated with alumina and monoclinic HBO_2. *Journal of Materials Science Letters*, 21(3), 209-212.

115. Lee, W. E., & Rainforth, M. (1994). Ceramic microstructures: property control by processing. Springer Science & Business Media.

116. Leo, S., Tallon, C., & Franks, G. V. (2014). Aqueous and nonaqueous colloidal processing of difficult-to-densify ceramics: suspension rheology and particle packing. *Journal of the American Ceramic Society*, 97(12), 3807-3817.

117. Leo, S., Tallon, C., Stone, N., & Franks, G. V. (2014). Near-net-shaping methods for ceramic elements of (body) armor systems. *Journal of the American Ceramic Society*, 97(10), 3013-3033.

118. Leu, M. C., Adamek, E. B., Huang, T., Hilmas, G., & Dogan, F. (2008). Freeform fabrication of zirconium diboride parts using selective laser sintering.

119. Levchik, G. F., Si, K., Levchik, S. V., Camino, G., & Wilkie, C. A. (1999). The correlation between cross-linking and thermal stability: Cross-linked polystyrenes and polymethacrylates. *Polymer Degradation and Stability*, 65(3), 395-403.

120. Levinson, L. (2020). Electronic Ceramics: Properties: Devices, and Applications. CRC Press.

121. Lewis, J. A. (2000). Colloidal processing of ceramics. *Journal of the American Ceramic Society*, 83(10), 2341-2359.

122. Li, H., Fan, H., Wang, B., Wang, C., Zhang, M., Chen, G., ... & Zhang, J. (2020). Mechanical and electrical properties of lithium stabilized sodium beta alumina solid electrolyte shaping by non-aqueous gelcasting. *Journal of the European Ceramic Society*, *40*(8), 3072-3079.

123. Li, S., Geng, Y., Zhao, T., Zhang, Q., & Yang, H. (2012). Effect of V_2O_5 on the aqueous tape casting of $Li_{1.075}Nb_{0.625}Ti_{0.45}O_3$ microwave ceramic. *Procedia Engineering*, 27, 1328-1333.

124. Li, S., Zhang, Q., Yang, H., & Zou, D. (2009). Fabrication and characterization of Li1+ x− yNb1− x− 3yTix+ 4yO3 substrates using aqueous tape casting process. *Ceramics International*, 35(1), 421-426.

125. Li, Y. Y., Perera, S. P., Crittenden, B. D., &Bridgwater, J. (2001). The effect of the binder on the manufacture of a 5A zeolite monolith. *Powder Technology*, 116(1), 85-96.

126. Lindqvist, K. M., & Carlström, E. (2005). Indirect solid freeform fabrication by binder assisted slip casting. *Journal of the European Ceramic Society*, 25(16), 3539-3545.

127. Liu, D. M. (1997). Influence of porosity and pore size on the compressive strength of porous hydroxyapatite ceramic. *Ceramics International*, *23*(2), 135-139.

128. Liu, G., & Li, J. (2013). High-gravity combustion synthesis: A fast and furnace-free way for preparing bulk ceramic materials. *Journal of Asian Ceramic Societies*, 1(2), 134-142.

129. Liu, G., Li, J., & Yang, Z. (2012). Melt-casting of translucent MgAl2O4 ceramics by combustion synthesis under high gravity. *Materials and Manufacturing Processes*, 27(6), 689-693.

130. Liu, K., Shi, Y., Li, C., Hao, L., Liu, J., & Wei, Q. (2014). Indirect selective laser sintering of epoxy resin-Al2O3 ceramic powders combined with cold isostatic pressing. *Ceramics International*, 40(5), 7099-7106.

131. Lukasiewicz, S. J. (1989). Spray-drying ceramic powders. *Journal of the American Ceramic Society*, *72* (4), 617-624.

132. Lv, X., Ye, F., Cheng, L., Fan, S., & Liu, Y. (2019). Binder jetting of ceramics: Powders, binders, printing parameters, equipment, and post-treatment. *Ceramics International*, 45(10), 12609-12624.

133. Marie, J., Bourret, J., Geffroy, P. M., Chartier, T., Bienia, M., Chaleix, V., ... & Smith, A. (2021). Impact of bio-based binders on rheological properties of aqueous alumina slurries for tape casting. *Journal of the European Ceramic Society*, 41(11), 5593-5601.

134. Marie, J., Bourret, J., Geffroy, P. M., Smith, A., Chaleix, V., &Chartier, T. (2017). Eco-friendly alumina suspensions for tape-casting process. *Journal of the European Ceramic Society*, 37(16), 5239-5248.

135. McKinney, D., & Sigmund, W. (2013). *Handbook of Advanced Ceramics: Chapter 11.1. 3. Colloidal Processing Fundamentals*. Elsevier Inc. Chapters.

136. McNulty, T. F., Mohammadi, F., Bandyopadhyay, A., Shanefield, D. J., Danforth, S. C., & Safari, A. (1998). Development of a binder formulation for fused deposition of ceramics. *Rapid Prototyping Journal*, *4*(4), 144-150.

137. Menard, K. P., & Menard, N. R. (2002). Dynamic mechanical analysis in the analysis of polymers and rubbers. *Encyclopedia of Polymer Science and Technology*, 1-33.

138. Michálek, M., Blugan, G., Graule, T., & Kuebler, J. (2015). Comparison of aqueous and non-aqueous tape casting of fully stabilized ZrO2 suspensions. *Powder Technology*, *274*, 276-283.

139. Millan, A. J., Nieto, M. I., & Moreno, R. (2002). Near-net shaping of aqueous alumina slurries using carrageenan. *Journal of the European Ceramic Society*, 22(3), 297-303.

140. Mistler, R. E. (1990). Tape casting: the basic process for meeting the needs of the electronics industry. *American Ceramic Society Bulletin*, 69, 1022-1026.

141. Mistler, R. E. (1995). The principles of tape casting and tape casting applications. *Ceramic Processing*, 147-173.

142. Mistler, R. E., & Twiname, E. R. (2000). Tape casting: theory and practice. *American ceramic society*.

143. Mistler, R. E., Bianchi, E., Wade, B., & Hurlbut, J. (2007). Evaluation of an environmentally friendly plasticizer for polyvinyl butyral for use in tape casting. Advanced Processing and Manufacturing Technologies for Structural and Multifunctional Materials: *Ceramic Engineering and Science Proceedings*, Volume 28, Issue 7, 27-34.

144. Mohanty, S., Rameshbabu, A. P., Mandal, S., Su, B., & Dhara, S. (2013). Critical issues in near net shape forming via green machining of ceramics: A case study of alumina dental crown. *Journal of Asian Ceramic Societies*, 1(3), 274-281.

145. Montanaro, L., Coppola, B., Palmero, P., & Tulliani, J. M. (2019). A review on aqueous gelcasting: A versatile and low-toxic technique to shape ceramics. *Ceramics International*, 45(7), 9653-9673.

146. Moon, J., Grau, J. E., Knezevic, V., Cima, M. J., & Sachs, E. M. (2002). Ink-jet printing of binders for ceramic components. *Journal of the American Ceramic Society*, *85*(4), 755-762.

147. Moreno, R. (1992). The role of slip additives in tape-casting technology. I: Solvents and dispersants. *American Ceramic Society Bulletin*, 71(10), 1521-1531.

148. Moreno, R. (2012). Colloidal processing of ceramics and composites. *Advances in applied ceramics*, 111(5-6), 246-253.

149. Moreno, R. (2020). Better ceramics through colloid chemistry. *Journal of the European Ceramic Society*, 40(3), 559-587.

150. Morissette, S. L., & Lewis, J. A. (1999). Chemorheology of aqueous-based alumina-poly (vinyl alcohol) gelcasting suspensions. *Journal of the American Ceramic Society*, 82(3), 521-528.

151. Moritz, T., & Richter, H. J. (2007). Ice-mould freeze casting of porous ceramic components. *Journal of the European Ceramic Society*, 27(16), 4595-4601.

152. Motyl, J. (1963). Spray Drying Ferrite Powder. Western Electric Eng, 7(3), 3-10.

153. Mukherjee, A., Maiti, B., Sharma, A. D., Basu, R. N., & Maiti, H. S. (2001). Correlation between slurry rheology, green density and sintered density of tape cast yttria stabilised zirconia. *Ceramics International*, 27(7), 731-739.

154. Muto, D., Hashimoto, S., Kondo, H., Daiko, Y., Honda, S., & Iwamoto, Y. (2020). Fabrication of highly isotropic porous alumina refractory clinkers consisting of platelets using a gelatin-sol. *Journal of Asian Ceramic Societies*, 8(2), 265-276.

155. Nahass, P., Rhine, W. E., & Pober, R. L. (1990). Comparison of aqueous and nonaqueous slurries for tape-casting, and dimensional stability in green tapes. *Ceramic Transactions*, 15 pp., 355.

156. Natividad, S. L., Marotto, V. R., Walker, L. S., Pham, D., Pinc, W., & Corral, E. L. (2011). Tape casting thin, continuous, homogenous, and flexible tapes of ZrB2. *Journal of the American Ceramic Society*, 94(9), 2749-2753.

157. Nawamawat, K., Sakdapipanich, J. T., Ho, C. C., Ma, Y., Song, J., & Vancso, J. G. (2011). Surface nanostructure of Hevea brasiliensis natural rubber latex particles. *Colloids and Surfaces A: Physicochemical and Engineering Aspects*, 390(1-3), 157-166.

158. Nayak, S., Singh, B. P., Besra, L., Chongdar, T. K., Gokhale, N. M., & Bhattacharjee, S. (2011). Aqueous tape casting using organic binder: a case study with YSZ. *Journal of the American Ceramic Society*, 94(11), 3742-3747.

159. Nettleship, I. (1996). Applications of porous ceramics. In Key Engineering Materials (Vol. 122, pp. 305-324). *Trans Tech Publications Ltd*.

160. Nie, J., Li, M., Liu, W., Li, W., & Xing, Z. (2021). The role of plasticizer in optimizing the rheological behavior of ceramic pastes intended for stereolithography-based additive manufacturing. *Journal of the European Ceramic Society*, 41(1), 646-654.

161. Nies, C. W., & Messing, G. L. (1984). Effect of glass-transition temperature of polyethylene glycol-plasticized polyvinyl alcohol on granule compaction. *Journal of the American Ceramic Society*, *67*(4), 301-304.

162. Nunn, S. D., Omatete, O. O., Walls, C. A., & Barker, D. L. (1994). Tensile strength of dried gelcast green bodies. In Proceedings of the 18th Annual Conference on Composites and Advanced Ceramic Materials—A: *Ceramic Engineering and Science Proceedings* (pp. 493-498). Hoboken, NJ, USA: John Wiley & Sons, Inc..

163. Nunn, S. D., & Kirby, G. H. (1996). Green Machining of Gelcast Ceramic Materlals. In Proceedings of the 20th Annual Conference on Composites, Advanced Ceramics, Materials, and Structures—A: *Ceramic Engineering and Science Proceedings* (pp. 209-213). Hoboken, NJ, USA: John Wiley & Sons, Inc.

164. Oberacker, R. (2011). Powder compaction by dry pressing. *Ceramics Science and Technology*, 3, 3-37.

165. Oezkan, B., Sameni, F., Karmel, S., Engstrøm, D. S., & Sabet, E. (2021). A systematic study of vat-polymerization binders with potential use in the ceramic suspension 3D printing. *Additive Manufacturing*, 47, 102225.

166. Ohji, T., & Fukushima, M. (2012). Macro-porous ceramics: processing and properties. *International Materials Reviews*, 57(2), 115-131.

167. Olhero, S. M., & Ferreira, J. M. F. (2002). Particle segregation phenomena occurring during the slip casting process. *Ceramics international*, *28*(4), 377-386.

168. Omatete, O. O., Janney, M. A., & Nunn, S. D. (1997). Gelcasting: from laboratory development toward industrial production. *Journal of the European Ceramic Society*, 17(2-3), 407-413.

169. Onoda Jr, G. Y. (1976). Theoretical strength of dried green bodies with organic binders. *Journal of the American Ceramic Society*, 59(5-6), 236-239.

170. Otitoju, T. A., Okoye, P. U., Chen, G., Li, Y., Okoye, M. O., & Li, S. (2020). Advanced ceramic components: Materials, fabrication, and applications. *Journal of Industrial and Engineering Chemistry*, 85, 34-65.

171. Pagnoux, C., Chartier, T., Granja, M. D. F., Doreau, F., Ferreira, J. M., & Baumard, J. F. (1998). Aqueous suspensions for tape-casting based on acrylic binders. *Journal of the European Ceramic Society*, 18(3), 241-247.

172. Paik, U., Hackley, V. A., Choi, S. C., & Jung, Y. G. (1998). The effect of electrostatic repulsive forces on the stability of BaTiO3 particles suspended in non-aqueous media. *Colloids and Surfaces A: Physicochemical and Engineering Aspects*, 135(1-3), 77-88.

173. Palmqvist, L., Lyckfeldt, O., Carlström, E., Davoust, P., Kauppi, A., & Holmberg, K. (2006). Dispersion mechanisms in aqueous alumina suspensions at high solids loadings. *Colloids and Surfaces A: Physicochemical and Engineering Aspects*, 274(1-3), 100-109.

174. Park, S. J., & Seo, M. K. (2011). Intermolecular force. *Interface science and technology*, 18, 1-57.

175. Pekor, C. M., Kisa, P., & Nettleship, I. (2008). Effect of polyethylene glycol on the microstructure of freeze-cast alumina. *Journal of the American Ceramic Society*, 91(10), 3185-3190.

176. Peng, E., Zhang, D., & Ding, J. (2018). Ceramic robocasting: recent achievements, potential, and future developments. *Advanced Materials*, 30(47), 1802404.

177. Piacenza, E., Presentato, A., & Turner, R. J. (2018). Stability of biogenic metal (loid) nanomaterials related to the colloidal stabilization theory of chemical nanostructures. *Critical reviews in biotechnology*, 38(8), 1137-1156.

178. Plucknett, K. P., Caceres, C. H., & Willinson, D. S. (1994). Tape casting of fine alumina/zirconia powders for composite fabrication. *Journal of the American Ceramic Society*, 77(8), 2137-2144.

179. Potoczek, M., Heneczkowski, M., & Oleksy, M. (2003). A new polyurethane binder providing high green strength of dry-pressed alumina. *Ceramics International*, 29(3), 259-264.

180. Prabhakaran, K., Narayanan, A., & Pavithran, C. (2001). Cardanol as a dispersant plasticizer for an alumina/toluene tape casting slip. *Journal of the European Ceramic Society*, 21(16), 2873-2878.

181. Promdej, C., Areeraksakul, S., Pavarajarn, V., Wada, S., Wasanapiarnpong, T., & Charinpanitkul, T. (2008). Preparation of translucent alumina ceramic specimen using slip casting method. *Journal of the Ceramic Society of Japan*, 116(1351), 409-413.

182. Pugh, R. J., & Bergstrom, L. (Eds.). (2017). Surface and colloid chemistry in advanced ceramics processing. CRC Press.

183. Rahaman, M. N. (2017). Ceramic processing and sintering. CRC press.

184. Raj, P. M., & Cannon, W. R. (2001). Mechanisms in Nonadueous High Solids Loading Dispersions. *Polymers in Particulate Systems: Properties and Applications*, *104*, 27.

185. Rao, R. R., & Kannan, T. S. (2001). Dispersion and slip casting of hydroxyapatite. *Journal of the American Ceramic Society*, 84(8), 1710-1716.

186. Reddy, N., & Yang, Y. (2010). Citric acid cross-linking of starch films. *Food Chemistry*, 118(3), 702-711.

187. Reed, J. S. (1995). Principles of ceramics processing. Second edn. John Wiley & sons, Inc.

188. Ren, L., Zeng, Y. P., & Jiang, D. (2009). Preparation of porous TiO2 by a novel freeze casting. *Ceramics international*, 35(3), 1267-1270.

189. Rice, R. W. (1993). Evaluating porosity parameters for porosity–property relations. *Journal of the American Ceramic Society*, 76(7), 1801-1808.

190. Richerson, D. W., & Lee, W. E. (2018). Modern ceramic engineering: properties, processing, and use in design. CRC press.

191. Rombouts, M., Deckers, J., Thijs, I., Deckx, J., & Kruth, J. P. (2012). Wax based binder for indirect selective laser sintering of alumina. *In Proceedings of the 5th International PMI Conference* (pp. 184-188).

192. Romdhane, M. R. B., Chartier, T., Baklouti, S., Bouaziz, J., Pagnoux, C., & Baumard, J. F. (2007). A new processing aid for dry-pressing: a copolymer acting as dispersant and binder. *Journal of the European Ceramic Society*, 27(7), 2687-2695.

193. Roosen, A. (2001). New lamination technique to join ceramic green tapes for the manufacturing of multilayer devices. *Journal of the European Ceramic Society*, 21(10-11), 1993-1996.

194. Ruys, A. J., & Sorrell, C. C. (1996). Slip casting alumina with Na-CMC. *American Ceramic Society Bulletin*, 75(11).

195. Sabree, I., Gough, J. E., & Derby, B. (2015). Mechanical properties of porous ceramic scaffolds: influence of internal dimensions. *Ceramics International*, 41(7), 8425-8432.

196. Sailaja, G. S., Ramesh, P., & Varma, H. K. (2007). Hydroxyapatite moldable formulation using natural rubber latex as binder. *Journal of Biomedical Materials Research Part B: Applied Biomaterials*, 82(1), 231-238.

197. Sanches, M. F., Vitorino, N., Freitas, C., Abrantes, J. C. C., Frade, J. R., Neto, J. R., & Hotza, D. (2015). Cellular ceramics by gelatin gel casting of emulsified suspensions with sunflower oil. *Journal of the European Ceramic Society*, 35(9), 2577-2585.

198. Sansatsadeekul, J., Sakdapipanich, J., & Rojruthai, P. (2011). Characterization of associated proteins and phospholipids in natural rubber latex. *Journal of Bioscience and Bioengineering*, 111(6), 628-634.

199. Schwentenwein, M., & Homa, J. (2015). Additive manufacturing of dense alumina ceramics. *International Journal of Applied Ceramic Technology*, 12(1), 1-7.

200. Sciancalepore, C., Moroni, F., Messori, M., & Bondioli, F. (2017). Acrylate-based silver nanocomposite by simultaneous polymerization–reduction approach via 3D stereolithography. *Composites Communications*, 6, 11-16.

201. Seeber, B. S. M., Gonzenbach, U. T., &Gauckler, L. J. (2013). Mechanical properties of highly porous alumina foams. *Journal of Materials Research*, *28*(17), 2281-2287.

202. Shah, R. B., Tawakkul, M. A., & Khan, M. A. (2008). Comparative evaluation of flow for pharmaceutical powders and granules. *Aaps Pharmscitech*, 9, 250-258.

203. Shahzad, K., Deckers, J., Zhang, Z., Kruth, J. P., & Vleugels, J. (2014). Additive manufacturing of zirconia parts by indirect selective laser sintering. *Journal of the European Ceramic Society*, 34(1), 81-89.

204. Shanefield, D. J. (2013). Organic additives and ceramic processing: with applications in powder metallurgy, ink, and paint. Springer Science & Business Media.

205. Shang, Q., Wang, Z., Li, J., Zhou, G., Zhang, H., & Wang, S. (2017). Gel-tape-casting of aluminum nitride ceramics. *Journal of Advanced Ceramics*, 6, 67-72.

206. Shapkin, N. P., Papynov, E. K., Shichalin, O. O., Buravlev, I. Y., Simonenko, E. P., Simonenko, N. P., ... & Drankov, A. N. (2021). Spark plasma sintering-reactive synthesis of SiC and SiC–HfB2 ceramics based on natural renewable raw materials. *Russian Journal of Inorganic Chemistry*, 66(5), 629-637.

207. Shende, R. V., & Lombardo, S. J. (2002). Determination of binder decomposition kinetics for specifying heating parameters in binder burnout cycles. *Journal of the American Ceramic Society*, 85(4), 780-786.

208. Sigmund, W. M., Bell, N. S., & Bergström, L. (2000). Novel powder-processing methods for advanced ceramics. *Journal of the American Ceramic Society*, 83(7), 1557-1574.

209. Singh, B. P., Bhattacharjee, S., Besra, L., Sengupta, D. K., & Misra, V. N. (2004). Use of Polymeric and other Organic Additives in Ceramic Slurry Processing for Casting—A Review. *Transactions of the Indian Ceramic Society*, 63(1), 1-8.

210. Singh, B. P., Menchavez, R., Takai, C., Fuji, M., & Takahashi, M. (2005). Stability of dispersions of colloidal alumina particles in aqueous suspensions. *Journal of colloid and interface science*, *291*(1), 181-186.

211. Siti Nuraya, A. S., Baharin, A., & Azura, A. R. (2019). Effect of potassium oleate (PO) on the colloid stability of high ammonia (HA) natural rubber latex (NRL) after the freezing and thawing processes. *Journal of Rubber Research*, 22, 13-21.

212. Smejda-Krzewicka, A., Olejnik, A., & Strzelec, K. (2020). The effect of metal oxide on the cure, morphology, thermal and mechanical characteristics of chloroprene and butadiene rubber blends. *Polymer Bulletin*, 77, 4131-4146.

213. Snijkers, F., De Wilde, A., Mullens, S., & Luyten, J. (2004). Aqueous tape casting of yttria stabilised zirconia using natural product binder. *Journal of the European Ceramic Society*, 24(6), 1107-1110.

214. Sofie, S. W., & Dogan, F. (2001). Freeze casting of aqueous alumina slurries with glycerol. *Journal of the American Ceramic Society*, 84(7), 1459-1464.

215. Somiya, S. (2013). Handbook of advanced ceramics: materials, applications, processing, and properties. Academic press.

216. Somton, K., Laoratanakul, P., & McCuiston, R. (2019). Effect of Binder Content on the Slip Rheology and Green Properties of Slip Cast Alumina. In Key Engineering Materials (Vol. 798, pp. 177-181). *Trans Tech Publications Ltd*.

217. Stevinson, B., Bourell, D. L., & Beaman, Jr, J. J. (2006). Dimensional stability during post-processing of selective laser sintered ceramic preforms. *Virtual and Physical Prototyping*, 1(4), 209-216.

218. Steyer, T. E. (2013). Shaping the future of ceramics for aerospace applications. *International Journal of Applied Ceramic Technology*, 10(3), 389-394.

219. Straus, S., & Madorsky, S. L. (1956). Thermal degradation of unvulcanized and vulcanized rubber in vacuum. *Industrial & Engineering Chemistry*, 48(7), 1212-1219.

220. Su, B., Dhara, S., & Wang, L. (2008). Green ceramic machining: A top-down approach for the rapid fabrication of complex-shaped ceramics. *Journal of the European Ceramic Society*, 28(11), 2109-2115.

221. Subramaniam, A. (1995). The chemistry of natural rubber latex. *Immunology and Allergy Clinics of North America*, 15(1), 1-20.

222. Subramanian, K., Vail, N., Barlow, J., & Marcus, H. (1995). Selective laser sintering of alumina with polymer binders. *Rapid Prototyping Journal*, 1(2), 24-35.

223. Sun, M. Q., Shen, P., & Jiang, Q. C. (2019). Fabrication and characterization of robust freeze-cast alumina scaffolds with dense ceramic walls and controllable pore sizes. *Journal of Materials Science*, 54, 5224-5235.

224. Szafran, M., Rokicki, G., & Wiśniewski, P. (2001). New water thinnable polymeric binders in die pressing of alumina powders. *Functional Gradient Materials and Surface Layers Prepared by Fine Particles Technology*, 75-80.

225. Szafran, M., Wisniewski, P., & Rokicki, G. (2004). Effect of glass transition temperature of polymeric binders on properties ceramic materials. *Journal of Thermal Analysis and Calorimetry*, 77, 319-327.

226. Taguchi, H., Takahashi, Y., & Miyamoto, H. (1985). Effect of milling on slip casting of partially stabilized zirconia. *Journal of the American Ceramic Society*, 68(10), C-264.

227. Taktak, R., Baklouti, S., & Bouaziz, J. (2011). Effect of binders on microstructural and mechanical properties of sintered alumina. *Materials Characterization*, 62(9), 912-916.

228. Tallon, C., & Franks, G. V. (2011). Recent trends in shape forming from colloidal processing: A review. *Journal of the Ceramic Society of Japan*, 119(1387), 147-160.

229. Tallon, C., Limacher, M., & Franks, G. V. (2010). Effect of particle size on the shaping of ceramics by slip casting. *Journal of the European Ceramic Society*, 30(14), 2819-2826.

230. Tallon, C., Moreno, R., Nieto, M. I., Jach, D., Rokicki, G., & Szafran, M. (2007). Gelcasting Performance of Alumina Aqueous Suspensions with Glycerol Monoacrylate: A New Low-Toxicity Acrylic Monomer. *Journal of the American Ceramic Society*, 90(5), 1386-1393.

231. Tanaka, S., Pin, C. C., & Uematsu, K. (2006). Effect of Organic Binder Segregation on Sintered Strength of Dry-Pressed Alumina. *Journal of the American Ceramic Society*, 89(6), 1903-1907.

232. Tang, H. H., Chiu, M. L., & Yen, H. C. (2011). Slurry-based selective laser sintering of polymer-coated ceramic powders to fabricate high strength alumina parts. *Journal of the European Ceramic Society*, *31*(8), 1383-1388.

233. Tang, Y., Miao, Q., Qiu, S., Zhao, K., & Hu, L. (2014). Novel freeze-casting fabrication of aligned lamellar porous alumina with a centrosymmetric structure. *Journal of the European Ceramic Society*, 34(15), 4077-4082.

234. The International Organization for Standardization (2014). Latex, Rubber—Determination of Total Solids Content (ISO Standard No. 124). 7th ed. Geneva, Switzerland: The International Organization for Standardization.

235. The International Organization for Standardization (2018). Rubber—Determination of ash- Part-1 combustion method. ISO 247-1: 2018 (E).

236. Trunec, M., & Maca, K. (2014). Advanced ceramic processes. In Advanced Ceramics for Dentistry (pp. 123-150). Butterworth-Heinemann.

237. Tseng, W. J., Liu, D. M., & Hsu, C. K. (1999). Influence of stearic acid on suspension structure and green microstructure of injection-molded zirconia ceramics. *Ceramics International*, 25(2), 191-195.

238. Tsetsekou, A., Agrafiotis, C., Leon, I., & Milias, A. (2001). Optimization of the rheological properties of alumina slurries for ceramic processing applications Part II: Spray-drying. *Journal of the European Ceramic Society*, *21*(4), 493-506.

239. Uhland, S. A., Holman, R. K., Morissette, S., Cima, M. J., & Sachs, E. M. (2001). Strength of green ceramics with low binder content. *Journal of the American Ceramic Society*, 84(12), 2809-2818.

240. Uppalapati, M., & Green, D. J. (2005). Effect of external lubricant on mechanical properties of dry-pressed green bodies. *Journal of the American Ceramic Society*, 88(6), 1397-1402.

241. Vallet-Regí, M. (2001). Ceramics for medical applications. Journal of the Chemical Society, Dalton Transactions, (2), 97-108.

242. Vinod, A., Sanjay, M. R., Suchart, S., & Jyotishkumar, P. (2020). Renewable and sustainable biobased materials: An assessment on biofibers, biofilms, biopolymers and biocomposites. *Journal of Cleaner Production*, 258, 120978..

243. Vlajic, M. D., & Krstic, V. D. (2002). Strength and machining of gelcast SiC ceramics. *Journal of Materials Science*, 37, 2943-2947.

244. Wang, S. F., Zhang, J., Luo, D. W., Gu, F., Tang, D. Y., Dong, Z. L., ... & Kong, L. B. (2013). Transparent ceramics: Processing, materials and applications. *Progress in solid state chemistry*, 41(1-2), 20-54.

245. Wei, Q., Wang, Y., Chai, W., Zhang, Y., & Chen, X. (2017). Molecular dynamics simulation and experimental study of the bonding properties of polymer binders in 3D powder printed hydroxyapatite bioceramic bone scaffolds. *Ceramics International*, *43*(16), 13702-13709.

246. Wei, Y., Zhang, H., Wu, L., Jin, L., & Liao, S. (2017). A review on characterization of molecular structure of natural rubber. *MOJ Polymer Science*, 1(6), 197-199.

247. Wiecinska, P., Graule, T., & Bachonko, M. (2015). Organic additives in gel-tape casting of ceramic powders–A novel approach to the problem of elasticity and cracking of thin tapes. *Journal of the European Ceramic Society*, 35(14), 3949-3957.

248. Wiecinska, P., Zurawska, A., Falkowski, P., Jeong, D. Y., & Szafran, M. (2020). Sweet ceramics: How saccharide-based compounds have changed colloidal processing of ceramic materials. *Journal of the Korean Ceramic Society*, 57, 231-245.

249. Wolny, W. W. (2004). European approach to development of new environmentally sustainable electroceramics. *Ceramics international*, 30(7), 1079-1083.

250. Wu, Q., Li, Y., Zhang, B., Liu, Y., Li, X., & Ji, H. (2023). A new gelcasting using Isobam both as dispersant and monomer. *Ceramics International*, 49 (10), 15560-15567.

251. Wu, X.L.K., & McAnany, W. J. (1995). Acrylic binder for green machining. *American Ceramic Society Bulletin*, 74(5), 61-64.

252. Wu, X. K., Whitman, D. W., Kaufell, W. L., Finch, W. C., & Cumbers, D. I. (1997, January). Acrylic binders for dry pressing ceramics. In 98th Annual Meeting and the Ceramic Manufacturing Council's Workshop and Exposition: Materials & Equipment/Whitewares: Ceramic Engineering and Science Proceedings (pp. 422-438). Hoboken, NJ, USA: John Wiley & Sons, Inc.

253. Wu, X., Weidner, A., Aneziris, C. G., & Biermann, H. (2022). Manufacture of carbon-bonded alumina based on a lactose-tannin binder system via slip casting. *Ceramics International*, 48(1), 148-156.

254. Xie, Z. P., Luo, J. S., Wang, X., Li, J. B., & Huang, Y. (2005). The effect of organic vehicle on the injection molding of ultra-fine zirconia powders. *Materials & Design*, 26(1), 79-82.

255. Xu, J., Zhang, Y., Gan, K., Zhang, X., Qu, Y., Ma, N., & Yang, J. (2015). A novel gelcasting of alumina suspension using curdlan gelation. *Ceramics International*, 41(9), 10520-10525.

256. Xu, Q., Gabbitas, B., Matthews, S., & Zhang, D. (2013). The development of porous titanium products using slip casting. *Journal of Materials Processing Technology*, 213(8), 1440-1446.

257. Xu, Q., Gabbitas, B., Matthews, S., & Zhang, D. (2014). The effect of binder and plasticizer on porous titanium compacts prepared by slip casting. *Procedia Materials Science*, *4*, 81-84.

258. Xu, X., Dong, X., Guo, A., Wang, M., Sui, G., & Liu, J. (2017). Effect of binder types on the properties of the mullite fibrous ceramics prepared by TBA-based gel-casting method. *Ceramics International*, 43(1), 228-233.

259. Xue, J., Dong, M., Li, J., Zhou, G., & Wang, S. (2010). Gelcasting of aluminum nitride ceramics. *Journal of the American Ceramic Society*, *93*(4), 928-930.

260. Yang, J., Yu, J., & Huang, Y. (2011). Recent developments in gelcasting of ceramics. *Journal of the European Ceramic Society*, 31(14), 2569-2591.

261. Yoon, B. H., Choi, W. Y., Kim, H. E., Kim, J. H., & Koh, Y. H. (2008). Aligned porous alumina ceramics with high compressive strengths for bone tissue engineering. *Scripta Materialia*, 58(7), 537-540.

262. Yoon, S. J., Shin, H. S., Lee, D. K., Kang, C. Y., Park, J. W., & Kim, H. J. (2001). Rheology of slurries and effects of polymer volume ratio in aqueous PZT tape casting. *The Korean Journal of Ceramics*, *7*(1), 16-19.

263. Young, A. C., Omatete, O. O., Janney, M. A., & Menchhofer, P. A. (1991). Gelcasting of alumina. *Journal of the American Ceramic Society*, 74(3), 612-618.

264. Zhang, C., Yang, J., Qiu, T., & Guo, J. (2012). Preparation of ZTA ceramic by aqueous gelcasting with a low-toxic monomer DMAA. *Ceramics International*, 38(4), 3063-3068.

265. Zhang, D., Zhang, Y., Xie, R., & Zhou, K. (2012). Freeze gelcasting of aqueous alumina suspensions for porous ceramics. *Ceramics International*, 38(7), 6063-6066.

266. Zhang, J., Jiang, D., & Lin, Q. (2005). Poly (vinyl pyrrolidone), a dispersant for non-aqueous processing of silicon carbide. *Journal of the American Ceramic Society*, 88(4), 1054-1056.

267. Zhang, N., Liu, Z., Du, Y., Yu, Q., Wang, S., Tan, G., ... & Ritchie, R. O. (2022). Facile processing of oriented macro-porous ceramics with high strength and low thermal conductivity. *Journal of the European Ceramic Society*, *42*(15), 7196-7202.

268. Zhang, T., Blackburn, S., & Bridgwater, J. (1994). Properties of ceramic suspensions for injection moulding based on agar binders. *British Ceramic Transactions*, 93(6), 229-233.

269. Zhang, Y., Hu, L., Han, J., & Jiang, Z. (2010). Freeze casting of aqueous alumina slurries with glycerol for porous ceramics. *Ceramics international*, 36(2), 617-621.

270. Zhang, Y., Xu, J., Qu, Y., Xi, X., & Yang, J. (2014). Gelcasting of alumina suspension using gellan gum as gelling agent. *Ceramics International*, 40(4), 5715-5721.

271. Zhang, Y., Zuo, K., & Zeng, Y. P. (2009). Effects of gelatin addition on the microstructure of freeze-cast porous hydroxyapatite ceramics. *Ceramics International*, 35(6), 2151-2154.

272. Zhou, C., Jiang, B., Fan, J., Mao, X., Pan, L., Jiang, Y., ... & Fang, Y. (2016). Translucent Al2O3 ceramics produced by an aqueous tape casting method. *Ceramics International*, 42(1), 1648-1652.

273. Zhu, J., Lai, Z., Yin, Z., Jeon, J., & Lee, S. (2001). Fabrication of ZrO2–NiCr functionally graded material by powder metallurgy. *Materials Chemistry and Physics*, 68(1-3), 130-135.

274. Zhu, X., Jiang, D., & Tan, S. (2002). The control of slurry rheology in the processing of reticulated porous ceramics. *Materials Research Bulletin*, 37(3), 541-553.

275. Zocca, A., Colombo, P., Gomes, C. M., & Günster, J. (2015). Additive manufacturing of ceramics: issues, potentialities, and opportunities. *Journal of the American Ceramic Society*, 98(7), 1983-2001.

276. Zuo, K. H., Zeng, Y. P., & Jiang, D. (2010). Effect of polyvinyl alcohol additive on the pore structure and morphology of the freeze-cast hydroxyapatite ceramics. *Materials Science and Engineering: C*, 30(2), 283-287.

List of publications based on the thesis

Paper Publications

1. Rakesh Krishnan,P.P., Vijayan, S., Wilson, P., Kumar, P. A., & Prabhakaran, K. (2021). Machinable green bodies by dry pressing of alumina powder using natural rubber latex as a cross-linkable binder. *Powder Technology*, 385, 227-233.
2. Rakesh Krishnan, P.P , P Arun Kumar, K Prabhakaran (2023). Natural rubber latex as a new binder for slip casting of alumina ceramics, *Journal of Rubber Research*, 1-11.
3. Rakesh Krishnan.P.P., Vijayan, S., Wilson, P., Kumar, P. A., & Prabhakaran, K. (2019). Aqueous tape casting of alumina using natural rubber latex binder, *Ceramics International*, 45 (15), 18543-18550.
4. Rakesh Krishnan.P.P, Kumar, P. A., & Prabhakaran, K. (2022). Freeze-gelcasting of aqueous alumina powder suspension using natural rubber latex. *Ceramics International*, 48(10), 14839-14848.
5. Rakesh Krishnan.P.P., Kumar, P. A., & Prabhakaran, K. (2023). Preparation of macroporous alumina ceramics by ice templating without freeze drying using natural rubber latex binder. *Journal of Porous Materials*, 1-9.

Conference papers

1. Aqueous tape casting of alumina using natural rubber latex, International Conference on Recent Trends in Materials Science and Technology, October 2018, Thiruvananthapuram.
2. Machinable alumina green bodies by powder pressing using natural rubber as a cross-linkable binder, National Conference on Recent Trends in Materials Science and Technology, December 2020, Thiruvananthapuram.
3. Freeze-gel casting of aqueous alumina powder suspension using natural rubber latex, National Conference on Recent Trends in Materials Science and Technology, December 2021, Thiruvananthapuram.

4. Preparation of macroporous alumina ceramics by ice templating without freeze drying using natural rubber latex binder, National Conference on Recent Trends in Materials Science and Technology, December 2022, Thiruvananthapuram.